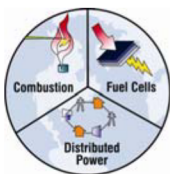**Energy Research and Development Division**
FINAL PROJECT REPORT

ECONOMICAL DISPATCH OF COMBINED COOLING, HEATING, AND POWER SYSTEMS WITH EMISSIONS CONSTRAINTS AND THERMAL LOAD FOLLOWING CAPABILITY

PREPARED BY:

Primary Author(s):
    Li Zhao
    Robert Flores
    Jacob Brouwer

Advanced Power and Energy Program
University of California, Irvine
221 Engineering Laboratory Facility
Irvine, California 92697-3550
Phone: 949-824-1999 | Fax: 949-824-7423
http://www.apep.uci.edu

Contract Number: PIR-09-013

Prepared for:

California Energy Commission

Mike Kane
Contract Manager

Aleecia Gutierrez
Office Manager
Energy Generation Research Office

Laurie ten Hope
Deputy Director
ENERGY RESEARCH AND DEVELOPMENT DIVISION

Robert P. Oglesby
Executive Director

PREFACE

The California Energy Commission Energy Research and Development Division supports public interest energy research and development that will help improve the quality of life in California by bringing environmentally safe, affordable, and reliable energy services and products to the marketplace.

The Energy Research and Development Division conducts public interest research, development, and demonstration (RD&D) projects to benefit California.

The Energy Research and Development Division strives to conduct the most promising public interest energy research by partnering with RD&D entities, including individuals, businesses, utilities, and public or private research institutions.

Energy Research and Development Division funding efforts are focused on the following RD&D program areas:

- Buildings End-Use Energy Efficiency

- Energy Innovations Small Grants

- Energy-Related Environmental Research

- Energy Systems Integration

- Environmentally Preferred Advanced Generation

- Industrial/Agricultural/Water End-Use Energy Efficiency

- Renewable Energy Technologies

- Transportation

Economical Dispatch of Combined Cooling, Heating, and Power Systems With Emissions Constraints and Thermal Load Following Capability is the final report for the Economical Dispatch of CCHP Systems with Emissions Constraints & Thermal Load Following Capability project (Grant Number PIR-09-013) conducted by Advanced Power and Energy Program, University of California, Irvine. The information from this project contributes to Energy Research and Development Division's Buildings End-Use Energy Efficiency Program.

For more information about the Energy Research and Development Division, please visit the Energy Commission's website at www.energy.ca.gov/research/ or contact the Energy Commission at 916-327-1551.

ABSTRACT

The research team developed economic dispatch strategies, which are analyzed and discussed in this report, to enable combined cooling, heat, and power technologies to reduce overall facility energy costs. The models have been built in the MATLAB-Simulink® framework using a method developed by the University of California, Irvine. In addition, the research team has developed the economic and environmental analyses strategies and models that are used in the project.

A microturbine generator is dispatched using different economic control strategies, reducing the cost of energy to the facility. Several industrial and commercial buildings and facilities are simulated using acquired dynamic electrical, heating, and cooling load data. Industrial and commercial utility rate structures are modeled after Southern California Edison and Southern California Gas Company tariffs and used to find energy costs for the simulated buildings and corresponding microturbine dispatch. Using these control strategies, building models, and utility rate models, the research team performed a parametric study examining various generator characteristics. An economic assessment of the distributed generation is then performed for both the microturbine generator and that parametric study. In addition, the researchers examined carbon and pollutant emissions from a Capstone C65 microturbine generator and estimated for the dispatch strategies. The criteria pollutant emissions were estimated using measured emissions levels for various amounts of heat recovery. These emission rates were compared to regulatory limits, the California electric grid emissions rates, and national grid emissions rates.

Finally, the novel control algorithms and architectures that were developed were also demonstrated to dispatch a microturbine generator in the Engineering Laboratory Facility of the University of California, Irvine. The control algorithms were translated to Siemens controls and were installed to demonstrate the novel control algorithms for economical dispatch of a CCHP system.

Keywords: CCHP, Economic Dispatch, Control Strategy, Energy Cost, Emission

TABLE OF CONTENTS

LIST OF FIGURES

vii

LIST OF TABLES

* **UNSOURCED TABLES WERE DEVELOPED BY THE PROJECT TEAM.**

EXECUTIVE SUMMARY

Introduction

This project enables using combined heat and power (CHP) in underutilized applications. With the emergence of technologies that can efficiently convert heat into cooling (for example, absorption chilling technology), considering combined cooling, heating, and power offers additional market opportunities that are of interest and can significantly contribute to meeting Public Interest Energy Research Program goals.

Combined cooling, heating, and power technology can support large energy efficiency improvements and significant reductions of greenhouse gas (primarily carbon dioxide [CO_2]) emissions. While combined cooling, heating, and power has been widely applied in large (>20 megawatts) applications, the smaller commercial and industrial applications between 500 kilowatts (kW) and 5 megawatts (MW) have not been fully exploited. Various estimates of the combined cooling, heating, and power market potential in the industrial sector are in the range of 30-90 gigawatts (GW) of electrical capacity. The "light" industrial market (defined here as 0.5 – 5 MW of electrical capacity) comprises about 60 percent of the total industrial combined cooling, heating, and power market potential. In addition, similar applications in the commercial and institutional market sectors are estimated to comprise about 75 GW of the market potential. As a result, the combined light industrial, commercial, and institutional combined cooling, heating, and power market potential ranges from 93 to 129 GW.

However, combined cooling, heating, and power in the smaller commercial and industrial applications are challenged by a host of barriers. These barriers include product performance and availability barriers; awareness, information, and education barriers; utility policies and regulatory barriers; planning, siting, and zoning barriers; and environmental regulation and supporting market infrastructure barriers. Among these barriers are three high priority challenges that must be overcome to enable the light industrial, commercial, and institutional adoption of combined cooling, heating, and power. These high priority challenges are:

1.   Lack of cost-competitive equipment options in the appropriate size range (0.5 – 5MW).

2.   Lack of information on the value of these smaller systems for potential users.

3.   Lack of controls sufficient to deal with the highly dynamic nature and relative noncoincidence of the thermal and electrical loads in many of these applications.

This research and development effort directly addresses these challenges and significantly contributes to increased combined cooling, heating, and power market penetration in the light industrial, commercial, and institutional sectors.

Project Purpose

Most commercial and industrial electrical loads are highly dynamic and typically not synchronized with local heating and cooling demands. These dynamics, together with utility charges and nonexport requirements, often make CHP/CCHP systems less cost-effective and less attractive to end users.

A new, dynamic combined heat and power/combined cooling, heating, and power system control approach is required to address this problem and overcome these barriers. The purpose of this research and development effortis to develop novel control strategies for dynamic economical dispatch of combined heat and power/combined cooling, heating, and power systems with emissions constraints and thermal load following capability (or the ability of the system to adjust the amount of heat energy supplied to match the amount required in real time). This new combined heat and power/combined cooling, heating, and power control technology will significantly contribute to increased CHP/CCHP market penetration in the light industrial, commercial, and institutional sectors of California. The novel control algorithms and technology will be developed based upon previous research, experience, and expertise at the University of California, Irvine (UCI), which directly addresses the high priority challenges in a wide variety of applications.

To meet the goal and address the problem, the research team has established a set of objectives as follows:

Objective 1: Develop first principles dynamic physical models of the CCHP technologies required for fundamental understanding of transient performance capabilities and interactions.

Objective 2: Acquire and assess dynamic loads from existing building types and applications and dynamic performance characteristics of CCHP technologies of interest.

Objective 3: Verify the dynamic model performance by comparing simulation results to existing CCHP performance.

Objective 4: Develop and test novel control algorithms and architecture for dynamic control of CCHP systems with economic and environmental constraints and goals.

Objective 5: Translate the novel control algorithms and architecture to the industrial partner (Siemens) controls hardware platform, and

Objective 6: Install & verify performance of the novel controls in a CCHP system.

Project Results

The first principles dynamic models for CCHP components and integrated systems technologies that are required for the project have been developed. The models have been built in the MATLAB-Simulink® framework using a method developed by UCI and described in detail in this report. In addition, the research team has developed the economic and environmental analyses, strategies, and models that were used in the project. The UCI method develops a physical model for each of the primary system components and then connects the components together to represent the CCHP system. The system dynamic models are then subjected to dynamic CCHP load demands and other deviations. In this fashion the dynamics of individual components, as well as interactions among system components, are captured to simulate the system dynamic response. In this report, the developments of all of the following dynamic models are presented: Micro-Turbine Generator, High-Temperature Polymer Electrolyte Fuel

Cell Model, Molten Carbonate Fuel Cell Model, Photovoltaic Model, Lead-Acid Battery Model, Lithium-Ion Battery Model, and Ultracapacitor Model.

A combined cooling, heating, and power system can provide many benefits over traditional central generation such as increased reliability and efficiency while reducing emissions. Despite these potential benefits, a CCHP system is generally not purchased unless it reduces energy costs. Economic dispatch strategies can be designed such that CCHP technologies reduce overall facility energy costs. In this report, a microturbine generator is dispatched using different economic control strategies, reducing the cost of energy to the facility. Several industrial and commercial facilities are simulated using acquired electrical, heating, and cooling load data. Industrial and commercial utility rate structures are modeled after Southern California Edison and Southern California Gas Company tariffs and used to find energy costs for the simulated buildings and corresponding microturbine dispatch. Using these control strategies, building models, and utility rate models, the research team performed a parametric study examining various generator characteristics. The team then performed an economic assessment of the distributed generation for both the microturbine generator and parametric study.

Without the ability to export electricity to the grid, the economic value of CCHP system is limited to reducing the costs that make up the cost of energy for a building. Any economic dispatch strategy must be built to reduce these costs. While the ability of CCHP system to reduce cost depends on factors such as electrical efficiency and operations and maintenance cost, the building energy demand being serviced has a strong effect on cost reduction. Buildings with low load factors (average power to peak power ratios) can accept distributed generation with higher operating costs (low electrical efficiency and/or high operations and maintenance cost) due to the value of demand reduction. As load factor increases, lower operating cost generators are desired due to a larger portion of the building load being met to reduce demand. In addition, buildings with large thermal demand have access to the least expensive natural gas, lowering the cost of operating distributed generation. Recovery of exhaust heat from the combined cooling, heating, and power system reduces cost only if the thermal demand of the buildings coincides with the electrical demand.

Capacity limits exist where annual savings from operation of distributed generation decrease if further generation is installed. For low operating cost generators, the approximate limit is the average building load. This limit decreases as operating costs increase. In addition, a high capital cost of distributed generation can be accepted if generator operating costs are low. As generator operating costs increase, capital costs must decrease if a positive economic performance is desired.

In addition, the carbon and pollutant emissions from a Capstone C65 MicroTurbine generator (were examined. Using the experimental efficiency, the research team estimated the carbon emissions. The criteria pollutant emissions were estimated using measured emissions levels for various amounts of heat recovery. The team compared these emission rates to regulatory limits, the California electric grid emission rate, and national grid emission rate. For each case, the team determined the amount of waste heat recovery that would lead to parity between a

Capstone C65 MicroTurbine generator and the different regulatory limits and grid emission rates.

Novel control algorithms and architecture were developed and tested to dispatch a microturbine generator in the Engineering Laboratory Facility in University of California, Irvine. The control algorithms have been translated to Siemens controls and were installed to demonstrate the novel control algorithms for economical dispatch of a CCHP system.

Project Benefits

This report provides CHP/CCHP system developers, installers or end users a detailed understanding of CHP/CCHP generator and component technology operating and performance characteristics required to successfully control highly integrated systems

The project supports the California Energy Commission's Energy Research and Development Division's goal to develop and help bring to market energy technologies that provide increased environmental benefits, provide greater system reliability, and lower system costs. This effort provides tangible benefits to electric utility customers through development of advanced controls for electricity generation technologies that exceed applicable standards to increase reductions in greenhouse gas emissions from electricity generation. This project will also lead to greater adoption of advanced electricity technologies that reduce the consumption of finite fossil fuels. Specifically, the novel controls advanced will make CHP/CCHP systems more capable of meeting demands for a larger cross-section of the potential market and will make market adoption of CHP/CCHP technology more rapid. Increasing the market potential and market adoption of CHP/CCHP technology will provide California ratepayers with the following specific benefits:

- Lower energy use (improved fuel use efficiency) that contributes to conservation of limited primary energy resources
- Reduced criteria pollutants that can lead to improved air quality
- Reduced greenhouse gas emissions, which contribute to meeting state goals for GHG reduction and lessens impacts on the global climate
- Lower ultimate cost of electricity and heat than would otherwise result due to energy that is saved and due to the increasing costs of emissions.

Finally, the project developed technology that would otherwise not be developed by competitive or regulated markets. These anticipated benefits are developed with very modest cost (about $400,000), since the project heavily leverages previous investment and uses significant previously developed expertise and resources.

CHAPTER 1:
First Principles Dynamic Models of CCHP Technologies Development and Verification

While the market potential and emissions reductions of Combined Cooling, Heat and Power (CCHP) use are significant, CCHP use is currently challenged by a host of barriers. The general problem is that, although CCHP technology could significantly contribute to reductions in energy use, criteria pollutant and green house gas emissions, market adoption and installation of CHP/CCHP technology is too slow. Contributing broadly to this fact and directly related to the general technical and market barriers listed above are three high priority challenges that must be overcome to enable higher adoption of CCHP technology. These high priority barriers include 1) Lack of cost-competitive options in the appropriate size range, 2) Lack of information on the value of these systems for potential users, and 3) Lack of controls sufficient to deal with the highly dynamic nature and relative non-coincidence of the thermal and electrical loads in many applications. The specific problem is that most commercial and industrial electrical loads are highly dynamic and typically not synchronized with local heating and cooling demands. These dynamics, together with utility charges and non-export requirements often make CHP/CCHP systems less cost effective and less attractive to end-users.

A new, dynamic CHP/CCHP system model and control approach is required to address this problem and overcome these barriers. In this chapter, first principles dynamic physical models are developed and verified for dynamic economical dispatch of CCHP systems with emissions constraints and thermal load following capability.

This chapter summarizes and describes the dynamic model development effort that has been completed for this project and describes the details of the models developed. This chapter contains the following sections: Micro-Turbine Generator (MTG), High Temperature Polymer Electrolyte Fuel Cell Model, Molten Carbonate Fuel Cell Model, Photovoltaic Model, Lead-acid Battery Model, Lithium-ion Battery Model, and Ultra-capacitor Model.

1.1   Microturbine Model (Capstone C65)

Steady state experimental data was taken from a Capstone C65 Microturbine operating from 5 kW to 65 kW in 1 kW increments. Data collected included information on actual power output, fuel consumption, and exhaust characteristics, including pollutant emission levels. The pollutant emissions for a Capstone C65 Microturbine generator at steady state operation for various part loads are shown in Figure 1.

Figure 1: NOx and CO Emissions for Capstone C65 Microturbine Generator for Steady-State Operation at Part Load
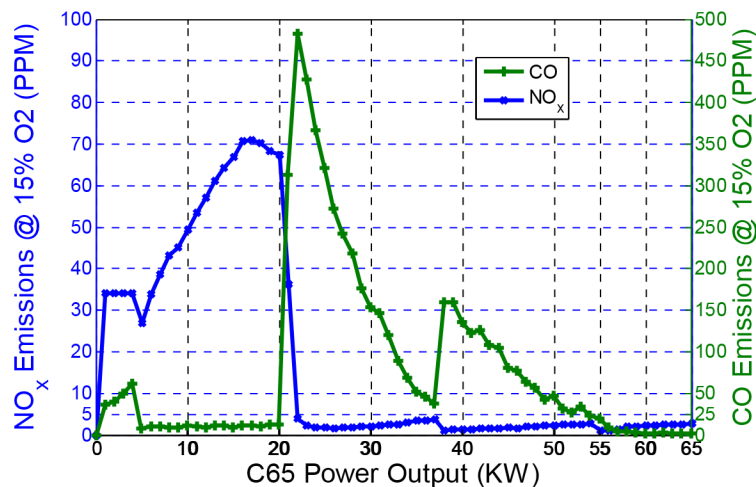
As seen in Figure 1, part load steady state emissions are significantly higher than operation near or at full load. While studies have shown that increased distributed generation penetration, including combustion based generators, can help improve overall air quality[1], emission factors based on operation at near or full load are assumed[2]. Continuous operation at part load would undoubtedly increase these distributed generation emission factors, potentially turning any air quality benefits into disadvantages. Regulation of emission limits for distributed generation exist in some parts of the United States[3], but generator operators needs to ensure that microturbine dispatch occurs at near or full load.

Any air quality improvements provide indirect benefits to the operator and, currently, would most likely not increase profitability of a microturbine investment. Operation at part load, however, does lead to reduced electrical efficiency, as shown in Figure 2.

This reduced efficiency at part load increases the cost of electricity produced by the generator, reducing the value of producing electricity on-site. With the highest efficiency occurring at near or full load and increased pollutant creation at part load, microturbine operation for a single generator will likely be limited to between 80 and 100 percent of maximum generator power to simultaneously achieve high electrical efficiency and low emissions dispatch.

---

1 Carreras-Sospedra, M., et al., **Central power generation versus distributed generation - An air quality assessment in the South Coast Air Basin of California**. Atmospheric Environment. 44(26): p. 3215-3223

2 Rodriguez, M.A., et al., **Air quality impacts of distributed power generation in the South Coast Air Basin of California 1: Scenario development and modeling analysis**. Atmospheric Environment, 2006. 40(28): p. 5508-5521.

3 Greene, N. and R. Hammerschlag, **Small and Clean Is Beautiful: Exploring the Emissions of Distributed Generation and Pollution Prevention Policies**. The Electricity Journal, 2000. 13(5): p. 50-60.

Figure 2: Part Load Electrical Efficiency of a Capstone C65 Microturbine Generator with Curve Fit
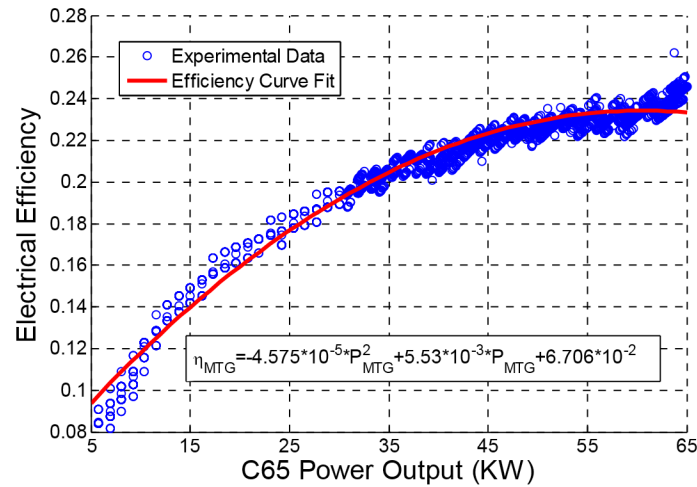
Ambient temperatures above 59 °F have a negative impact on power. As ambient temperature increases beyond this value, the maximum power produced decreases due to a lower air density at elevated ambient temperatures[4]. This temperature derate was captured by operating the C65 MTG at full load for various temperatures during the summer. Using this data, a look-up table was built that captures the temperature derate due to ambient temperature and is shown in Figure 3.

Figure 3: Temperature Derate Due to Ambient Temperature of a Capstone C65 Microturbine Generator

---
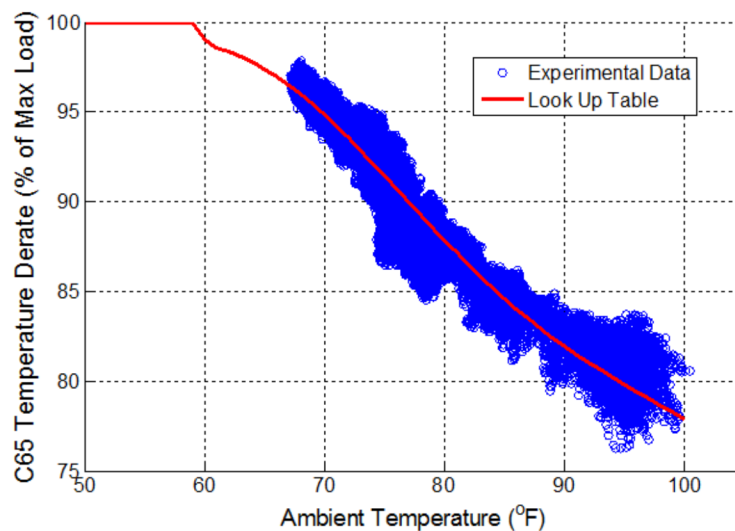
4 Goldstein, H.L., et al., **Gas-fired Distributed Energy Resource Technology Characterizations**. 2003: National Renewable Energy Laboratory.

Available waste heat also changes based on generator power setting. Using a mass flow curve supplied to APEP from Capstone and temperature information taken from the generator, the available waste heat at part load operation was found using the equation below.

$$\dot{E} = \dot{m}_{exhaust} * (Cp_{exhaust}(T) * T_{exhaust} - Cp_{ambient}(T) * T_{ambient})$$

Figure 4: Available Heat for the Capstone C65 Microturbine Generator Operation at Part Load for Various Ambient Temperatures
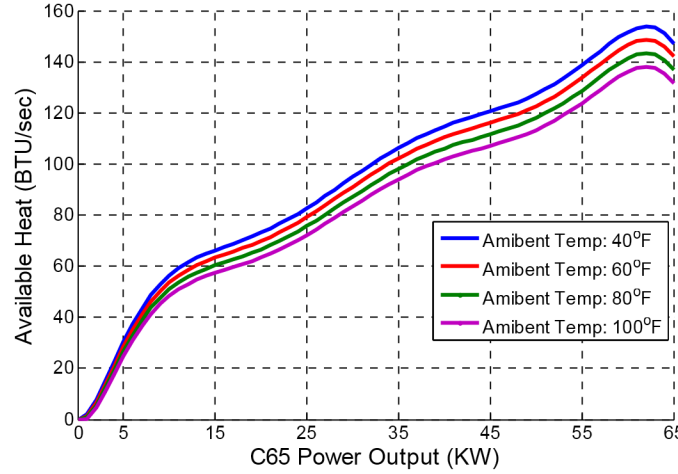
Available waste heat, according to Eq. 1 changes due to ambient temperature, with available heat being reduced at elevated ambient temperatures. The available waste heat at part load operation used for the C65 model for various ambient temperatures is shown in Figure 4 6. Capital cost of a Capstone C65 Microturbine Generator is assumed to be $2700 per kW.

1.2 High-Temperature Polymer Electrolyte Fuel Cell Model

In Proton Exchange Membrane (PEM) fuel cells, the electrolyte material that are widely used is perfluorosulfonic acid (PFSA). In the family of PFSA, the material Nafion, which was developed by Dupont®, has good durability and fairly high proton conductivity. The use of phosphoric acid-doped polybenzimidazole (PBI) membrane is intended to raise the operating temperature of PEM fuel cells. PBI membrane possesses desirable characteristics such as high proton conductivity at temperatures up to 200ºC, good tolerance of CO and SO_2 when operating at high temperature up to 200ºC. PEM fuel cells using PBI membrane can operate at higher temperature and possess good features as shown above. Other undesirable characteristics of PBI are low proton conductivity at low temperature, low solubility of oxygen, and evaluation of stack components including bipolar plate, seals and coolant, and thermal and water management. To evaluate the effect of using a high temperature PEM fuel cell (HTPEMFC) couple with a micro-CHP for heating purpose, a first-principle model has been developed.

1.2.1 Model Description

A first-principle HTPEMFC model has been developed using the MatLab-Simulink® interface. The temperature, species concentrations of the control volumes throughout the system are

determined from the first principles conservation equations. Temperatures of the solids are resolved using the ordinary differential equation below:

$$\rho V C \frac{dT}{dt} = \sum Q'_{in}$$

The temperature of the gas channel and coolant control volumes is determined by solving the dynamic energy conservation equation in the form:

$$NC_V \frac{dT}{dt} = \sum \dot{N}_{in} h_{in} - \sum \dot{N}_{out} h_{out} + \sum Q_{in}$$

Where $\dot{N}_{in} h_{in}$ represent the enthalpy flux into the control volume, $\dot{N}_{out} h_{out}$ the enthalpy flux out of the control volume, N is the molar capacity, or total number of moles, C_V is the constant volume gas specific heat capacity.

Species mole fractions at the exit of each bulk fluid control volume are determined from the dynamic species conservation equation:

$$\frac{d(N\vec{X})}{dt} = \dot{N}_{in}\vec{X}_{in} - \dot{N}_{out}\vec{X}_{out} + \sum \vec{\Phi}$$

Where $\vec{X}$ is the species mole fraction vector and $\vec{\Phi}$ is the species diffusion flux from adjacent control volumes.

The major assumptions of the model are: 1) Only major species in the gas stream are considered in the model: CH_4, CO, CO_2, H_2, H_2O, N_2, O_2; 2) All gases are ideal gases; 3) Control volumes have a single lumped temperature, pressure, and set of species mole fractions; 4) Uniform gas pressure along the streams. Thus, the pressure drop along the gas flow channels and gas diffusion layer (GDL) are neglected; 5) the solid GDL and membrane electrode assembly (MEA) have a lumped temperature; 6) each cell in the fuel cell is identical. Thus the performance of the stack can be evaluated using the performance of a single cell. 7) Quasi-steady electrochemistry is assumed, since the electrochemistry is rapid (occurring at time scales on the order of 10^{-3} s; 8) A single activation polarization equation is used to capture the effects of all physical and chemical processes that polarize the charge transfer process; 9) All reactants generate their ideal number of electrons, and no fuel or oxidant crosses the electrolyte.

1.2.1.1 PBI Fuel Cell

The model is developed with emphasis on electrochemical reaction with these assumptions: 1) The system distributes air, fuel, and coolant evenly across all cells; 2) All cells are identical. Thus modeling of one cell is sufficient to predict the performance of the stack; 3) Heat loss is negligible. The fuel cell is discretized in the direction that is normal to the flow. The control volumes are: anode bipolar plat, anode GDL, electrolyte, cathode gas diffusion layer, bipolar plat, coolant and end plate, as shown in Figure 5.

Figure 5: PBI Fuel Cell Control Volume Definitions

BP	Anode	GDL	MEA	GDL	Ca	BP	Coolant	Coolant plate

The reactions that happen in the anode and cathode compartments are:

$$H_2 + O^{2-} \rightarrow H_2O + 2e^-$$

$$\frac{1}{2}O_2 + 2e^- \rightarrow O^{2-}$$
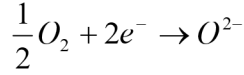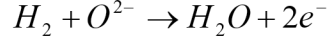
The reaction rate of consumption and creation are calculated using Faraday's Law.

$$r_{H_2} = -\frac{i}{2 \cdot F \cdot 1000}$$

$$r_{H_2O} = \frac{i}{2 \cdot F \cdot 1000}$$

In which F is the Faraday constant, i is the current, and r is the reaction rate. The model also captures the species diffusion between the gas channel, GDL, and electrodes using standard approach of calculating the mass transport coefficient ($\bar{g}_m$):

$$\bar{g}_m = \frac{\text{Sh} \cdot \bar{\text{D}}_\text{m}}{\text{D}_\text{H}}$$

Where Sh is the Sherwood number, $\bar{D}_o$ is the diffusion coefficient, and $\bar{D}_m$ is the hydraulic diameter of the gas flow channel. The diffusion coefficients for species are functions of temperature and pressure and are modified via the Bruggeman correlation to account for the effects of porosity and tortuosity in the GDL as follows:

$$\bar{D}_m = \bar{D}_o \left(\frac{T}{T_o}\right)^{3/2} \left(\frac{P_o}{P}\right)$$

$$\bar{D}_m^{eff} = \varepsilon^{1.5} \cdot \bar{D}_m$$

Where $\bar{D}_o$ is the species diffusion coefficient at standard pressure and temperature, $\bar{D}_m^{eff}$ is the effective species diffusion coefficient and ε is the GDL porosity. The species diffusion flux between the GDL and bulk gasses is then as:

$$\bar{R}_{dif} = A \cdot \cfrac{1}{\cfrac{1}{\bar{g}_m} + \cfrac{t_{gdl}}{\bar{D}_m^{eff}}}$$

$$\bar{\Phi} = \bar{R}_{dif} \cdot \left(\bar{C}_2 - \bar{C}_1 \right)$$

After participating in electrochemical reaction, the cathode exhaust recirculates to the fuel processing unit, and the anode exhaust enters the combined heating and power (CHP) unit.

1.2.1.2 Fuel Processing Unit

The fuel processing system consists of an auto thermal reactor, a high temperature shift reactor, and heat exchangers to preheat the fuel and regulate the anode inlet temperature. The auto thermal reactor process uses rate reaction developed by Yuan et al.[5]. The model takes into account the convection heat transfer between the gas stream and the catalyst bed to determine the temperature of the gas stream and the temperature of the catalyst according to the equation:

$$Q_a = h_c \cdot A_c \cdot V_c \cdot (T_a - T_c)$$

Where h_c is the convective coefficient between catalyst and gases, A_c is the convective efficient area per volume of the catalyst. The High Temperature Shift reactor captures the reaction:

$$CO + H_2O \rightleftharpoons H_2 + CO_2$$

Using the internal reforming of mechanism for solid oxide fuel cell, as outlined by Aguiar et al.[6] and the catalyst used is $Ni/MgAl_2O_4$. The operating temperature of the HTS is ~400°C.

1.2.1.3 Heat Exchanger

The heat exchanger model is a counter-flow shell-and-tube heat exchanger model. In the normal direction to the flow, the heat exchanger is discretized into three nodes: hot stream, wall, and cold stream. The main assumptions of the models are: 1) Heat transfer between the fluid and the wall is dominant in compared to the heat transfer along the fluid stream; 2) All streams are symmetric, thus simulating along one channel is sufficient to capture the temperature profile along the heat exchanger. A description of the resistive thermal flow network of the heat exchanger can be found in Figure 2. Tuning of the heat exchanger model is accomplished by varying physical parameters of the heat exchanger such as tube length, tube diameter, and number of tubes.

---

5 L. Yuan, J. Brouwer, and G.S. Samuelsen. **Dynamic Simulation of an Autothermal Methane Reformer.** in 2nd International Conference on Fuel Cell Science, Engineering and Technology. 2005. Rochester, NY.

6 P. Aguiar, D. Chadwick, and L. Kershenbaum, **Modelling of an indirect internal reforming solid oxide fuel cell**. *Chemical Engineering Science,* 2002. 57(10): p. 1665-1677.

Figure 6: Heat Exchanger Heat Transfer Network
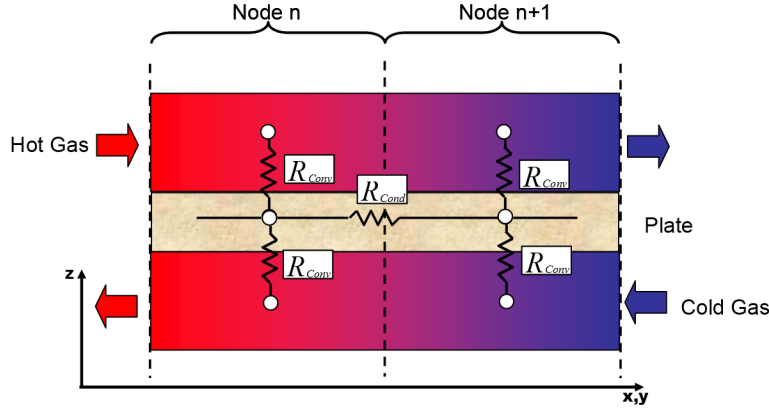
1.2.2 Model Verification

The simulation results of the voltage and the current agree well with the experiment data as shown in Figure 7.

Figure 7: HTPEMFC Stack Voltage and Current
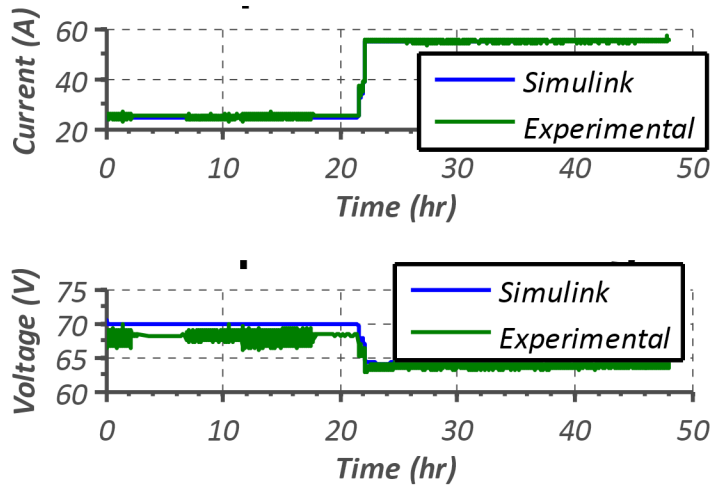
1.3 Molten Carbonate Fuel Cell Model

A spatially-and temporally-resolved fuel cell model has been developed using the MatLab-Simulink® interface. The model incorporates necessary terms for Molten Carbonate Fuel Cell (MCFC) simulations and is derived from first principles. Spatial resolution allows for analysis of the internal temperature profile and thus internal heat transfer must be modeled with precision. The analysis allows for local evaluation of electrochemical activity and potential using local

12

pressure, temperature, and concentration values. Internal reforming rates are evaluated locally and local heat generation calculated from the difference in chemical potential energy and local electrical power production.

1.3.1 Model Description

1.3.1.1 Species Conservation

Each spatially resolved segment, or node, of the fuel cell accounts for the changing concentration of each species through mass conservation of each element and known reaction processes. The expression assumes a perfectly stirred reactor with the exit conditions representing the concentrations throughout the control volume.

$$\frac{R_{REFORM} + R_{CONSUME} + \dot{N}_{in}X_{in} - \dot{N}_{out}X_{out}}{\frac{P_j V_j}{R_U T_j}} = \frac{dX_i}{dt}$$

Where the following apply:

$$\dot{N}_{out} = \dot{N}_{in} + \sum (R_{REFORM} + R_{CONSUME})$$

$$X_{out} = \int \frac{dX_i}{dt}$$

$$R_{CONSUME} = \frac{\alpha \cdot i}{nF}$$

$R_{REFORM,CONSUME}$ Rate of species reform/consumed $(kmol/s)$

i Nodal Current $(coulombs/s)$

F Faradays Constant $\left(\frac{coulombs}{mole\ of\ electrons}\right)$

$\dot{N}_{in,out}$ Flow rate in/out of node $(kmol/s)$

$X_{in,out}$ Species concentration in/out of node

P_j Local Pressure (kPa)

V_j Volume of channels in node (m^3)

R_U Universal Gas Constant $(kJ/kmol \cdot K)$

$\frac{dX_i}{dt}$ Rate of change in species $(1/s)$

The consumption rates for the cathode and anode are based upon the two half reactions for a molten carbonate and solid oxide fuel cell. The half-reactions of the MCFC consume carbon dioxide and oxygen in the cathode to produce carbonate ions while hydrogen molecules and carbonate ions react in the anode to produce carbon dioxide and water. The balance of electrons passes through an external circuit providing for the useful power of the chemical reactions.

13

Cathode: $\frac{1}{2}O_2 + CO_2 + 2e^- \rightarrow CO_3^{2-}$

Anode: $H_2 + CO_3^{2-} \rightarrow CO_2 + H_2O + 2e^-$
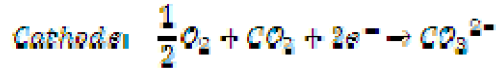
The reaction rate is arranged in an array of seven species specified below. A positive reaction rate indicates the production of that species while a negative rate indicates consumption.

$$species = [CH_4 \quad CO \quad CO_2 \quad H_2 \quad H_2O \quad N_2 \quad O_2]$$

$$R_{CONSUME,Cathode} = \begin{bmatrix} 0 & 0 & \frac{-1 \cdot i}{2F} & 0 & 0 & 0 & \frac{-1 \cdot i}{4F} \end{bmatrix}$$

$$R_{CONSUME,Anode} = \begin{bmatrix} 0 & 0 & \frac{1 \cdot i}{2F} & \frac{-1 \cdot i}{2F} & \frac{1 \cdot i}{2F} & 0 & 0 \end{bmatrix}$$

1.3.1.2 Reformation

Reformation occurs within the anode and any external reforming chamber, and is a function of the local pressure, temperature, and species.

$$R_{REFORM} = f(P, T, X_{out})$$

The internal and external reformation of methane as well as the water gas shift chemistry utilized in the model is based on the well established kinetic reaction mechanisms, presented in Equations below. Through well documented experiments the authors outlined three important reaction mechanisms and the corresponding rate equations. Three reaction mechanisms are responsible for the conversion of methane and steam into hydrogen and carbon dioxide.

$$CH_4 + H_2O \rightarrow CO + 3H_2$$

$$CO + H_2O \rightarrow CO_2 + H_2$$

$$CH_4 + 2H_2O \rightarrow CO_2 + 4H_2$$
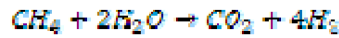
The rate equations for these three reactions above are presented below and implemented directly into the model in each node.

$$r_1 = \frac{k_1}{P_{H_2}^{2.5}} \left(P_{CH_4} P_{H_2O} - \frac{P_{H_2}^3 P_{CO}}{K_{p,1}} \right) / (DEN)^2$$

$$r_2 = \frac{k_2}{P_{H_2}} \left(P_{CO} P_{H_2O} - \frac{P_{H_2} P_{CO_2}}{K_{p,2}} \right) / (DEN)^2$$

$$r_3 = \frac{k_3}{P_{H_2}^{3.5}} \left(P_{CH_4} P_{H_2O}^2 - \frac{P_{H_2}^4 P_{CO_2}}{K_{p,3}} \right) / (DEN)^2$$

Where:

$$DEN = 1 + K_{CO} P_{CO} + K_{H_2} P_{H_2} + K_{CH_4} P_{CH_4} + \frac{K_{H_2O} P_{H_2O}}{P_{H_2}}$$

$$k_i = A_i exp\left(-\frac{E_i}{RT}\right)$$

14

$$k_j = A_j exp\left(-\frac{\Delta H_j}{RT}\right)$$

$$Reaction\ Rate = r_i * n_i * SA_{channels} * ActiveCatalyst$$

r_i Reaction rate $(kmol/m^2 * s)$

n_i Reaction effectiveness

$SA_{channels}$ Reaction surface area (m^2)

$ActiveCatalyst$ Surface Catalyst

P_j Local Partial Pressure (kPa)

$K_{p,i}$ Reaction equilibrium constant

k_i Arrhenius equation reaction constant

K_j Van't Hoff equation reaction constant

The constants used in these expressions are presented in the Table 1 and Table 2.

Table 1: Reformation Constants

Rate Constant	Activation Energy (kJ/mol)	Pre-exponential factor	Rate Constant	Heat of absorption (kJ/mol)	Pre-exponential factor
k_1	240.1	4.225×10^{15} (kmol·MPa$^{(0.5)}$/kgcat·h)	K_{CO}	-70.65	8.23×10^{-5} (MPa^{-1})
k_2	67.13	1.955×10^6 (kmol/kgcat·h·MPa)	K_{CH4}	-38.28	6.65×10^{-4} (MPa^{-1})
k_3	243.9	1.020×10^{15} (kmol·MPa$^{(0.5)}$/kgcat·h)	K_{H2O}	88.68	1.77×10^5 (unit less)
			KH_2	-82.9	6.12×10^{-9} (MPa^{-1})

Table 2: Equilibrium Constants

Equilibrium Constant		Dimensions
K_{p1}	$= 1.198 \times 10^{19}\cdot exp(-26830/T)$	$(MPa)^2$
K_{p2}	$= 1.77 \times 10^{-2}\cdot exp(4400/T)$	$(MPa)^0$
K_{p3}	$= K_{p1}\cdot K_{p2}$	$(MPa)^2$

1.3.1.3 Inlet Composition

Molten carbonate fuel cells require sufficient carbon dioxide in the cathode inlet stream for the carbonate forming reduction reaction to proceed. Determining correct inlet concentrations and flow rates requires several assumptions or a detailed understanding of the system configuration. Typically for MCFC systems the exhaust supplies the necessary CO_2 by mixing with the inlet air stream, thus the exact concentration depends upon the exhaust composition and amount of recirculated gas. Solutions require multiple iterations for steady state models or a short period of convergence with dynamic state models. Calculating inlet conditions rather than specifying them allows direct comparison of different system parameters without the influence of arbitrary variations in fuel and air specifications. The parameter under investigation, steam to carbon ratio, recirculation or utilization, can be varied independently. Table 3 lists the reference conditions for a MCFC running at a steam to carbon ratio of 2, fuel utilization of 80 percent, and no recirculation. The fresh fuel stream flows directly from a pre-heater into the reformer compartment.

Table 3: Reference Molten Carbonate Inlet Concentrations

Compartment	CH_4	CO	CO_2	H_2	H_2O	N_2	O_2
Reformer	0.2798	0.005	0.0346	0.1168	0.5662	0.0	0.0
Cathode	0.0	0.0	0.1041	0.0	0.1137	0.6332	0.149

The composition of the cathode inlet stream plays a significant role on the overall performance of the cell. A reduction in oxidant concentration at the cell inlet reduces oxidant partial pressure throughout the cell. This negatively impacts the local Nernst potential and loss terms, thereby producing more heat and reducing the efficiency of the cell. Cathode recirculation, if present, can increase or decrease the oxidant concentration at the inlet. Cathode recirculation diminishes oxygen concentration when diluting ambient air, but increases CO_2 concentration for MCFC.

A molten carbonate fuel cell recycles CO_2 from the anode compartment and post combustor into the cathode inlet stream. The anode off gas is diluted with atmospheric air, and the resulting inlet species distribution is calculated. The following expressions determine the inlet concentrations.

$$X_{CO_2} = \frac{\left\{\dot{n}\left(X_{CH_4} + X_{CO} + X_{CO_2}\right)\right\}_{An,exit} + R\left(\dot{n}\left(X_{CO_2}\right)\right)_{Cath,exit}}{\left\{\dot{n}\right\}_{Cath,inlet}}$$

$$X_{H_2O} = \frac{\left\{\dot{n}\left(2X_{CH_4} + X_{H_2} + X_{H_2O}\right)\right\}_{An,exit} + R\left(\dot{n}\left(X_{H_2O}\right)\right)_{Cath,exit}}{\left\{\dot{n}\right\}_{Cath,inlet}}$$

$$X_{O_2} = \left(X_{O_2}\right)_{Air}\left(1 - \frac{\left\{\dot{n}\left(1 + 2X_{CH_4}\right)\right\}_{An,exit}}{\left\{\dot{n}\right\}_{Cath,inlet}}\right)$$

16

$$X_{N_2} = 1 - X_{O_2} - X_{H_2O} - X_{CO_2}$$

Water has a high heat capacitance, and can be used within the stack for temperature management. However, the addition of water in the anode compartment reduces the fuel concentration and thus the Nernst potential, possibly reducing the overall efficiency of the stack. When the MCFC stack is combined with the rest of the components in the hybrid system, the steam to carbon ratio can be adjusted as an additional control mechanism. The steam from a Rankine bottoming cycle can be added to a natural gas stream to reach a specified steam to carbon ratio when no anode recycle is employed. The reference steam to carbon ratio is 2:1; for each carbon atom flowing into the stack, two water molecules are also supplied. Table 4 presents the composition of fuel supplied to the MCFC stack.

Table 4: Example Molten Carbonate Inlet Concentrations

Compartment	CH_4	CO	CO_2	H_2	H_2O	N_2	O_2
Steam	0.0	0.0	0.0	0.0	1.0	0.0	0.0
Natural Gas	0.8	0.0	0.05	0.1	0.0	0.05	0.0
S/C = 2.0	0.2963	0.0	0.01852	0.03704	0.6296	0.01852	0.0

The flow rate into the reformer is controlled to maintain specific fuel utilization by measuring the instantaneous current produced, and supplying enough available hydrogen to produce that current at a specified utilization factor. The following expressions are important in determining the fuel flow rate into the fuel cell, and fuel utilization is an important parameter that can be manipulated to control stack conditions.

$$Util_{fuel} = \frac{H_{2,consumed}}{H_{2,avail}}$$

$$H_{2,consume} = \frac{n_{cell} \cdot J \cdot A_{Cell}}{2 \cdot F}$$

$$H_{2,avail} = n_{fuel} * \left(4 \cdot X_{CH_4} + X_{CO} + X_{H_2} \right)$$

Air utilization is calculated by comparing the oxygen supplied and consumed. Air flow is controlled by the inlet and exhaust stream temperatures, not air utilization. Higher air utilization implies a more efficiently fuel cell that requires less cooling air. At high air utilization local Nernst potential decreases dramatically as the partial pressure of the oxidant approaches zero in downstream nodes. This impact is enhanced in systems operating on pure oxygen rather than atmospheric air at 21 percent oxygen.

1.3.1.4 Energy Balance

Each component of the cell is given the conservation of energy treatment resulting in a unique expression for each. Several intrinsic and extrinsic properties of the stack and the anode,

cathode, and electrolyte material properties are needed to complete these expressions and are detailed in Table 5.

Table 5: Molten Carbonate Fuel Cell Parameters

Component	Parameter	Value	Units
Stack	Length	1.2	(m)
	Width	0.8	(m)
Bipolar Plate	Thickness	0.02	(m)
	Density	7900	(kg/m^3)
	Specific Heat	611	(J/kg*K)
	Conductivity	25.4	(W/m*K)
Anode	Channel Height	0.004	(m)
	Channel Width	0.004	(m)
	Wall Thickness	0.005	(m)
Cathode	Channel Height	0.005	(m)
	Channel Width	0.006	(m)
	Wall Thickness	0.006	(m)
Electrolyte	Membrane Thickness	0.001	(m)
	Plate Density	2702	(kg/m^3)
	Plate Specific Heat	1146	(J/kg*K)
	Plate Conductivity	218	(W/m*K)
Reformer	Channel Height	0.005	(m)
	Channel Width	0.003	(m)
	Wall Thickness	0.001	(m)

The resulting expressions from this conservation of energy analysis are presented below. The subscript a refers to the anode gas stream, e to the PEN, c to the cathode gas stream, o to the oxidant side of the separator plate, and f to the fuel side of the separator plate except for the following exceptions. The subscripts $n+1$ and $n-1$ refer to the subsequent and previous nodes in the direction of air flow, $r+1$ and $r-1$ refer to the nodes to the right and left respectively, and $h+1$ and $h-1$ refer to the nodes above and below.

h_c Local heat transfer coef. $(W/m^2 K)$

h Specific enthalpy $\left(\frac{kJ}{kMol}\right)$

Δh_{rxn} Heat of Reaction $\left(\frac{kJ}{kMol}\right)$

Δh_i Change in sensible enthalpy of species i $\left(\frac{kJ}{kMol}\right)$

$\dot{n}$ Flow rate $(kMol/s)$

$A_{x/y}$ Contact area between x and y (m^2)

T Temperature (K)

P_j Local Partial Pressure (kPa)

$Q_{ion\,transfer}$ Enthalpy of transport ion*rate of transfer (kW)

t_i Thickness of component i (m)

k_{cond} Local heat conduction $(W/m \cdot K)$

Q_{gen} Heat generated by electrochemical reaction (kW)

Anode/Fuel Stream:

$$\frac{dT_a}{dt} = \frac{\left[\begin{array}{c} h_c \cdot A_{anode/electrode} \cdot (T_e - T_a) \\ + h_c \cdot A_{anode/fuel\,sep} \cdot (T_f - T_a) \\ + (h \cdot \dot{n})_{fuel\,in} - (h \cdot \dot{n})_{fuel\,out} + Q_{ion\,transfer} \end{array}\right]}{C_p \frac{P_a V_a}{R_U T_a}}$$

Cathode/Air Stream:

$$\frac{dT_c}{dt} = \frac{\left[\begin{array}{c} h_c \cdot A_{cath/elec} \cdot (T_e - T_c) \\ + h_c \cdot A_{cath/ox\,sep} \cdot (T_o - T_c) \\ + (h \cdot \dot{n})_{air\,in} - (h \cdot \dot{n})_{air\,out} - Q_{ion\,transfer} \end{array}\right]}{C_p \frac{P_c V_c}{R_U T_c}}$$

Electrolyte Energy Balance:

$$\frac{dT_e}{dt} = \frac{\left[\begin{array}{c} \frac{k_{cond}}{t_f/2} \cdot A_{elec/fuel\,sep} \cdot (T_f - T_a) \\ + h_c \cdot A_{cath/elec} \cdot (T_e - T_c) \\ \frac{k_{cond}}{t_o/2} \cdot A_{elec/ox\,sep} \cdot (T_o - T_e) \\ + h_c \cdot A_{elec/cath} \cdot (T_c - T_e) \\ + \frac{k_{cond}}{l_{node}/2} \cdot t_{elec} \cdot w_{node} \cdot (T_{n-1} + T_{n+1} - 2T_e) \\ + \frac{k_{cond}}{w_{node}/2} \cdot t_e \cdot l_{node} \cdot (T_{r-1} + T_{r+1} - 2T_e) \\ + Q_{gen} \end{array}\right]}{\rho_e \cdot C_e \cdot V_e}$$

Where:

19

$$Q_{gen} = \frac{i}{2F}\left(\Delta h_{rxn} + \Delta h_{H_2O} - \Delta h_{H_2} - \tfrac{1}{2}\Delta h_{O_2}\right) - V \cdot i$$

Oxidant Separator Plate:

$$\frac{dT_o}{dt} = \frac{\begin{bmatrix} \frac{k_{cond}}{t_o/2} \cdot A_{node} \cdot (T_{h-1} - T_o) \\ + h_{conv} \cdot A_{oxsep/anth} \cdot (T_n - T_o) \\ + \frac{k_{cond}}{t_o/2} \cdot A_{oxsep/elec} \cdot (T_e - T_o) \\ + \frac{k_{cond}}{l_{node}/2} \cdot t_o \cdot w_{node} \cdot (T_{n-1} + T_{n+1} - 2T_o) \\ + \frac{k_{cond}}{w_{node}/2} \cdot t_o \cdot l_{node} \cdot (T_{r-1} + T_{r+1} - 2T_o) \end{bmatrix}}{\rho_o \cdot C_o \cdot V_o}$$

Fuel Separator Plate:

$$\frac{dT_f}{dt} = \frac{\begin{bmatrix} \frac{k_{cond}}{t_f/2} \cdot A_{node} \cdot (T_{h+1} - T_f) \\ + h_{conv} \cdot A_{fuel\,sep/cath} \cdot (T_{cath} - T_f) \\ + \frac{k_{cond}}{t_o/2} \cdot A_{fuel\,sep/elec} \cdot (T_{elec} - T_{fu}) \\ + \frac{k_{cond}}{l_{node}/2} t_f w_{node}(T_{n-1} + T_{n+1} - 2T_f) \\ + \frac{k_{cond}}{w_{node}/2} t_f l_{node}(T_{r-1} + T_{r+1} - 2T_f) \end{bmatrix}}{\rho_f \cdot C_f \cdot V_f}$$

1.3.1.5 Energy Balance

The Nernst Equation is applied specifically to the operation of a molten carbonate fuel cell and presented below. When applied to the Nernst potential equation the half-reactions occurring in the anode and cathode compartments of an MCFC form an expression for the open circuit potential.

$$E = E^0 + \frac{R_U T}{2F} ln\left(\frac{P_{H_2}}{P_{H_2O}P_{CO_2}}\right)_{Anode} + \frac{R_U T}{2F} ln\left(P_{O_2}{}^{1/2}P_{CO_2}\right)_{Cathode}$$

Assuming the pressures in the anode and cathode compartments are equal this expression can be reduced by combining logarithms and using only the cathode pressure. This results in the following simplified expression.

$$E = E^0 + \frac{R_U T}{2F} ln\left(\frac{X_{H_2}X_{O_2}{}^{1/2}X_{CO_2\,Cathode}}{X_{H_2O}X_{CO_2\,Anode}} P_{Cathode}{}^{1/2}\right)$$

20

$$E^Q = \frac{-\Delta \bar{g}_f{}^Q}{nF}$$

Where:

E		Nernst Potential $(Volts)$
E^Q		Ideal Reversible Cell Potential $(Volts)$
R_U		Universal Gas Constant $(kJ/kmol \cdot K)$
T		Electrolyte Temperature $(Kelvin)$
F		Faradays Constant $(coulombs/mol)$
P_i		Partial Pressure of species i normalized by atmospheric pressure
X_i		Mole Fraction of Species i $(unitless)$
$\Delta \bar{g}_f{}^Q$		Change in Gibbs energy of formation $(kJ/kmol)$
n		# of electrons involved in reaction $(unitless)$

1.3.1.6 Polarization Losses

Activation losses: The activation losses is encapsulated in the fundamental equation of electrochemical kinetics, know commonly as the Butler-Volmer equation:

$$j = j_0{}^Q \left(\frac{c_R^s}{c_R^{Q_s}} e^{\alpha n F \eta / (RT)} - \frac{c_P^s}{c_P^{Q_s}} e^{-(1-\alpha)nF\eta/(RT)} \right)$$

Where:

j		Exchange Current Density $(Amps/m^2)$
$j_0{}^Q$		Exchange Current Density at Standard Concentrations $(Amps/m^2)$
$c_{R/P}^s$		Actual Surface Concentrations (reactants/products)
$c_{R/P}^{Q_s}$		Reference Concentrations (reactants/products)
α		Symmetry of Activation Barrier $(unitless)$
n		Number of Electrons in Reaction $(unitless)$
η		Activation Overpotential $(Volts)$

The shape of the Butler-Volmer equation lends itself to simplification. For extremely low activation polarization, less than 15mV, a linear approximation is accurate. A first order Taylor expansion results in the first equation below. For higher polarizations, 50-100mV, an exponential approximation is employed resulting in the second equation below. This is further simplified, by solving directly for the activation over-potential, resulting in the more common form of the Tafel equation shown below that is utilized in this model.

$$j = j_0 \frac{nF\eta_{act}}{RT}$$

$$j = j_0 e^{\alpha nF\eta_{act}/RT}$$

$$\eta_{act} = -\frac{RT}{\alpha nF}\ln j_0 + \frac{RT}{\alpha nF}\ln j$$

Ohmic losses: Electrical resistance of the electrodes and electrolyte results in the single largest source of energy loss incurred during typical fuel cell operation. Due to their highly porous structure, and high operating temperatures, the electrode materials conduct electrons from the Triple Phase Boundary (TPB) poorly. The ions being conducted across the electrolyte also encounter significant resistance, and can account for up to 70 percent of the total Ohmic loss. Electrolyte resistance exhibits a strong dependence on both temperature and thickness. Though thinner electrolytes offer less resistance the electrolyte must remain thick enough to prevent leakage, crossover of reactants or products, and withstand the thermal and physical stresses of the stack. The electrode and electrolyte resistances can be combined as resistors in series to form a single effective resistance. The effective resistance modeled in these experiments is taken from the empirical test cell data gathered by Rivera of UCI, and follows the correlation below.

$$ASR_{eff} = C_2 + C_1 * T$$

This results in an Area Specific Resistance (ASR). Fuel cells are typically compared on a per-unit-area basis to relate small test cells to full size operational models. When using ASR it is important to account for the current density when calculating the actual cell resistance. This is utilized in the nodal design of the model by calculating the local resistance with needing to know the resistance of the entire plate. The final equation needed to find the local Ohmic loss is expressed below.

$$\eta_{Ohmic} = \frac{i}{A_{cell}} * ASR_{eff} = j * ASR_{eff}$$

Concentration Losses: Concentration losses arise from a physical limitation of gaseous flow to the reaction sites. As the cell produces current it must be continually supplied with reactants at the TPB, however, at some rate the supply of reacting species cannot diffuse through the electrode quick enough. This is known as the limiting current density, and will reduce the operating voltage all the way to zero. Reactant concentration affects the fuel cell performance in two specific ways, through the Nernst potential and through the reaction kinetics. The actual theoretical potential of the cell is found by using the reactant concentrations at the TPB, not in the bulk flow. Thus by comparing the Nernst potential using the slightly different reactant concentrations we can derive the first portion of the concentration loss.

$$\eta_{conc1} = \left(E^0 + \frac{R_U T}{2F}\ln\frac{1}{c_R^0}\right) - \left(E^0 + \frac{R_U T}{2F}\ln\frac{1}{c_R^*}\right) = \frac{R_U T}{2F}\ln\frac{c_R^*}{c_R^0}$$

The relationship between the concentration of the bulk flow and at the TPB can be put in terms of the current and diffusivity rates in the following expression. Taking the limiting case of zero reactants at the TPB, letting $c_R^s = 0$, we can define a limiting current density, j_L.

$$c_R^s = c_R^0 - \frac{j\delta}{nFD^{eff}} = \frac{j_L\delta}{nFD^{eff}} - \frac{j\delta}{nFD^{eff}}$$

Combining these equations forms the first portion of the concentration loss equation.

$$\eta_{conc1} = \frac{R_UT}{2F}\ln\frac{j_L}{j_L - j}$$

Reaction kinetics is also heavily dependent upon reactant concentrations at the TPB. Once again the difference in concentration between the bulk flow and TPB can be modeled and input into the Tafel Equation. This simplification of the more general Butler-Volmer expression is valid, because concentration losses are most likely to have an effect in the high current density regimes where the Tafel Expression is valid. This results in a similar loss term.

$$\eta_{conc2} = \frac{R_UT}{2\alpha F}\ln\frac{j_L}{j_L - j}$$

Combining the above with the previous expression yields the net concentration loss term.

$$\eta_{conc} = \left(1 + \frac{1}{\alpha}\right)\frac{R_UT}{2F}\ln\frac{j_L}{j_L - j}$$

1.3.1.7 Model Parameters

The open circuit voltage found using the Nernst Equation must be adjusted to account for the three types of voltage loss detailed above. The values used for the constants in the voltage loss equations are shown in Table 6.

Table 6: Voltage Loss Parameters for MCFC

Constant	Value	Units
j_l	4000	Amps/m^2
C_1	6.667×10^{-7}	Ohm·m^2/K
C_2	4.7833×10^{-4}	Ohm·m^2
α	0.4	unit less
j_o	50	Amps/m^2

1.3.2 Model Testing

To test the robustness of the model, and gain insight into the steady state behavior of the fuel cell a multi-parameter variation was undertaken. The important variables manipulated during these tests were power density, steam to carbon ratio, fuel utilization, and temperature rise

23

across the stack. Airflow was controlled to maintain the desired average PEN operating temperature of 650°C. The following data presents the power produced, amount of cooling air required, peak electrolyte temperature, and thermodynamic efficiency under the applied conditions. This study will help determine the ideal conditions to operate the fuel cell at in conjunction with the turbomachinery. It is obvious that higher operating voltages result in better fuel cell performance, but decrease the power density of the fuel cell and the amount of high temperature gas available to drive the turbomachinery. A portion of the initial test matrix and results are shown in Table 7.

Table 7: Operating Condition Test Matrix and Initial Results

ΔT	Steam to Carbon	CO_2	Voltage	Current	Air Flow	Power	Efficiency	Peak Temp
(K)	H_2O:C	%	(volts)	(amps)	(mol/s)	(watt/cell)	%	(K)
100	3:1	10	0.70	535.2	0.0449	374.6	53.51	973.0
100	3:1	15	0.71	595.8	0.0484	423.1	54.27	975.8
100	2:1	10	0.70	567.5	0.0541	397.2	53.51	977.4
100	2:1	15	0.72	553.3	0.0481	398.4	55.04	978.2
100	2:1	20	0.72	623.6	0.0524	448.9	55.03	979.4
75	2:1	15	0.745	400.6	0.0472	298.4	56.95	965.4
50	2:1	15	0.76	320.3	0.0588	243.5	58.10	953.4

1.4 Photovoltaic Model

1.4.1 Model Description

Solar photovoltaic (PV) electricity sources convert sunlight directly into electricity through the use of semiconductor technology. Sunlight is composed of photons that have energy proportional to their frequency (f) according to $E = hf$, where h is Planck's constant. When the photon hits a semiconductor, it will either be reflected or transfer its energy to the surface. If this energy is greater than the band gap of the material, an electron will be promoted from the valence band to the conduction band. In this way, the heart of a PV cell is a current source: photons strike a surface to emit electrons. This in itself will not produce electricity, as without the presence of an electric field, the electron will fall back into the 'hole' created by its absence. However, the silicon material can be doped with atoms that have either 3 (p-type) or 5 (n-type) valence electrons. The lattice structure of silicon is achieved with four valence electrons, so the addition of an n-type impurity will cause four of those electrons to participate in the lattice structure and leave one essentially 'free' electron. Similarly, a p-type dopant will create a hole. Both these materials are electrically neutral, but due to the structure, when put together, the free electrons tend to migrate to the holes, which creates an intrinsic electric field in the material that

is called a p-n junction. Now, when a photon strikes the semiconductor, the electron will have the force of an electric field and provide current[7]. However, this p-n junction also creates a diode in parallel with the current source that must be accounted for in the PV model. The resistance of the current through the semiconductor material and contacts creates a series resistance with the current source and diode as well. Thus the simplest PV cell model is presented with current source, diode, and resistance in Figure 8.

Figure 8: Simple Electric Schematic of a Solar PV Cell
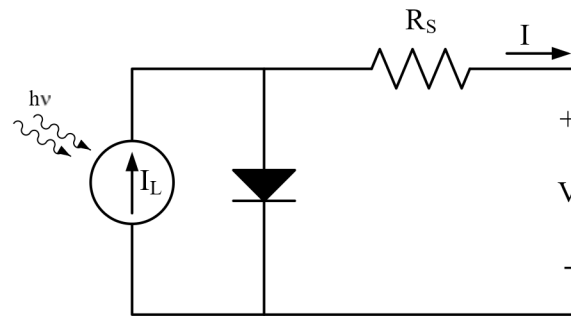
1.4.1.1 Irradiation Module

Solar power-producing devices such as photovoltaics are capable of producing electrical power from both direct and indirect light inputs. Therefore, the total irradiation that is incident on the photovoltaic cell must be calculated from the different irradiation components. Calculation of the in-plane irradiation on the solar array is done using the exact model constructed by Heling[8]. The model reads files containing hourly data for different types of solar insolation for a given location: Direct "beam" insolation (B) is the component of the sun's radiation which arrives on a horizontal surface at ground level without interruption, in a straight line from the sun. Indirect "diffuse" insolation (D) is the component of the sun's radiation which arrives at a horizontal surface at ground level after being reflected from atmospheric objects such as clouds and airborne particles. An additional given parameter is the global horizontal irradiation (H), which is the amount of total (beam and diffuse) irradiation striking a horizontal surface at ground elevation. The model uses the different insolation types to calculate in-plane beam irradiation (I_b), the in-plane diffuse irradiation (I_d), and the in-plane irradiation that is reflected from the ground (I_r). The total in-plane irradiation on the solar panel is then:

$$ I = I_b + I_d + I_r $$

The in-plane beam irradiation is calculated according to the following method using the solar declination and the true solar time. The solar declination (δ), which is the angle between the

---

7 J. J. Kraushaar and R. A. Ristinen, *Energy and Problems of a Technical Society*, 2nd ed: John Wiley & Sons, 1993.

8 M. G. Heling, **Assesment of the zero-emission vehicle, shared-use station car (ZEV-SUSC) mobility concept with a focus on energy and environmental sustainability**, Master thesis, University of California, Irvine, 2008.

earth's equatorial plane and a straight line drawn between the center of the earth and the center of the sun, is calculated for locations north of the equator as:

$$\delta = 23.45^\circ \sin\left[\frac{360(d_n + 284)}{365}\right]$$

where d_n is the serial number of the day of the year. The true solar time, which is the difference between noon and the considered hour of the day in terms of a complete revolution of the earth, is calculated as:

$$\omega = 15 \times (TO - AO - 12) - (LL - LH)$$

where TO is the local time, AO is the time by which the clocks are advanced ahead of local time zones, LL is the longitude of the site in consideration, and LH is the reference longitude of the local time zone encompassing the site in consideration. Note that TO and AO are in hours, and LL, LH are in degrees.

The solar declination and true solar time used to calculate the angle of solar incidence θ_s, which is the angle between the sun and the line that perpendicular to the face of the photovoltaic array, calculated as:

$$\cos\theta_s = \sin\delta\sin\phi\cos\beta - \sin\delta\cos\phi\sin\beta\cos\alpha + \cos\delta\cos\phi\cos\beta\cos\omega + \ldots$$

$$\cos\delta\sin\varphi\sin\beta\cos\alpha\cos\omega + \cos\delta\sin\alpha\sin\omega\sin\beta.$$

where ϕ corresponds to the latitude of the site under consideration.

The total in-plane beam irradiation is then calculated by:

$$I_b = B\max(0, \cos\phi_s)$$

The total in-plane reflected irradiation can also be calculated by:

$$I_r = \rho_g H \frac{1 - \cos\beta}{2}$$

Where ρ_g is the reflectivity of the ground. The in-plane diffuse irradiation is calculated according to the model presented by Perez[9], represented by:

$$\theta_Z = \cos\phi\cos\delta\cos\omega + \sin\phi\sin\delta$$

---

[9] R. Perez and P. Ineichen, **Modeling daylight at availability and irradiance components from direct and global irradiance.** Solar Energy, 1990. 44(5): p. 271-289.

$$I_d = D\left[\frac{(1-F_1')(1+\cos\beta)}{2} + F_1'\frac{a}{b} + F_2'\sin\beta\right]$$

Where F_1 and F_2 are functions of the sky condition 9, and θ_Z is the solar zenith angle as calculated[10]. The values for a and b are calculated according to:

$$a = \max(0, \cos\theta_S)$$

$$b = \max(0.087, \cos\theta_Z)$$

1.4.1.2 Fixed-Plate Solar Photovoltaic Module

The PV model captures the effect of solar irradiance, cloud cover, and ambient temperature on the array output power, dynamically capturing the intermittent nature of solar PV power. The model integrates (1) an equivalent circuit model for power output and (2) an energy balance based PV cell temperature model. The developed model is tuned to represent experimentally measured data of a Solarex MSX-60 panel installed on top of the Engineering Laboratory Facility at the University of California, Irvine. The developed module model output is scaled to simulate any sized solar installation parametrically.

The Power Block model was developed based on an equivalent circuit representation of a solar cell as presented by Walker[11], with temperature dependence of the diode saturation current (I_o) and photo-current (I_L), and the inclusion of a series resistor.

The current output of the PV cell is equal to the difference between the current source (I_L) and the diode current (I_D). The diode current can be expressed according to the Shockley equation, which is presented in the following Equation.

$$I_D = I_0\left(e^{V_D/nV_T} - 1\right)$$

Where I_0 is the reverse bias saturation current and V_T is the thermal voltage $V_T = kT/q$. For the thermal voltage, k is the Boltzmann constant, T is temperature in Kelvin, and q is the elementary charge of an electron. V_D is the voltage across the diode, and n is a quality factor of the semiconductor, generally between 1 and 2 with 1.2 used herein[11].

Thus, the overall current produced by the PV cell is:

$$I = I_L - I_0\left(e^{q(V+IR_s)/nkT} - 1\right)$$

The current source photo-current, I_L, is directly proportional to irradiance, G. The photo-current is generally constant for a specific irradiance and temperature and has a linear dependence with temperature. The equation for photo-current at any irradiance and temperature is thus[11]:

---

[10] J. A. Duffie and W. A. Bechman, **Solar Engineering of Thermal Processes**, John Wiley & Sons, 1991.

[11] G. Walker, Evaluating MPPT Converter **Topologies Using a MATLAB PV Model**, Journal of Electrical and Electronics Engineering, Australia, vol. 21, pp. 49-55, 2001.

$$I_L = \frac{G * I_{SC(T_2,nom)}}{G_{(nom)}}\left(1 + K_0 \frac{(T - T_1)}{(T_2 - T_1)}\right)$$

$$K_0 = \frac{(I_{SC(T_2)} - I_{SC(T_1)})}{I_{SC(T_1)}}$$

The reverse bias saturation current, I_0, is shown below from[12].

$$I_0 = I_{0(T_1)} * \left(\frac{T}{T_1}\right)^{3/n} * e^{-qV_g\left(nk\left(\frac{1}{T}-\frac{1}{T_1}\right)\right)}$$

$$I_{0(T_1)} = I_{SC(T_1)} / \left(e^{qV_{OC}/T_1 \cdot nkT_1} - 1\right)$$

Which can be evaluated directly with known constants and from values on the data sheet. The specific panel modeled here is the Solarex MSX-60 PV panel, which is a 60W panel comprised of 36 series-connected cells. The array open circuit voltage (VOC), at 25°C is 21.0V, and the short circuit current, I_{SC}, is 3.74 A. The I_{SC} increases to 3.92 A at 75°C. The Rs is found to be about 8mΩ[11].

Cell Temperature Block: The temperature of the solar cell is determined by applying conservation of energy to a control volume encompassing the entire 5 kW solar array. Heat transfer due to convection and radiation was resolved, however conduction was assumed to be negligible since the contact area of the panel interconnects with the roof is very small:

$$\rho \forall C_v \frac{dT_s}{dt} = Q_{rad} - Q_{conv} - Q_{rad,loss} - W$$

Convective heat transfer was determined using a turbulent-flow Nusselt number approach for a flat plate:

$$\overline{Nu} = \frac{\bar{h}L}{k_f} = 0.664 \, \mathrm{Re}_L^{0.5} \, \mathrm{Pr}^{0.33}$$

Where Re_L is the Reynolds number of the ambient flow, Pr is the Prandtl number, k_f is the thermal conductivity of the ambient air, L is the length of the plate, and A_s is the surface area of the array. For the case of the solar panel, the length of the plate is taken to be the diagonal of the panel area.

The density, dynamic viscosity, thermal conductivity and Prandtl number are temperature dependent. The velocity of the ambient air is taken from measured wind speed data in the Santa Ana region for the appropriate time period.

---

[12] J. A. Gow and C. D. Manning, **Development of a photovoltaic array model for use in power-electronics simulation studies**, Electric Power Applications, IEE Proceedings -, vol. 146, pp. 193-200, 1999.

Radiative heat transfer was modeled using the grey body assumption, where the temperature of the grey surface is set to the ambient temperature:

$$Q_{rad} = \left(G_{measured} - \varepsilon\sigma\left(T_s^4 - T_\infty^4\right)\right)A_s$$

Where $G_{measured}$ is the in-plane solar irradiation on the panel, calculated from the irradiation module. In addition, a radiative heat loss was included to account for the absorptivity of the ambient atmosphere and any cloud cover that might be present. This loss is also modeled with a grey body, where the temperature of the grey body is set to the ambient temperature minus 2 degrees Kelvin, and the emissivity of the gray body is dependent on the ambient relative humidity and cloud condition:

$$Q_{rad,loss} = \varepsilon(\%RH, \text{Cloud})\sigma A_s \left(T_s^4 - \left(T_\infty - 2\right)^4\right)$$

Where:

$$\varepsilon(\%RH, \text{Cloud}) = 1 - \left(\frac{\varepsilon_{RH} + \varepsilon_{Cloud}}{2}\right)$$

Where ε_{RH} and ε_{Cloud} are the emissivity indices of the grey surface due to relative humidity and cloud cover, respectively:

Table 8: Relative Humidity Emissivity Indices

Relative Humidity (%)	Relative Humidity Index
RH < 65%	0
65%< RH < 70%	0.1
70% < RH < 75%	0.25
75% < RH < 80%	0.4
80% < RH < 85%	0.5
85% < RH	0.8

Table 9: Cloud Condition Emissivity Indices

Cloud Condition	Cloud Condition Index
Clear	0
Few	0
Scattered	0.05
Broken	0.25

| Overcast | 0.65 |
| Haze | 0.8 |

This approach greatly simplifies the calculations needed to determine the temperature of the solar cell. Notice that as the cloud cover or relative humidity increases, the radiation loss decreases, representing the effects of atmospheric radiation absorption and re-radiation. This assumption was made since it was deemed unnecessary to develop a physics of weather simulation for the purpose of determining the temperature of the solar cell, since the variation in the performance of the cell over the temperature range considered is relatively small, however it is significant enough to be included.

1.4.2 Model Verification

The model was constructed to simulate the performance of a Solarex MSX-60 60W solar panel array. Model verification of the power module is carried out by comparing simulation results to power data obtained from a 3.85 kW solar array on the rooftop of the Engineering Laboratory Facility at the University of California, Irvine. The simulated irradiation and cell temperature were used as inputs to the power module, and the results were compared to the measured power data. The individual 60W panel was scaled up to 3.85 kW for comparison.

The combined model was validated against measured power, cell temperature, and irradiation data from a 3.85 kW solar panel array on the roof of the Engineering Laboratory Facility at the University of California, Irvine.

Figure 9: Model Verification (a) Power Module, (b) Irradiation Model, (c) Temperature Module
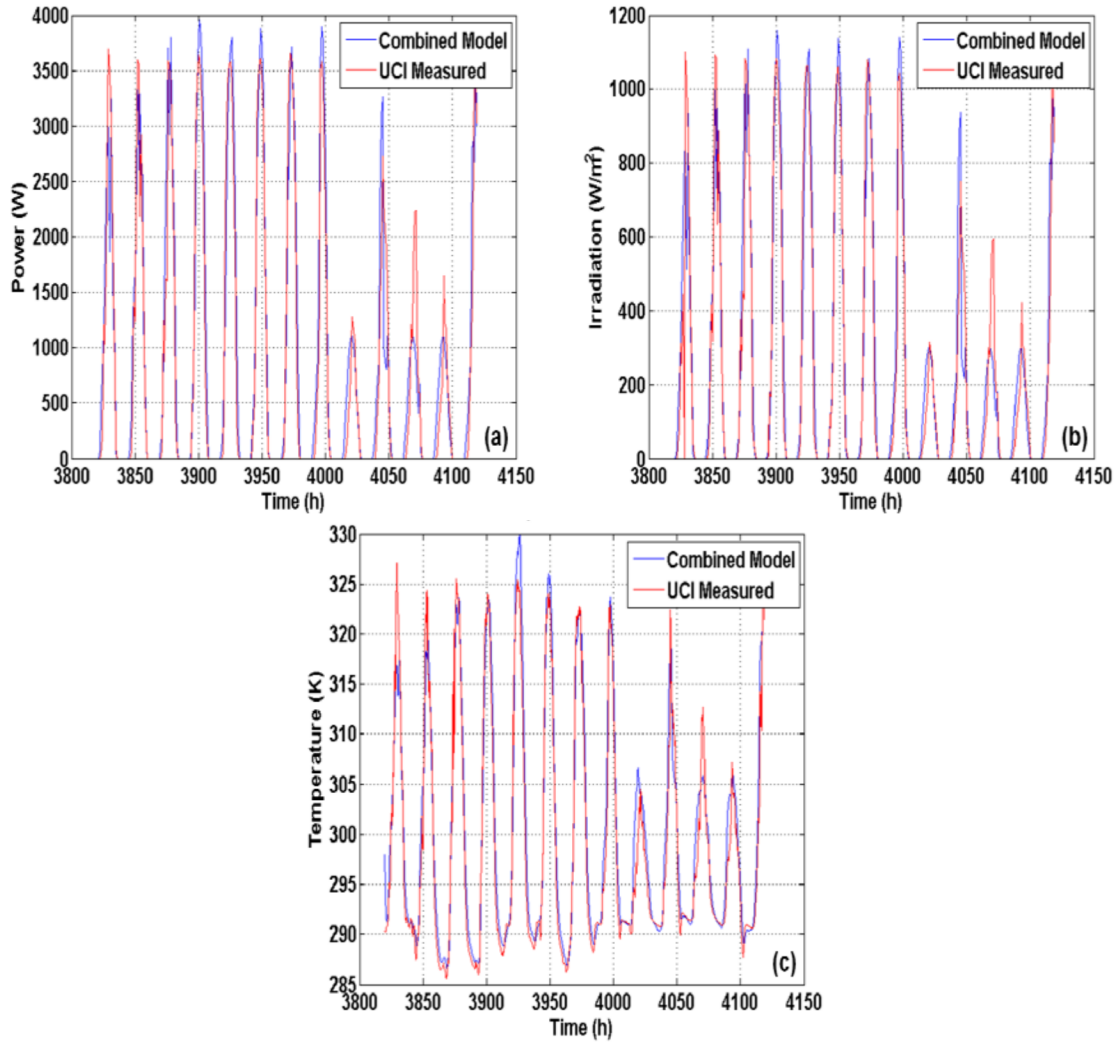
From Figure 9, the combined model results match with the measured data with an average error of 1.36% on a power output basis. Therefore, it is safe to assume that a more detailed model for determining the effective irradiation, power output, or cell temperature is not necessary for this level of analysis.

1.5 Lead-acid Battery Model

1.5.1 Model Description

A lead-acid battery dynamic model based on equivalent circuit is developed. The model is designed to accept inputs for current and ambient temperature, and the outputs are battery voltage, state of charge (SOC) and battery electrolyte temperature. The equivalent circuit network represented in Figure 10 constitutes the basis on which the battery model developed in

this report[13]. There were mainly three sub models: charge and capacity sub model, thermal (electrolyte heating) sub model and circuit network sub model. The model developed had been demonstrated to have accuracy satisfactory for majority of uses[14]. The dynamic model developed can be used for 1) simulate battery behavior under different operating conditions (both charge and discharge processes), 2) state of charge estimation, battery monitoring and diagnostics when lead acid battery is contained in on-line systems.

The temperature of battery is modeled by the energy balance equations. In the battery operation, the heat generation is ascribed to the ohmic heating by the sum of the energy charged and discharged from the battery (I^2R). The heat dissipation is modeled by free convection and radiation processes described in the Equation below. The convection coefficient (h) is evaluated based on empirical correlation of external free convection flows and Nusselt number.

$$Heat\ loss = q_{conv} + q_{rad} = h\pi D(T_s - T_{ambient}) + \varepsilon\pi D\sigma(T_s^4 - T_{ambient}^4)$$

Figure 10: Lead-acid Battery Equivalent Circuit
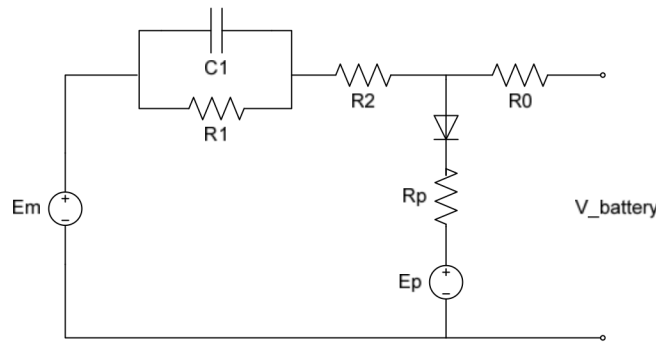
1.5.2 Model Verification

Model parameters were determined starting from sets of lab tests of real lead-acid batteries and empirical parameters used in literatures' models[15]. The parameter identification was simplified since some of the parameters can be taken as constant for all the batteries built with the same technology. The model was validated in conjunction with identifying the model parameters under various operating conditions.

---

[13]   M. Ceraolo, **New dynamical models of lead-acid batteries**. IEEE Transactions on Power Systems, 2000. 15(4): p. 1184-1190.

[14] M. Chen and G.A. Rincon-Mora, **Accurate electrical battery model capable of predicting, runtime and I-V performance.** IEEE Transactions on Energy Conversion, 2006. 21(2): p. 504-511.

[15] S. Barsali and M. Ceraolo, **Dynamical models of lead-acid batteries: Implementation issues.** IEEE Transactions on Energy Conversion, 2002. 17(1): p. 16-23.

The simulated battery behaviors agreed well with the experiment data in the literatures[13, 14, 15]. Some representative simulation results of a 2V 250Ah Lead-acid battery are shown in Figure 11, Figure 12, and Figure 13. Discharge (from fully charged) processes under various constant discharging currents (25A, 50A, 125A, 200A and 250A) starting are shown in Figure 11. The temperature effect on discharging is presented in Figure 12, in which a fully charge battery being discharged at current of 125A under various ambient temperatures. Figure 13 presents the simulation of transient behaviors of the battery discharging under constant currents (0.2C for 2 hours and 4 hours) followed by rest periods (in which the current is zero) at 20°C.

Figure 11: Discharge under Constant Current, 20°C
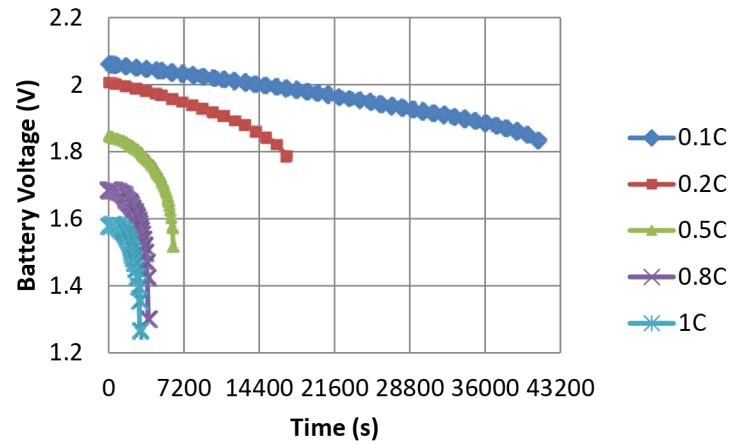
Figure 12: Discharge under 0.5C at Various Ambient Temperatures
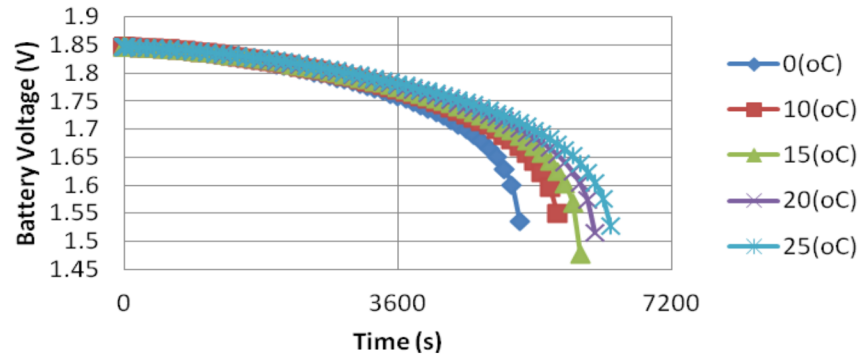
Figure 13: Discharge under 0.2C current step at 20°C
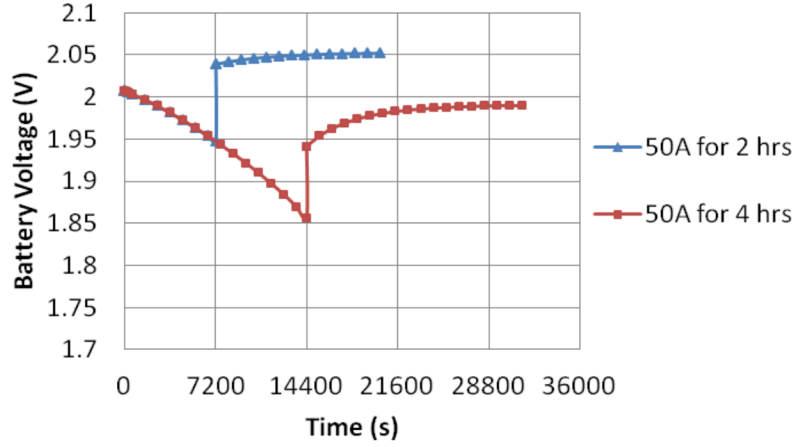
1.6   Lithium-ion Battery Model

1.6.1   Model Description

A generic Lithium-ion battery dynamic model is developed and validated with a 3.3V 2.3Ah Lithium-ion battery (ANR26650M1, A123Systems®) based on a model proposed in[16] and the implemented battery model in SimPowerSystems™ in MATLAB/Simulink®. The model is using SOC as input and battery voltage as output, and simulated using a simple controlled voltage source in series with a constant resistance. The equivalent circuit of the non-linear battery model proposed in[16] is showed in Figure 14 and the parameters are listed in Table 10. Based on the discharge characteristics, all the parameters of the equivalent circuit can be modified to represent a particular battery type.

Figure 14: Non-linear Battery Model

$$E = E_0 - K\frac{Q}{Q - it} + A\exp(-B \cdot it)$$

---
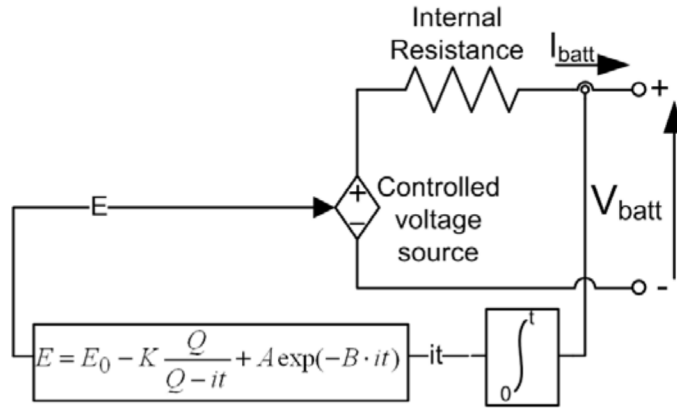
[16] Tremblay, O., L.A. Dessaint, and A.I. Dekkiche. **A Generic Battery Model for the Dynamic Simulation of Hybrid Electric Vehicles**. in Vehicle Power and Propulsion Conference, 2007. VPPC 2007. IEEE. 2007.

Table 10: Battery Model Parameters

E (V)	No load voltage
E_0(V)	Battery constant voltage
Q (Ah)	Battery capacity
R(Ω)	Internal resistance
K(V)	Polarization voltage
A(V)	Exponential zone amplitude
B(Ah)$^{-1}$	Exponential zone time constant inverse

The model developed is based on specific assumptions: 1) the internal resistance is assumed constant during the charge and the discharge cycles and does not vary with the amplitude of the current, 2) the parameters of the model are extracted from discharge characteristics and assumed to be the same for charging, 3) the capacity of the battery doesn't change with the amplitude of current, 4) the temperature doesn't affect the model's behavior, and the battery model is simulated the battery behavior at 25°C. 5) the Self-Discharge of the battery is not simulated, and 6) the battery has no memory effect.

1.6.2 Model Verification

A series of voltage response experiment results for a higher power rechargeable Lithium-ion (ANR26550M1) battery under various constant discharging current were obtained from A123systems® and presented in Figure 15 and Figure 16. Fully charged batteries (SOC=100 percent) are discharged under 0.43C, and 4.35C, respectively.

According to Figure 15, which compares manufacture experimental results and our simulated voltage responses relative to complete discharges at 1A, the model developed accurately simulated the discharging processes starting from full charge (SOC=100 percent) to nominal voltage (3.3V). While from nominal voltage to recommended cut off voltage (2V), the simulation results are not agreed very well with the manufacture's data.

With increased discharge current to 4.35C (10A) presented in Figure 16, the simulation result agreed well with the manufacture data at the exponential zone where the beginning of the discharge, and power output is slightly larger from 3.2 V to cut off voltage.

Figure 15: Discharge Characteristics at 25°C, 1A
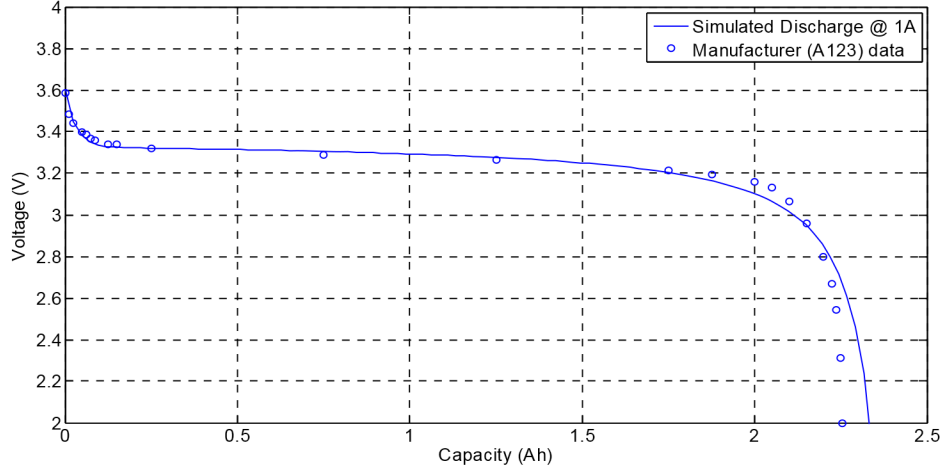
Figure 16: Discharge Characteristics at 25°C, 10A
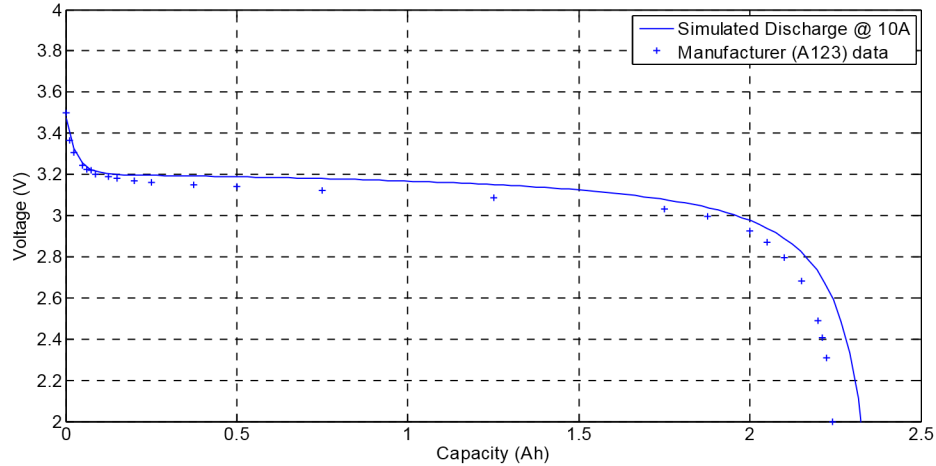
1.7 Ultra-capacitor Model

Ultracapacitors or electric double layer capacitors (EDLC) are electrical energy storage devices which have significantly larger energy density as compared to common capacitors, and larger power density compared to conventional batteries. Ultracapacitors present the lowest cost per Farad, extremely high cycling capability and long shelf life (when using carbon electrode), and are environmentally safe[17]. Because of these unique characteristics, ultracapacitors are utilized in a wide range of applications, such as electric vehicles and distributed generation systems. The feature of larger energy density is mainly due to the enormous surface area created by the porous (carbon) electrodes and the small charge separation created by the dielectric separator in ultracapacitors[17].

---

[17] Burke, A., **Ultracapacitors: why, how, and where is the technology**. Journal of Power Sources, 2000. 91(1): p. 37-50.

1.7.1 Model Description

Dynamic modeling and simulation of ultracapacitors are very important for evaluating and understanding the ultracapacitor behavior under different operating conditions in various applications. The most commonly used model of ultracapacitor is the classical RC equivalent circuit model, which consists of a capacitance (C), an equivalent series resistance (ESR) representing the charging and discharging resistance, and an equivalent parallel resistance (EPR) that accounts for the self discharging losses[18] [19]. In spite of being useful for many applications, this simple resistor and capacitor network model is insufficient to describe accurately the dynamics of an ultracapacitor[20]. Because of the porous nature of the ultracapacitor electrodes, the capacitive interface is not localized in a plain area but spreads into the inner of the highly distributed pores. Hence, the theoretical model was then developed to be a highly distributed R-C network which composed of many non linear resistors and capacitor leading to different time constants.

In this project, a dynamic ultracapacitor model based on a new equivalent circuit is developed and the model can predict the dynamic response of several types of ultracapacitors having different capacity and rated voltage values under various operating conditions. Further, an ultracapacitor bank built by arranging single ultracapcacitors in series is also developed and verified. Dynamic simulations are performed in MATLAB/Simulink® environment with Simpowersystem toolbox, and the simulations results were compared to the data provided by ultracapacitor manufacturer (Maxwell®).

The equivalent ultracapacitor circuit used in the model is shown in Figure 17. The single resistor of R1 represents the terminal interconnects resistance. While the resistor ESR represents the equivalent series resistance of the combined effect of interconnects, metal foil current collectors and interfacial resistance of carbon electrodes. Compared to the traditional RC network, the Cauer I network used in this study gives more insight into the origins of the three time constant approximation of an ultracapacitor model[21]. The branch of ESR-C_f, R_{d1}-C_{d1}, and R_{d2}-C_{d2} account for the highly distributed effects of carbon matte resistance, ionic conduction, and Helmholtz double layer capacitances existing at "macro", "meso" and "micro" pores in the electrodes, respectively[21]. The resistor R_{leak} represents the self-discharge behavior of ultracapacitor, and which is important factor to determine the duration time of stored energy at open circuit.

---

[18] Uzunoglu, M. and M.S. Alam, **Dynamic modeling, design and simulation of PEM fuel cell/ultra-capacitor hybrid system for vehicular applications**. Energy Conversion and Management, 2007. 48(5): p. 1544-1553.

[19] Vural, B., et al. **A dynamic ultra-Capacitor model for vehicular applications**. in Clean Electrical Power, 2009 International Conference on. 2009.

[20] Belhachemi, F., S. Rael, and B. Davat. **A physical based model of power electric double-layer supercapacitors.** in Industry Applications Conference, 2000. Conference Record of the 2000 IEEE. 2000.

[21] Miller, J.M., P.J. McCleer, and M. Cohen, **Ultracapacitors as Energy Buffers in a Multiple Zone Electrical Distribution System**, Maxwell Technologies, Inc.

Figure 17: Equivalent Circuit Model of Ultracapacitor
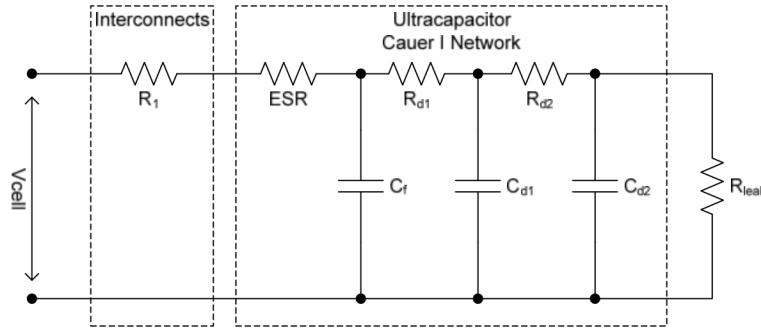
1.7.2 Model Verification

In this project, MATLAB/Simulink® is used to develop the dynamic ultracapacitor model. To test the developed dynamic model, various charge/discharge conditions are used in DC regime. The extraction of model parameters is achieved by comparing the simulation results and the data provided by Maxwell®. In this section, a Maxwell® 2000 F ultracapacitor (BCAP2000-P270, rated as 2000F, 2.7V) is first simulated and verified. By varying model parameters with the same equivalent circuit, a Maxwell® 3000F ultracapacitor (BCAP3000-P270, rated as 3000F, 2.7V) is then simulated and verified. Further, to simulate an ultracapacitor bank, a Maxwell® 16V ultracapacitor module (BMOD0500-P016) is simulated and verified. Three types of ultracapacitors and their rated voltages and capacitances are listed in Table 11.

Table 11: Commercial (Maxwell®) Ultracapacitors Simulated

Ultracapacitor	Capacitance (F)	Rated Voltage (V)	Rated ESR (mΩ)
BCAP2000-P270	2000	2.7	0.35
BCAP3000-P270	3000	2.7	0.29
BMOD0500-P016	500	16.2	2.4

1.7.2.1 Single Ultracapacitor Rated at 2000F, 2.7V

Constant current tests represent a basic and a widely used characterization method that is useful to determine the rated capacitance and the equivalent series resistance (ESR)[22]. A series of voltage response experiment results for BCAP2000-P270 under various constant discharging current was obtained from Maxwell® and presented in Figure 18. According to Figure 18, which compares Maxwell® experimental results and our simulated voltage responses relative

---

[22] Lajnef, W., et al., **Characterization methods and modelling of ultracapacitors for use as peak power sources**. Journal of Power Sources, 2007. 168(2): p. 553-560.

to complete discharges at various constant currents, the model developed accurately simulated the discharging processes starting from full charge. In Figure 19, voltage response results when discharging the ultracapacitor with constant power provided by Maxwell® and our simulation results were presented, and it can be seen that the results obtained by the simulation are in good agreement with the experimental results of Maxwell® for BCAP2000-P270 in the range of 1.35V-2.7V at various constant power. For capacitance and ESR characterization of ultracapacitor products, Maxwell® uses a constant current test method called 6-step process. In terms of BACP2000-P270 ultracapacitor, a test including charge device to rated voltage at 250 A, rest, discharge device to one-half its rated voltage at 250 A, rest, and end test after discharge to a low safe voltage (<0.1V). Maxwell® provided the experiment results and simulation results obtained using their model which are shown in Figure 20. The simulation result obtained by the model developed in this study was also showed in Figure 20, which is also in good agreement with the experiment data. Figure 20 also indicate that the model developed by Maxwell® is more accurate than the one developed in this study in terms of the dynamic response at 250A discharging rate. The model developed in this project is more accurate when discharging occurs at lower current (≤200A). The parameter values for BCAP2000-P270 model are listed in Table 12.

Figure 18: Simulation and Experimental Results for a 2000F Ultracapacitor (Maxwell® BCAP2000-P270) Discharging at Various Constant Current
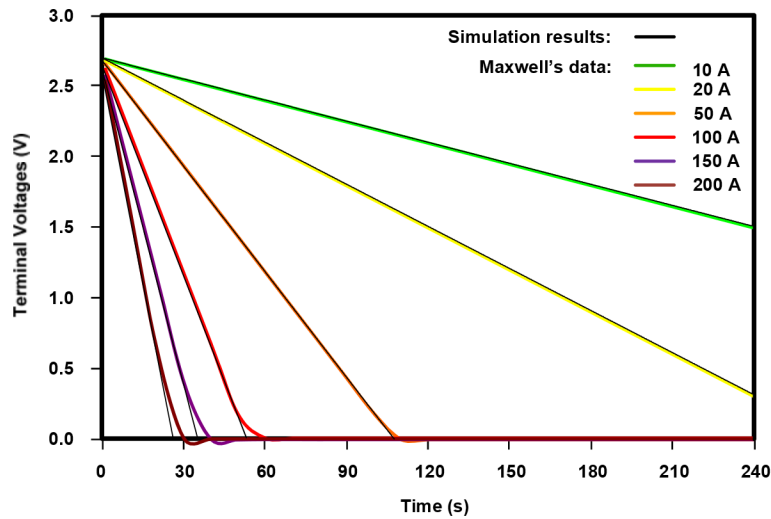
Figure 19: Simulation and Experimental Results for a 2000F Ultracapacitor (Maxwell® BCAP2000-P270) Discharging at Various Constant Power
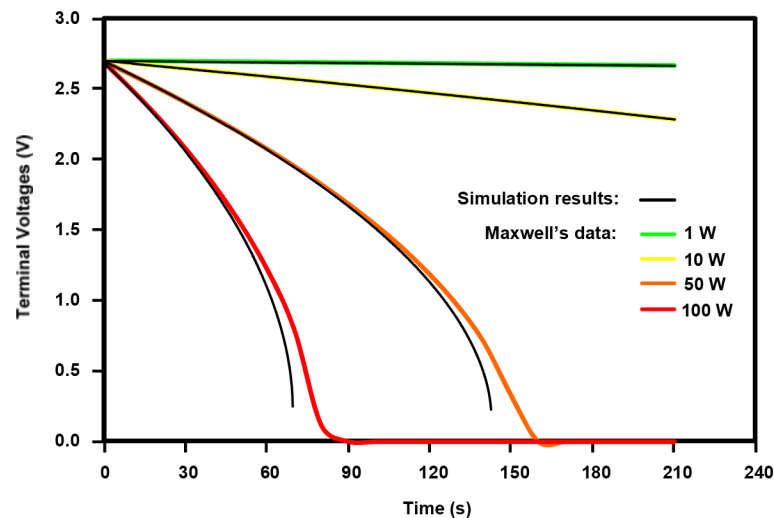
Figure 20: Simulation and Experimental Voltage Response Results for a 2000F Ultracapacitor (Maxwell® BCAP2000-P270) under 6-step Test Procedure
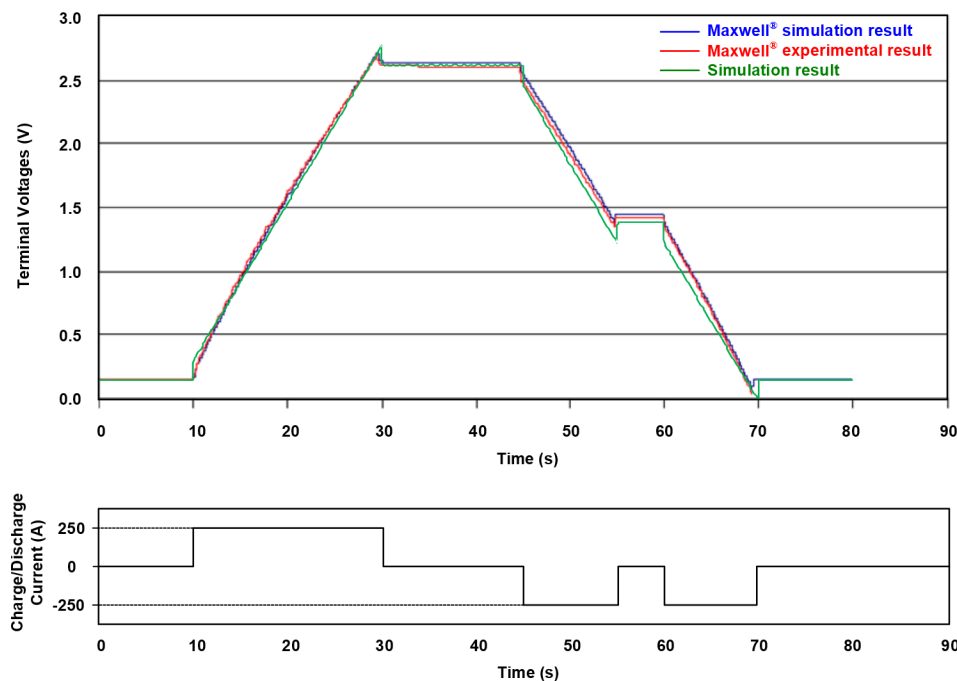
1.7.2.2 Single Ultracapacitor Rated at 3000F, 2.7V

By varying model parameters of the ultracapacitor model developed, Maxwell® BCAP3000-P270 was simulated and the simulation results were compared to the manufacture data and presented in Figure 21 and Figure 22, and the parameter values for BCAP3000-P270 model are listed in Table 12. As shown in Figure 21, the model developed accurately simulated the

40

discharging processes starting from full charge under various discharging current. And it also can be seen that the discharging results obtained by the simulation are in good agreement with the experimental results in the range of 1.35V-2.7V at various constant power in Figure 22. The model developed in this project shows higher accuracy at lower constant power discharge rate.

Figure 21: Simulation and Experimental Results for a 3000F Ultracapacitor (Maxwell® BCAP3000-P270) Discharging at Various Constant Current
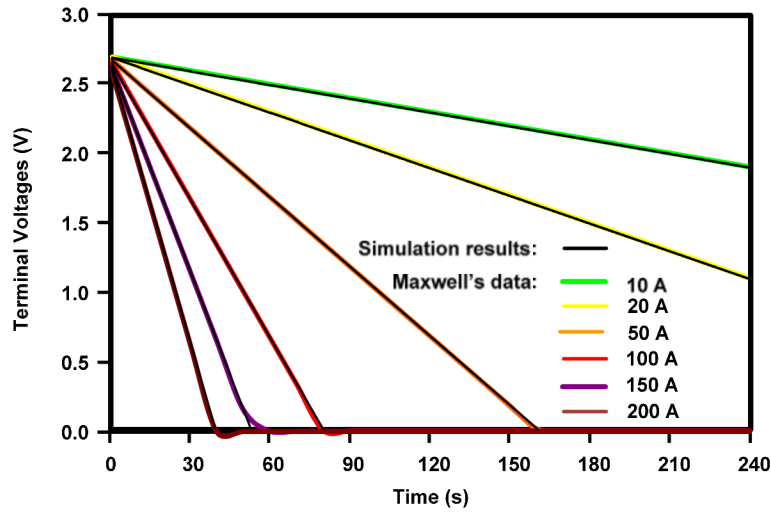
Figure 22: Simulation and Experimental Results for a 3000F Ultracapacitor (Maxwell® BCAP3000-P270) Discharging at Various Constant Power

41
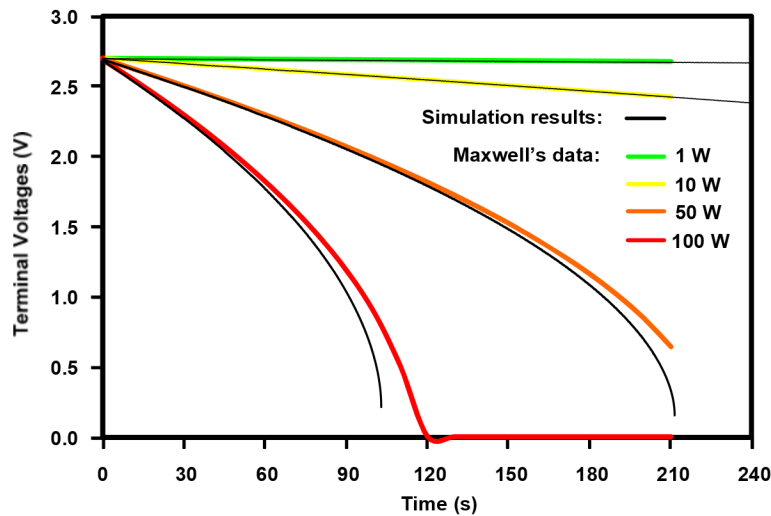
Table 12: Model Parameters for BCAP2000 and BCAP3000 Ultracapacitor

Parameters	BCAP2000 MODEL	BACP3000 MODEL
R_1	0.213 mΩ	0.18 mΩ
ESR	0.35 mΩ	0.29 mΩ
R_{d1}	0.142 mΩ	0.12 mΩ
R_{d2}	0.355 mΩ	0.3 mΩ
C_f	800 F	1200 F
C_{d1}	880 F	1320 F
C_{d2}	320 F	480 F
R_{leak}	675 Ω	675 Ω

1.7.2.3 Ultracapacitor Bank Rated at 500F, 16.2V

In practical applications, the certain amount of terminal voltage and energy or the capacitance of ultracapacitor storage system can be achieved by stacking multiple ultracapacitors in series and/or parallel. The terminal voltage required determines the number of capacitors that must be connected in series to form a bank and the total capacitance the total equivalent circuit resistance can be calculated as:

$$C_{total} = N_P \cdot \frac{C}{N_s}$$

$$R_{total} = N_s \cdot \frac{ESR}{N_P}$$

Where N_s is the number of ultracapacitors connected in series, N_P is the number so series strings in parallel, C is the capacitance for single ultracapacitor, ESR is equivalent series resistance for single ultracapacitor, C_{total} is the total system capacitance, and R_{total} is the total system resistance. By calculation, the Maxwell® BMOD0500-P016 is made up of 6 Maxwell® BCAP3000-P270 in series in terms of rated operating voltage and capacitance.

After the single ultracapacitor (BCAP3000-P270) is simulated and verified, a 16.2 V ultracapacitor bank model is developed by connecting 6 single ultracapacitor equivalent circuit models in series. The simulation results are compared to manufacturer's data and showed in Figure 23 and Figure 24.

Depending on the physical structure nature, the maximum voltage that can be applied across a single ultracapacitor is limited, typically 2.5~2.7V. Exceeding of this voltage will lead to a reduction of the lifetime or even catastrophic failure. As a consequence of this limitation, many of such cells have to be connected in series for applications required higher operating voltage, especially in automotive and distributed energy uses. When connecting many ultracapacitors in series, a disadvantage of this high voltage ultracapacitor series module is the asymmetrical balance of the voltage. If there is difference in the values of each ultracapacitor in series, the total voltage over the series connection will not be equally distributed between the different ultracapacitor which resulted in asymmetrical voltage distribution. With increasing

charge/discharge cycles, a local over-voltage could appear over one of several ultracapacitors and decrease the lifetime. Ultracapacitor series model developed in this study assumed that component as ideal ultracapacitors with identical capacitance and leakage current, thus voltage balancing would not be an issue. In terms of operation, there are several ways to balance the ultracapacitor series module, such as passive voltage balancing and active voltage balancing. A limitation of the model developed is that the temperature is not consider and assumed all ultracapacitors working at room temperature (25°C).

Figure 23: Simulation and Experimental Results for a 500F Ultracapacitor (Maxwell® BMOD0500-P016) Discharging at Various Constant Current
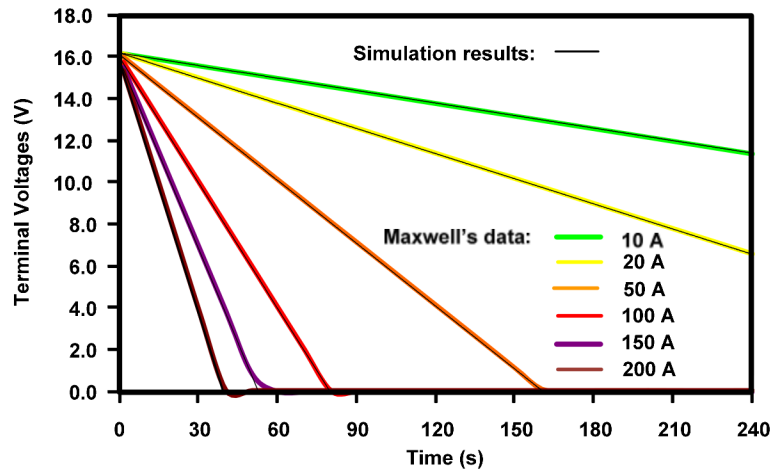
Figure 24: Simulation and Experimental Results for a 500F Ultracapacitor (Maxwell® BMOD0500-P016) Discharging at Various Constant Power

43
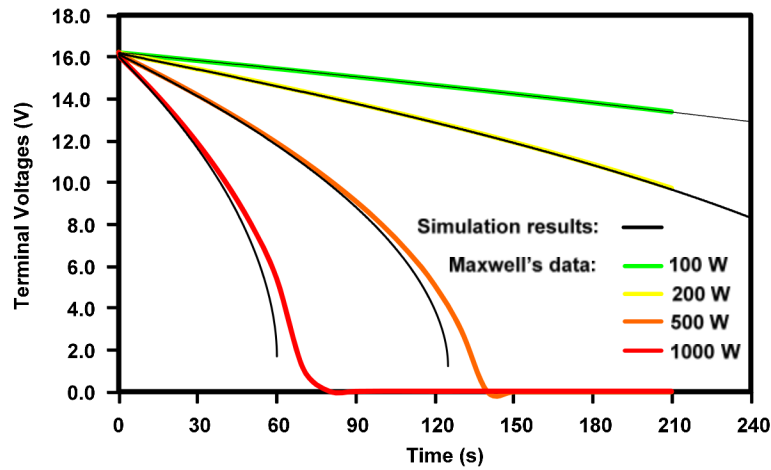
CHAPTER 2:
Economic Dispatch of CCHP System Models Development

2.1 Electric and Natural Gas Rate Structure Models

2.1.1 Electric Rate Structure Model

Electric rate structures are typically broken down into fixed, energy (aka volumetric), and demand charges. The methods by which these charges are calculated vary amongst utilities and rate structures (e.g., time of use, declining block, and fixed or non-time of use rate). As a result, the calculation of charges can vary drastically between utilities and tariffs. It is therefore important to capture the general characteristics of an electric rate structure and how it functions as a whole, as opposed to specific individual charges associated with a particular rate structure.

For example, some common charges can be broken down into non-time of use (non-TOU) and time of use (TOU) charges. These charges often vary with season, with higher charges for seasons when total utility demand is highest. Non-TOU energy charges consist of a flat rate that applies to all of the energy consumed by a customer. Non-TOU demand charges are often determined by the largest load recorded for that billing period. As for TOU energy charges, they depend on what time the energy is consumed. TOU energy rates are generally highest during periods of high electrical demand ("on-peak"), lower for periods of moderate electrical demand ("mid-peak"), and lowest during periods of low electrical demand ("off-peak"). TOU demand charges are determined by the largest load recorded during a specific time period during the billing period. If a declining block rate is being used, the charge is reduced with increased electricity consumption. Many declining block rate structures are presented in a three tier structure separated by levels of electricity consumption, with electricity becoming progressively less expensive as the customer reaches each new tier. The electrical rate structures used in this work were based on the structures used by Southern California Edison (SCE).

SCE rate structures for commercial and industrial buildings are broken down by maximum yearly customer demand. Customers with loads greater than 20 kW are offered the choice between at least two different rate structure types: (1) TOU-A, which has larger energy charges than TOU-B; and (2) TOU-B, which has higher demand charges than TOU-A. Both rate structures contain TOU energy charges, and both TOU and non-TOU demand charges. SCE defines "summer" as June 1st through October 1st, and "winter" as all other times. During the summer, the on-peak hours are 12:00 p.m. to 6:00 p.m., the mid-peak hours from 8:00 a.m. to 12:00 p.m. and 6:00 p.m. to 11:00 p.m., and off-peak hours are all other hours. During the winter, on-peak hours do not exist, mid-peak hours are from 8:00 a.m. to 9:00 p.m., and off-peak hours are all other hours. Energy charges versus time of day for summer and winter season are shown for TOU8 in Figure 25 and Figure 26. Figure 26 shows the percentage of a year for which each peak period is applicable. A non-TOU demand charge of $11.88 per kW is applicable for all months and is determined by the highest 15 minute average demand in a month. During the summer, TOU demand charges exist for both on-peak and mid-peak, and are $19.49 per kW and

$5.46 per kW respectively. These are determined by the highest 15 minute average demand during the peak period in a month. All SCE tariffs for buildings with maximum yearly load over 20 kW are shown in Table 13. The rate structures shown in Table 13 are applicable to customers who do not have Distributed Generation (DG).

Figure 25: Southern California Edison TOU8 Energy Charge versus Time of Day for Summer and Winter Seasons
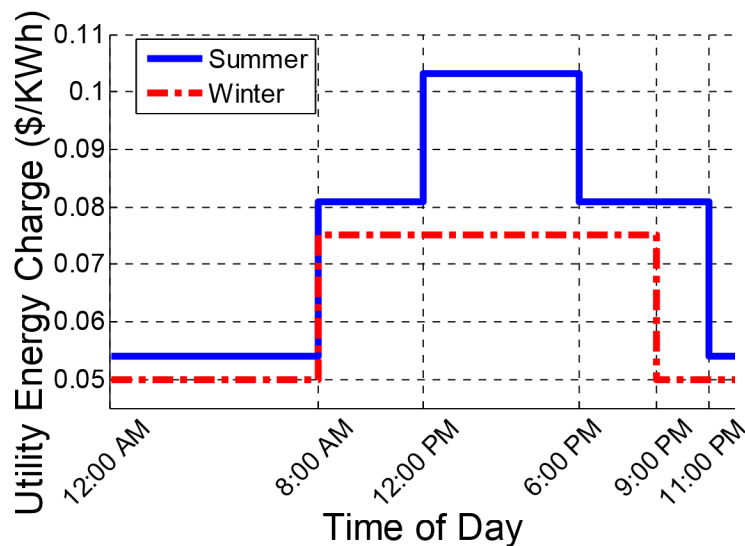
Source: Southern California Edison (SCE).

Figure 26: Percentage of the Year Comprising Each of the Southern California Edison Peak Periods

Source: Southern California Edison (SCE).

45
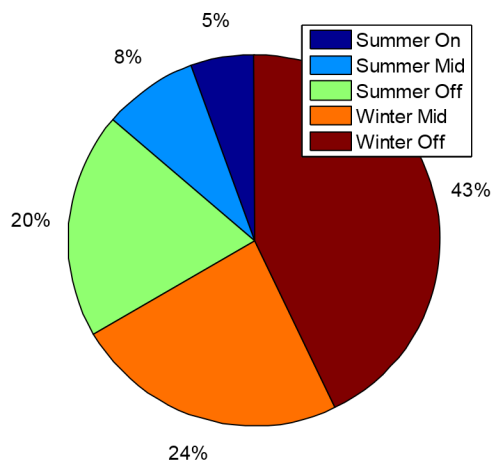
Table 13: Southern California Edison Energy and Demand Charges for Commercial and Industrial Buildings with Loads Larger Than 20 KW

SCE Tariff			GS-2		GS-3		TOU8	
Applicable Building Size (kW)			20-200		200-500		>500	
Rate Structure Type			TOU-A	TOU-B	TOU-A	TOU-B	TOU-A	TOU-B
Energy Charges	Summer	On ($/kWh)	$0.37809	$0.13667	$0.28163	$0.11855	$0.36288	$0.10323
		Mid ($/kWh)	$0.14311	$0.08398	$0.12820	$0.08493	$0.13528	$0.08078
		Off ($/kWh)	$0.05511	$0.05511	$0.06507	$0.05950	$0.05407	$0.05407
	Winter	Mid ($/kWh)	$0.08066	$0.08066	$0.06992	$0.06394	$0.07505	$0.07505
		Off ($/kWh)	$0.05183	$0.05183	$0.05273	$0.04819	$0.04980	$0.04980
Demand Charges	Summer	Non-TOU ($/kW)	$12.18	$12.18	$13.30	$13.30	$11.88	$11.88
		On TOU ($/kW)	N/A	$14.94	N/A	$12.96	N/A	$19.49
		Mid TOU ($/kW)	N/A	$4.57	N/A	$3.08	N/A	$5.46
	Winter	Non-TOU ($/kW)	$12.18	$12.18	$13.30	$13.30	$11.88	$11.88

Source: Southern California Edison (SCE).

2.1.2 Natural Gas Rate Structure Model

Natural gas utilities usually sell their gas in a block structure. These block structures can have a single price for all gas used or be a three tiered declining block structure, with gas becoming progressively less expensive as the customer reaches each new tier. The standard charge is dollars per therm. Southern California Gas Company (SCG) is a major provider of natural gas to many of SCE's customers, providing a declining block structure for commercial and industrial users. Like many natural gas utilities, SCG's rates take into account the distribution and fuel costs. While distribution costs have been observed to be relatively stable for SCG, fuel costs regularly change depending on the price of natural gas. As a result, while natural gas rate structures are relatively simple, changes in fuel cost because regular changes in customer prices. Prior work has shown that fuel price has a large impact on distributed generation economics. However, due to increased reserves and production of natural gas, prices have been "depressed… to the lowest levels in a decade"[23], leading to price projections that remain low in

---

[23] Gilbert, D., Fowler, T., **Natural Gas Glut Pushes Exports**, Wall Street Journal. 2012: U.S. Edition.

the near future[24]. While energy price projections have been shown to be inaccurate[25], a distributed generation investment that pays back in a reasonable time period should reduce the risk of exposure to natural gas price volatility. As a result, the natural gas rate model will follow SCG prices effective June 10th, 2012. This rate structure is as follows: $0.81115 for the first 250 therms, $0.56622 for the next 3,917 therms, and $0.402 for all other therms.

2.2 Building Models

Building models were developed using electrical load data showing energy consumption in 15 minute increments acquired from 38 buildings throughout Southern California, 12 of which had corresponding thermal loads. The characteristics of data obtained from buildings with both electrical and thermal loads are shown in Table 14.

Table 14: Characteristics of Collected Building Data

Building Name	Building Type	Data Length (Months)	Annual Average Electrical Load (kW)	Average Monthly Max Electrical Load (kW)	Average Monthly Heating (Therms)	Annual E/T ratio	Coincident Electrical & Heating During On/Mid-Peak
UCI Croul	College/ University	12	201.0	332.6	2301.4	2.18	58.18%
US Navy Palmer Hall	Hotel	14	203.9	272.3	1111.8	4.58	95.14%
UCI Bren	College/ University	12	206.7	340.3	1197.9	4.23	34.06%
UCI Cal IT2	College/University	12	420.8	677.2	4217.7	2.5	14.18%
UCI Natural Science 2	College/ University	12	447.8	732.6	7761.3	1.44	19.60%
UCI Natural Science 1	College/ University	12	505.7	828	6413.3	1.93	94.08%
Hyatt Irvine	Hotel	12	719.2	1016.8	13321.5	1.35	99.94%
SCAQMD	Commercial	24	1011.6	1774.7	28615.3	0.86	59.57%
St. Regis	Hotel	24	1367.4	1848.2	14814.1	2.3	99.85%
Patton State	Hospital	14	1679.4	2579.2	41393.1	1.36	72.79%
Loma Linda VA	Hospital	10	3089.4	3915.1	66474.3	1.24	94.74%
Long Beach VA	Hospital	13	3510.0	4832	46819.5	1.81	53.76%
LACCD Southwest	Commercial	17	57.7	430.44593	N/A	N/A	N/A

[24] United States. Office of Energy Markets and End Use. and United States. Energy Information Administration. Office of Integrated Analysis and Forecasting., **Annual energy outlook. 2012**, The Office : Supt. of Docs., U.S. G.P.O., [distributor]: Washington, D.C. p. v.

[25] Smil, V., **Perils of Long-Range Energy Forecasting: Reflections on Looking Far Ahead.** Technological Forecasting and Social Change, 2000. 65(3): p. 251-264.

College Cox Bldg							
UCI ELF	College/University	24	81.0	429.6637	N/A	N/A	N/A
UCI MSTB	College/University	12	99.1	351.16163	N/A	N/A	N/A
LA-ISD El Monte Health Center	Hospital	14	112.6	504.81778	N/A	N/A	N/A
Stater Brothers #171 Hidden Valley	Grocery	15	170.5	709.20741	N/A	N/A	N/A
Canon B	Commercial	16	173.5	753.25778	N/A	N/A	N/A
Stater Brothers #175 Fontana	Grocery	15	175.3	717.63407	N/A	N/A	N/A
LA-ISD Van Nuys Court House East & West	Commercial	19	179.2	696.52	N/A	N/A	N/A
Stater Brother #124 Laguna Hills	Grocery	15	219.1	858.18519	N/A	N/A	N/A
Stater Brothers #170 Corona	Grocery	15	225.5	888.12296	N/A	N/A	N/A
LA-ISD Hall of Records	Commercial	19	227.5	670.32148	N/A	N/A	N/A
Canon A	Commercial	16	236.6	924.92	N/A	N/A	N/A
LA-ISD Norwalk Court House	Commercial	19	290.6	697.44	N/A	N/A	N/A
LA-ISD Roybal Health Center	Hospital	19	330.3	823.7437	N/A	N/A	N/A
LA-ISD Pomona Court House North	Commercial	19	345.6	831.67852	N/A	N/A	N/A
LA-ISD Mental Health Court	Commercial	19	351.7	1171.2222	N/A	N/A	N/A
Canon A and B	Commercial	16	399.4	1114.7511	N/A	N/A	N/A
Grocery Store	Grocery	23	457.9	643.71704	N/A	N/A	N/A
LA-ISD Pasadena Court House	Commercial	19	501.0	868.13185	N/A	N/A	N/A
US Navy Commissary Naval Base San Diego	Grocery/Food	14	535.8	618.12296	N/A	N/A	N/A
Jamboree Center #4	Commercial	20	701.3	1433.6519	N/A	N/A	N/A
Jamboree Center#3	Commercial	20	748.9	1488.8222	N/A	N/A	N/A

Chino Women's Prison	Jail/Prison	26	757.8	1134.851 9	N/A	N/A	N/A
Jamboree Center #5	Commercial	20	771.0	1369.715 6	N/A	N/A	N/A
The Island Hotel	Hotel	10	848.1	977.8355 6	N/A	N/A	N/A
CA Rehab Center	Jail/Prison	25	995.3	1653	N/A	N/A	N/A

Table 14 shows the type of building load, length of data acquired, the average electrical load for the year, the average monthly maximum electrical load, the average amount of heating required per month, the electrical to thermal load ratio, and the amount of time that both an electrical and heating load are present at the same time during on and mid peak electrical periods. All buildings monitored experienced typical diurnal load behavior, with the highest demand being experienced during on or mid peak periods.

Since the price of electricity changes between the winter and summer season, financial analysis using the building data could be improperly skewed; extra winter months would depress total potential savings while extra summer months would inflate potential savings. For Southern California Edison, the proper seasonal ratio is 4 summer months to 8 winter months, or one summer month to every two winter months. If the acquired building data did not meet this criterion, representative summer and winter months for the building were added in order to create the proper seasonal month ratio.

2.3   Finance Models

A finance model was developed in order to determine the appropriate cost of capital associated with investment in DG, track the cumulative costs of energy, and determine the simple payback of the investment.

The cost of capital associated with investment in DG would come in the form of a loan used to assist the purchase of the DG. It was assumed that the loan would cover 80 percent of the purchase cost of the equipment and the other 20 percent would be funded directly by the investor. The cost of this loan to the investor was summed up in a monthly debt payment, calculated through the following equation:

$$Monthly\ Debt\ Payment = \frac{Principal \cdot i}{1 - (1 + i)^{-n}}$$

where i is the interest rate, principal is the total loan amount, and n is the debt term. For this study, the interest rate was set to eight percent and the debt term was set to 10 years.

The cumulative cost of energy was determined first by using the electric parent rate structure and natural gas rate structure to determine the baseline case (no DG) for the cost of energy. Then, after the dispatch strategy had been applied to the building load using the generator specifications assigned to the model, the cost of energy was calculated using the electric standby rate structure, natural gas rate structure, and determining the O&M from the generator

dispatch. These costs were summed and compared to the baseline case, allowing for the monthly savings to be calculated. These savings were used to represent future energy savings also. The cost of capital was then applied through the life of the loan, allowing for savings including capital costs to be determined.

Many investment criteria exist for judging the quality of DG investment[26]. The criteria picked for this study was simple payback. While other criteria include the time value of money, simple payback is a good indicator of investment potential; other criteria do not give positive investment reviews unless simple payback occurs in a timely manner.

Since cost of capital is included through the first ten years, payback lengths that do not occur within this time frame can have exaggerated paybacks due to this additional cost that stops at the end of year ten. As a result, payback is determined to occur when the cumulative savings, starting with the initial 20 percent of the purchase price invested, is greater than zero and does not subsequently turn negative.

2.4 Economic Dispatch Strategy

The following assumptions were made in developing the economic dispatch strategy:

• Onsite generation is limited to real power and heat. No ancillary products or services are considered.

• Benefits associated with reliability of onsite generation are not included.

• Installed generation is always available.

• A building's electrical load is met at all times. Any load not met by distributed generation is met by purchasing electricity from the grid.

• Onsite generation is not allowed to produce more electricity than the building requires.

• A building's thermal load is met at all times. Any load not met by distributed generation is met by a natural gas boiler. Boiler efficiency is set at 90 percent.

• If more heat is produced than needed through onsite generation, excess heat is vented to the atmosphere.

• Electrical and thermal storage is not considered.

• Generator warm up costs are not considered.

• Maximum system efficiency is 80 percent.

• Only up to 60 percent of the heat produced by onsite generation can be captured.

---

[26] Biezma, M.V. and J.R.S. Cristóbal, **Investment criteria for the selection of cogeneration plants - a state of the art review**. Applied Thermal Engineering, 2006. 26: p. 583-588.

- The only economic benefit of investment in distributed generation is reduction in electricity and natural gas bills.

- Individual microturbine operation range is limited from near full to full power (80-100 percent).

- All operations and maintenance costs (O&M) associated with a microturbine are considered to be variable.

- Installation of DG switches the building electrical rate structure from the parent structure to the standby structure.

DG dispatch strategies have been used to measure DG performance with respect to its ability to meet building loads through electrical and/or heat tracking[27][28], as well as its ability to minimize the cost of energy[29]. One example of a cost minimization dispatch strategy is The Distributed Energy Resource Customer Adoption Model (DER-CAM), which were applied[8] to produce an optimal, cost-minimizing operating schedule for onsite generation. DER-CAM, however, was intended to work with multiple DG systems much more complicated than an MTG with heat recovery. A more simple dispatch strategy can be used to minimize costs in situations using a single DG system such as an MTG.

A cost minimizing dispatch strategy utilizes DG only when it reduces total energy costs. Energy costs are generally comprised of electricity demand and energy charges, and natural gas energy charges. An economic dispatch strategy was therefore developed to utilize DG only when it minimizes these charges. Also, because demand charges are determined by the average electrical load over 15 minute increments, the dispatch strategy was designed to create an operating schedule resolved to the same time increment. It was also designed to block dispatch when the building load is less than the minimum power setting of the generator due to the fact that the generator cannot export electricity or operate below its minimum power setting.

2.4.1 Demand Charge Reduction

The dispatch strategy used in this study gives priority to minimizing demand and electrical energy charges as these costs can be significantly higher than the cost of natural gas. Because demand charges are determined by the highest 15 minute average demand in a billing cycle (30 days), spikes in the electrical load that have little to no impact on the energy charge can cause a large demand charge increase. Thus, priority is given to minimizing demand charges first.

---

[27] Medrano, M., et al., **Integration of distributed generation systems into generic types of commercial buildings in California**. Energy and Buildings, 2008. 40(4): p. 537-548.

[28] Ruan, Y., et al., **Optimal option of distributed generation technologies for various commercial buildings**. Applied Energy, 2009. 86(9): p. 1641-1653

[29] Siddiqui, A., et al., **Distributed Generation with Heat Recovery and Storage**. Journal of Energy Engineering, 2007. 133(3): p. 181-210.

Since demand charges are determined by the highest 15 minute average demand, or maximum utility demand (MUD), the simplest way to reduce these charges is to operate any onsite generation to keep the maximum utility demand from rising during any billing period. For generators sized smaller than the maximum building load, the MUD can only be reduced from the maximum building load to the maximum building load minus the maximum output of the generator. With perfect foresight of a building electrical demand, the generator can be turned on at precisely the right moments to ensure that demand charges are reduced as much as possible. Realistically, though, this is not possible and a more practical strategy must be adopted.

One such strategy is to set a demand threshold at the beginning of a month. This threshold is set at the average daily maximum demand of the prior month (or a representative month from the previous year) minus the capacity of the installed generation. Whenever the building load increases beyond this threshold, the generator is dispatched in order to ensure that the MUD does not increase. If the building load increase beyond the demand threshold is larger than the maximum output of the installed generation, then MUD increases to fulfill the unmet building load. Since demand charges have increased with the new MUD, the prior demand threshold must be increased to equal the new MUD; only dispatch occurring when the building load is surpassing the new demand threshold will reduce demand charges. This process repeats itself till the end of the month, at which point the demand threshold is reset in preparation for the next month. This demand reduction strategy is performed for all TOU and non-TOU demand charges.

For the standby electrical rate structure outlined in section 2.4.1, demand charges during the summer are determined by when the MUD occurs in addition to the size of the MUD. Winter demand charges are non-TOU, with no value being added by shifting MUD from mid-peak to off-peak. For summer operation, ensuring that the MUD occurs away from on- and mid-peak times can be more important than reducing the MUD. Demand shifting only occurs if the MUD happens on- or mid-peak. Prior to this occurrence, demand reduction as outlined above is performed.

If the MUD occurs on- or mid-peak, then demand shifting is performed by allowing the utility demand to surpass the prior MUD during lower cost periods. On-peak demand shifting translates into letting mid- or off-peak load increase while mid-peak demand shifting translates into letting off-peak load increase. While demand shifting consists of allowing the MUD to increase away from on- or mid-peak, demand reduction still occurs during the process of demand shifting if possible. For generators with a minimum dispatch constraint (e.g., a microturbine can be turned down to only 80 percent of full power), the generator is dispatched only if the building load is greater than the prior MUD by the minimum generator dispatch power. Otherwise, the generator is left off. Performing demand shifting ensures that not only is the MUD reduced, but demand charge rates are minimized. If demand shifting is being performed, dispatch aimed at reducing electrical energy and natural gas energy charges is blocked.

This dispatch strategy is illustrated in Figure 27 for a microturbine with a maximum output of 65 kW and minimum power setting of 50 kW operating at a grocery store. During Fri-01, the

generator only operates whenever the building load surpasses the MUD, ensuring that demand charges do not increase. During Sat-02 and Sun-03, the MUD is allowed to increase, shifting the time of MUD from on-peak to off-peak. While the MUD increases, the shift from on-peak to off-peak demand charges reduces overall costs. The demand threshold increases with the MUD and following Sun-03, the generator is only dispatched when the building load surpasses the increased demand threshold. This ensures that demand charges do not increase and are not shifting from off-peak to mid- or on-peak.

Figure 27: One Week Example of Demand Reduction and Shifting Strategy for a Grocery Store with a Single 65 kW Generator with a Minimum Power Setting of 50 kW
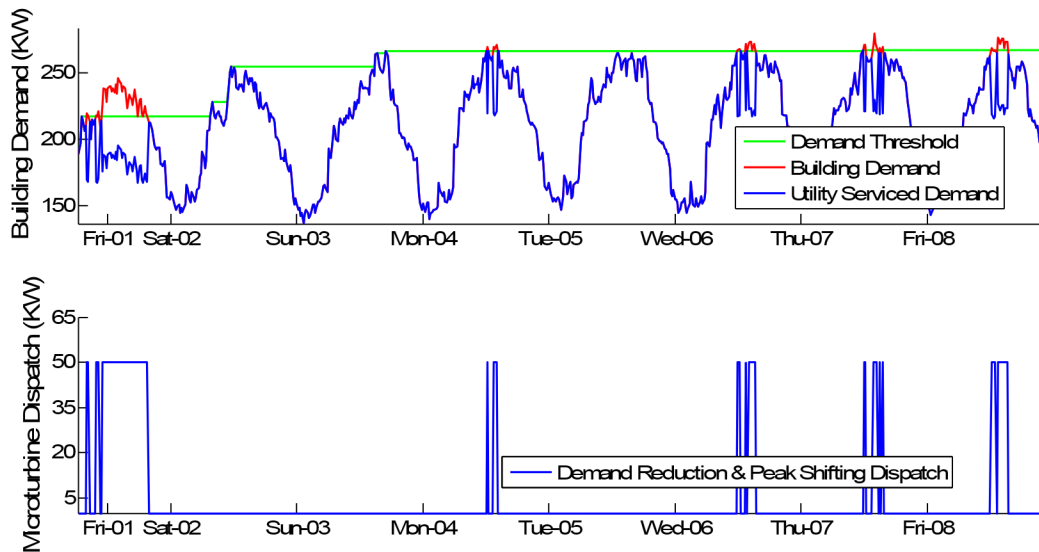
The demand reduction dispatch strategy is further illustrated in Figure 28for a microturbine with a maximum output of 65 kW and minimum power setting of 50 kW operating at Canon B. Figure 28 occurs during a month where demand shifting has no value so demand reduction is the only cost reducing activity available. It can be seen in Figure 28 that the microturbine is only dispatched when the building demand surpasses the prior maximum utility demand. Throughout much of the week, this activity occurs with the microturbine being set to its minimum power level. However, the microturbine power level is increased throughout the week to full power in an effort to keep the MUD from increasing; this behavior is successful in the early portion of Figure 28, but the load increases prove to be too large for a single microturbine to meet, resulting in a slight increase in MUD.

53

Figure 28: One Week Example of Demand Reduction for Canon B with a Single 65 kW Generator with a Minimum Power Setting of 50 kW
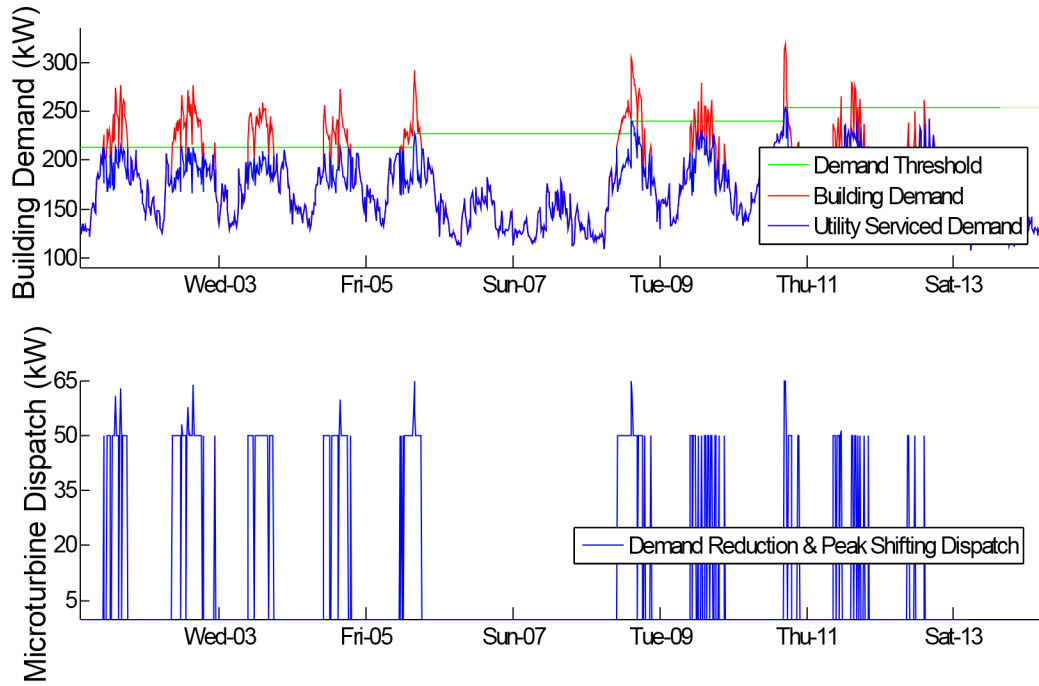
2.4.2 Electrical Energy Replacement Dispatch

Electrical energy is more expensive to purchase from a utility than an equivalent amount of energy from natural gas. As a result, if demand shifting is not occurring, electrical energy is generated if the cost on onsite generated energy is less expensive than what is offered by the electrical utility. With the cost of onsite generation being created by the fuel required to operate the generator and O&M, the cost of a kWh is:

$$Cost_{kWh} = \frac{C_1 * Cost_{NG}}{\eta_{elec}} + Cost_{O\&M}$$

which has units of \$/kWh. $Cost_{kWh}$ is the cost of a kWh from onsite generation, $Cost_{NG}$ is the cost of fuel $\left(\frac{\$}{Therm}\right)$, η_{elec} is the electrical efficiency of the onsite generation, $Cost_{O\&M}$ is the cost of operations and maintenance $\left(\frac{\$}{kWh}\right)$, and C_1 is the conversion factor between the energy unit of fuel and a kWh. If the $Cost_{kWh}$ is less than the cost of grid electricity and demand shifting is not occurring, the generator is operated.

2.4.3 Electrical Energy and Thermal Energy Replacement

Captured waste heat produces heating that would have otherwise been met through the firing of a boiler using additional natural gas. If both demand reduction and electrical energy replacement do not reduce energy costs and a thermal load exists, the addition of captured waste heat has the potential to cause onsite generation to be less expensive than the otherwise necessary grid electricity and fuel purchases to meet the building electrical and thermal load.

The cost of onsite generation is similar to the equation above with the addition of a term that includes savings due to waste heat recovery and is:

$$Cost_{kWh} = \frac{C_1 * Cost_{NG}}{\eta_{elec}}\left[1 - (\eta_{MAX} - \eta_{elec})\frac{\varepsilon_{hr}}{\varepsilon_{boiler}}\right] + O\&M$$

where η_{MAX} is the maximum system thermal efficiency achievable, ε_{hr} is the effectiveness of waste heat recovery, and ε_{boiler} is the efficiency of the boiler that would have been used to supply the thermal load the waste heat recovery is meeting. Eq. 3 calculates the cost to produce one kWh of electrical energy while also taking into account those avoided natural gas purchases that would otherwise be necessary for heating. If $Cost_{kWh}$ is less than the cost of grid electricity, the generator operation could potentially reduce energy costs. The generator is set to produce enough electricity so that all of the available waste heat is utilized. If this power setting is higher than the capacity of the generator, then the power setting is reduced to the maximum capacity. If the power setting is lower than the minimum allowable power of the generator, then the cost of producing the additional electricity is calculated using Eq. 2. The cost of producing the electricity onsite with partial heat recovery is then compared to the cost of purchasing the electricity and natural gas from a utility, with the cheaper option being selected.

The electrical energy and thermal energy replacement dispatch strategy is presented in Figure 29. Until 23:00 (11:00 p.m.) the generator can produce electricity and heat at a lower cost than can be purchased. However, the generator is turned to its minimum power setting because not all heat is being utilized, except for heat demand spikes, where the generator power setting is observed to increase to full power. At 23:00, the price of electricity changes from the mid-peak price to off-peak. This reduction in price coupled with an insufficient thermal load leads to the generator not operating during the off peak except for the two heat demand spikes. Once 8:00 is reached the following morning, grid electrical energy is charged at mid-peak rates, and the generator starts operation again.

Figure 29: Example of Electrical Energy and Thermal Energy Replacement for UCI Croul with a 180 kW Generator with a Minimum Power Setting of 144 kW during a Night in the Summer Season
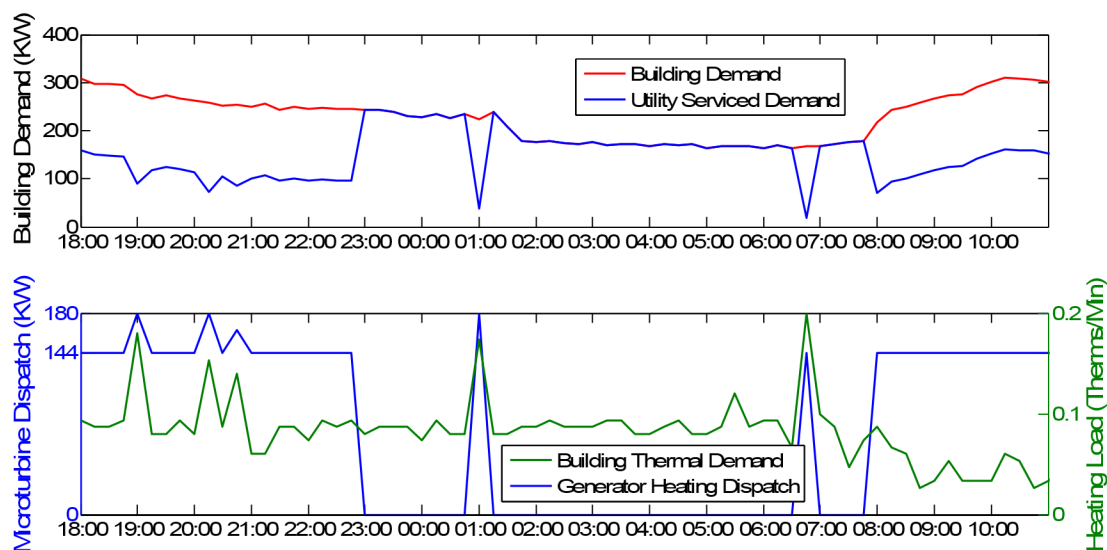
Figure 30 shows the economic dispatch strategy operating during a summer week for Canon A with a 400 kW generator with 20 percent turndown, utilizing demand reduction, electrical energy replacement, and electrical energy and thermal energy replacement whenever these activities reduce energy costs. During the first day (Sunday), off-peak electricity is available and no energy replacement is possible. Demand charge reduction is possible, but the generator produces as little electricity possible to accomplish this task. In the middle of the week, electrical energy and thermal energy replacement is possible during the mid-peak period. However, not all of the available heat is utilized, so the generator continues to operate at its minimum power setting. As the building demand increases during mid-peak, demand reduction activities result in generator operation before the dispatch strategy can check if electrical and thermal energy replacement is possible. During on-peak, electrical energy replacement is possible even without thermal energy replacement, and the generator power setting is increased to full power in order to produce as much electricity as possible. These cost reducing activities occur for all on-peak and mid-peak. When the end of the week is reached (Saturday), off-peak rates apply, resulting in demand reduction being the only cost reducing activity available to the generator.

56

Figure 30: Example of the Economic Dispatch Strategy for Canon A with a 400 kW Generator with a Minimum Power Setting of 320 kW during a Week in the Summer Season
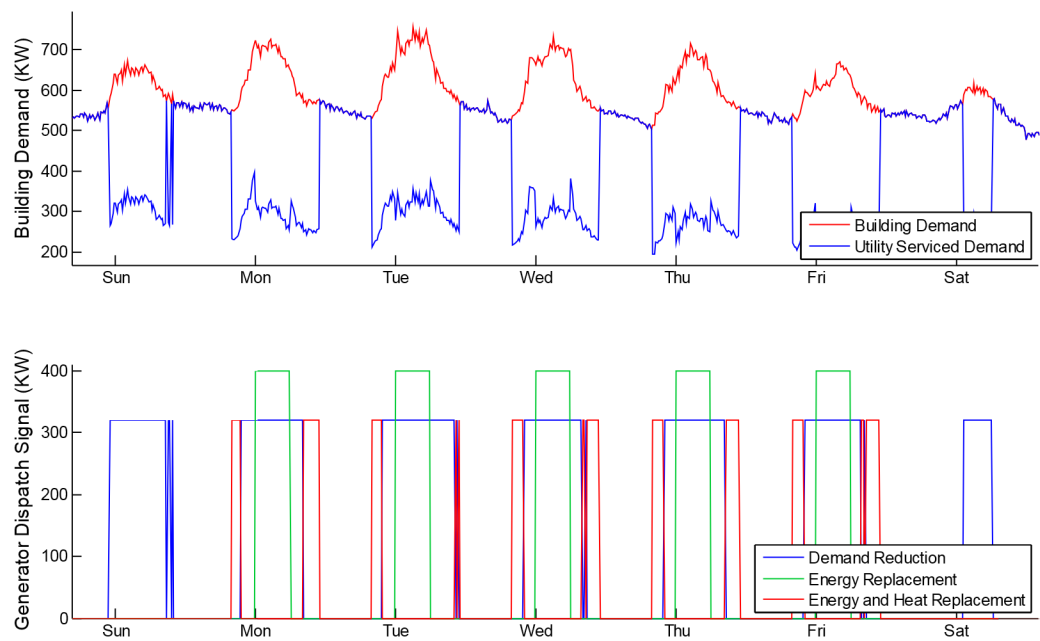
CHAPTER 3:
Economic Dispatch and Emissions of a C65 Microturbine Generator

Economic dispatch of a C65 Microturbine Generator (MTG) can occur under many different scenarios. First, depending on any agreements made between the generator operator and the electric utility, either the standby or parent rate structure can be used to charge for utility electricity service. If the parent rate structure is being used, the rate structure can be further broken down (Such as TOU-A and TOU-B). The products utilized by the generator operator can be electric only or both electricity and heat. Operation can be further altered by whether or not additional charges such as departing load are applied, which would add an additional $0.01493 per kWh generated on-site[30], increasing the O&M charge associated with the generator. These different scenarios were investigated with the results being presented and analyzed in this chapter. Three different parameters, load factor, average monthly heating load, and coincidence between electrical and thermal loads are used throughout this chapter to divide the results into groups. The load factor is the ratio between the average building load and the maximum building load. Each building has unique energy demand and DG operation can differ depending on how much generation is installed and the three parameters mentioned. While these three parameters do not capture all of the building energy demand behavior, they are useful for characterizing the buildings used in this study as well as allowing for the numerous results produced by yearlong simulations to be understood.

3.1 Baseline Building Energy Cost

Using the electrical and natural gas rate structures outlined in the previous chapter, the baseline cost of energy was determined for the 38 buildings discussed in Section 2.2. Each building was analyzed for use of both the TOU-A or TOU-B rate structure, with the less expensive rate being picked as the baseline electrical cost for that building. The difference between TOU-A and TOU-B is that TOU-A has higher energy charges while TOU-B has higher demand charges. The electric energy cost incurred to meet each building annual energy demand using grid electricity is shown in Table 15. The thermal energy cost to meet each of the building annual heat demand profiles using a natural gas-fired boiler with 90 percent efficiency are presented in Table 16.

---

[30] Southern California Edison, **Schedule DL-NBC Departing Load Nonbypassable Charges**. 2010.

Table 15: Cost of Electricity for Building Models using only Grid Electricity to Meet all Electrical Demand

Building Name	Annual Average Electrical Load (kW)	Average Monthly Load Factor	Annual Electric Utility Bill ($/Year)	Annual Cost of Electricity ($/kWh)	Summer Cost of Electricity ($/kWh)	Winter Cost of Electricity ($/kWh)	Difference over Other Rate (%)
LACCD Southwest College Cox Bldg	58.5	0.46	$69,711.42	$0.1412	$0.1555	$0.1234	6.81%
UCI ELF	81.1	0.25	$118,183.73	$0.1664	$0.1958	$0.1518	9.84%
UCI MSTB	99.1	0.53	$105,259.42	$0.1117	$0.1378	$0.1004	6.66%
LA-ISD El Monte Health Center	112.9	0.62	$120,818.19	$0.1245	$0.1425	$0.1133	7.45%
Stater Brothers #171 Hidden Valley	170.8	0.74	$160,743.38	$0.0948	$0.1196	$0.0796	9.06%
Canon B	172.6	0.55	$170,541.36	$0.1097	$0.1322	$0.0964	7.82%
Stater Brothers #175 Fontana	176.6	0.66	$151,462.17	$0.0867	$0.0981	$0.0795	8.33%
LA-ISD Van Nuys Court House East & West	182.7	0.43	$242,631.00	$0.1458	$0.1866	$0.1232	3.92%
UCI Croul	201.1	0.61	$189,350.78	$0.1065	$0.1259	$0.0949	8.43%
US Navy Palmer Hall	203.1	0.77	$172,544.19	$0.0965	$0.1043	$0.0922	9.07%
UCI Bren	206.7	0.57	$185,917.27	$0.1040	$0.1347	$0.0910	6.04%
Stater Brother #124 Laguna Hills	218.0	0.71	$188,206.23	$0.0873	$0.1382	$0.0634	5.30%
Stater Brothers #170 Corona	226.7	0.59	$202,082.49	$0.0898	$0.1434	$0.0632	5.06%
Canon A	232.3	0.44	$285,189.49	$0.1359	$0.1614	$0.1194	6.80%
LA-ISD Hall of Records	234.8	0.63	$263,295.43	$0.1232	$0.1479	$0.1097	6.00%

Building Name	Annual Average Electrical Load (kW)	Average Monthly Load Factor	Annual Electric Utility Bill ($/Year)	Annual Cost of Electricity ($/kWh)	Summer Cost of Electricity ($/kWh)	Winter Cost of Electricity ($/kWh)	Difference over Other Rate (%)
LA-ISD Norwalk Court House	291.6	0.45	$341,792.31	$0.1288	$0.1649	$0.1084	5.82%
LA-ISD Roybal Health Center	335.9	0.61	$370,866.93	$0.1212	$0.1507	$0.1051	7.47%
LA-ISD Mental Health Court	362.5	0.31	$535,065.15	$0.1621	$0.2107	$0.1328	2.35%
LA-ISD Pomona Court House North	373.3	0.61	$423,287.23	$0.1245	$0.1333	$0.1179	8.11%
Canon A and B	399.0	0.51	$451,459.03	$0.1253	$0.1487	$0.1103	7.45%
UCI Cal IT2	420.8	0.64	$407,970.87	$0.1097	$0.1257	$0.1003	5.93%
UCI Natural Science 2	447.8	0.67	$430,361.44	$0.1087	$0.1195	$0.1028	5.64%
Grocery Store	452.7	0.74	$403,960.12	$0.0977	$0.1239	$0.0851	7.81%
UCI Natural Science 1	505.7	0.66	$488,401.57	$0.1120	$0.1278	$0.1024	5.71%
LA-ISD Pasadena Court House	507.3	0.62	$507,945.50	$0.1100	$0.1370	$0.0956	7.68%
US Navy Commissary Naval Base San Diego	540.1	0.86	$455,974.63	$0.0904	$0.0880	$0.0920	7.67%
Jamboree Center #4	702.2	0.45	$813,680.78	$0.1291	$0.1599	$0.1119	5.45%
Hyatt Irvine	719.2	0.69	$663,527.48	$0.1050	$0.1283	$0.0923	6.54%
Jamboree Center#3	752.4	0.44	$852,260.67	$0.1262	$0.1669	$0.1048	4.34%
Chino Women's Prison	760.4	0.69	$715,045.37	$0.1113	$0.1175	$0.1072	6.47%

Building Name	Annual Average Electrical Load (kW)	Average Monthly Load Factor	Annual Electric Utility Bill ($/Year)	Annual Cost of Electricity ($/kWh)	Summer Cost of Electricity ($/kWh)	Winter Cost of Electricity ($/kWh)	Difference over Other Rate (%)
Jamboree Center #5	771.0	0.49	$832,648.82	$0.1203	$0.1527	$0.1024	6.22%
The Island Hotel	843.6	0.78	$719,190.62	$0.1033	$0.1208	$0.0911	7.12%
CA Rehab Center	997.1	0.60	$1,001,744.74	$0.1144	$0.1289	$0.1054	6.29%
SCAQMD	1011.6	0.56	$1,016,566.94	$0.1121	$0.1292	$0.1018	4.36%
St. Regis	1365.7	0.75	$1,225,125.51	$0.1010	$0.1206	$0.0899	7.78%
Patton State	1701.3	0.69	$1,670,207.67	$0.1066	$0.1118	$0.1031	8.13%
Loma Linda VA	3093.9	0.80	$2,709,063.10	$0.0926	$0.1098	$0.0796	8.41%
Long Beach VA	3496.4	0.73	$3,198,358.62	$0.1019	$0.1128	$0.0958	7.56%

Table 16: Cost of Natural Gas for Building Models using only a Boiler to Meet all Thermal Demand

Building Name	Average Monthly Thermal Load (Therms)	Annual Natural Gas Bill ($/Year)	Average Natural Gas Price ($/Therm)
US Navy Palmer Hall	1111.8	$8,750.15	$0.5956
UCI Bren	1197.9	$9,418.63	$0.5897
UCI Croul	2301.4	$17,166.20	$0.5594
UCI Cal IT2	4217.7	$29,203.04	$0.5193
UCI Natural Science 1	6413.3	$40,704.72	$0.4760
UCI Natural Science 2	7761.3	$47,615.83	$0.4601
Hyatt Irvine	13321.5	$76,685.39	$0.4317
St. Regis	14814.1	$84,491.62	$0.4265
SCAQMD	28615.3	$152,345.62	$0.3993
Patton State	41393.1	$157,895.29	$0.3979

Building Name	Average Monthly Thermal Load (Therms)	Annual Natural Gas Bill ($/Year)	Average Natural Gas Price ($/Therm)
Long Beach VA	46819.5	$240,892.01	$0.3949
Loma Linda VA	66474.3	$328,076.11	$0.3921

Table 15 shows average electrical demand, average monthly summer load factor, annual electrical bill, annual cost per kWh, summer cost per kWh, winter cost per kWh, and the percent difference between the less expensive and more expensive rate structures for each of the buildings studied. Table 16 shows the average monthly thermal load, the annual cost of natural gas if a 90 percent efficient boiler is used to meet the thermal load, and the resulting average price of natural gas for the 12 buildings for which thermal load data were available. Comparing the annual cost of electricity to natural gas shows the difference in value between the two energy sources. Since natural gas must be put through further processes to convert the chemical energy into a useful source of energy like electricity, it has a lower value than electricity. For example, a natural gas price of $0.50 per therm converts to a price of $0.0171 per kWh. It is improper to compare fuel and electricity on this basis since natural gas is a raw fuel and electricity was created from burning a raw fuel[31]. However, comparing the two energy sources on a cost basis illustrates the point that electricity charges comprise the majority of energy costs generated by a building and that the electrical loads generated by the building models are more expensive to meet than the thermal loads.

For nearly all buildings, TOU-B was less expensive than TOU-A; UCI ELF was the single exception where TOU-A was less expensive than TOU-B. The total annual cost of electricity can be seen to increase as the average electrical load increases. For all buildings, the cost per kWh is greater in the summer than the winter. Despite these predictable trends, the cost per kWh of each building and the percent difference between the baseline rate structure (TOU-B for all buildings except UCI ELF) and the other more expensive rate structure that the building operator can choose between can vary dramatically. These differences can be partially explained by the building demand dynamics, which are somewhat characterized by the load factor. This correlation is shown for the annual cost of electricity versus the load factor in Figure 31. As seen in Figure 31, as the average load factor decreases the cost of electricity increases. Load factor decreases as the maximum load deviates further from the average load. This increased maximum demand due to a shrinking load factor causes demand charges to increase.

Examples of building with various load factors are shown in Figure 32. The different buildings shown in Figure 32 illustrate a wide range of load factors. US Navy Commissary have a high load factor, shown by the consistently high level of demand. UCI Natural Science 1 has a

---

[31] Fumo, N. and L.M. Chamra, **Analysis of combined cooling, heating, and power systems based on source primary energy consumption**. Applied Energy. 87(6): p. 2023-2030.

smaller load factor, but still experiences a moderately large base load demand. Jamboree Center #3 consistently experiences high levels of demand during the middle of the day, punctuated by the largest demand at the beginning of each day, and is followed by low night time demand. UCI ELF has a relatively low base load and experiences demand surges that can be over eight times the size of the average load, resulting in a low load factor.

Buildings such as the US Navy Commissary experience a low cost of electricity because the maximum demand of the building is not significantly increasing the maximum utility demand far beyond the average demand. For other buildings with lower load factors, the demand charge is set by building demand that deviates further and further from the average demand causing for each kW of demand charge to be created using fewer kWh. For example, UCI ELF experiences demand charges created from a peak building demand that is greater than 600 kW but experiences energy charges for a building that has an average load of approximately 80 kW. The demand dynamic variations that cause these large demand charges do not consume a lot of energy relative to the total energy consumed by the building for the billing period. As a result, this increased demand causes the total price of electricity to increase. The ELF building exhibits this sort of low load factor and high electricity prices primarily because it contains several large industrial type loads.

Figure 31: Annual Cost of Electricity versus Average Electrical Demand Load Factor with Curve Fit
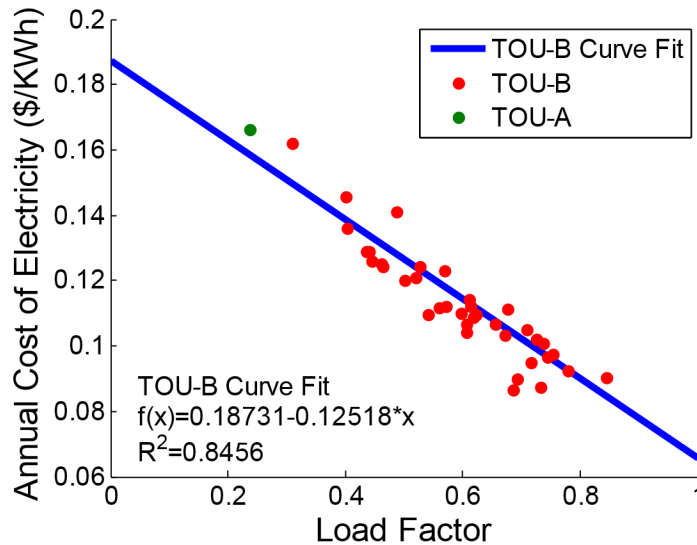
Figure 32: Portions of Building Load Data from US Navy Commissary, UCI Natural Science 1, Jamboree Center #3, and UCI ELF, Illustrating the Types of Building Loads that Lead to Different Load Factors
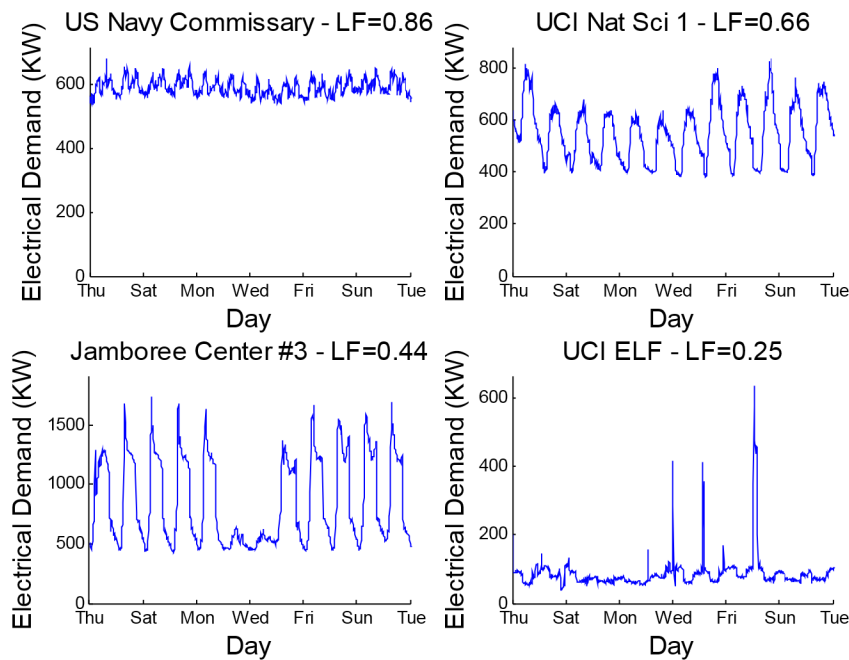
The difference between TOU-A and TOU-B is that the bulk of charges for TOU-A rest in the energy charges and for TOU-B in the demand charges. These differences, however, are only experienced during the summer since winter charges are the same for both rate structures. As load factor decreases, the difference between the two rate structures decreases due to increasing demand charges. This reduction in difference between the two rate structures shows that the

impact of shifting charge emphasis from demand to energy recedes as load factor decreases. The difference between the two rates and average load factor is shown in Figure 33.

Figure 33: Percent Difference between TOU-A and TOU-B for the Annual Total Cost of Electricity versus Load Factor with Resulting Linear Curve Fit
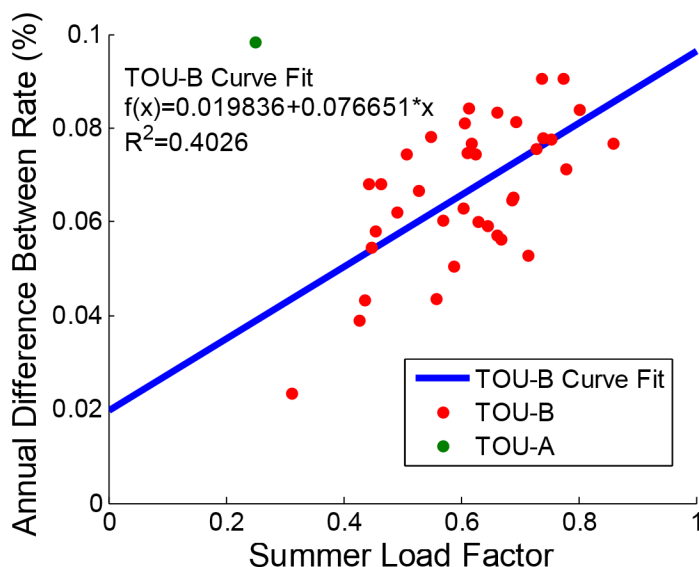
Figure 33 shows the percent different in annual electricity cost between the less and more expensive rate structures. All data points shown, except for the single TOU-A point belonging to UCI ELF, belong to buildings that experience lower electricity costs under TOU-B. It also shows that while other factors not included here influence the difference between TOU-A and TOU-B, the average load factor does help capture the general behavior of the difference of the two rates shrinking as load factor decreases. The spread of the data is created for two reasons. The average load factor is a combination of data from every month of building data. Some months, a building might experience a lower load factor than what is typically experienced, causing for a lower difference between TOU-A and TOU-B to occur for that single month. In more extreme cases, such as for UCI Cal IT2, while total annual cost of electricity is less expensive under TOU-B, individual months that have low load factors can experience lower cost of electricity under TOU-A.

Attempts to include other variables were made using analysis of variance methods available in the Design of Experiments (DOEx) software used here. Other metrics, such as the standard deviation of the load factor, summer on-peak and mid-peak load factors, and amount of load occurring during on-peak and mid-peak periods, were found to be insignificant. Since, as mentioned above, the difference in TOU-A and TOU-B is created by different summer charges, only the load factors from summer months were considered when creating the average load factor, which created the best fit while performing analysis of variance. The low R2 value of using only the summer load factor suggests that improvements can be made in predicting the difference between TOU-A and TOU-B. One way this could be accomplished is to determine the difference in cost for every kW of demand charge if that kW were to be charged on TOU-A versus TOU-B. This work falls outside the scope of this study and the summer load factor is

65

sufficient for understanding the difference between the two rates. Also, not enough low load factor buildings are used in this study to characterize what type of demand dynamic variations prefer TOU-A.

Cost of natural gas is easier to resolve versus the building load due to the simplicity of the rate structures for natural gas. Since a declining block rate structure is being employed, the price of natural gas decreases with increased consumption. While total cost increases with larger thermal demand, average price of purchased fuel decreases. This is illustrated in Figure 34 along with the Tier-2 and Tier-3 price of natural gas. Moderate increases to thermal loads smaller than 10,000 therms per month lead to large reductions in average fuel cost. As the thermal load increases, reduction in price decreases as it approaches the Tier-3 natural gas price. Past 30,000 therms per month, large increases in monthly thermal load are required in order to further reduce the average price.

Figure 34: Average Price of Natural Gas versus Average Monthly Heating Demand for the 12 Buildings that Have both Electrical and Heating Load Data
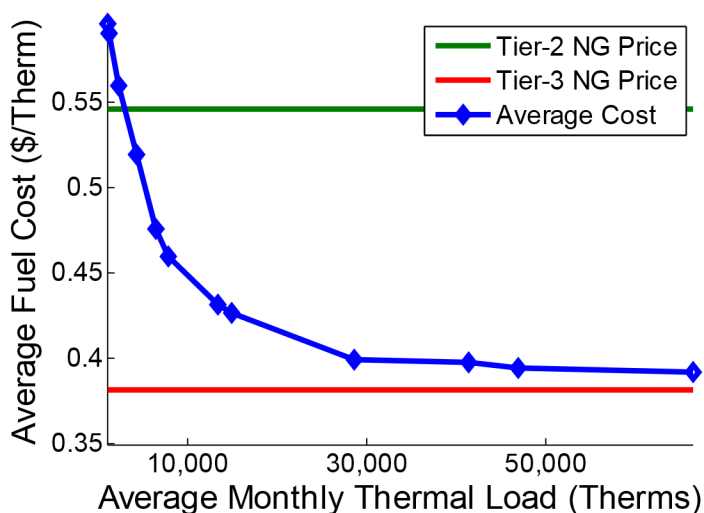
3.2   Economic Dispatch of a C65 Microturbine

3.2.1 Standby Electric Rates

Standby electric rates in the current analyses are only applicable for TOU-B rates. Standby rates designed by SCE only apply to demand charges, with energy charges being calculated according to the parent rate structure. As a result, using the high TOU-A energy charges and including standby demand charges would add additional demand charges not experienced under the parent TOU-A rate structure, increasing the cost of electricity. The single building in this study that does prefer TOU-A (UCI ELF) has a low load factor and experiences the energy costs of all buildings. Installing on-site generation could lower their electricity bill, but applying standby demand charges and TOU-A energy charges would at best not raise energy cost and increase the cost of electricity if the maximum utility demand occurs during on- and mid- peak periods during the summer. Due to this, only TOU-B rates are considered for the standby electric dispatch.

66

3.2.1.1 Electric Only Analyses

For generators that offer electricity as their only product, the cost reducing operation of the generator is demand reduction, demand shifting, and electric energy replacement. Performing demand reduction and demand shifting occurs regardless of the cost of electrical energy. Electrical energy replacement occurs only when the electricity produced by the generator is available at a lower cost than what is currently available for purchase from the electrical utility. The cost of producing electricity using a C65 MTG using the maximum and cost of natural gas is shown below in Table 17. Table 17 shows in column two the cost of natural gas to produce a single kWh for the three different natural gas tiers. The third and fourth column show the total cost to generate electricity by adding O&M cost to the cost of natural gas found in column 2. The O&M charges shown in Table 17 were taken as the cost of O&M for the C65 MTG ($0.03 per kWh) and the cost of O&M plus the departing load charge ($0.01493 per kWh), for a total cost of $0.04493 per kWh.

Table 17: Cost of Electricity for a C65 MTG in Southern California

Natural Gas Cost		Total Cost ($/kWh)	
Natural Gas Tier	Fuel Cost ($/kWh)	O&M=$0.04493	O&M=$0.03
Tier I	$0.1150	$0.1599	$0.1450
Tier II	$0.0794	$0.1243	$0.1094
Tier III	$0.0555	$0.1004	$0.0855

For a C65 MTG producing electricity only with an O&M cost of $0.04493 per kWh, the only peak period the generator can produce electricity at a lower cost than purchasing it from SCE is during summer on-peak and if Tier III natural gas is being used. If the departing load charge is not included and O&M costs are reduced, the C65 MTG can still only produce less expensive energy during on-peak times if Tier III natural gas is achieved. As a result, the C65 MTG is limited in its ability to provide energy replacement to, at maximum, approximately five percent. Due to this limitation, demand reduction and demand shifting activities account for the majority of C65 MTG operation. Installing an MTG to provide base load power would reduce demand charges, but would also replace less expensive electricity available from SCE. Losses created from full time operation would reduce the savings from demand reduction and demand shifting activity, weakening the economic case for purchase and operation of a C65 MTG.

Note that the Tier of natural gas price that is achieved depends upon the natural gas consumption of the building. In this study, all natural gas consumption is assumed to be due to heating, ventilation, and air conditioning. However, in actual practice, natural gas consumption can be caused by many more activities and operations. It is important to note that the heating load in this study can be synonymous with any natural gas consumption in actual practice.

Installing an MTG to reduce and eliminate the building electrical demand dynamic variation could reduce electricity costs enough to result in a short payback length. Sufficient savings can be realized by using the C65 MTG to supply the dynamic portion of a building load that lead to high demand charges, resulting in a short payback length on the investment. This leads to installed capacity smaller than the building load. The ability of the generator to perform demand reduction and demand shifting relies on the size of installed capacity relative to the size of the building. For some of the buildings in this study, a single C65 MTG is as large as 80 percent of the average load, while for others, is less than five percent.

In order to compensate for this difference, each building and generator simulation was first performed with a single generator. If the building and generator combination experienced payback, an additional generator was added to the generator set, and the economic analysis was performed again. This cycle was repeated until the generator combination did not experience payback, at which point the simulation was terminated. The payback length results for all building and generator combinations using an O&M charge of $0.04493 per kWh is shown in Figure 35. Figure 35 uses the installed capacity versus building average (ICBA) and installed capacity versus building maximum (ICBM) ratios as a basis for comparison. ICBA is the capacity of installed generation over the average electrical demand of the building. ICBM is the capacity of installed generation over the maximum electrical demand of the building. Increasing the amount of DG installed at a building increases both ICBA and ICBM. Due to the large differences in building load size and behavior, ICBA and ICBM are used to normalize the amount of installed generation between the buildings. Instead of discussing absolute amount of installed capacity at each building, ICBA and ICBM relates the amount of installed capacity to how much of the building average and maximum electrical demand can be met by the installed generation.

Figure 35: Payback Length for All Building and Generator Combinations Versus ICBA and ICBM
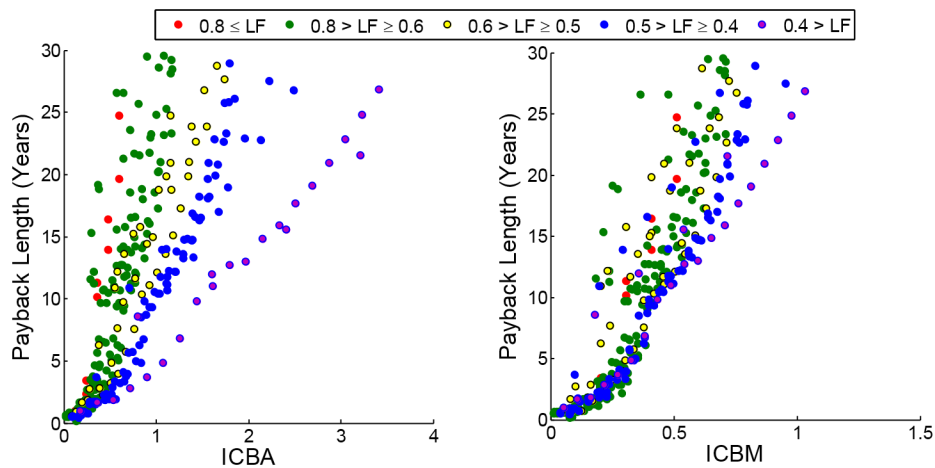
As seen in Figure 35, payback length can be short for some building and generator combinations. Length of payback increases with more installed generation. The amount of installed generation can differ depending on the building dynamics. Buildings with lower load factors can have more generation installed versus their average electrical demand than

buildings with high load factors for the same payback length. With the C65 MTG mostly unable to produce electricity at a lower cost than what is offered by the electrical utility, demand reduction and demand shifting operation reduces demand charges while replacing less expensive electricity purchased from a utility with more expensive electricity generated on-site.

The building demand dynamic variations that contribute to load factor are of much greater magnitude for low load factor buildings. With these larger dynamic variations deviating further from the average building load, more C65 MTG capacity can be installed for low load factor buildings relative to the average building demand since the demand reduction and demand shifting operation will only occur due the portion of the building load that is dynamic, not the base load. As load factor increases, less on-site generation can be installed since the dynamic variation of the building load is reduced. When comparing the payback length to the installed capacity relative to the maximum building demand, it can be seen in Figure 35 that buildings with lower load factors also can tolerate more on-site capacity than buildings with high load factors, but the difference between the buildings is not as great as when comparing the installed capacity to the average building demand. For all buildings, installation on a C65 MTG will take longer than 10 years if the installation is larger than half the average maximum building demand.

During most C65 MTG operation, the energy produced on-site is more expensive than what is available from the electric utility. Performing demand reduction and demand shifting reduces demand charges, but the fuel and O&M charges associated with MTG operation are more expensive than comparable energy charges; the more energy created on-site for the building, the more likely payback length will be extended. This is shown in Figure 36, which displays the percent of the building load met by C65 MTGs versus payback length. The legend in this figure breaks the data down between the average monthly heating loads and has units of therms per month.

Figure 36: Building Load Met versus Payback Length for all Building and Generator Combinations
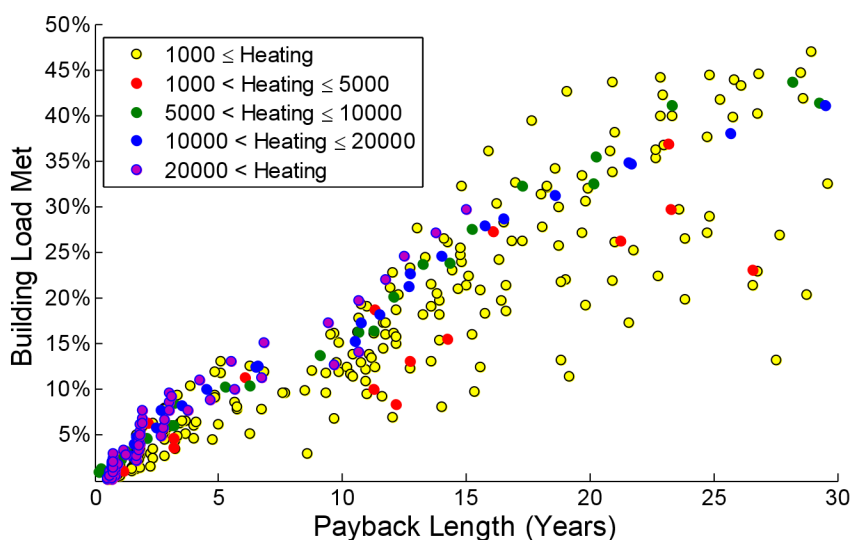
Buildings that experience a higher average heating load also experience lower natural gas cost per therm purchased. This benefit is experienced by the C65 MTG, with lower cost fuel being available to the generator. Buildings with higher monthly heating loads can have more of their building load replaced during demand reduction and demand shifting than buildings with lower average heating loads. However, for all buildings, the more building load that is met, the more likely payback length will be extended. Even with the benefit of lower fuel costs, buildings that have high average monthly heating loads still can only meet a small portion of their building load and still expect a quick payback. This point is illustrated further in Figure 37 and Figure 38. Figure 37 shows the percent of how much of the reduction to the electrical utility bill was created due to demand reduction and demand shifting activity versus building load met. Assuming an O&M charge of $0.04493 per kWh, Figure 38 shows the percent of how much of the reduction to the electrical utility bill was created due to demand reduction and demand shifting activity versus payback length. As more of the building load is met, the amount of total electrical savings that is attributed to reduced demand charges is reduced, regardless of load factor. This is true except for a few data points that represent buildings with low load factors. These data points are due to UCI ELF, which prefers TOU-A over TOU-B for its baseline energy costs. For UCI ELF, switching to a standby rate shifts the energy charges from the more expensive TOU-A rates to the less expensive TOU-B rates while keeping demand charges low. As a result, significant savings can be found before meeting any of the building demand simply from switching energy rates to the less expensive TOU-B rates while keeping demand charges low.

Figure 37: Percentage of Electricity Cost Reduction that is attributed to Demand Charge Reduction versus Percentage of Building Load Met
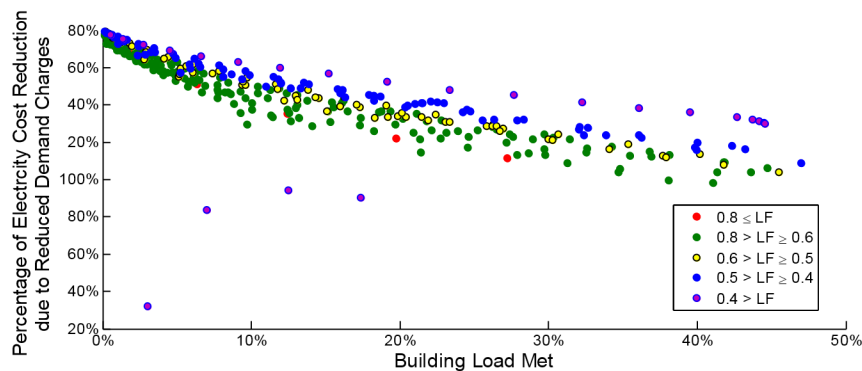
Figure 38: Percentage of Electricity Cost Reduction that is attributed to Demand Charge Reduction versus Payback Length
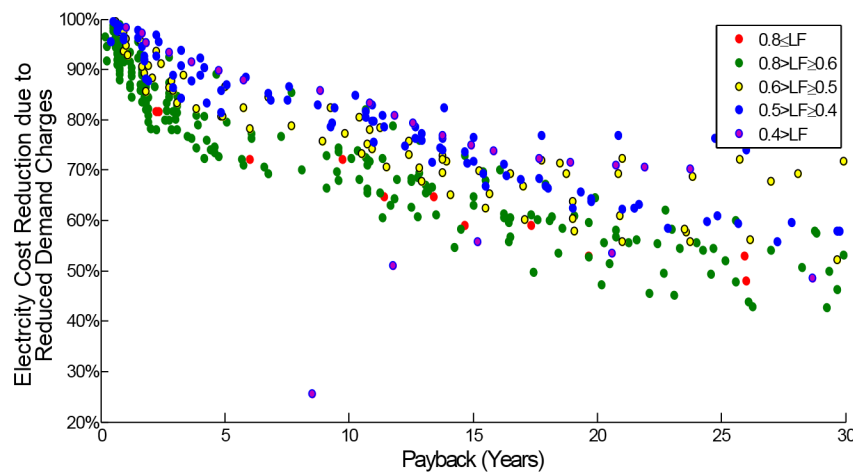
For all other cases, utility electricity costs are reduced as more of the building load is met due to building energy being met by on-site generation. However, except for UCI ELF, as the demand charge reduction becomes a smaller percentage of total utility electricity cost savings, payback length is increased. This is due to replacing the building energy with more expensive energy generated on-site. In fact, as more electrical energy is met by electricity produced from a C65 MTG, the increased fuel and O&M costs reduce overall savings to a fraction of the savings produced by demand reduction and demand shifting.

Figure 39 shows the percentage of total energy savings over demand charge reduction versus payback length. Whenever a building has total savings that are less than the demand charge reduction (all data points less than 100 percent), another factor, such as increased fuel and O&M costs are reducing total savings. Again, the effect of switching UCI ELF to standby rates is seen, where the data points from this building deviating sharply from the rest of the data points. The black line at 100 percent in Figure 39 shows where total savings are equal to total demand charges. As the savings from reduced demand charges are offset due to increases in fuel and O&M costs, total savings begins to shrink, extending payback length. For high load factor buildings, more building demand must be met in order for the C65 MTG to maximize demand charge reductions, leading to high fuel and O&M costs.

For low load factor buildings, a smaller portion of building energy is met. As a result, demand charge savings are still nearly fully realized and are not diluted by high fuel and O&M costs. Despite this, length of payback still increases as C65 MTG capacity increases. Payback length is extended due to larger on-site capacity and larger capital costs. Increasing on-site capacity does lead to further demand reduction. However, for demand shifting, once the maximum utility demand has been shifted away from on- and mid-peak for all summer months, no more savings from demand shifting can be realized since the lowest demand charge rate has been achieved. As a result, further increased capacity does not lead to more savings from demand shifting, only demand reduction. Even though the majority of demand charge savings for low load factor buildings are not offset by high fuel and O&M cost, the increased capital cost and associated

71

loan payments reduce total savings and extend length of payback. This also occurs with high load factor buildings, but high load factor buildings also face the issue of having to replace larger amounts of electrical energy using expensive on-site generation to reduce and shift demand instead of purchasing the electrical energy from a utility.

Figure 39: Percent of Total Savings that are produced by Demand Reduction versus Payback Length
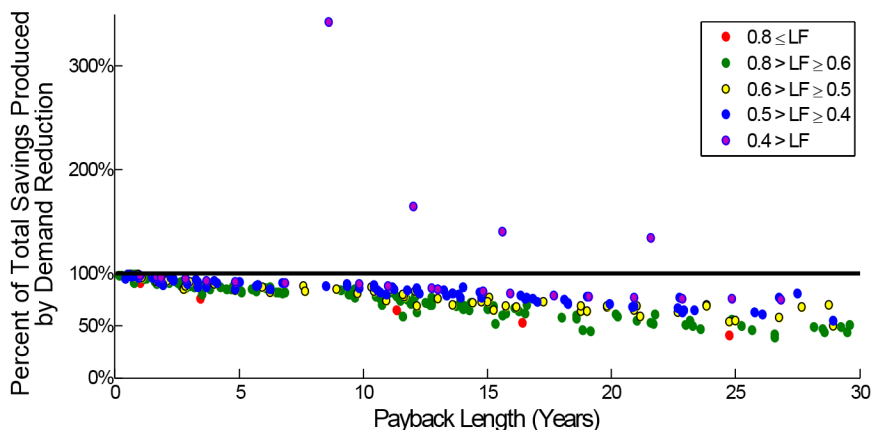
Capacity factor for the different building and generator combinations can vary. Capacity factor is used throughout this study as a tool for comparing the operation of different size generators to each other. Since heat recovery is being considered for part of this study, it is defined as the amount of energy used by the generator, both thermal and electrical, versus the amount of energy that could have been produced over the simulation time. The yearly capacity factor of the different combinations versus payback length is shown in Figure 40, broken down between different load factor ranges. Capacity factor is heavily dependent on load factor. As discussed earlier, buildings with high load factors must replace more energy than low load buildings to reach the same level of demand charge reduction from the same generator. This translates to a higher capacity factor for buildings that have high load factors and the opposite for buildings that have low load factors. Note that the longer payback lengths correlate to the larger installed capacities. Higher capacity factors are required for demand charge reductions to be maximized for these larger capacity installations. Capacity factor also depends upon the price of fuel available to the generator. As stated earlier, buildings with larger average heating loads have less expensive fuel. This less expensive fuel can also translate to a higher capacity factor, as shown in Figure 41.

When comparing Figure 40 to Figure 41, it can be seen that many of the high load factor buildings also have the highest heating loads. This is beneficial for the high load factor buildings by providing the least expensive fuel to on-site generation. However, it is clear from Figure 40 that high load factor buildings utilize their generators more often than low load factor buildings. It is difficult to separate the effects of building load factor and average monthly heating other than to say that high load factor buildings utilize their generators more often and that the low fuel cost helps reduce losses generated from producing expensive electricity on-site

instead of purchasing it from a utility. Regardless, the capacity factors of the generators presented here is far below what is actually capable of the generators.

Figure 40: Yearly Capacity Factor of Generators Installed on-site versus Payback Length Separated by Load Factor
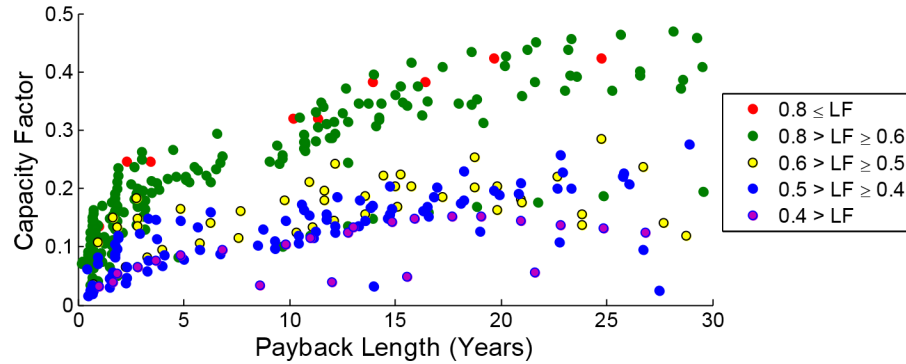
The number of generators installed on-site varies depending on building size.

Figure 41: Yearly Capacity Factor of the Generator Installed in various Buildings and Dispatched to Reduce Demand Charges versus Payback Length Separated by Average Monthly Heating Load
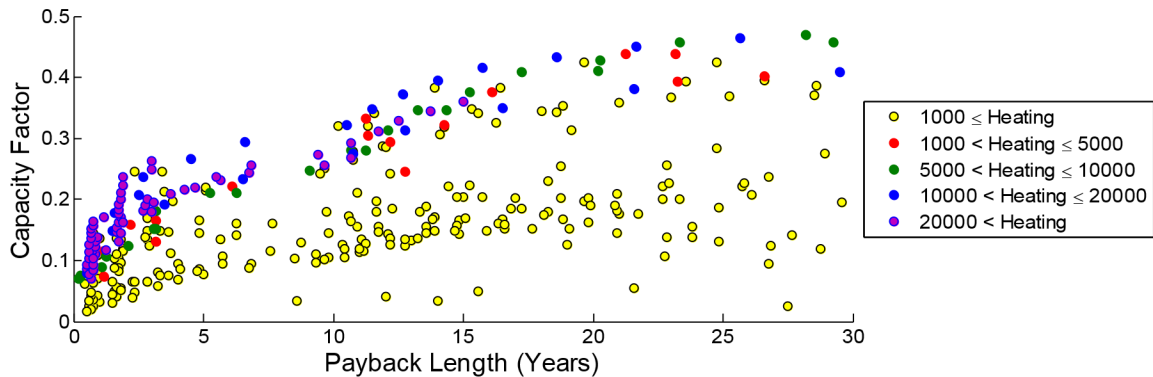
In order to achieve a shorter payback and higher capacity factor, the efficiency of the generator must increase, O&M must decrease, or other products, such as waste heat, must be utilized in order to improve the economic value of the C65 MTG. Reducing capital cost would also aid in improving the economic potential of this type of on-site generation. Of these three options, the addition of heat recovery is the only one that can be readily implemented by a building operator.

3.2.1.2 Heat Recovery Analyses

The addition of heat recovery utilizes the waste heat produced by the exhaust of the generator to help meet heating loads that would have been otherwise met through the firing of a natural gas boiler. This waste heat, which otherwise would have been vented to the environment and wasted, can reduce the amount of natural gas required to heat the building, improving the economics of MTGs. The value of recovered heat was calculated along with the total cost of

73

electricity and the percent reduction in cost of electricity for a C65 MTG supplying electricity only in Table 18 for all natural gas Tiers.

Table 18: Cost of electricity for a C65 MTG using Waste Heat Recovery in Southern California

Value of Recovered Heat		O&M=$0.04493/kWh		O&M=$0.03/kWh	
Natural Gas Tier	Recovered Heat Savings ($/kWh)	Total Cost ($/kWh)	Cost Reduction	Total Cost ($/kWh)	Cost Reduction
Tier I	$0.0434	$0.1166	27.1%	$0.1016	29.9%
Tier II	$0.0299	$0.0944	24.1%	$0.0795	27.4%
Tier III	$0.0209	$0.0795	20.8%	$0.0646	24.5%

The value of the recovered heat decreases for each subsequent Tier because the cost of natural gas is decreasing; the value of replaced heat is reduced with increased natural gas use. Despite this, heat recovery can reduce the cost of electricity as produced by a C65 by up to approximately 30 percent. These values, however, only apply if the heat being produced by a C65 MTG is utilized. Utilization of the heat requires that the building heating demand not only coincide with electrical demand, but the magnitude of the heating load be equal or greater than what is offered by the C65 MTG. If the heating load is coincident but the magnitude of the demand is smaller than what is produced, the values presented in Table 18 only apply to the kWh that is required to be generated in order to produce the waste heat needed to meet the thermal load. The cost of all additional kWh generated above what is required to produce waste heat sufficient to meet the thermal load has the same as outlined in Table 17.

With the inclusion of heat recovery, a C65 MTG is capable of producing electricity at a lower cost than what is available for purchase from SCE during summer mid-peak in addition to summer on-peak. If O&M is reduced to $0.03 per kWh, a C65 MTG is capable of producing electricity at a lower cost than what is available for purchase from SCE during winter mid-peak also. The ability of a C65 MTG to produce electricity at a lower cost during these peak periods depends on if the heat being produced is utilized by the building.

Fewer of the building models used in this study have heating load data, leading to 12 buildings being used to analyze the inclusion of heat recovery. Figure 42 shows payback length for building and C65 MTGs that are capable of waste heat recovery with an O&M charge of $0.04493 per kWh. Buildings with lower load factors are able to have larger installed capacity relative to the average building electrical demand. When comparing capacity to the average building maximum electrical demand, a separation is seen between low and high load factor buildings, but the difference is smaller than for comparing the capacity to the average building electrical demand. Similar to a C65 MTG supplying electricity only, payback length decreases as on-site generation meets more of building load, as shown in Figure 43. Also similar to a C65 MTG supplying electricity only and shown in Figure 44, as installed capacity increases, more of the building load is met during cost reducing operation. The majority of savings are produced

from reduced demand charges and payback length increases as reduced demand charges become a smaller portion of the reduced electrical utility bill due to replacing inexpensive SCE electricity with more expensive electricity on-site, as shown in Figure 45.

Figure 42: Payback Length versus ICBA and ICBM assuming Waste Heat is recovered for Various Generator-Building Combinations
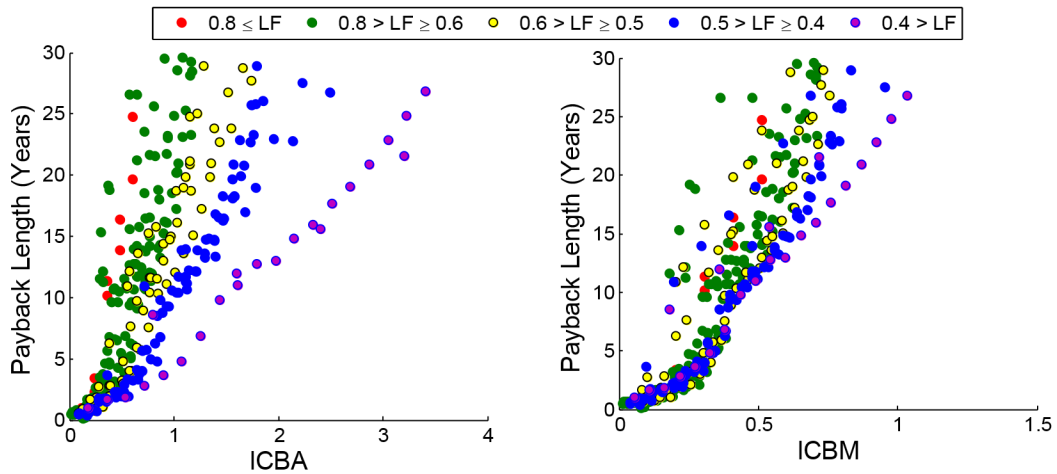
Figure 43: Building Load Met versus Simple assuming Heat Recovery for the Various Generator-Building Combinations

75
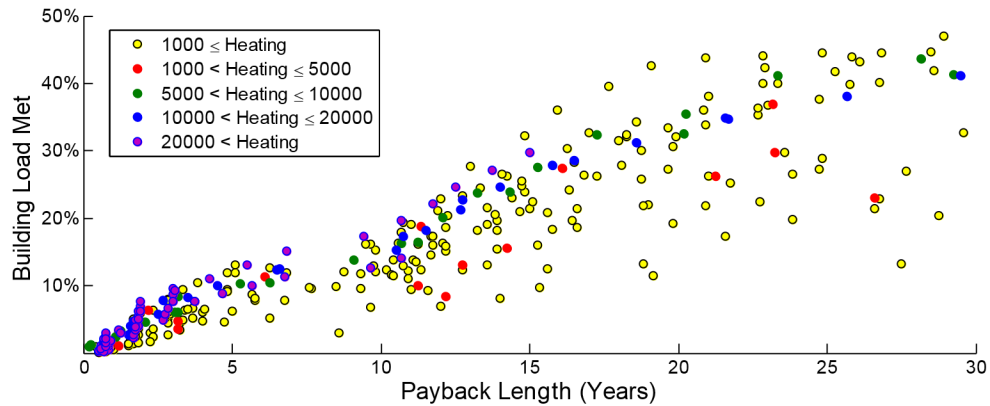
Figure 44: Building Load Met versus ICBM assuming Heat Recovery for the various Generator-Building Combinations
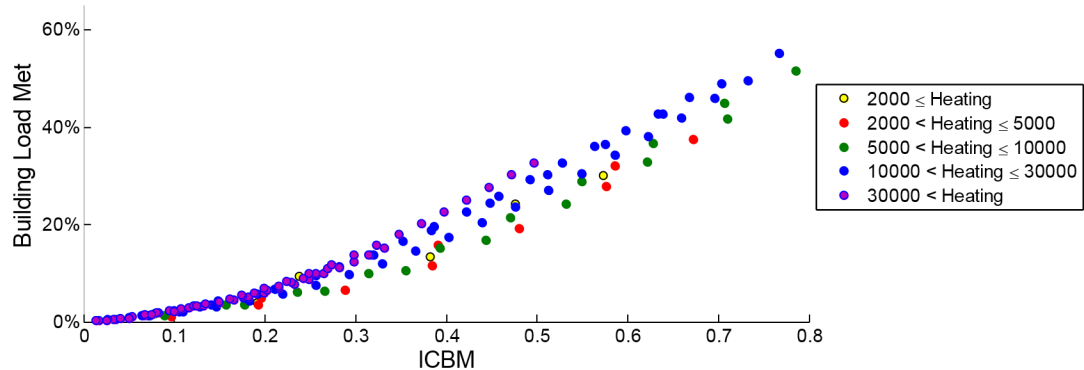
Figure 45: Percentage of Electricity Cost Reduction that is attributed to Demand Charge Reduction versus Payback Length assuming Heat Recovery for the Various Generator-Building Combinations
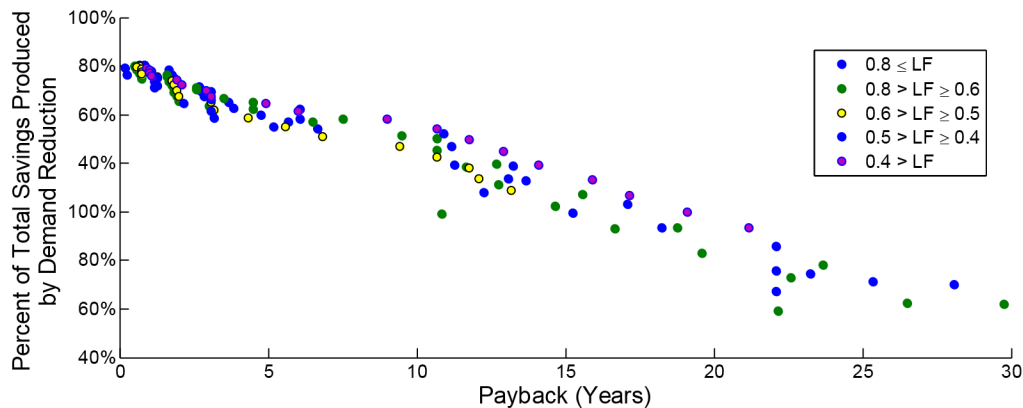
The most significant difference between the operation of a C65 MTG where the waste heat is captured and where the waste heat is not captured is operation during the summer mid-peak. When heat recovery is performed, electrical and thermal energy replacement during summer mid-peak is possible if Tier III natural gas is available and if there is a coincident demand for the heat. The summer mid-peak capacity factor for the different buildings is shown versus payback length and ICBM in Figure 46 with the data separated by the average monthly heating load.

Figure 46: Summer Mid-peak Capacity Factor versus Payback Length and ICBM Separated by Average Heating Load assuming Heat Recovery for the Various Generator-Building Combinations
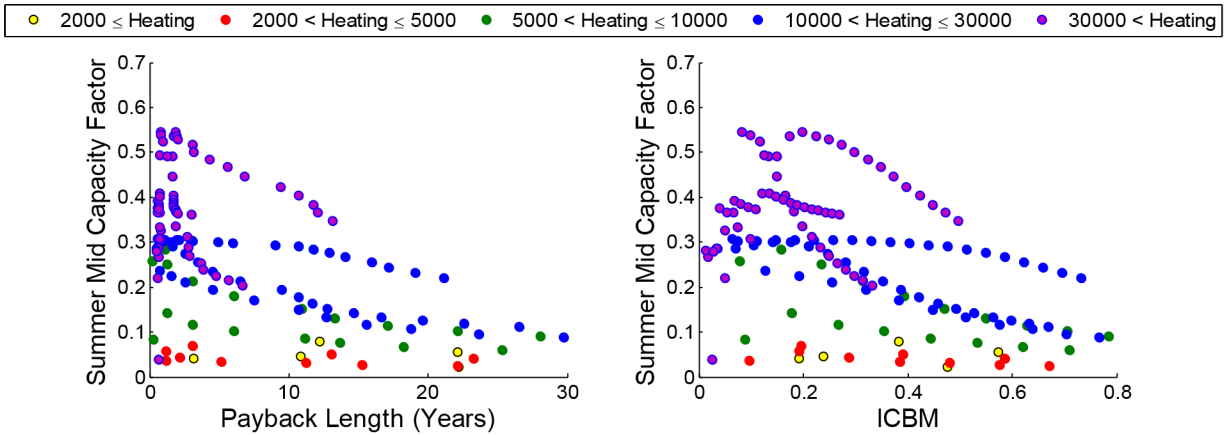
Buildings with larger heating loads have the largest capacity factor during the summer mid-peak. Only buildings that reach Tier III are capable of electrical and thermal energy replacement. These buildings with large heating loads also possess heating loads that are highly coincident, as seen in Figure 47. Figure 47 shows the same information as Figure 46 but with the building and generator combinations being separated by coincidence between the heating and electrical demand of the building. Figure 47 shows that large levels of coincidence are required for increased operation during summer mid-peak. The US Navy Palmer Hall building has coincidence of over 90 percent but still maintains a low summer mid-capacity factor of less than 0.1. This is because while US Navy Palmer Hall has high coincidence, the average monthly heating load is small and the required Tier III gas is not achieved, making electrical and thermal energy replacement not possible. Figure 46 shows that as installed capacity increases, capacity factor drops. Figure 46 and Figure 47 also show that for buildings with large average monthly heating loads and high levels of coincidence, a high summer mid-peak capacity factor is not always achievable. Sufficient heat must be utilized from the C65 MTGs in addition to access Tier III natural gas and the existence of coincidence. This is shown in Figure 48, which shows the summer mid-peak capacity factor versus the heat utilized. For buildings that access Tier III natural gas and have high coincidence, if sufficient heat is not utilized, the summer mid-peak capacity factor remains low.

Figure 47: Summer Mid-peak Capacity Factor Versus Payback Length Separated by Coincident Electrical and Heating Demand Assuming Heat Recovery for the Various Generator-Building Combinations
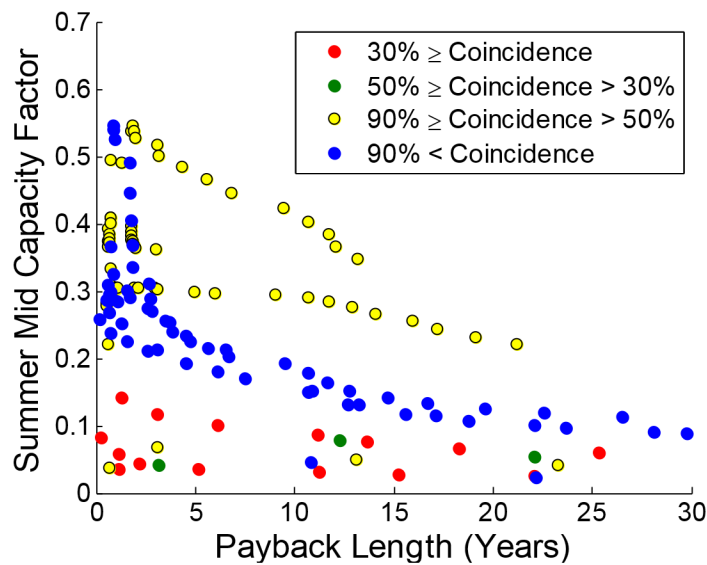
Figure 48: Summer Mid-peak Capacity Factor Versus Heat Utilized Separated by Coincident Electrical and Heating Demand Assuming Heat Recovery for the Various Generator-Building Combinations
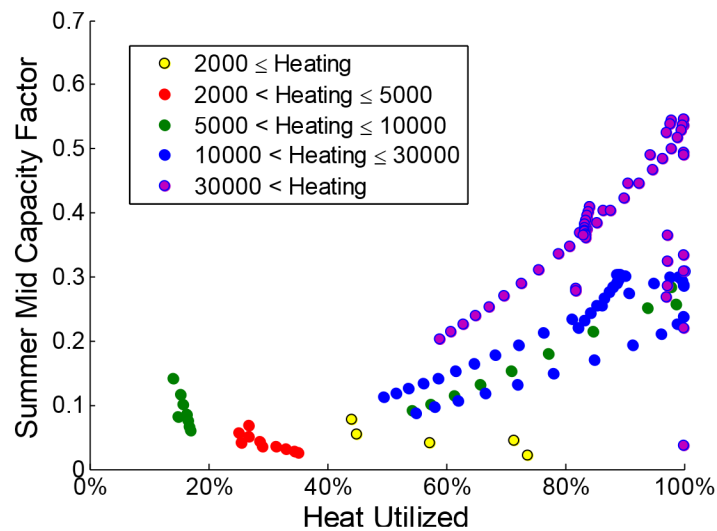
Since the efficiency of a C65 MTG is low, much energy in the form of waste heat is available. A potential benefit of distributed generation being that due to the proximity of the generator to the end user, higher efficiencies can be achieved. This benefit is not achievable for a C65 MTG unless a high degree of waste heat available is utilized. Figure 49 shows the total system efficiency of all building and generator combinations versus the utilized waste heat with the

data separated by the level of coincidence for each building. Total efficiency has a linear relationship with heat utilized according to Figure 49, with higher system efficiency being achieved when more waste heat is utilized.

Figure 49: Total System Efficiency Versus Utilized Waste Heat for all Building and Generator Combinations using Waste Heat Recovery for the Various Generator-Building Combinations
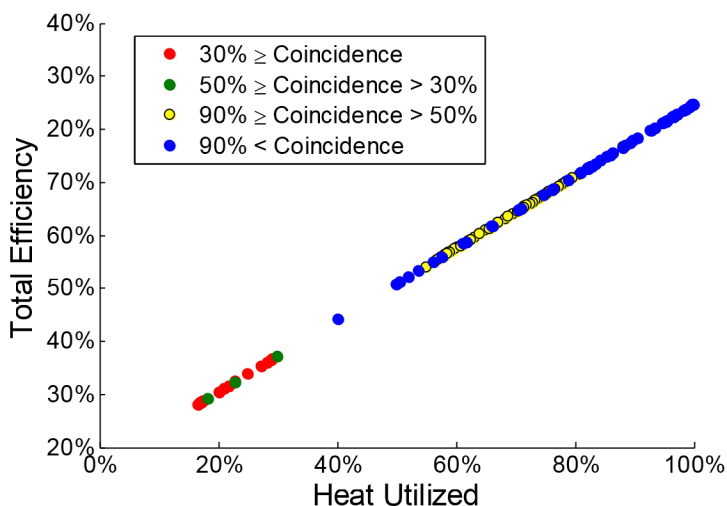
The decision to include heat recovery would add additional cost to a DG installation. If the primary goal of the installed DG is to reduce total costs, then an individual analysis of the building load and proposed DG system would be prudent in order to understand the projected financial and operational performance of any proposed on-site generation. General guild lines can be derived from the analysis above, such as a sufficient heating load is required so that Tier III natural gas is achieved by the building and that the heating demand is large enough to utilize the majority of the available waste heat while being coincident with the electrical load, but individual building analysis can be performed to give insight into the financial and operational benefits of on-site generation using heat recovery. This is briefly performed for two buildings; UCI Natural Science 1 (UCI Nat Sci1) and UCI Natural Science 2 (UCI Nat Sci2) by comparing the scenario where the buildings have an O&M cost of $0.04493 per kWh with no heat recover to the scenario where they have the same O&M cost and are capable of waste heat recovery. These two buildings were picked due to their similar average electrical demand and load factor and similar average monthly thermal demand while having different levels of coincident electrical and thermal loads (UCI Nat Sci1 has coincident electrical and thermal loads for approximately 95 percent of the year while UCI Nat Sci2 has coincident loads for approximately 20 percent of the year).

This difference in coincidence affects the change in payback length, as shown for both buildings in Figure 50. Decreases in payback length can be seen for UCI Nat Sci1, with heat recovery helping large installations payback faster. UCI Nat Sci2 does not experience reduced payback

length due to waste heat recovery except for systems that payback slowly. Also shown in Figure 50 is the behavior of the financing payments made to pay for the capital cost required to purchase the on-site generation. Since the life of the loan made for the purchase of on-site generation is 10 years, once the loan has been paid off, savings that were previously being offset by loan payments are now realized by the building operator or investor. This causes a step increase in savings that happens the first month after the loan life has ended, causing the slope of payback length to decrease suddenly at approximately 10 years.

Figure 50: Change in Payback Length due to the Addition of Waste Heat Recovery Versus ICBA for UCI Nat Sci1 and UCI Nat Sci2
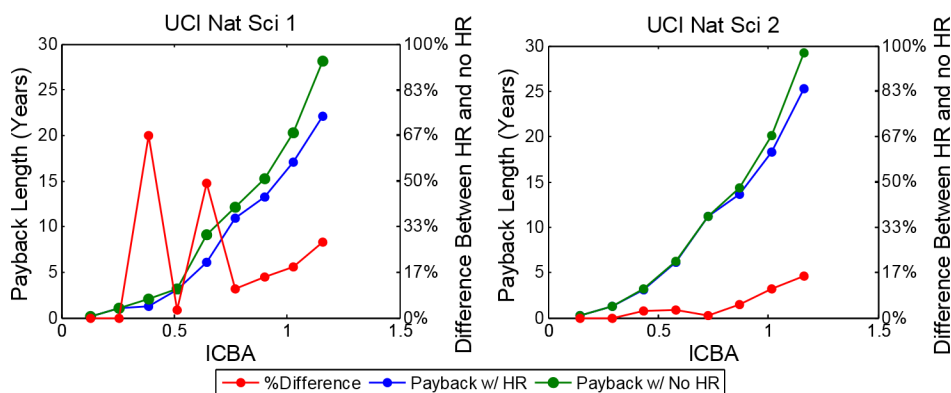
Yearly capacity factor for both UCI Nat Sci1 and UCI Nat Sci2 experience little change due to the addition of heat recovery as shown in Figure 51. The increased capacity factor is most noticeable for both buildings at smaller installed capacities. UCI Nat Sci1 does experience a much greater increase to capacity factor. This increase is primarily due to an increase in the summer mid-peak capacity factor as shown in Figure 52. During this peak period, capacity for smaller installations increase by over a factor of 10 for UCI Nat Sci1. While the increase for UCI Nat Sci2 is nearly 50 percent, this increase is dwarfed in comparison to the increase experienced by UCI Nat Sci1.

80

Figure 51: Change in Yearly Capacity Factor due to the Addition of Waste Heat Recovery Versus ICBA for UCI Nat Sci1 and UCI Nat Sci2
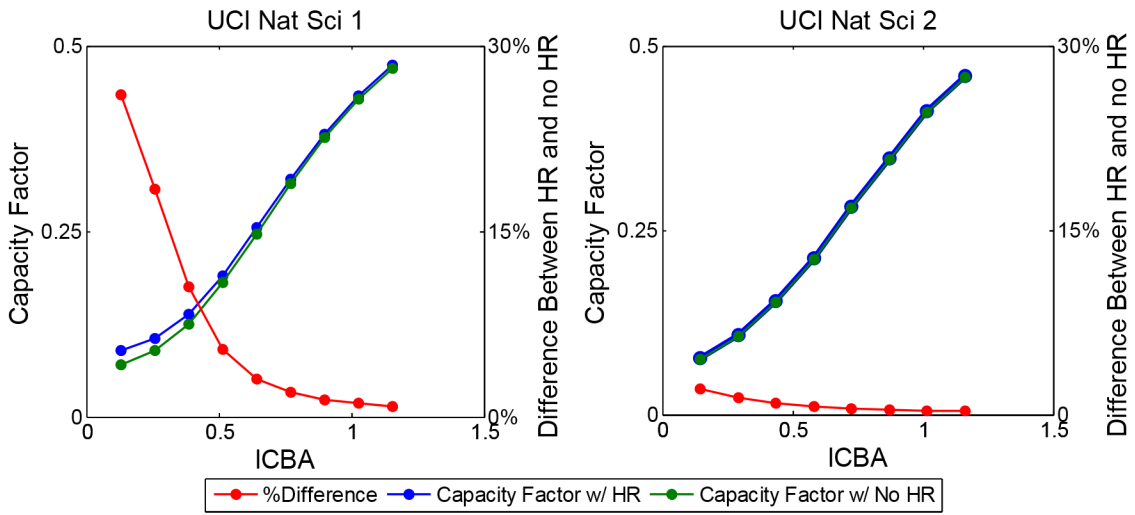
Figure 52: Change in Summer Mid-peak Capacity Factor due to the Addition of Waste Heat Recovery Versus ICBA for UCI Nat Sci1 and UCI Nat Sci2
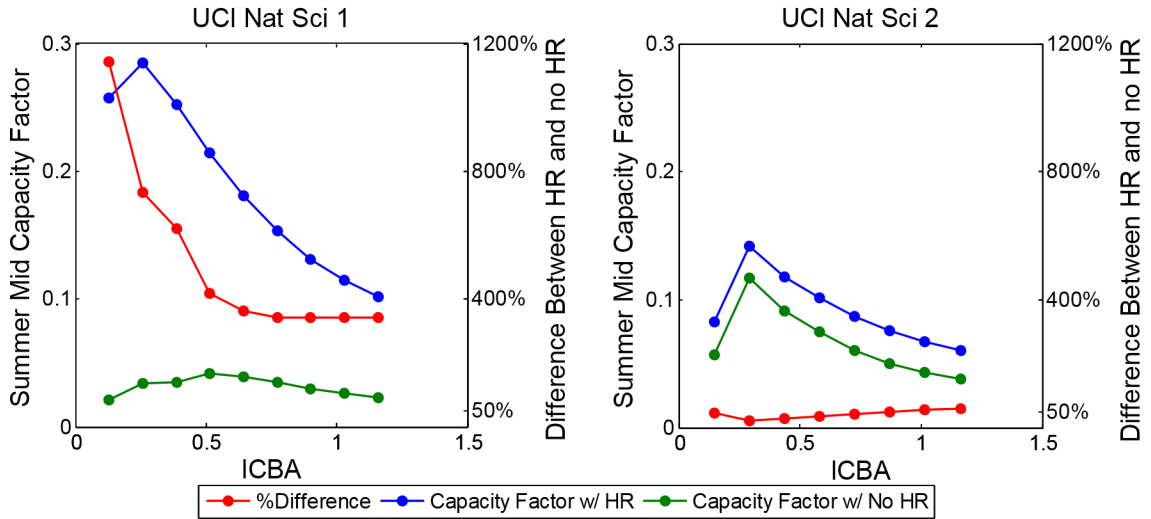
Despite this large increase for UCI Nat Sci1, the actual capacity factor for small installations still remains relatively small and does not translate to a much larger annual capacity factor. This is due to the issue of larger installations of C65 MTGs producing more heat than can fully be utilized by the building. The utilized waste heat, total system efficiency, and portion of the yearly heat load met are shown versus the installed capacity in Figure 53. As capacity increases, waste heat utilized decreases because the building heating demand is not large enough to fully utilize the waste heat produced by the C65 MTGs, leading to decreased capacity factor at higher installations for peak periods such as the summer mid-peak as shown in Figure 52.

Figure 53: Utilized Waste Heat, Percentage of Building Heating Load Met, and Total System Efficiency Versus ICBA for UCI Nat Sci1 and UCI Nat Sci2
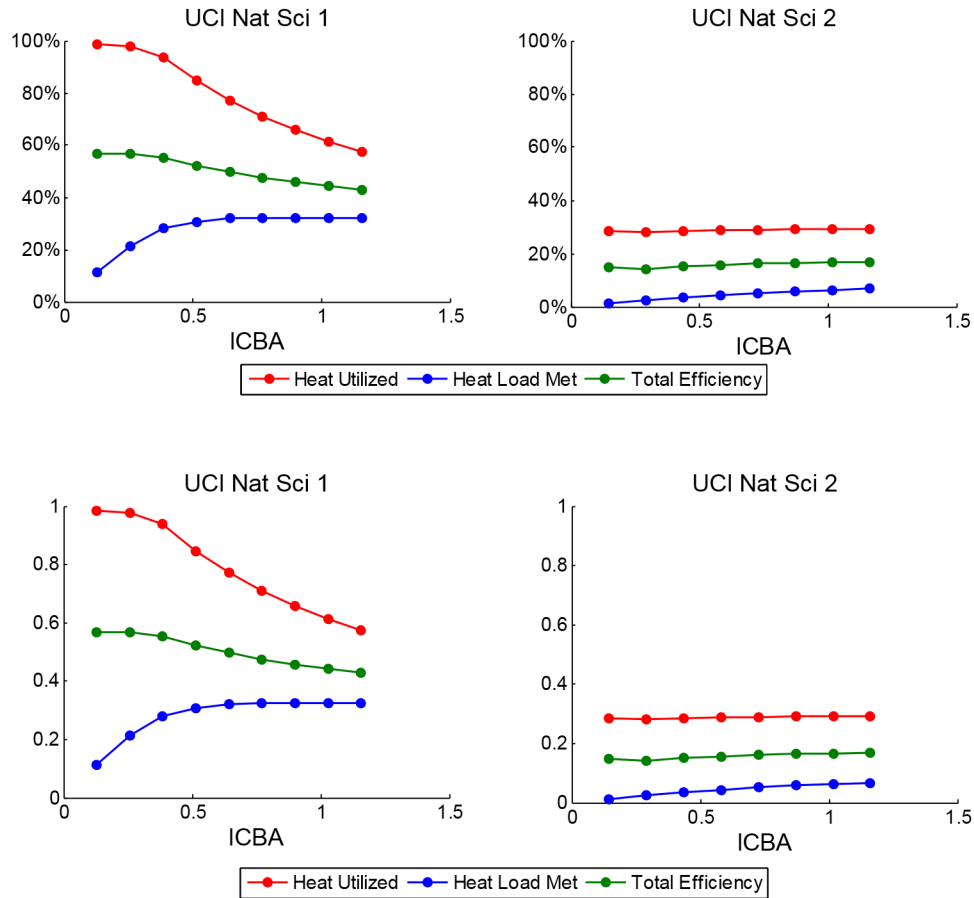
The portion of the heat load met in Figure 53 for UCI Nat Sci1 appears to have semi-asymptotic behavior, turning into a flat line shortly after the capacity of roughly the average electrical demand of the building has been installed. The capacity factor of any building and generator combination is low for peak periods where energy replacement is not possible due to operation only occurring when electrical demand needs to be reduced or maximum demand can be shifted. During these peak periods where energy replacement is not possible, the majority of the heating load is met through firing a gas boiler, not through waste heat capture. As a result, heating loads during entire peak periods, such as all off-peak during summer and winter, are almost exclusively met without using on-site generation and waste heat capture. This leads to the amount of heating load that is actually met through waste heat recovery to be a portion of the total heat load. In order to increase the amount of heating that waste heat capture replaces, generator operation costs must be reduced to the point where it is less expensive to produce electrical and thermal products on-site instead of purchasing them elsewhere.

The largest increase for capacity factor occurs for smaller capacity installations due to the full utilization of the available waste heat. This does not correspond to the largest decrease in payback length. With savings created from demand shifting not increasing once the maximum utility demand has been shifted to off-peak regardless of additional installed capacity, smaller capacity that achieves these demand shifting savings have the smallest payback length. The savings derived from demand shifting are much greater than the savings derived from heat recovery. While demand charge savings drive quick payback, not waste heat recovery, the utilization of waste heat can also produce savings sufficient to warrant the purchase the necessary equipment needed to perform waste heat recovery.

Removing the departing load charge from the cost of O&M, lowering the O&M charge to $0.03 per kWh, allows for a C65 MTG supplying both electricity and heat to perform electrical and thermal energy replacement during the winter mid-peak. The same issues exist during winter mid-peak as for all other peak periods where electrical and thermal energy replacement is possible; both electrical and thermal products produced by the generator must be utilized at the same time and generator operation costs must be low enough to make the products offered by on-site generation economically competitive with the same products offered by local utilities. Of the other potential scenarios, the scenario of a C65 MTG operating with O&M costs of $0.03 per kWh while capturing waste heat is the first case that has potential to perform any type of energy replacement during the winter season.

Payback length for a C65 MTG with waste heat recovery is improved for all systems. The largest improvemensts occer for high load factor buildings with high coincidence between electrical and thermal loads. For these buildings, demand reduction and demand shifting operation do not experience as great of losses due to producing expensive electricity on-site. This is shown in Figure 54, which shows the payback length of all building and genrator combination versus ICBA and ICBM broken down by load factor. While there is still a difference between the different buildings depending on load factor, this difference is smaller when comparing payback length versus ICBM. Buildings with low load factors still benefit from being able to reduce their maximum electrical utility demand using less energy, helping to reduce the production of expensive electricity on-site during periods of little or no thermal demand, but the ability of high load factor buildings to operate at near parity or at lower cost than utility supplied electricity improves the economic and financial potential of on-site generation.

Figure 54: Payback Length Versus ICBA and ICBM Broken Down by Load Factor Assuming Waste Heat is Recovered and an O&M Charge of $0.03 per kWh for the Various Generator-Building Combinations
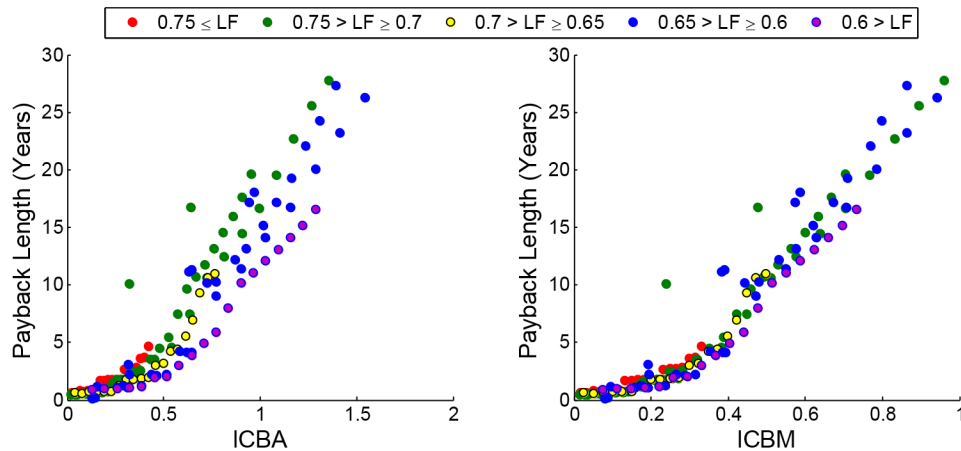
Some buildings with high load factors still experience trouble paying back quickly. This is due to these buildings being unable to reach Tier III natural gas, as shown in Figure 55, which shows the payback length of all building and genrator combination versus ICBA and ICBM broken down by average monthly heating load. Figure 55 shows that buildings that are unable to reach Tier III natural gas are unable to payback as fast as similarlly sized installations at buildings that do reach Tier III natural gas.

Figure 55: Payback Length Versus ICBA and ICBM Broken Down by Average Monthly Heating Load Assuming Waste Heat is Recovered and an O&M Charge of $0.03 per kWh for the Various Generator-Building Combinations
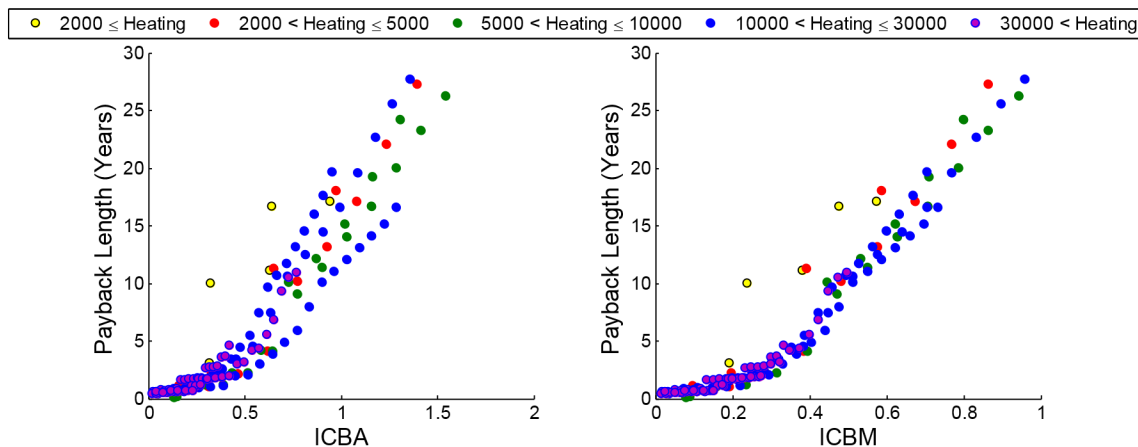
Different behavior is also observed with the yearly capacity factor of the generators. Compared to other scenarios, C65 MTGs with a $0.03 per MWh O&M charge and waste heat recovery can operate during the majority of all on- and mid-peak periods, regardless of season. This causes

84

for the capacity factor of generators to be much higher for smaller on-site capacity while maintaining a quick payback. This is illustrated in Figure 56, which shows the yearly capacity factor versus payback length and ICBA with the building and generator combinations separated by the level of coincidence each building has between its electrical and thermal loads.

Figure 56: Yearly Capacity Factor of DG Versus Payback Length and ICBA Broken Down by Coincidence of Electrical and Thermal Loads Assuming Waste Heat is Recovered and an O&M Charge of $0.03 per kWh for the Various Generator-Building Combinations
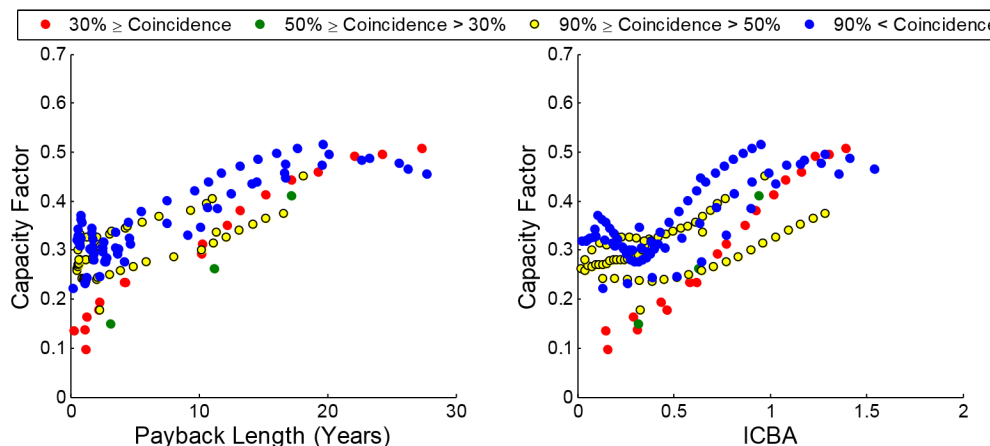
The primary reason for this increase in capacity factor is due to an increase of capacity factor during the winter mid-peak, as shown in Figure 57 for winter mid-peak capacity factor versus payback length and ICBA with the building and generator combinations separated by the level of coincidence each building has between its electrical and thermal loads. Figure 57 shows that buildings with high levels of coincident electrical and thermal loads are able to produce high capacity factors. These high capacity factors are due to the ability of the on-site generation to perform electrical and thermal energy replacement. Similarly sized generators that do not provide a thermal product are only able to provide demand reduction during the winter season and have much lower capacity factors for the same payback length and installed capacity.

85

Figure 57: Winter Mid-peak Capacity Factor of DG Versus Payback Length and ICBA Broken Down by Coincidence of Electrical and Thermal Loads Assuming Waste Heat is Recovered and an O&M Charge of $0.03 per kWh for the Various Generator-Building Combinations
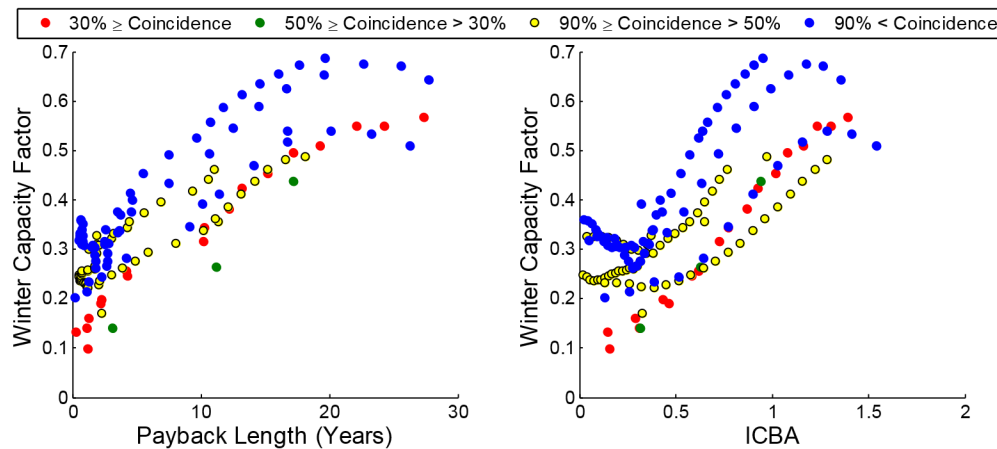
Despite these improvements in the generators ability to perform energy replacement during the winter, a C65 MTG is unable to produce electricity at a less expensive rate during off-peak for the entire year. Both summer and winter off-peak consist of approximately 63 percent of the year. While operation during off-peak may not be desired, any improvement that allows for energy replacement during off-peak also improves cost reducing operation during all other peak periods.

Examining individual buildings reveals the benefits of being able to operate with a $0.03 per kWh O&M charge with waste heat recovery. Comparing UCI Nat Sci1 to UCI Nat Sci2 shows that the ability to perform energy replacement during winter mid-peak period improves the economics of on-site generation while also allowing for a larger capacity factor. This analysis was performed by comparing the scenario where the generator is providing electricity only to the scenario where both electric and thermal products are available. For both scenarios, an O&M cost of $0.03 per kWh is used. The dispatch strategy operating a single microturbine is shown for UCI Nat Sci 1 in Figure 58 and UCI Nat Sci 2 in Figure 59. While the two buildings both have a large thermal load, it is apparent from comparing the two figures that UCI Nat Sci 1 has a much more coincident thermal load than UCI Nat Sci 2. In fact, the UCI Nat Sci 2 thermal demand, which consistently has a larger thermal demand than UCI Nat Sci 1, is punctuated by short periods of very large demand followed by no demand at all. This difference is also apparent in the dispatch of the microturbine. During mid-peak, the microturbine at UCI Nat Sci 1 is consistently operated due to a highly coincident thermal demand. The UCI Nat Sci 2 microturbine is operated sporadically, whenever there is coincidence between the electrical and thermal loads. This behavior exhibited by both UCI Nat Sci 1 and UCI Nat Sci 2 is typical of any generator that needs heat recovery in order to provide energy replacement.

Figure 58: Dispatch Strategy for a Single Microturbine Highlighting Electrical and Thermal Energy Replacement for UCI Nat Sci 1 during a Typical Winter Week Assuming O&M cost of $0.03 per kWh
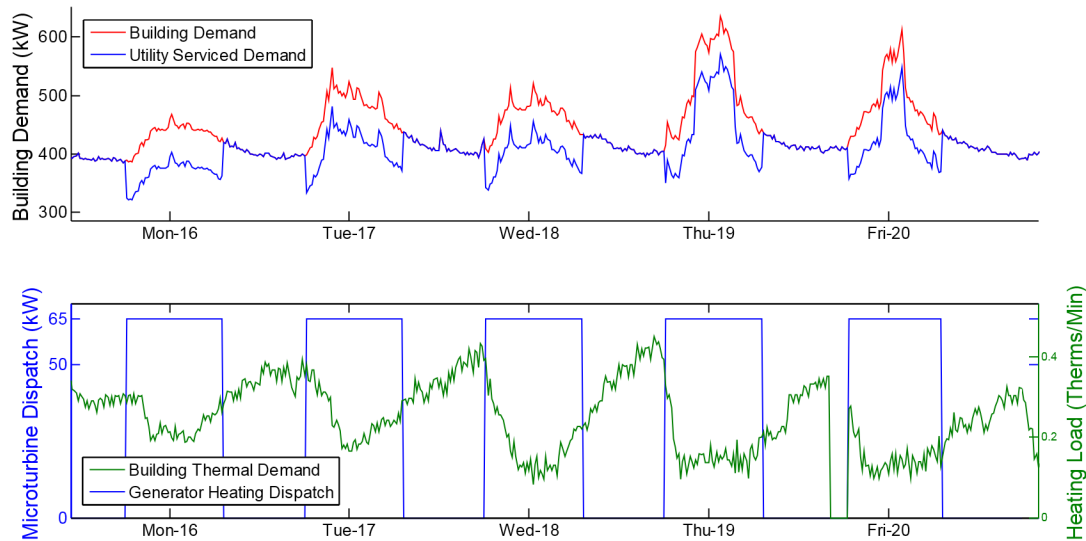
Figure 59: Dispatch Strategy for a Single Microturbine Highlighting Electrical and Thermal Energy Replacement for UCI Nat Sci 2 during a Typical Winter Week Assuming O&M cost of $0.03 per kWh
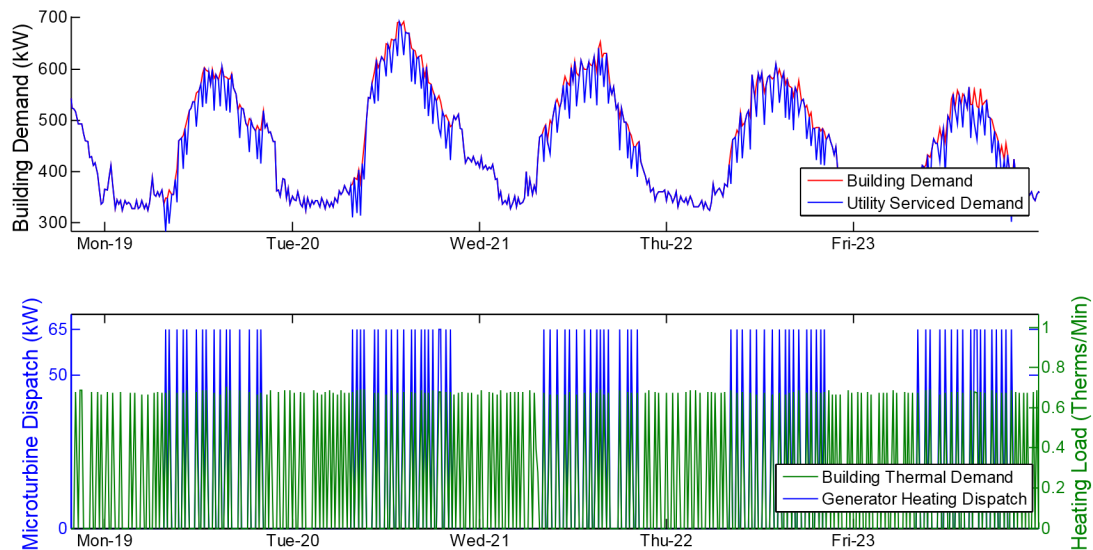
A single microturbine installed at either UCI Nat Sci 1 can only meet a fraction of the buildings electrical demand and more microturbines must be installed if a large portion of the electrical load is to be met on-site. However, as more microturbines are installed, their ability to provide electrical and thermal energy replacement is diminished due to the fact that much more heat

than is needed is available from the microturbines. As a result, even for a building with a highly coincident thermal load, if the thermal load is not large enough, only a portion of the installed capacity can be utilized to electrical energy and thermal energy replacement. This is evident in Figure 60, which shows four microturbines with a total capacity of 260 kW installed at UCI Nat Sci 1 during a typical summer day. Due to this plot being taken from a summer day, on-peak electrical energy replacement is possible without the assistance of heat recovery. However, this portion of the dispatch is ignored in order to simplify Figure 60, and only energy replacement is considered when heat recovery is needed. Despite having a total capacity of 260 kW, the full capacity of the generator is not used through the entire week for the purposes of electrical energy and thermal energy replacement. Even though the thermal load is coincident with the electric load, not enough thermal demand exists to use the full capacity of the microturbines, and capacity factor during mid-peak is reduced. As microturbine capacity is installed, more heat must be utilized for electrical energy and thermal energy replacement. If that heat is not utilized, operation of the microturbines is either reduced or blocked.

Figure 60: Dispatch Strategy for Four Microturbines with a Total Capacity of 260 kW Highlighting Electrical and Thermal Energy Replacement for UCI Nat Sci 1 during a Typical Summer Week Assuming O&M Cost of $0.03 per kWh
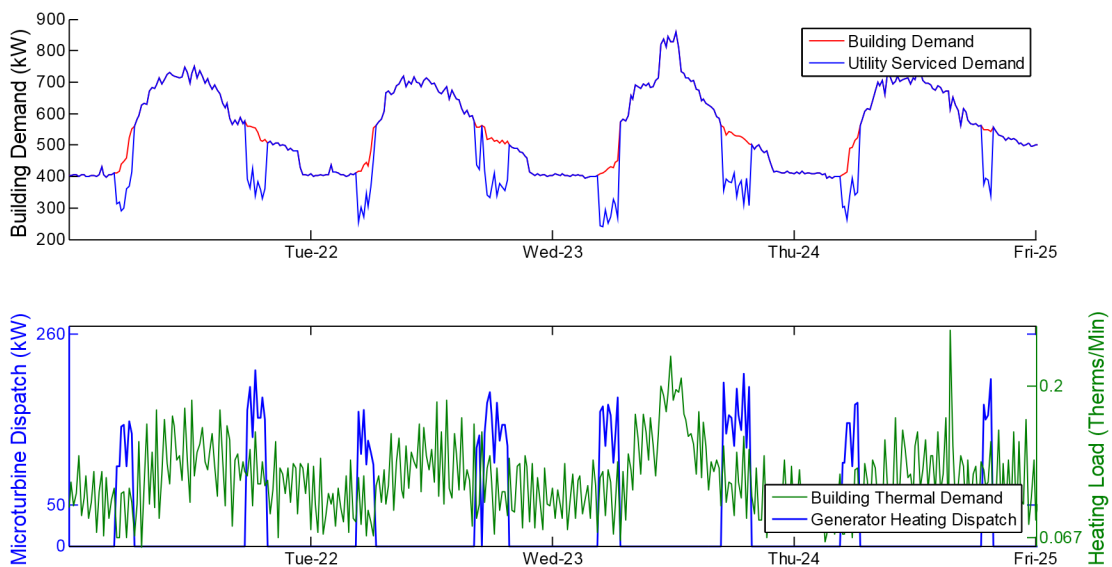
Figure 61 shows the payback length for UCI Nat Sci1 and UCI Nat Sci2 versus ICBA. Reduction in payback length occurs for both buildings except for generators that can meet only a small portion of the average electrical demand. This reduction is consistently greater for UCI Nat Sci1 due the higher level of coincidence between the electrical and thermal loads, allowing for more of the generator waste heat to be utilized. The greatest reduction for UCI Nat Sci1 occurs for installed capacity that had a payback length of approximately 10 years. This level of installed capacity was unable to payback when producing electricity only during the life of the loan used

to cover the capital cost of on-site generation. The capture and utilization of waste heat allows for this investment to payback before the length of the loan, causing for a large decrease in the length of payback.

Figure 61: Change in Payback Length due to the Addition of Waste Heat Recovery Versus ICBA for UCI Nat Sci1 and UCI Nat Sci2 with $0.03 per kWh O&M Charge
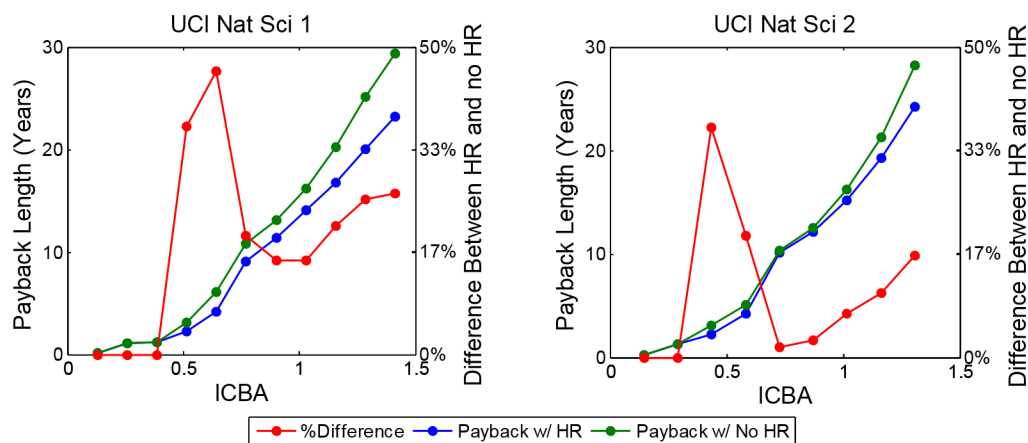
Capacity factor also increases for both building, as seen in Figure 62 which shows the change in capacity factor versus ICBA. Both buildings experience large increases in capacity factor, as opposed to the slight increase in capacity factor for generators operating with an O&M charge of $0.04493 as seen in Figure 52. By utilizing the waste heat produced by generators at these buildings, the peak period where energy replacement is possible has been expanded from summer on-peak to include both summer and winter mid-peak. Again, UCI Nat Sci1 experiences a greater change in capacity factor due to the high level of coincidence between its electrical and thermal loads. However, for both buildings, the capacity factors of on-site generation with and without waste heat recovery become equivalent at larger levels of installed capacity. At these larger levels of installed capacity, demand reduction occurs more often, resulting in increased generator operation to maximize the demand reduction potential of the on-site generation. Even though a difference is not seen between generators capable of waste heat recovery and generators that are not, capturing waste heat for these larger installations assist in reducing payback length.

Figure 62: Change in Yearly Capacity Factor due to the Addition of Waste Heat Recovery Versus ICBA for UCI Nat Sci1 and UCI Nat Sci2 with $0.03 per kWh O&M Charge
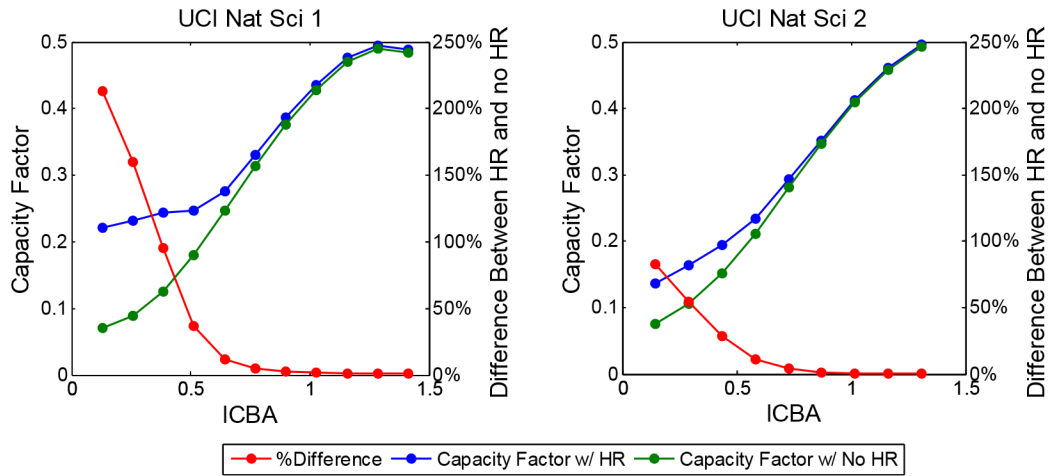
3.2.2   Parent Utility Electric Rates

Standby rates are applicable for customers who have on-site generation. SCE, however, has ultimate discretion on what rate is applied to a customer. Results from previous section has shown that, unless additional charges such as the departing load charges are relaxed and much of the generator waste heat is recovered and used, it is difficult to perform any form of energy replacement throughout the year. As a result, maximum savings for most buildings come from small installations that meet only a fraction of the building electrical load but are large enough to shift maximum summer demand from on-peak to mid- or off-peak, reducing the rate at which demand charges are applied. SCE can decide that the building load met by on-site generation is not sufficient to warrant the use of standby rates and shift the customer back to parent rates applicable to buildings that do not generate electricity on-site.

Demand shifting does not have the same value for parent rates as it does for standby rates. During the summer, on- and mid-peak each have their own separate demand charge that is applied to the maximum utility demand that occurs during the applicable peak period in addition to the non-TOU demand charge that is applied to the monthly maximum utility demand. Shifting the monthly maximum utility demand away from on- and mid-peak to off-peak does not reduce the rate at which all demand charges are applied as it does with standby rates, it only reduces the maximum utility demand used to determine the on- and mid-peak demand charges. As a result, the economic demand strategy shifts from attempting to shift maximum utility demand to minimizing the maximum utility demand during each individual peak period in addition to attempting to perform energy replacement whenever possible.

Fuel and O&M cost are independent of electric rate structure and the cost of energy produced from a C65 MTG are the same as shown in the previous section.

90

3.2.2.1 Electric Only Analyses

Economic dispatch for the parent rate structure can occur according to two different rate structures; TOU-A and TOU-B. Generator dispatch changes between these two rate structures based off of the different energy and demand charges.

TOU-B Rate Structure

Dispatch under the TOU-B rate structure uses the same energy charges as dispatch using the standby rate structure. With the value of demand shifting being reduced, demand charge savings are produced by reducing maximum utility demand during the individual peak periods during the summer and monthly maximum utility demand during the winter. Demand charge reduction depends on installed capacity. Figure 63 shows the percentage of standby demand charge reduction realized under the parent rate structure versus ICBA and separated by load factor. Figure 63 compares the difference in demand charge reduction between parent and standby rates for the same building and generator combinations. Demand charge reductions are significantly reduced for small installations, but as installed capacity increases, parent rate demand charge reductions surpass standby rate demand charge reductions. This occurs because operation under the standby rate structure allowed maximum utility demand during summer off-peak to increase in order to ensure that demand charge rates are reduced as much as possible. Parent rate operation minimizes maximum utility demand during all peak periods, reducing maximum utility demand during off-peak periods.

Figure 63: Percent of Standby Demand Charge Reduction Realized under Parent Rate Structures Assuming O&M cost of $0.04493 per kWh for the Various Generator-Building Combinations
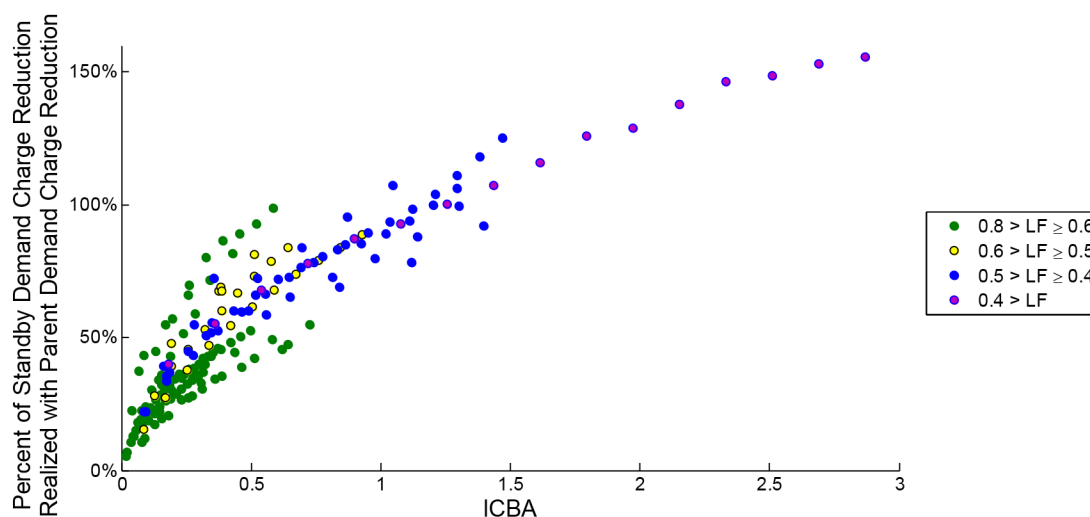
These reductions in parent rate demand charges occurs at the expense of meeting a larger portion of the building load, as seen in Figure 64, which shows the percent of building load met by on-site generation versus ICBA. The C65 MTG is mostly unable to produce electrical energy at a lower cost than what is offered to the customer by SCE, causing for savings derived from demand charge reduction to be offset by losses produced from generating electricity on-site.

Figure 64: Percent of Building Load Met Versus ICBA Assuming O&M Cost of $0.04493 per kWh for the Various Generator-Building Combinations
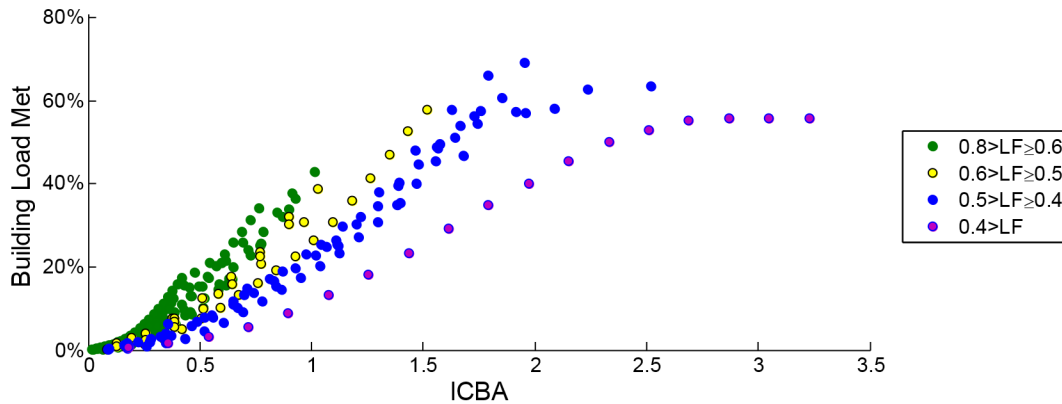
The additional electrical energy on-site reduces total savings. This combined with savings from demand shifting being nonexistent cause for total energy savings under parent rate structures to be a fraction of standby rate savings. This is shown in Figure 65, which shows the percentage of standby rate structure savings that are produced under parent rate structures versus ICBA and separated by load factor. Figure 65 compares the difference in savings between parent and standby rates for the same building and generator combinations.

Figure 65: Percent of Standby Total Energy Savings Realized under Parent Rate Structures Assuming O&M Cost of $0.04493 per kWh for the Various Generator-Building Combinations
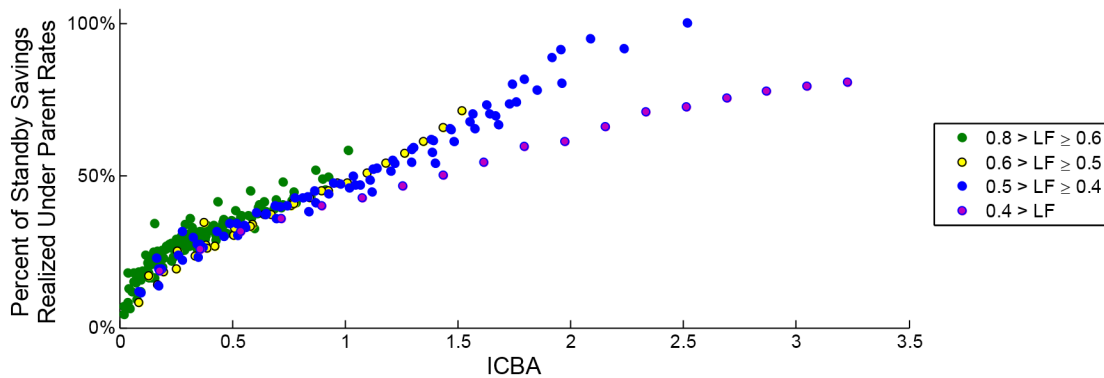
Savings are reduced when using the parent rate structure, especially for smaller installations, which have virtually all standby rate savings disappear. A larger portion of standby savings are realized as more on-site capacity is installed. However, it was shown that payback length is extended with larger installations due in part to the inability of total energy savings to offset the required loan payments to cover the capital cost of installing C65 MTGs. This inability to cover

the loan payments is increased further for the parent rate structure, which have savings that are a fraction of standby rate savings. This inability to cover the loan payments is shown in Figure 66, which shows the percentage of total energy savings that are required to cover the corresponding loan payment versus ICBA. For Figure 66, all loan payments are larger than 100 percent of the savings produced from C65 MTG operation. The portion of loan payments not met by energy savings are met by the customer, ensuring that payback for all building and generator combinations will not be met until the loan has been paid off and the original capital along with additional investment required to make the loan payments are recovered. Figure 66 shows that buildings with lower load factors are able to more closely meet their loan payments with their energy savings at larger installations, but no building and generator combination is able to meet their monthly loan payments with total energy savings alone.

Figure 66: Percentage Total Energy Savings that are Equivalent to Loan Payment Versus ICBA Assuming O&M Cost of $0.04493 per kWh for the Various Generator-Building Combinations
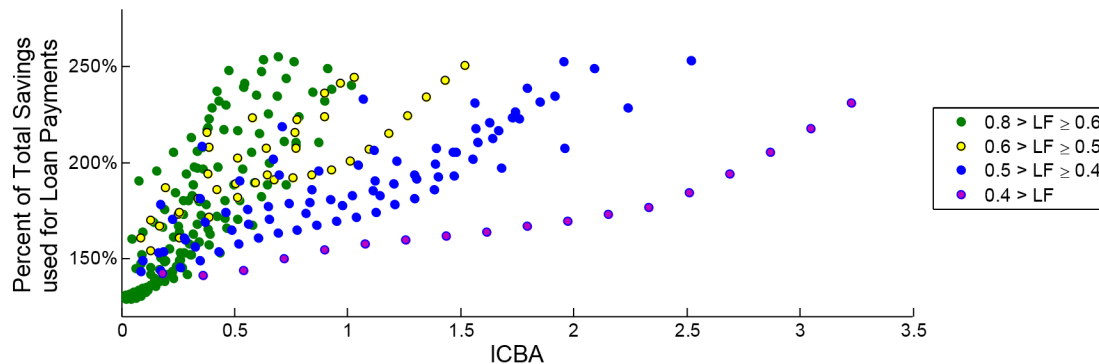
Payback, as a result, does not happen for any building before the end of the life of the loan, as seen in Figure 67. Figure 67 shows payback length for all building and generator combinations versus ICBA and ICBM, separated by building load factor. As with standby rates, there is a distinction between how much on-site generation can be installed on-site, with buildings with low load factors accepting more on-site generation than buildings with high load factors. Also, buildings with load factors greater than 0.8 that did pay back under standby rates do not pay back under the parent rate structure and are not shown in Figure 67. Regardless of a building size that is able to accept more or less on-site generation, the smallest installations take over 15 years to pay back and installing additional on-site capacity is shown to extend the length of the payback period.

Figure 67: Payback Length Versus ICBA and ICBM Assuming O&M Cost of $0.04493 per kWh for the Various Generator-Building Combinations
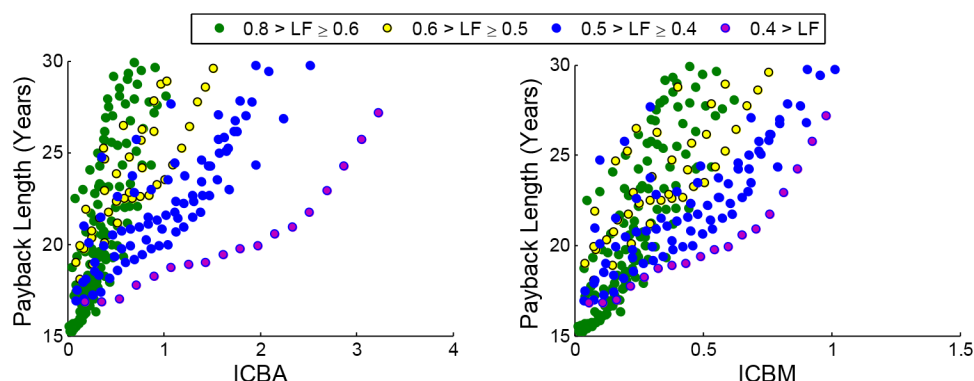
This long payback does not mean that reduced energy costs are not produced, just that the savings are unable to overcome the loan payments required to purchase the generator. Payback length is directly linked to the ability or inability of the energy savings to meet the cost of capital. Figure 68 shows the percentage of total energy savings that are required to cover the corresponding loan payment versus payback length. By reducing the percentage total savings required to pay off the corresponding loan payment, payback length is reduced, which can be accomplished by either increasing the total energy savings or reducing capital cost.

Figure 68: Percentage Total Energy Savings that are Equivalent to Loan Payment Versus Payback Length Assuming O&M Cost of $0.04493 per kWh for the Various Generator-Building Combinations
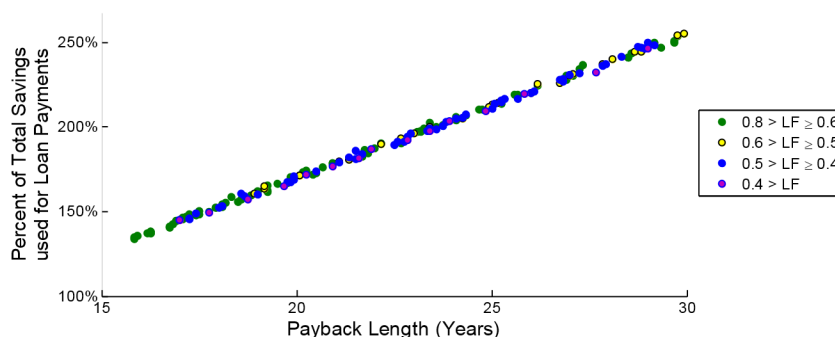
Capacity factor, as shown in Figure 69, increases as installed capacity increases. With the C65 generator unable to produce electricity at a less expensive rate than what can be purchased from SCE, generator operation occurs primarily due to demand reduction. Further increased generation has larger demand reduction potential but must operate more often to reduce demand. Capacity factor increases due to increased operation required to reduce demand

charges for all buildings except for low load factor buildings. Capacity factor increases then decreases for low load factor buildings because while the larger installations are capable of more demand reduction than smaller installations, the highly dynamic nature of low load factor buildings only utilize the fully full capacity of on-site generation for short periods of time. Operation time of on-site generation increases with larger installations but the average power setting decreases with increased capacity for low load factor buildings. This results in the decreasing capacity factor for some low load factor buildings.

Figure 69: Annual Capacity Factor Versus ICBM and Payback Length Assuming O&M Cost of $0.04493 per kWh for the Various Generator-Building Combinations
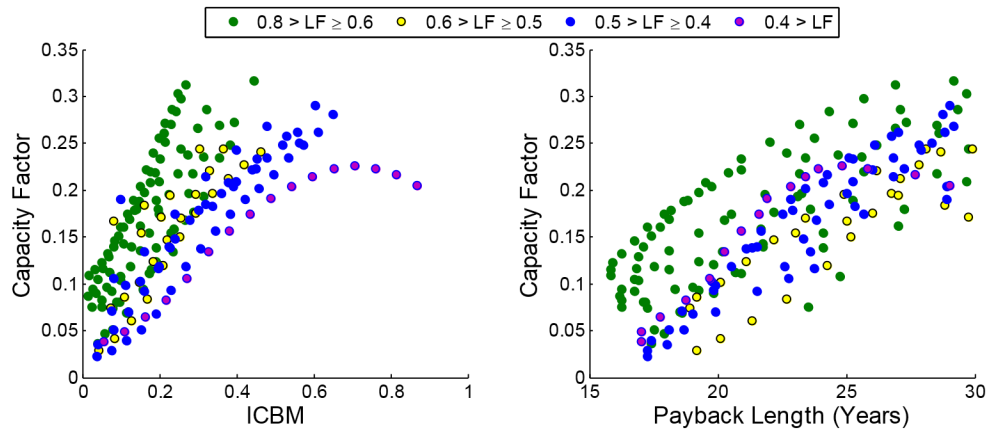
Reducing O&M cost by eliminating the departing load charge does not make energy replacement possible during any other peak period that was not possible before but does lead to some improvement to the economic performance of C65 MTGs; the lower O&M cost reduce losses generated by producing expensive electricity on-site. Capacity factor for the reduced O&M cost does not differ from Figure 69. Payback length is reduced for all building and generator combinations, however, the increased energy savings cannot meet the required loan payments, and payback does not occur until after the life of the loan, as shown in Figure 70, which shows payback length versus ICBA and ICBM for all building and generator combinations assuming an O&M cost of $0.03 per KWh.

Figure 70: Payback Length Versus ICBA and ICBM for all Building and Generator Combinations Assuming O&M Cost of $0.03 per kWh for the Various Generator-Building Combinations
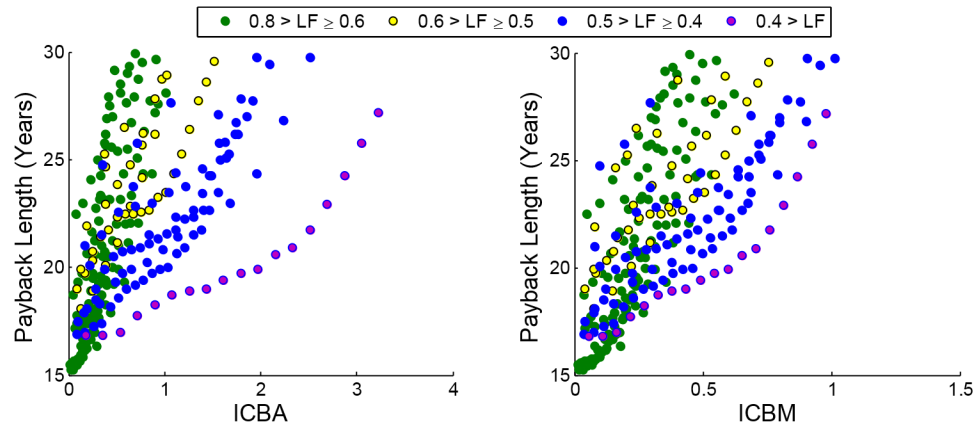
TOU-A Rate Structure

The only building that prefers TOU-A for its baseline electrical rate is UCI ELF, which also experiences the highest electrical costs per kWh. Besides UCI ELF, using the TOU-A rate to determine the cost of utility electricity does not result in payback for any other building and generator combination. Since the cost of electricity produced by a C65 MTG is generally more expensive than what can be purchased from SCE, the goal of operation is to reduce or eliminate the building electrical load dynamics that result in a low load factor and high demand charges. The TOU-A rate only works with a building that has the lowest load factor, and all other buildings experience a rise in overall electricity costs when switching their building to the TOU-A rate structure, as shown in Table 15 with the difference between the baseline rate (TOU-B for all buildings besides UCI ELF) and the other rate option. This cost increase eliminates any savings from using on-site generation, blocking payback from occurring.

Payback does occur for the UCI ELF, as seen in Figure 71, which shows payback length versus ICBA and ICBM for UCI ELF. Prior work has shown that buildings with low load factors are capable of accepting more on-site generation than buildings with high load factors, and UCI ELF is no exception. As with all other buildings, the amount of building load that is met increases as more on-site capacity is installed, as seen in Figure 72. Payback length also increases in part due to replacing less expensive utility electricity with more expensive electricity generated on-site.

Figure 71: Payback Length Versus ICBA and ICBM for UCI ELF under TOU-A Rates Assuming O&M Cost of $0.04493 per kWh
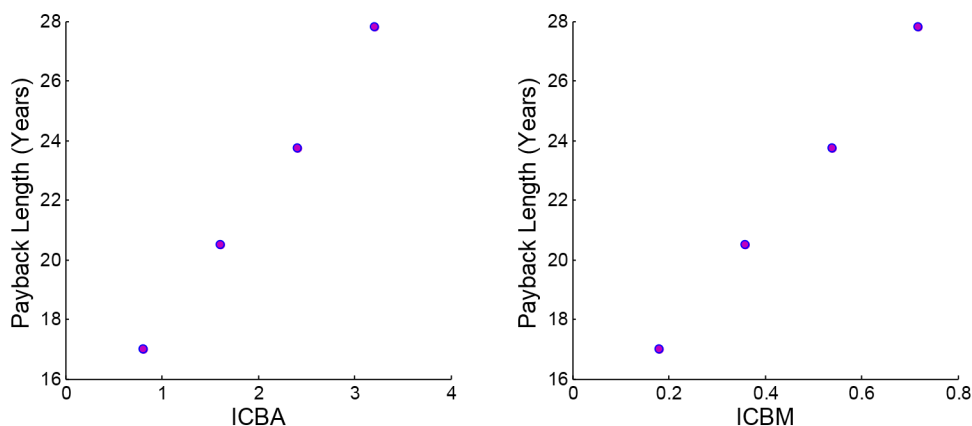
Figure 72: Building Load Met Versus ICBM and Payback Length for UCI ELF under TOU-A Rates Assuming O&M Cost of $0.04493 per kWh
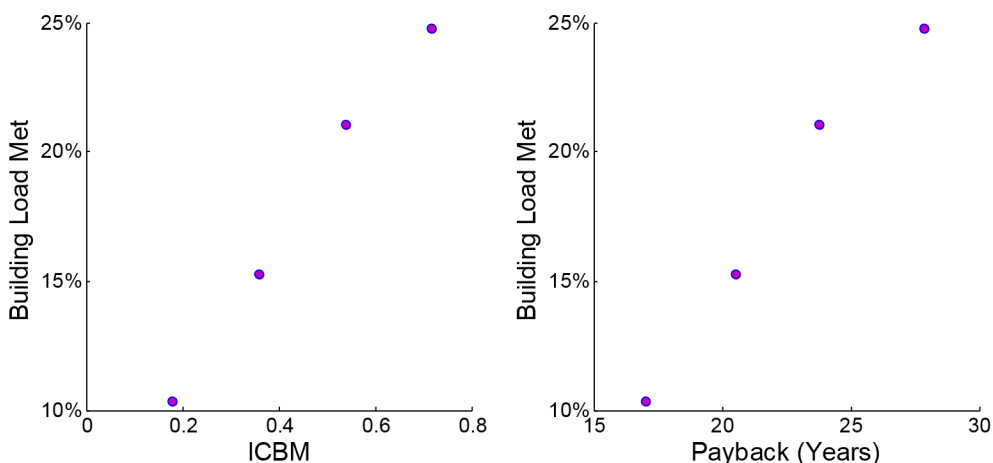
Capacity factor, as seen in Figure 73 versus ICBM and payback length, decreases with more on-site capacity. Due to the extremely dynamic nature of the UCI ELF building, the on-site generation is used sparingly since the demand surge that can be eliminated are short in duration. Also, as on-site generation increases, the full capacity of the generators is not required to meet every demand surge and only a portion of the on-site generation is used to reduce maximum utility demand, reducing capacity factor further. Reducing O&M cost to $0.03 per kWh reduces payback length slightly, as seen in Figure 74. However, capacity factor and building load met does not change.

Figure 73: Yearly Capacity Factor Met Versus ICBM and Payback Length for UCI ELF under TOU-A Rates Assuming O&M Cost of $0.04493 per kWh
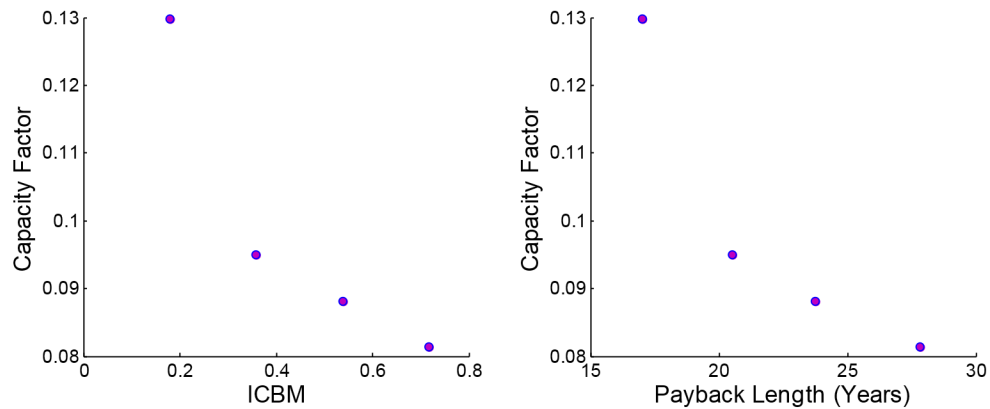
Figure 74: Payback Length Versus ICBA and ICBM for UCI ELF under TOU-A Rates Assuming O&M Cost of $0.03 per kWh
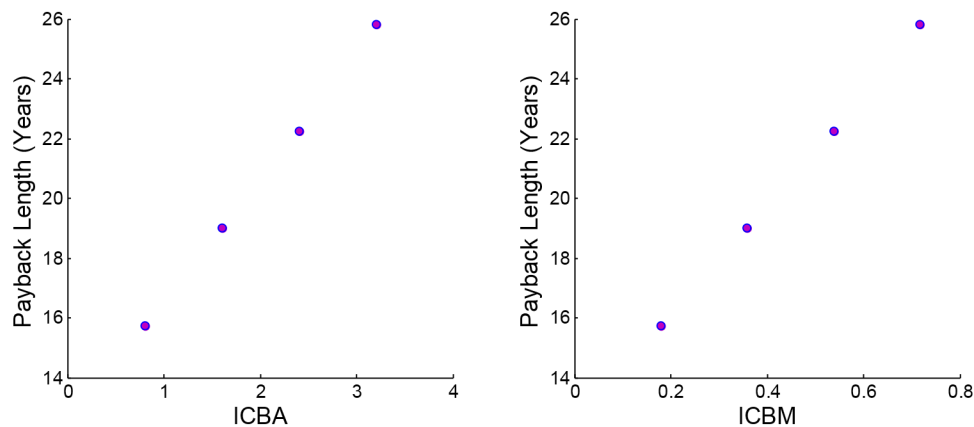
3.2.2.2 Heat Recovery Analyses

Each building that has a corresponding heating load prefer TOU-B over TOU-A for the baseline cost of electricity. Due to this, any building that prefers TOU-B must overcome the cost difference between TOU-B and TOU-A in addition to loan payments if the building is switched over to TOU-A when on-site generation is added. No building and generation combination is capable of this when heat recovery is added while installing C65 MTGs, just like it was not possible for building and generator combinations where only electricity was generated on-site. With no building and generator combination paying back under TOU-A, payback analysis only occurs for building and generator combinations operating under TOU-B. It is possible for a generator that offered both electricity and heat that is installed at a building that prefers TOU-A

to payback, but none of the building models used for examining heat recovery prefer TOU-A for their baseline electricity costs.

Payback length is reduced as a result of heat recovery for both O&M costs of $0.04493 and $0.03 per kWh. Figure 75 and Figure 76 show payback length versus ICBA and ICBM for O&M cost of $0.04493 and $0.03 per kWh respectively. The same issues of requiring coincidence between electrical and thermal loads, significant heat recovery, and the least expensive natural gas exist under the parent rate structure. Both Figure 75 and Figure 76 show that for smaller installations, the buildings with the largest heating loads, which also tend to be the most coincident for the models used, pay back the quickest. Reducing O&M cost by eliminating the departing load allows for heat and energy replacement to be possible during the winter mid-peak, which is reflected by the on-site generation investment paying back the fastest of all scenarios presented, as seen in Figure 76.

Figure 75: Payback Length Versus ICBA and ICBM Assuming Parent Rate Structure, Waste Heat is Recovered, and an O&M Charge of $0.04493 per kWh for the Various Generator-Building Combinations
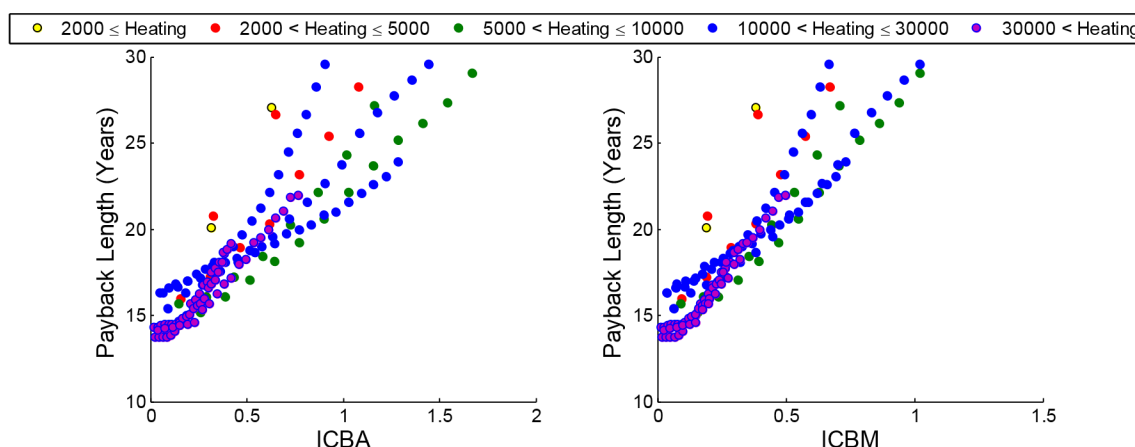
Regardless of these results, it is apparent that attempts to reduce O&M cost and include heat recovery cannot match the savings generated by demand shifting that can be accomplished when operating under utility standby rates. The high operating cost and difficulty of providing energy replacement associated with using C65 MTGs hamper the economic attractiveness of this form of generation under parent and standby rates, but it is obvious that standby rates, not the parent rates, are much more favorable to this form of DG.

3.3   Improvements to C65 Microturbine Economic Performance

The results in Section 3.1 and 3.2 showed that it can be difficult for a C65 MTG to perform economic energy replacement unless Tier 3 natural gas is being available. During the winter season, utilization of the heat produced by a C65 MTG is necessary for economic energy replacement to be realized. If these requirements are not met, a C65 is limited to demand reduction and economic energy replacement during summer on-peak, which consists of approximately five percent of the year. Under both the standby and parent rate structures, it is difficult for large installations of C65 MTGs to produce enough savings to pay back the required initial investment quickly. While these results are accurate, the whole microturbine potential is not recognized or fully covered.

The preceding analysis assumed that the base operations and maintenance cost is $0.03 per kWh (the additional departing load charge is due to operating within the SCE service area) and capital cost of a C65 MTG is $2700 per kW. Both of these costs are relatively high and have an adverse effect on economic performance; the high operations and maintenance cost suppresses economic energy replacement while the high capital cost stifles quick payback of the initial investment.

While the operations and maintenance and capital cost are accurate, they are not guaranteed to be the true cost of every C65 MTG or other commercially available MTG. Lower operations and

maintenance cost may be achieved through increased operation. This increased operation may operate outside the economic dispatch strategy developed through this work, but can be a method for lowering operations and maintenance cost. More importantly, as MTGs achieve greater market penetration and the number of generators requiring maintenance increases, operations and maintenance cost will decrease as competition to meet the larger maintenance requirement increases.

Capital cost is a combination of the purchase cost of the generator from the manufacturer and the cost to install the generator on-site. Similar to maintenance cost, the purchase cost of the generator will decrease as the demand for MTGs increase due to lower production cost for manufacturers. Installation cost depends on complexity of the installation and decreases for buildings and structures where installation is simple. As a result, it is currently possible to install a C65 MTG with lower capital cost than is assumed in this study.

The possibility of having lower operations and maintenance and capital cost is very real. Lowering operations and maintenance cost significantly improves the ability of a C65 MTG to perform economic energy replacement while lowering capital cost reduces the savings that must be realized in order to pay back the initial investment. However, instead of only performing a parametric study covering lower operations and maintenance costs as well as capital costs in an effort to only show the economic potential of a C65 MTG, the varied parameters are expended to include other factors to include other DG technologies. The results of this parametric study are discussed in the next section.

3.4   Parametric Study

Section 3.2 discussed the economics of using C65 MTGs to provide on-site generation. The models used to accomplish this can be modified to capture the behavior of other types of generators, such as larger MTGs, reciprocating engines, and fuel cell systems. Performing this for individual generators can provide valuable insights into the economics associated with these generators, but a parametric study examining a wide range of generator characteristics can determine which operating characteristics and economic factors most significantly contribute to cost effective dispatch of DG. Previous sections showed the importance of the building heating load impact on fuel cost as well as heat recovery analysis. As a result, only buildings with heating loads were examined in the current parametric study.

The installed capacity versus building average (ICBA) and installed capacity versus building maximum (ICBM) ratios are used extensively in this section. ICBA is the capacity of installed generation over the average electrical demand of the building. ICBM is the capacity of installed generation over the maximum electrical demand of the building. Increasing the amount of DG installed at a building increases both ICBA and ICBM. Due to the large differences in building load size and behavior, ICBA and ICBM are used to normalize the amount of installed generation between the buildings. Instead of discussing absolute amount of installed capacity at each building, ICBA and ICBM relates the amount of installed capacity to how much of the building average and maximum electrical demand can be met by the installed generation.

Capacity factor is used throughout this study as a tool for comparing the operation of different size generators to each other. Since heat recovery is being considered for part of this study, it is possible to define capacity factor as the amount of energy used by the generator, both thermal and electrical, versus the amount of energy that could have been produced over the simulation time. However capacity factor for all analysis is considered to only be the amount of electrical energy produced versus the amount of electrical energy that could have been produced. Thermal energy is considered by examining how much of the thermal energy produced by the generator is utilized; it is not directly considered in the calculation of capacity factor.

3.4.1 Standby Electric Rates

3.4.1.1 Electric Only

<u>Efficiency, O&M, and Fuel Cost Effects</u>

Economic DG operation occurs when the cost of energy for a building can be reduced. Demand charge reduction occurs regardless of the cost of producing energy on-site. However, savings from reduced demand charges decrease if grid electricity is replaced with more expensive electricity generated on-site. During periods when demand reduction is not needed, energy replacement using DG occurs only when energy produced on-site is less expensive than what can be purchased from a utility. In contrast with demand charge reduction, efficiency, O&M cost, fuel cost, and the cost of grid electricity dictate whether or not energy replacement can occur. Capacity factor of an installed system depends on how much these cost reducing activities can be performed. Capacity factor for UCI Bren and Patton State Hospital using the economic dispatch strategy and a generator sized to half the average applicable building load is shown in Figure 77.

Figure 77: Predicted Capacity Factor Versus Electrical Efficiency for a) UCI Bren and b) Patton State Hospital using Economic Dispatch Strategy. Installed Systems are sized to 50% of Average Building Load
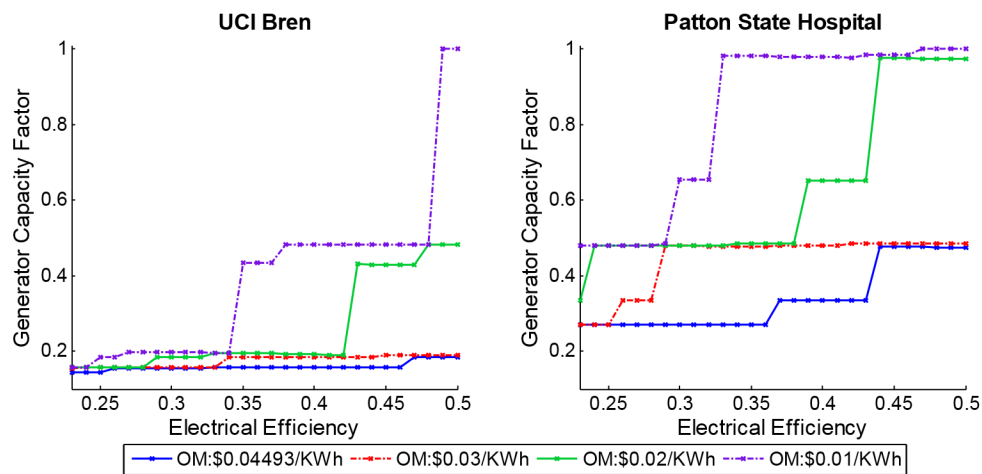
Capacity factor for all systems is lowest when DG efficiency is also low, with demand reduction being the only cost reduction activity available to the DG. While increasing efficiency reduces operating cost for the DG, the cost of electricity is not continuous and an increase in efficiency does not translate into a linear increase in capacity factor. For each electrical peak period, an efficiency target must be met in order for energy replacement to occur. Prior to reaching this efficiency target, increases to efficiency only improve savings during peak periods where energy replacement was already possible. Energy replacement for other peak periods, however, is not allowed until the applicable efficiency target is surpassed. Once this target has been surpassed, energy replacement is possible for the entire new peak period, leading to a step increase in capacity factor. The efficiency target for the winter mid peak is shown in Figure 78.

A system that does not meet the target presented in Figure 78 for a given fuel and O&M cost can still potentially provide energy replacement during more expensive summer on- and mid-peak periods, but, referring to Figure 26, this operation is limited to approximately 13 percent of the year, and demand reduction is the only cost reducing activity during the winter. Even with the inclusion of winter mid-peak, if a system is unable to operate during any off-peak time, energy replacement is blocked for approximately 63 percent of the year.

Another way to improve capacity factor is through reduced O&M costs. For both buildings, higher O&M suppress DG operation but the effects differ between buildings. While UCI Bren struggles to have a capacity factor higher than 20 percent for high O&M, Patton State Hospital achieves a capacity factor of nearly 50 percent. This capacity factor for the highest O&M charge ($0.04493 per kWh) only occurs at extreme efficiencies unachievable by current and projected MTGs. Reducing O&M to $0.03 per kWh leads to capacity factors of 50 percent at 30 percent efficiency. The difference between the $0.03 per kWh and $0.04493 per kWh charge is the departing load charge applied to buildings serviced by SCE.

While much can be explained using the electrical energy rate structures and O&M costs, there is a fundamental difference between the capacity factors of the two buildings shown in Figure 77. Patton State Hospital has a thermal load that is 34.6 times larger than the thermal load for UCI Bren. Despite the difference, both buildings use the same natural gas rate structure; before the least expensive Tier 3 is available, 4163 therms of Tier 1 and Tier 2 natural gas must be consumed. Patton State Hospital readily and quickly consumes 250 therms in the first day of each month, reducing natural gas prices to the Tier 2 rate, and consumes 4163 therms in 4 days to move into Tier 3 rates. On the other hand the UCI Bren building can only get to Tier 2 natural gas after 7 days of operation and never reaches the Tier 3 rate. Due to this difference, the fuel available to Patton State Hospital is less expensive and the capacity factor is increased.

Other buildings display similar trends due to larger native thermal load. Two of these buildings are UCI Natural Science 2 (6.5 times larger thermal load than UCI Bren) and SCAQMD (23.9 times larger thermal load than UCI Bren). All three buildings have an electrical load factor of approximately 0.6. Larger thermal loads lead to reaching Tier 3 natural gas and a lower average fuel cost; SCAQMD experiences lower gas cost than UCI Natural Science 2, which experiences lower gas cost than UCI Bren.

Figure 78: Required DG Electrical Efficiency to Reach Parity with Grid during Winter Mid-peak Period
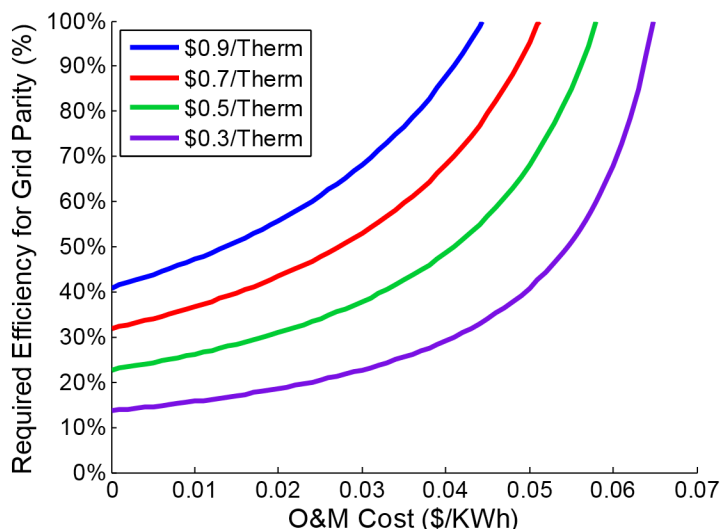
For a given natural gas and O&M cost, electrical efficiency above the plotted line guarantees the ability to produce electricity at a lower cost than purchasing it from the grid.

Fuel cost has one of the largest effects on DG and MTG economics, with high fuel cost eliminating benefit and low cost creating it. Figure 79 shows the predicted payback length for an installed system versus electrical efficiency and O&M cost as well as the reduction in payback length for UCI Natural Science 2 and SCAQMD. All installed system was sized to approximately 50 percent of the maximum building load (165 kW for UCI Bren, 345 kW for UCI Natural Science 2, and 850kW for SCAQMD), has 20 percent turndown, and has a capital cost of $2400 per kW. Shown for UCI Bren, electrical efficiency and O&M charges have a strong influence on payback length with shortest payback occurring when electrical efficiency is high and O&M is low.

Figure 79: Payback Length Plot Versus Electrical Efficiency and O&M for UCI Bren and the Corresponding % Difference in Payback Length due to Larger Heating Load for UCI Bren to UCI Natural Science 2 and UCI Bren to SCAQMD
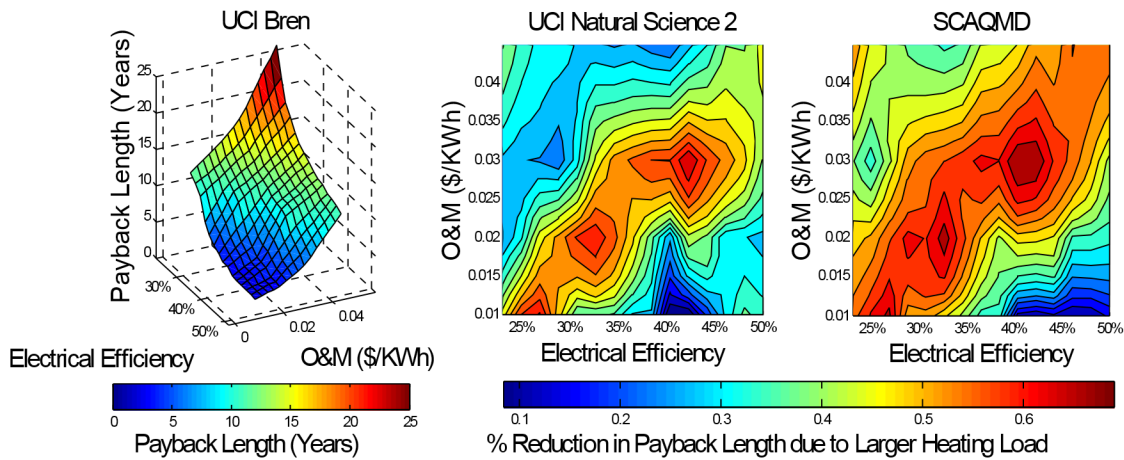
All buildings have a DG system sized to 50 percent of the maximum load, have 80 percent turndown, and capital cost is $2400 per kW to install.

As expected, the further the system moves towards low electrical efficiency and high O&M, the payback length increases. The relationship between capacity factor and payback length can be seen when comparing Figure 79 to Figure 77 for UCI Bren. Capacity factor increases as one reduces the cost of operation. Further dispatch of a system beyond demand reduction does not occur until savings can be generated during other peak times. As this cost reducing value is increased through higher efficiency, lower O&M, or achieving lower fuel costs, payback length is reduced.

As payback length increases, a gradient shift at ten years occurs for UCI Bren. Financing payments end at the ten year mark, and energy savings that were previously funding loan payments are realized by the investor, instantaneously increase in net savings. This sudden reduction in energy costs causes the brief gradient reduction, which occurs across the line moving from low electrical efficiency and low O&M to high electrical efficiency and high O&M.

When compared to UCI Bren, payback length is reduced for UCI Natural Science 2 for all electrical efficiencies and O&M costs, displaying the benefit of reduced fuel costs. Maximum benefit is seen for generators that had a payback length of approximately 10 years for UCI Bren. These equivalently sized systems that were unable to produce savings sufficient to overcome the financing payments required for UCI Bren, but are able to for UCI Natural Science 2 due to lower fuel cost.

Payback length is also reduced for all systems that lie beyond the gradient shift for UCI Bren. Decreasing the fuel price reduces losses generated during demand reduction activity while also enabling energy replacement. SCAQMD experiences further reductions to payback length due to an even larger thermal load. Reduced payback length occurs despite the greater total

investment required by UCI Natural Science 2 (2.1 times greater than UCI Bren) and SCAQMD (5.15 times greater than UCI Bren).

Installed Capacity and Turndown

Limits to generator turndown reduce the ability of on-site generation to operate at lower power levels. As DG capacity increases, to any beyond the average building load, the ability to turndown becomes more important to ensure that DG operation does not create excess electricity. If the building electrical demand is less than the minimum power setting allowable to the installed DG, on-site power generation is blocked, regardless of the economic potential of operation. In this instance, the installed DG is oversized for the current building load and does not produce any power due to the inability to export the additional power not consumed by the building. Figure 80 shows, for UCI Cal IT2, the percentage of the year generators with different turndown ability are oversized. The bottom x-axis shows ICBA and the top shows the ICBM. A generator with turndown of 20 percent starts to become oversized around 0.8 ICBA and 0.5 ICBM. A generator with turndown of 50 percent starts to become oversized at approximately 1.4 ICBA and 0.9 ICBM. A generator with turndown of 80 percent never becomes oversized, and capacity that meets the full building load can be installed without limiting time of operation available to the generator. Buildings with higher load factor than UCI Cal IT2 experience similar behavior with regards to generator turndown.

Figure 80: Percent of Year the Installed DG is Oversized for the Building Electrical Demand Versus ICBA and ICBM for UCI Cal IT2
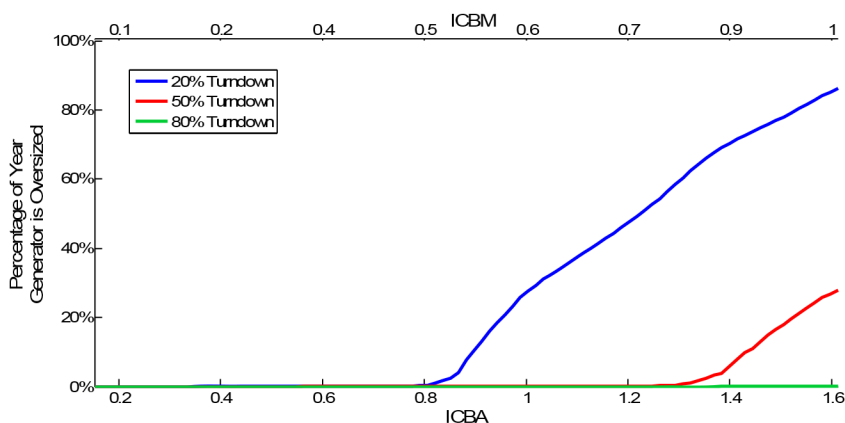
Increasing DG capacity requires larger total investment. Depending on the building and generator, increased capacity may be desired. However, total savings start to decline if too much capacity is installed. Figure 81 shows for UCI Cal IT2 the annual savings (with loan payments included) and payback length versus installed capacity. The bottom x-axis shows ICBA and the top shows the ICBM. Due to UCI Cal IT2's low load factor (i.e., more dynamic); turndown effects are more valuable for UCI Cal IT2 than for a building with a high load factor. The annual savings shown in Figure 81 include the loan payments required to pay off the

capital cost associated with purchase of the generator. Three generators with different turndown abilities are shown. Electrical efficiency is 50 percent, O&M is $0.01 per kWh, and capital cost is $2400 per kW. While this is an extreme case that is currently unachievable using MTGs, Figure 81 presented a scenario where electrical energy produced on-site is always cheaper than purchasing electrical energy from the grid.

Figure 81: Impact of Increased Capacity on Annual Savings and Payback Length Versus ICBM and ICBA for UCI Cal IT2. System Has an Electrical Efficiency of 50% and O&M Cost is $0.01 per kWh. Capital Cost of DG is $2400 per kW
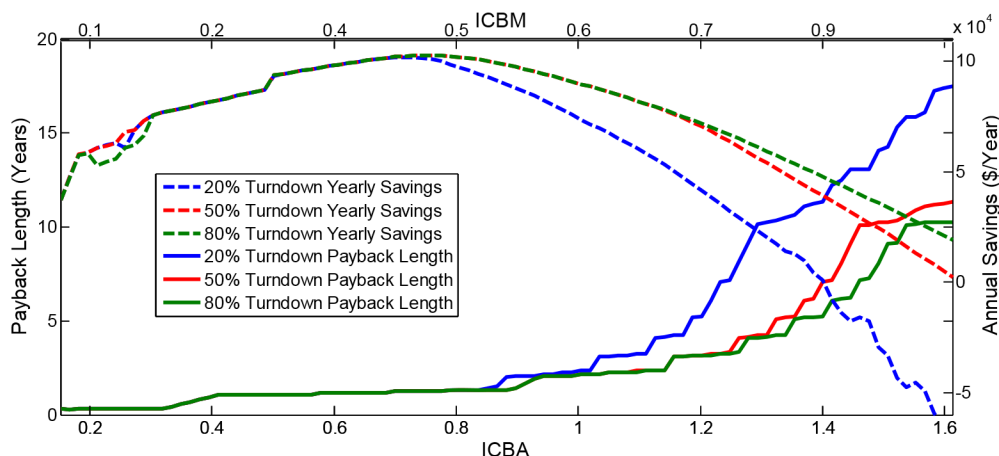
Capacity factor also suffers as installed generation increases beyond 0.8 ICBA, as seen in Figure 82 along with the percentage of the building load met by on-site generation. Low turndown generators remain inactive due to being oversized for the load, reducing capacity factor. High turndown machines experience a low capacity factor due to increased part load operation. For generators sized above the building average load, the full capacity is seldom used, with the additional capacity remaining unused and stranded While increased capacity of the system has the capability of producing cost efficient electricity, only a portion of the installation can consistently provide this service, putting the burden to payback the system investment on a fraction of the generator. As a result, the annual savings decrease and payback length is increased. Capacity factor at low levels of capacity is not one due to demand shifting activities blocking full power operation during summer mid- and off-peak. The building load met by the 80 percent turndown generator does not increase at large levels of installed capacity due to the minimum import restriction applied to grid connected buildings with DG.

Maximum annual savings occur at slightly below where the installed capacity is equal to the average building load. Capacity factor for this generator is near one, with nearly identical operation between the different generators regardless of turndown. The full cost reducing potential is achieved for these generators because no operation restrictions are created by an oversized installation or extended part load operation.

Figure 82: Yearly Capacity Factor and Percentage of Building Load Met Versus ICBM and ICBA for UCI Cal IT2. System Has an Electrical Efficiency of 50% and O&M Cost is $0.01 per Kwh
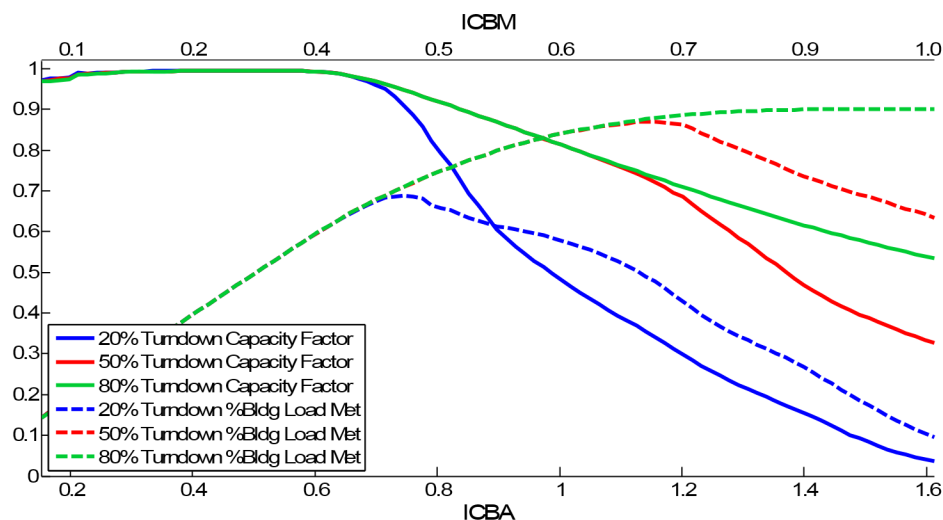
Allowing the generator to either export electrical energy or provide grid support would improve the economics of larger generators by allowing the unused capacity to be utilized. However, unless the value of these ancillary markets is equivalent in value to replacing grid electricity, the economics of additional capacity beyond the average building load suffer.

The individual bills that determine the total cost of electricity also change depending upon DG capacity and turndown. The annual cost of utility electricity decreases as a larger portion of the building electrical demand is met by on-site generation while natural gas and O&M costs increase with on-site electricity generation. Financing costs increase as further generator capacity is installed. The annual cost for utility electricity, natural gas, O&M, financing, and resulting savings for UCI Cal IT2 is shown in Figure 83 versus ICBA for an on-site generator that has DG turndown of 20 percent. Figure 83 shows how the different costs increase and decrease as on-site capacity increases. The top border of Figure 83 represents the baseline cost of energy, or the cost required to meet the electrical and thermal demand of the building if no on-site generation is installed.

The initial savings seen in Figure 83 are a result of switch the UCI Cal IT2 building from its parent electrical rate structure to the standby electrical rate structure. As generation capacity increases, electrical utility cost decreases while savings increase. However, after approximately 0.8 ICBA, electrical utility cost starts increasing and savings decrease, corresponding to the point in Figure 81 where annual savings start to decrease. The minimum electrical utility cost occurs at slightly more installed capacity than where maximum savings occur, showing that the installed capacity where savings are maximized does not match up where electrical utility costs are minimized. Electrical utility costs increase shortly after 0.8 ICBA due to the on-site generation being oversized for the building, blocking all on-site electricity generation and forcing the building to purchase electricity to meet the building demand.

Figure 83: Annual Cost of Energy Separated into Utility, O&M, and Financing Cost with Corresponding Savings for UCI Cal IT2 Versus ICBA
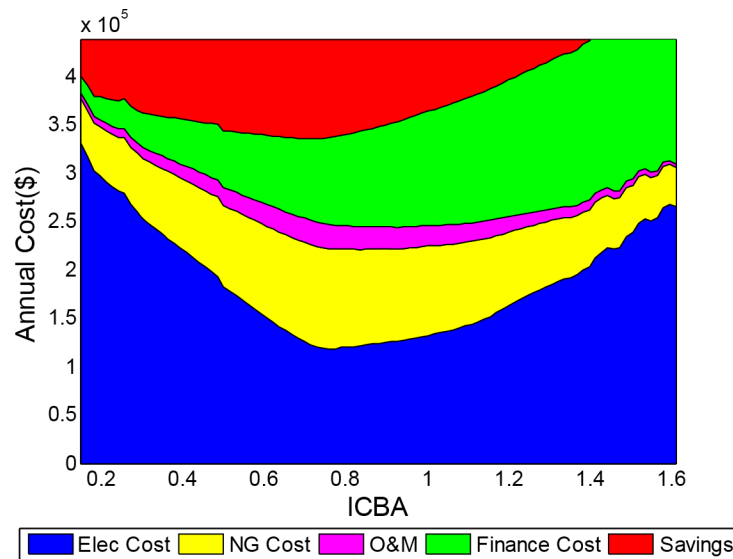
System has an electrical efficiency of 50 percent, O&M cost is $0.01 per kWh, and turndown of 20 percent. Capitol cost of DG is $2400 per kW.

At large levels of installed capacity, the finance cost becomes a large portion of the annual cost of energy, reducing and eliminating savings produced from on-site generation. This cost starts to nearly be equivalent to the cost of electricity, which remains the primary cost of energy due to the inability of on-site generation to operate because of little turndown ability.

Figure 84 shows the different annual cost of electricity when DG turndown is increased to 50 percent. At this level of turndown ability, on-site generation is able to replace more of the building load, and utility electrical costs are reduced even further. However, as with Figure 83, maximum savings do not correspond to minimum utility electricity cost, with an even larger difference between these two levels of on-site generation occurring in Figure 83. As installed capacity increases past 1.2 ICBA, the on-site generator starts to become oversized for portions of the building load, as seen in Figure 81, blocking generator operation and forcing the building to purchase electricity from the electrical utility in order to satisfy building demand.

Even with the increase in electrical utility cost with larger on-site capacity, the primary source of energy cost stems from the purchase and operation of on-site generation. Financing, O&M, and increases in natural gas cost account for over half of total annual energy costs. Savings, at larger levels of on-site capacity, are reduced and nearly disappear. As savings shrink, the total annual cost of energy using on-site generation approaches the baseline cost of having no generation on site. Since the annual cost of energy with on-site generation is nearly the same as not having generation on-site, the payments made to meet the cost of energy have just been shifted away from the electrical utility and towards covering financing cost, O&M, and natural gas.

Figure 84: Annual Cost of Energy Separated into Utility, O&M, and Financing Cost with Corresponding Savings for UCI Cal IT2 Versus ICBA

System has electrical efficiency of 50 percent, O&M cost is $0.01 per kWh, and turndown of 50 p34c3n5. Capitol cost of DG is $2400 per kW.

Table 19 and Table 20 show for all 12 buildings the installed capacity required to reach the maximum annual energy savings and the minimum electrical utility cost for on-site generation that has an electrical efficiency of 50 percent, O&M cost of $0.01 per kWh and a capital cost of $2400 per kW. Table 19 shows this information using ICBA and Table 20 shows it using ICBM. For all buildings, maximum savings is achieved at approximately the same level of installed capacity, regardless of turndown. SCAQMD experiences the largest increase in capacity when moving from a low to high turndown generator with less than 19 percent in additional capacity required to achieve maximum savings when turndown ability is increased. SCAQMD has the lowest load factor of the 12 buildings with electrical and thermal load data. This low load factor translates to larger dynamic variation, with demand dynamic variation that include electrical demand surges as well as sudden decreases in demand. Higher turndown generators are able to handle these sudden decreases better than lower turndown generators. However, the increase in annual savings due to installing a larger generator with greater turndown is only 6.5 percent greater than the annual savings achieved by the low turndown machine.

In addition to maximum savings being achieved at approximately the same level of installed capacity, regardless of DG turndown, minimum electrical utility cost is always achieved at a level of installed capacity that is greater than the level where maximum savings are achieved. For some buildings, the difference between these two levels of on-site generation is not large, such as for Patton Hospital, but additional capacity is always required it minimum electrical utility cost is desired over maximum savings.

110

Table 19: ICBA Comparison of Installed Capacity Required to Reach Maximum Annual Energy Savings Versus Installed Capacity Required to Reach Minimum Electrical Utility Cost

Building	Maximum Savings (ICBA)			Minimum Electrical Utility Cost (ICBA)		
	20% Turndown	50% Turndown	80% Turndown	20% Turndown	50% Turndown	80% Turndown
Hyatt Irvine	0.654	0.668	0.668	0.954	1.090	1.240
Loma Linda VA	0.622	0.622	0.622	0.927	1.194	1.194
Long Beach VA	0.761	0.761	0.761	0.895	1.175	1.175
Patton Hospital	0.724	0.785	0.785	0.755	1.170	1.540
SCAQMD	0.907	0.924	1.076	0.991	1.294	1.479
St Regis	0.875	1.007	1.007	0.901	1.127	1.233
UCI Bren	0.798	0.814	0.798	0.878	1.245	1.421
UCI Cal IT2	0.715	0.760	0.760	0.760	1.156	1.338
UCI Croul	0.755	0.755	0.755	0.894	1.311	1.511
UCI Nat Sci 1	0.703	0.734	0.734	0.812	1.203	1.484
UCI Nat Sci 2	0.801	0.817	0.817	0.832	1.248	1.294
US Navy Palmer Hall	0.837	0.917	0.917	0.877	1.196	1.196

System has an Electrical Efficiency of 50% and O&M Cost is $0.01 per kWh. Capital Cost of DG is $2400 per Kw

Table 20: ICBM Comparison of Installed Capacity Required to Reach Maximum Annual Energy Savings Versus Installed Capacity Required to Reach Minimum Electrical Utility Cost

Building	Maximum Savings (ICBM)			Minimum Electrical Utility Cost (ICBM)		
	20% Turndown	50% Turndown	80% Turndown	20% Turndown	50% Turndown	80% Turndown
Hyatt Irvine	0.463	0.472	0.472	0.675	0.771	0.877
Loma Linda VA	0.491	0.491	0.491	0.731	0.941	0.941
Long Beach VA	0.551	0.551	0.551	0.648	0.850	0.850
Patton Hospital	0.471	0.511	0.511	0.491	0.761	1.001
SCAQMD	0.517	0.527	0.613	0.565	0.738	0.843
St Regis	0.646	0.744	0.744	0.666	0.833	0.911
UCI Bren	0.485	0.495	0.485	0.533	0.756	0.863
UCI Cal IT2	0.444	0.473	0.473	0.473	0.718	0.832
UCI Croul	0.457	0.457	0.457	0.541	0.792	0.914
UCI Nat Sci 1	0.429	0.448	0.448	0.496	0.735	0.906
UCI Nat Sci 2	0.490	0.499	0.499	0.509	0.763	0.791
US Navy	0.623	0.682	0.682	0.653	0.890	0.890

Palmer Hall						

System has an Electrical Efficiency of 50% and O&M Cost is $0.01 per kWh. Capital Cost of DG is $2400 per Kw.

Figure 85 shows the individual costs that make up the cost of electricity for on-site generation that has 20 percent turndown. Figure 86 and Figure 87 show the same information for on-site generation that has 50 percent and 80 percent turndown respectively. All three figures show that maximum savings are achieved early due to switching from the parent electrical rate structure to the standby electrical rate. These figures also show that savings shrink and disappear as more on-site capacity is installed. Each figure also shows that savings produced by reducing the electrical utility cost are counteracted by increased natural gas and O&M cost. In addition to these cost increases, finance cost reduced savings derived from demand charge reduction, eliminating total energy savings quickly. In each figure, savings disappear at approximately a 0.8 ICBA. Low turndown generators have their operation blocked due to being oversized for the electrical at this ICBA, and experience smaller losses as a result of the purchase and operation of on-site generation, but savings during the life of the loan are eliminated for all generators, regardless of turndown, at approximately 0.8 ICBA.

Figure 85: Annual Cost of Energy Separated into Utility, O&M, and Financing Cost with Corresponding Savings for UCI Cal IT2 Versus ICBA
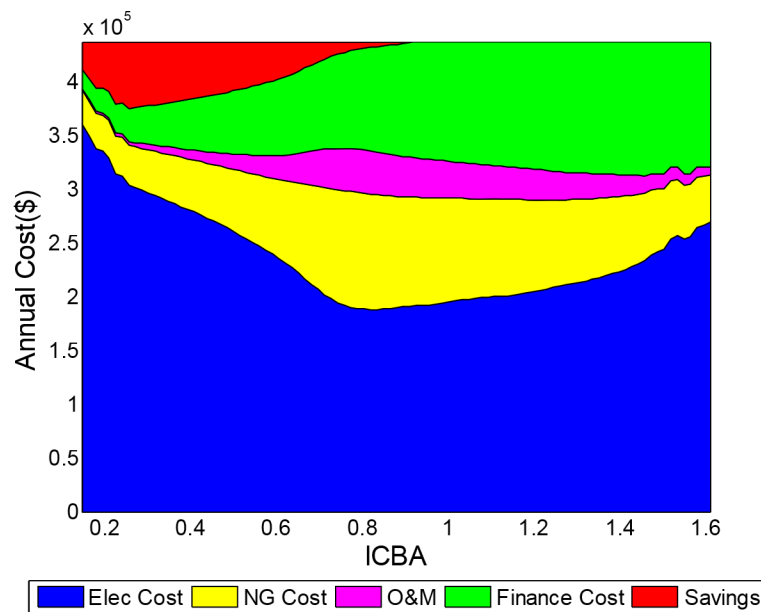
System has an Electrical Efficiency of 25%, O&M Cost is $0.03 per kWh, and Turndown of 20%. Capital Cost of DG is $2400 per Kw.

Figure 86: Annual Cost of Energy Separated into Utility, O&M, and Financing Cost with Corresponding Savings for UCI Cal IT2 Versus ICBA
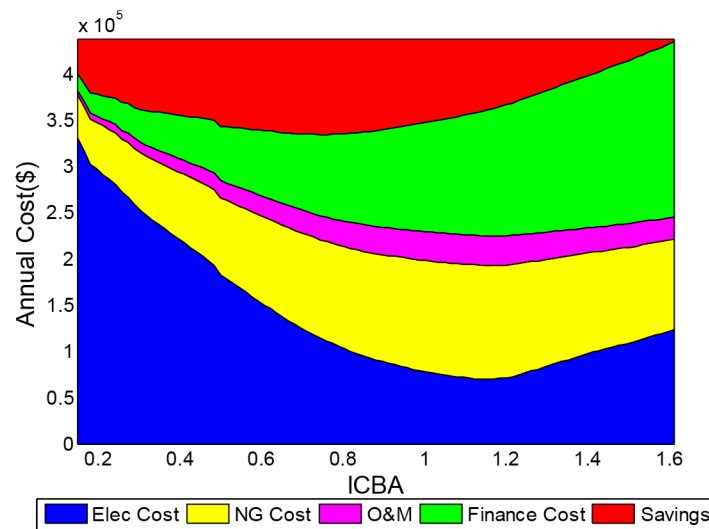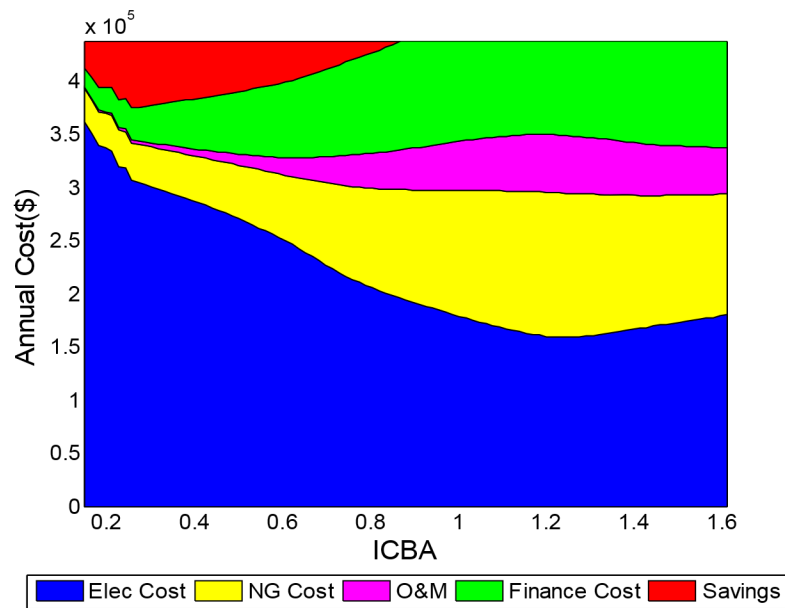

System has an Electrical Efficiency of 25%, O&M Cost is $0.03 per kWh, and Turndown of 50%. Capital Cost of DG is $2400 per kW.

Figure 87: Annual Cost of Energy Separated into Utility, O&M, and Financing Cost with Corresponding Savings for UCI Cal IT2 Versus ICBA
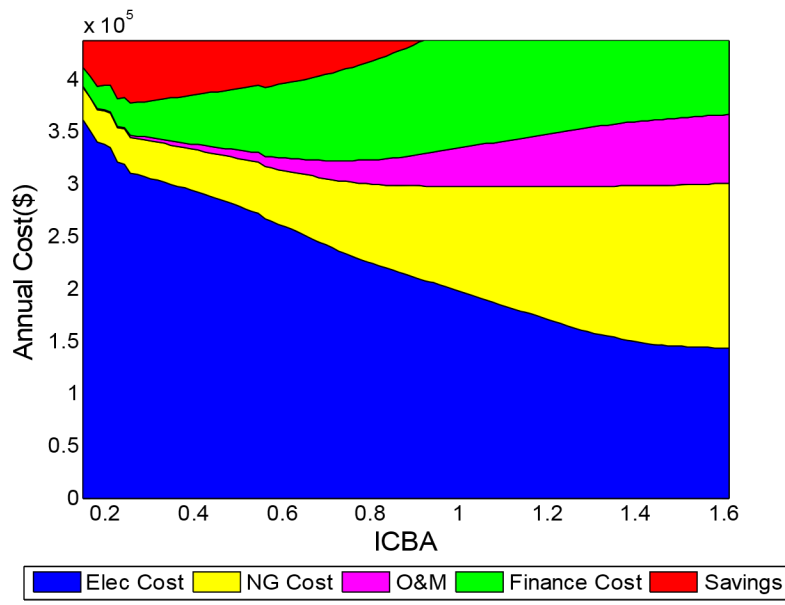
System has an Electrical Efficiency of 25%, O&M Cost is $0.03 per kWh, and Turndown of 80%. Capital Cost of DG is $2400 per kW.

Table 21 and Table 22 show for all 12 buildings the installed capacity required to reach the maximum annual energy savings and the minimum electrical utility cost for on-site generation that has an electrical efficiency of 25 percent, O&M cost of $0.03 per kWh and a capital cost of $2400 per kW. Table 21 shows this information using ICBA and Table 22 shows it using ICBM. For all buildings, maximum savings occur for small levels installed capacity, much smaller than what is required to achieve minimum electrical utility cost. The largest amount of installed generation relative to the building load required to achieve maximum savings occurs for SCAQMD. This is most likely due to SCAQMD having a low load factor, allowing for more on-site generation to be installed relative to its building load than other buildings with higher load factors.

Table 21: ICBA Comparison of Installed Capacity Required to Reach Maximum Annual Energy Savings Versus Installed Capacity Required to Reach Minimum Electrical Utility cost

Building	Maximum Savings (ICBA)			Minimum Electrical Utility Cost (ICBA)		
	20% Turndown	50% Turndown	80% Turndown	20% Turndown	50% Turndown	80% Turndown
Hyatt Irvine	0.136	0.136	0.136	1.036	1.254	1.417
Loma Linda VA	0.191	0.127	0.191	0.927	1.270	1.270
Long Beach VA	0.267	0.267	0.267	0.908	1.389	1.389
Patton Hospital	0.216	0.231	0.246	0.755	1.201	1.540
SCAQMD	0.521	0.706	0.723	1.008	1.496	1.748
St Regis	0.252	0.345	0.411	0.914	1.365	1.365
UCI Bren	0.319	0.319	0.319	0.926	1.517	1.517
UCI Cal IT2	0.259	0.259	0.259	0.821	1.278	1.612
UCI Croul	0.170	0.170	0.170	0.925	1.665	1.665
UCI Nat Sci 1	0.250	0.234	0.234	0.828	1.312	1.640
UCI Nat Sci 2	0.154	0.154	0.154	0.847	1.294	1.649
US Navy Palmer Hall	0.146	0.160	0.213	0.877	0.877	0.877

System has an Electrical Efficiency of 25% and O&M Cost is $0.03 per kWh. Capital Cost of DG is $2400 per Kw.

Table 22: ICBM Comparison of Installed Capacity Required to Reach Maximum Annual Energy Savings Versus Installed Capacity Required to Reach Minimum Electrical Utility cost

Building	Maximum Savings (ICBM)			Minimum Electrical Utility Cost (ICBM)		
	20% Turndown	50% Turndown	80% Turndown	20% Turndown	50% Turndown	80% Turndown
Hyatt Irvine	0.096	0.096	0.096	0.732	0.887	1.002
Loma Linda VA	0.150	0.100	0.150	0.731	1.001	1.001
Long Beach VA	0.193	0.193	0.193	0.657	1.005	1.005

Building	Maximum Savings (ICBM)			Minimum Electrical Utility Cost (ICBM)		
	20% Turndown	50% Turndown	80% Turndown	20% Turndown	50% Turndown	80% Turndown
Patton Hospital	0.140	0.150	0.160	0.491	0.781	1.001
SCAQMD	0.297	0.402	0.412	0.575	0.853	0.996
St Regis	0.186	0.255	0.304	0.676	1.009	1.009
UCI Bren	0.194	0.194	0.194	0.562	0.921	0.921
UCI Cal IT2	0.161	0.161	0.161	0.510	0.794	1.002
UCI Croul	0.103	0.103	0.103	0.559	1.007	1.007
UCI Nat Sci 1	0.153	0.143	0.143	0.506	0.801	1.002
UCI Nat Sci 2	0.094	0.094	0.094	0.518	0.791	1.008
US Navy Palmer Hall	0.109	0.119	0.158	0.653	0.653	0.653

System has an Electrical Efficiency of 25% and O&M Cost is $0.03 per kWh. Capital Cost of DG is $2400 per kW.

Almost all installed generators will fall somewhere between the two scenarios one with high electrical efficiency and low O&M cost, and the other with low electrical efficiency and high O&M cost. The points illustrated but these two scenarios apply to all peak periods and generator scenarios. If energy replacement is possible, the value of DG decreases if the full capacity of the on-site generation is not utilized. If energy replacement is not possible, the value of DG decreases when the capacity required to provide demand shifting and demand reduction has been surpassed since every unit of energy produced during demand reduction activity reduced total savings.

The levels of capacity listed in Table 19, Table 20, Table 21, and Table 22 where maximum savings are achieved do not necessarily correspond to shortest payback length. For most buildings, shortest payback length occurs at either the minimum generator capacity tested in this study or for the generator capacity required to shift maximum utility demand during the summer away from on-peak and mid-peak to off-peak. This is due to the value produced from virtually eliminating on-peak and mid-peak demand charges through the use of a small generator relative to the building electrical demand is large. The levels of capacity where maximum savings occur mark where further installed capacity is likely to experience extended payback length.

3.4.1.2 Waste Heat Recovery

Economic Effect

Waste heat recovery (HR) replaces thermal loads that would have been met by the firing of a natural gas boiler with heat produced during DG operation. Additional savings from HR can enable operation of a generator that previously could not compete with the grid when producing electricity only. This has a strong effect on the efficiency target presented in Figure

115

78, leading to lower efficiency generators reaching parity with the grid due to HR. As HR increases, the efficiency target is lowered, as shown in Figure 88.

Figure 88: Required DG Electrical Efficiency to Reach Parity with Grid during Winter Mid-peak Period with Waste Heat Recovery
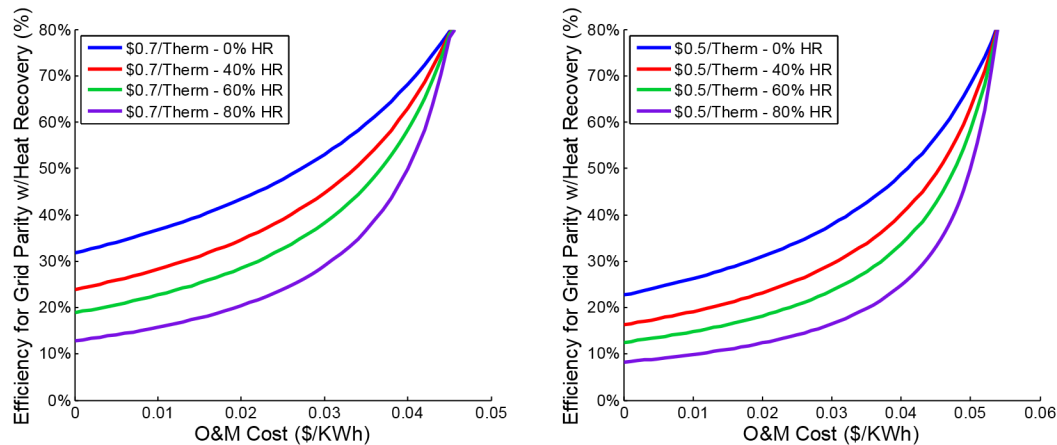
For a Given Natural Gas and O&M Cost, and Utilization of Available Heat, Electrical Efficiency Above the Plotted Line Guarantees the Ability to Produce Electricity at a Lower Cost than Purchasing it from the Grid.

The economic benefit of HR does have barriers before it can be realized. First, the thermal load must be coincident with the electrical load. If this does not happen, then the economic benefit of HR does not exist. This is particularly important during summer on- and mid-peaks as well as winter mid-peak where the price of electricity is most expensive. If the generator is relying on HR to make energy replacement possible, operation depends on coincidence. For electric only systems already capable of energy replacement, HR can further improve savings if coincidence exists.

Figure 89 shows the reduction in payback length from capturing available waste heat for UCI Cal IT2 and St. Regis. The installed generator is sized to 50 percent of the average building load installed, has 20 percent turndown, at a capital cost of $2400 per kW. The inclusion of heat recovery reduces payback length for almost all efficiency and O&M and, at worst, does not increase payback length. However, UCI Cal IT2 has a thermal load characterized by sporadic thermal demand, with 14 percent of the thermal load coinciding with on-peak and mid-peak periods for winter and summer. Very little waste heat is utilized and payback length is marginally improved. St. Regis has a thermal load that is nearly always coincident. The inclusion of heat recovery leads to decreases in payback length by up to 50 percent. High heat utilization is experienced, leading to high total system efficiency. Payback length reduction is greatest for low to mid efficiency machines since they offer more heat than high efficiency generators and tend to have longer payback lengths than higher efficiency systems with equivalent O&M. These regions of O&M and electrical efficiency also benefit from heat recovery

due to improved energy replacement ability. With the inclusion of heat recovery, electrical and thermal energy replacement is possible during peak periods where electrical energy alone is not possible.

Figure 89: Percent Reduction in Payback Length due to Waste Heat Recovery for UCI Cal IT2 and St. Regis for 0.5 ICBA
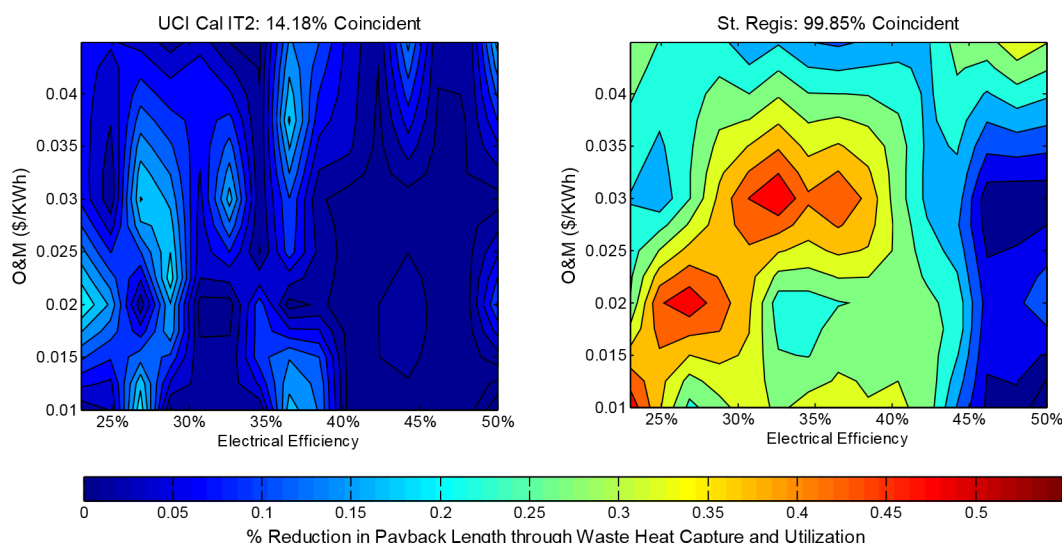
DG Capital Cost is $2400 per kW.

Realistically, the inclusion of heat recovery increases capital cost. While the increase in capital cost may make sense for a high coincidence building like St. Regis, the lack of coincidence may discourage the required investment for heat recovery at UCI Cal IT2. The lack of coincidence may increase payback length because the cost of installing the heat recovery equipment may never be recovered.

Waste heat recovery, as seen in Figure 89, is most beneficial for generators with low to mid electrical efficiency and mid to low O&M cost. Despite the improved savings for buildings with large and coincident thermal loads, the amount of installed capacity where maximum savings occur do not change from the levels for maximum savings for generators providing electricity only. For intermediate electrical efficiencies and O&M costs, it is possible to install more on-site capacity if the inclusion of waste heat recovery makes energy replacement possible. This increased capacity, however, is dependent on the scale and coincidence of the building thermal load, and does not surpass the level of generation where maximum savings occur established in Table 19 and Table 20.

Capacity Factor Effect

For generators that require HR to make energy replacement possible, coincidence must exist along with a large enough thermal demand to make sure that HR produces savings during

energy replacement. If the thermal demand is not large enough, electrical and thermal energy replacement is not possible regardless of coincidence. Off-peak operation is possible if enough thermal demand is present, as shown by the generator operation that mirrors the spikes in thermal demand. However, once the thermal spike subsides, not enough waste heat is utilized by the building and the generator shuts down, avoiding losses created by producing expensive energy on-site instead of purchasing it from the grid. An increase in thermal demand during this period would utilize more of the heat that is available from the generator, creating the savings from heat recovery necessary for electrical and thermal energy replacement.

Capacity factor has been shown to change due to heat recovery. For low efficiency and high O&M generators, capacity factor of the generator can improve significantly during peak periods where energy replacement is only possible when waste heat is utilized. Expanding the scope of the study by including a wide range of efficiencies and O&M costs helps to understand the impact of the inclusion of waste heat recovery. Figure 90 shows for UCI Bren, the yearly capacity factor for on-site generation for four O&M costs versus electrical efficiency. DG capacity is 50 percent of the average building electrical demand and turndown is 20 percent. Yearly capacity factor using waste heat recovery and not using waste heat recovery, as well as the percentage increase due to the utilization of waste heat recovery is shown. The highest O&M cost shows nearly no change in capacity factor, regardless of efficiency. As O&M cost decreases to $0.03 per kWh, increase in capacity factor does not occur until high efficiency is met. While the increase at this O&M cost and high efficiency is high relative to the capacity factor for operation in electric only mode, a large portion of the on-site capacity remains unused. This is also true for O&M cost of $0.01 per kWh, which experiences increase in capacity factor at lower electrical efficiencies but still like a large portion of the capacity unused. Large increases in capacity factor are seen for an O&M cost of $0.01 per kWh. The large increase in capacity factor at approximately 35 percent electrical efficiency helps the DG to achieve and surpass the efficiency target required to reach cost parity with the grid, shifting the electrical efficiency where a jump in capacity factor occurs for electric only operation to a lower level of electrical efficiency when waste heat is recovered. All other electrical efficiencies experience consistent increase in capacity factor from between a 20 to 40 percent increase.

Figure 90: Capacity factor versus electrical efficiency for UCI Bren with and without Waste Heat Recovery
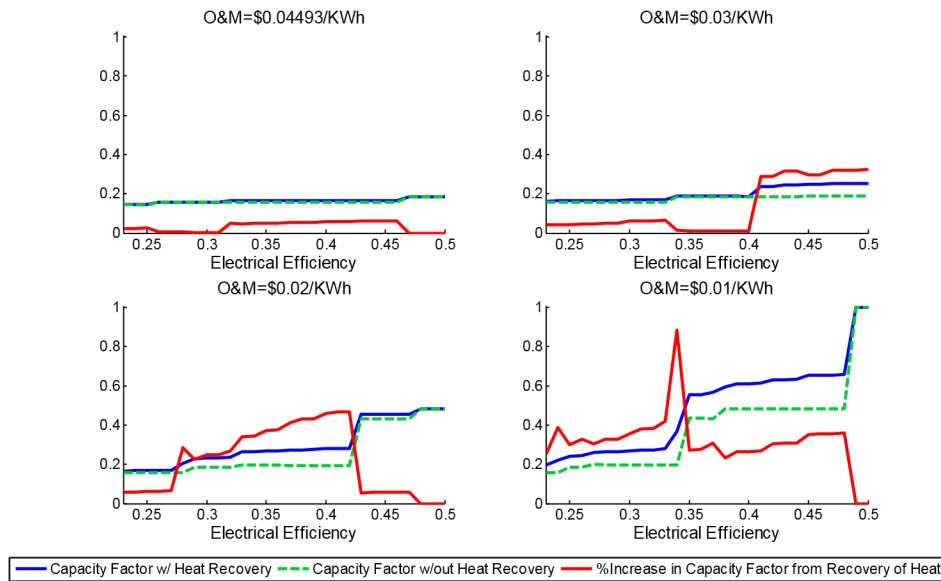
Installed systems are sized to 50% of average building load.

While coincidence between electrical and thermal loads for UCI Bren is relatively low, enough coincidence does exist in order to achieve a modest increase in capacity factor at some O&M cost and electrical efficiency combinations. Reducing coincidence, however, can eliminate even these small capacity factor increases. UCI Cal IT2, which has coincidental demand approximately 14 percent of the year, experiences approximately no increase in capacity factor due to waste recovery, as shown in Figure 91 regardless of O&M cost and electrical efficiency. Despite having a larger heating load than UCI Bren, the lack of coincidence virtually eliminates any increases in capacity factor due to waste heat recovery for UCI Cal IT2.

Figure 91: Capacity factor versus electrical efficiency for UCI Cal IT2 with and without waste heat recovery. Installed systems are sized to 50% of average building load
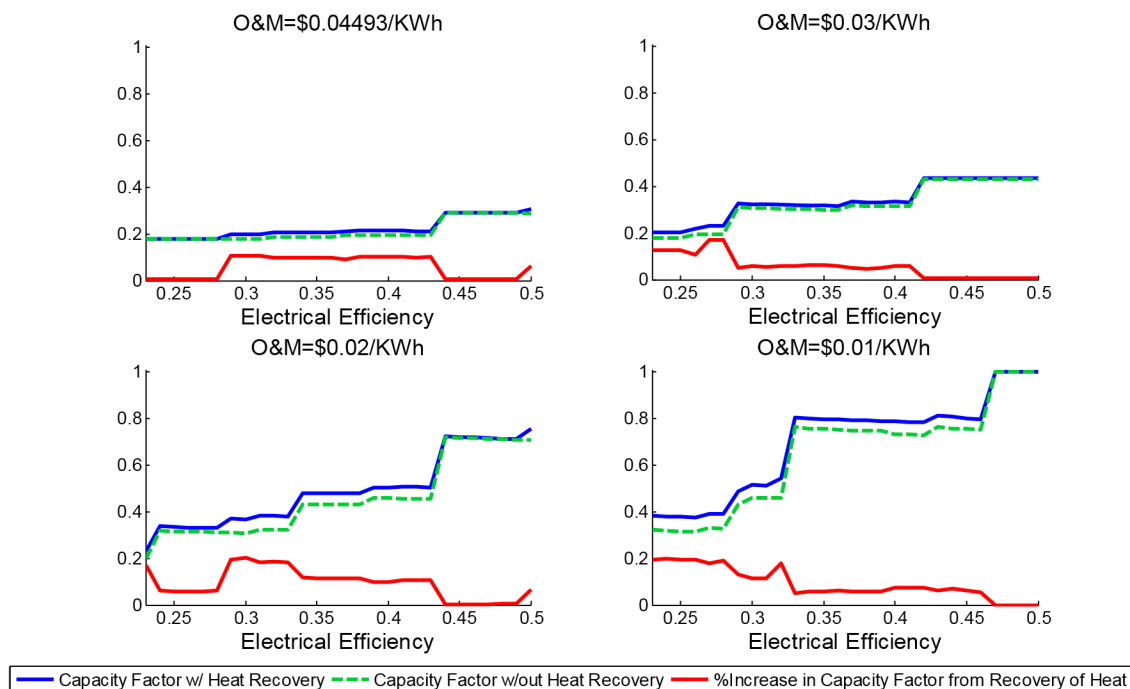
UCI Bren is not an ideal candidate for heat recovery. Due to the low coincidence between electrical and thermal loads, only a portion of available waste heat can be used. US Navy Palmer Hall has a similarly sized heating load to UCI Bren but a much higher level of coincidence. The capacity factor for a system in electric only mode and a system with waste heat recovery as well as the difference between these two capacity factors is shown for US Navy Palmer Hall in Figure 92. US Navy Palmer Hall naturally has a higher capacity factor than UCI Bren due to demand shifting and demand reduction. Marginal difference exists between the percentage increase in capacity due to waste heat recovery for US Navy Palmer Hall and UCI Bren. Even though a high level of coincidence exists for US Navy Palmer Hall, there is little difference between the increases in capacity due to waste heat recovery between US Navy Palmer Hall.

Figure 92: Capacity Factor Versus Electrical Efficiency for US Navy Palmer with and without Waste Heat Recovery
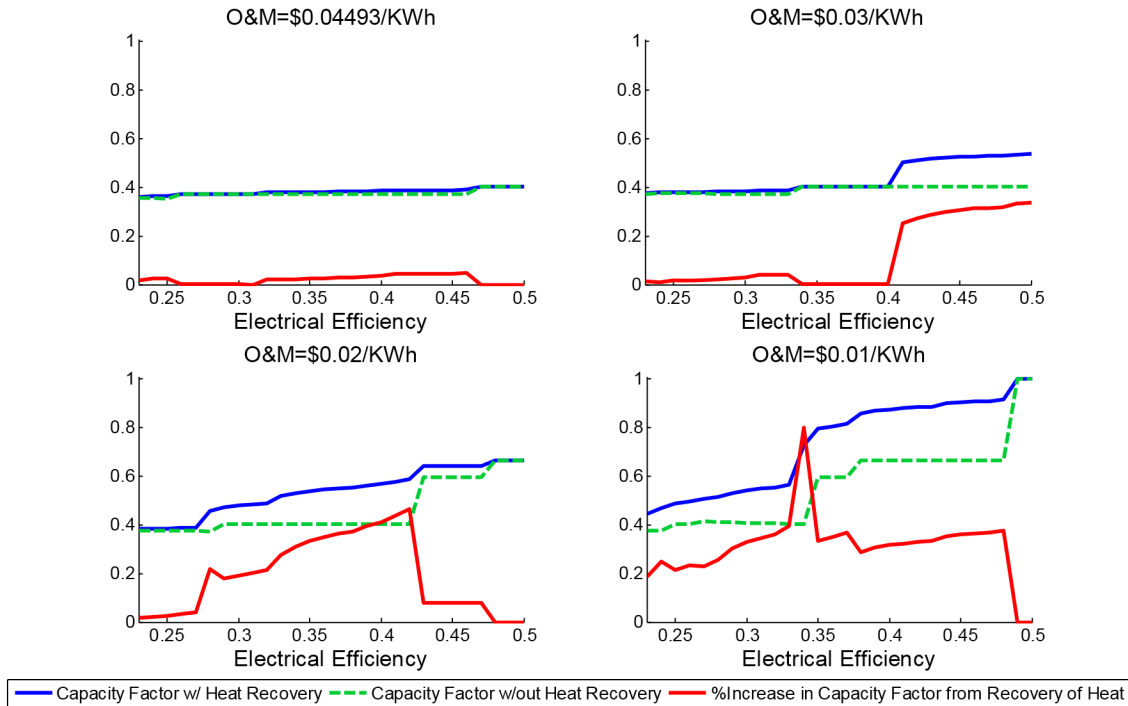
Installed systems are sized to 50% of average building load

Assuming that a high level of coincidence is achieved, the least expensive natural gas is available, and high levels of waste heat is utilized, significant increases in capacity factor can be realized. Figure 93 shows the yearly capacity factor for Patton State Hospital, which achieves Tier III natural gas due to a large heating load and has a high level of coincidence. Moderate increases to capacity factor is seen even for high O&M cost, except for electrical efficiencies between 30 and 40 percent for O&M cost of $0.03 per kWh. For lower O&M cost, close to maximum capacity factor is achieved at much lower electrical efficiencies. Figure 93 and Patton State Hospital is representative of all buildings that have large heating loads and increased coincidence.

Figure 93: Capacity Factor versus Electrical Efficiency for Patton State Hospital with and without Waste Heat Recovery
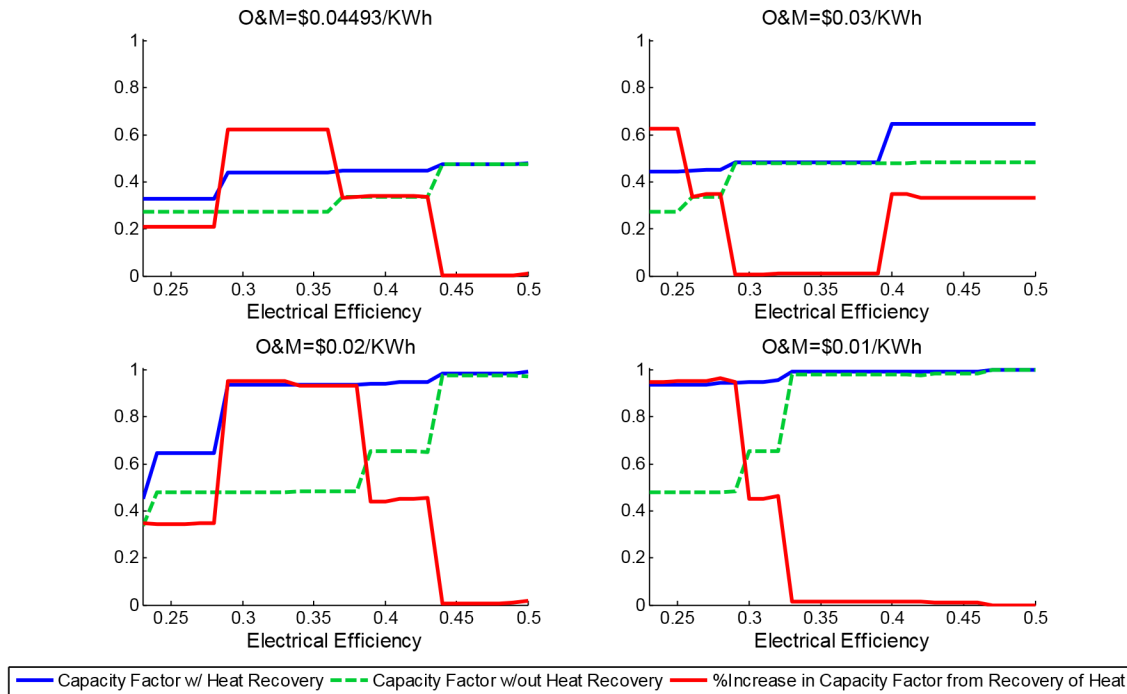
Installed systems are sized to 50% of average building load.

By utilizing waste heat, the potential exists to replace a large portion of the building heating load with the captured heat. The percentage of building load met for US Navy Palmer Hall and on-site generation with 80 percent turndown, broken down by O&M cost, is shown in Figure 94. Approximately 95 percent of the heating load for US Navy Palmer Hall is coincident with the electrical demand. Figure 94 shows that a large portion can be met, depending on electrical efficiency and amount of installed capacity relative to the building electrical demand. For all O&M costs, generators with low electrical efficiencies provide more heat to the building than high electrical efficiency generators. This allows for low efficiency generators to meet a larger portion of the building heating load. However, even high efficiency generators can meet a large portion of the building heating load is enough capacity is installed.

Figure 94: Building Heating Load Met for US Navy Palmer Hall, Broken Down by O&M Cost
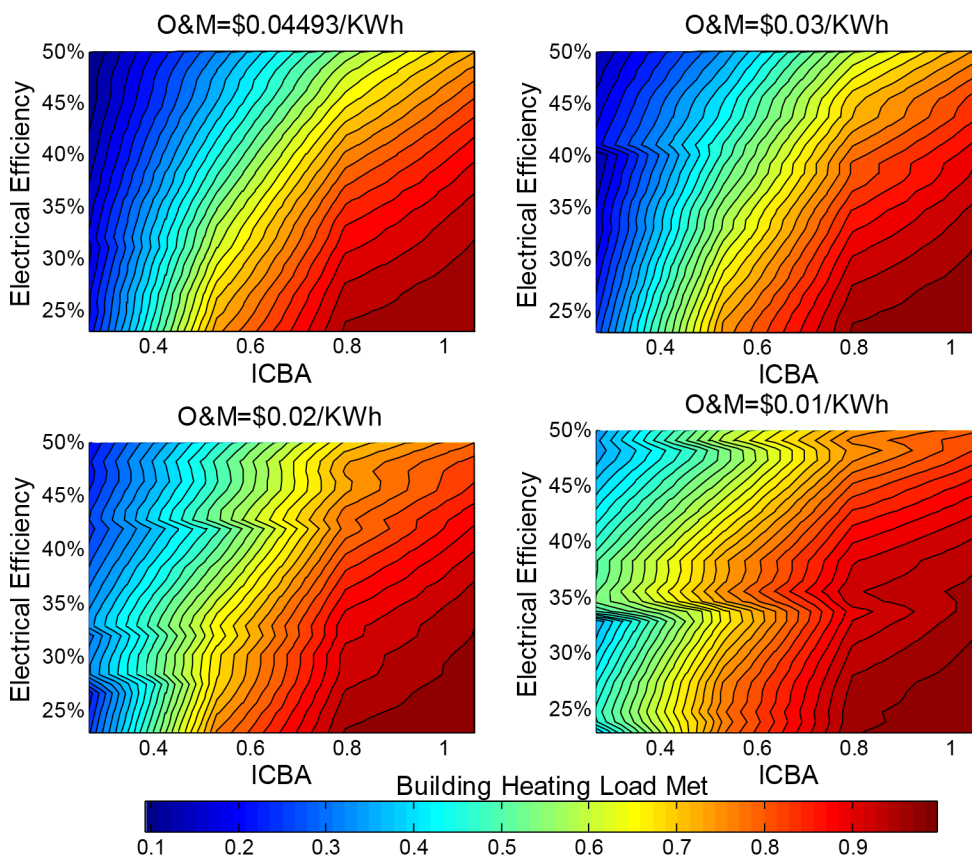
Building heating load met is determined for a given electrical efficiency and ICBA.

Capacity factor also has a strong impact on the building heat load that is met by on-site generation. Figure 92 shows for some O&M cost, particularly lower O&M cost, step increases in capacity factor as electrical efficiency increases. This can also be seen in Figure 94 while increasing electrical efficiency for constant ICBA, particularly for lower O&M cost. When these step increases in capacity factor occur, a portion of the building load that was being met through traditional means is met through waste heat recovery. This leads to higher efficiency generators meeting a larger portion of the building heating load. Despite offering less heat per unit of electrical energy created, these higher efficiency generators are able to operate during more peak periods and produce more waste heat overall.

Generator turndown also affects the ability of on-site generation to meet building heating load. If a generator is oversized, neither the electrical nor the heating demand can be satisfied using on-site generation. Figure 95 shows the percent of building heating load met for US Navy Palmer Hall, separated by turndown, when O&M cost is $0.03 per kWh And 80 percent and 50 percent turndown generators can meet a large portion of the building heating load, regardless of amount of installed capacity. Twenty percent turndown generators, however, starts to experience a reduction in the amount of building load met shortly after 0.8 ICBA. This is due to

the on-site generation being oversized for the building load, blocking operation of the on-site generation.

Figure 95: Building Heating Load Met for US Navy Palmer Hall, Broken Down by Turndown
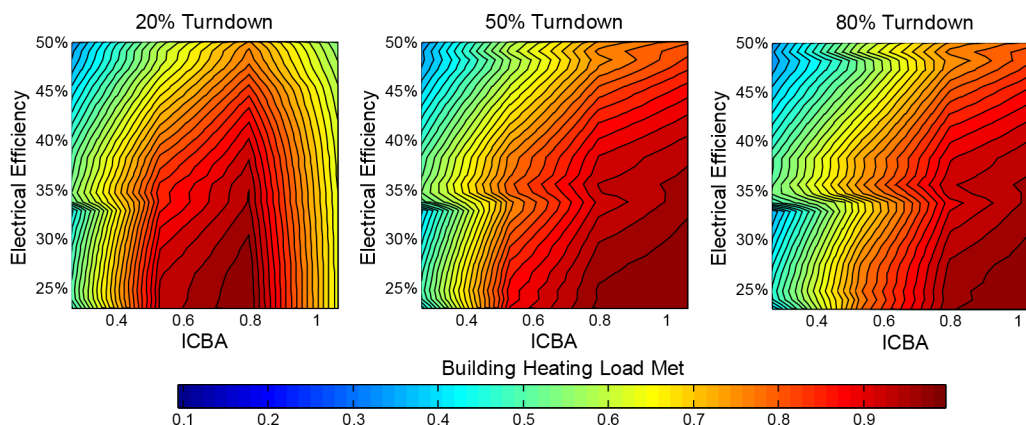
O&M Cost is $0.03 per kWh. Building heating load met is determined for a given electrical efficiency and ICBA.

Coincidence must exist between electrical and thermal loads in order for the building heating load to be met also. Figure 96 shows the percentage of building load met for UCI Cal IT2 and on-site generation with 80 percent turndown, broken down by O&M cost. Approximately 14 percent of the heating load for UCI Cal IT2 is coincident with the electrical demand. The same trends seen for US Navy Palmer Hall, with lower efficiency machines being able to meet more of the building load than higher efficiency machines and that step increases in the capacity factor, as shown for UCI Cal IT2, lead to higher efficiency machines producing more heat in total than lower efficiency machines due to increased operation. However, at maximum, only a little over 35 percent UCI Cal IT2's heating load can be met by using waste heat recovery. This value is considerably less as electrical efficiency increases and amount on on-site generation capacity decreases.

Having the option to utilize waste heat does not always translate into a full utilization of this product. Figure 97 shows, for US Navy Palmer Hall and an O&M cost of $0.03 per kWh, the percent of waste heat utilized in meeting the building's heating load. Smaller generators experience a higher utilization of their available waste heat, with nearly all of the available waste heat being utilized for high efficiency generators. This occurs due to the large coincidence between the electrical and thermal loads of the building and the ability of the thermal load to utilize heat produced by on-site generation. Despite experiencing a high level of heat utilization, only a small portion of the total heating load is met through waste heat utilization.

124

Figure 96: Building heating load met for UCI Cal IT2, broken down by O&M cost
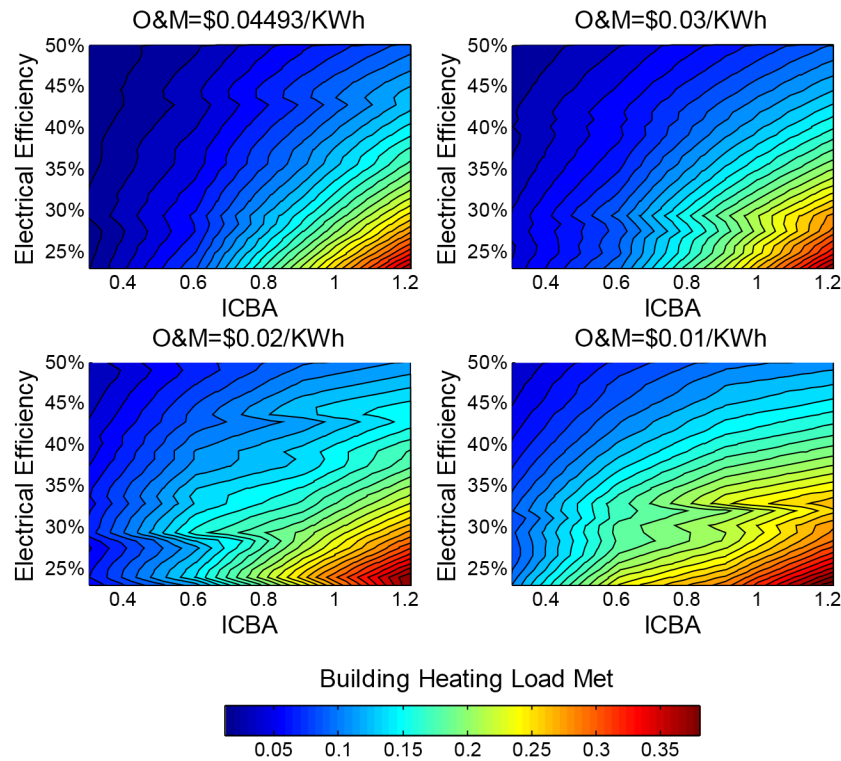
Building heating load met is determined for a given electrical efficiency and ICBA.

Figure 97: Waste heat utilized for US Navy Palmer Hall, broken down by O&M cost broken down by turndown
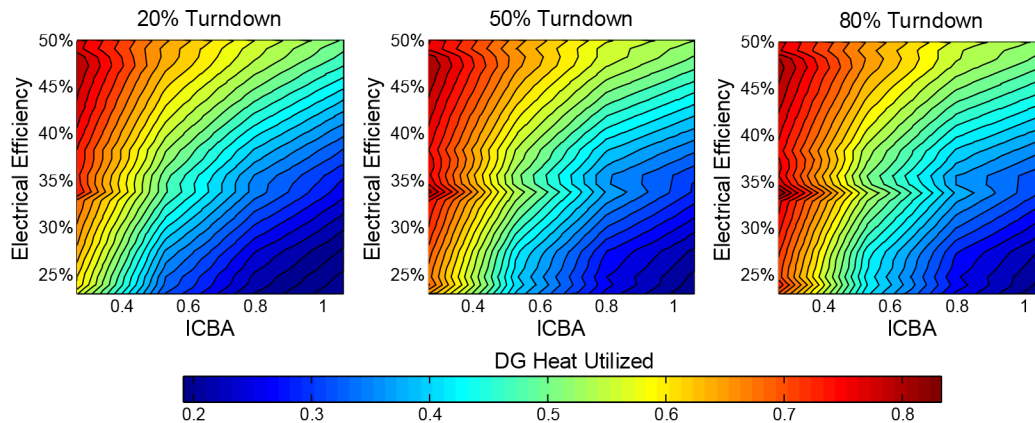
O&M cost is $0.03 per kWh. Waste heat utilized is determined for a given electrical efficiency and ICBA.

As electrical efficiency decreases and installed capacity increases, a higher portion of the building heating load is met, but waste heat utilization decreases. Increasing turndown improves waste heat utilization. A low turndown machine must operate at a higher power

setting, producing a large amount of heat relative to lower possible power settings. This heat may not be completely utilized by the building. Increasing turndown allows for the on-site generation to be operated at a lower power setting so that the amount of heat demanded by the building is produced by the generator, maintaining high heat utilization while meeting a large portion of the building heat load. Turndown affects peak period operation when energy replacement is possible when electricity and heat loads must both be satisfied. Peak periods when electrical energy replacement is possible without waste heat recovery, the maximum amount of electricity is produced, regardless of waste heat utilization.

Reducing coincidence between building electrical and thermal demand can change the amount of heat utilization experienced by a similarly sized generator. Figure 98 shows, for UCI Cal IT2, the percent of waste heat utilized in meeting the building's heating load for an O&M cost of $0.03 per kWh. Capacity factor for high efficiency generators is approximately twice as large as the capacity factor for low efficiency generators for UCI Cal IT2, as shown in Figure 91. This increase in capacity factor occurs for the building, regardless of waste heat recovery, and can be attributed to a more efficient generator being able to perform electrical energy replacement for a whole peak period. This operation occurs regardless of waste heat recovery, leading to the production of waste heat that is never used. Generators with lower electrical efficiencies that attempt to perform energy replacement must replace both electrical and thermal loads, causing for operation to occur only when both loads are coincident. This leads to higher waste heat utilization for smaller generators with low electrical efficiency, but also results in a low capacity factor due to lack of coincidence. As more capacity is installed, operation occurs more frequently due to demand reduction and demand shifting activities. The additional waste heat created during these activities is not used, leading to a reduction in waste heat utilization.

Figure 98: Waste heat utilized for UCI Cal IT2, broken down by O&M cost broken down by turndown
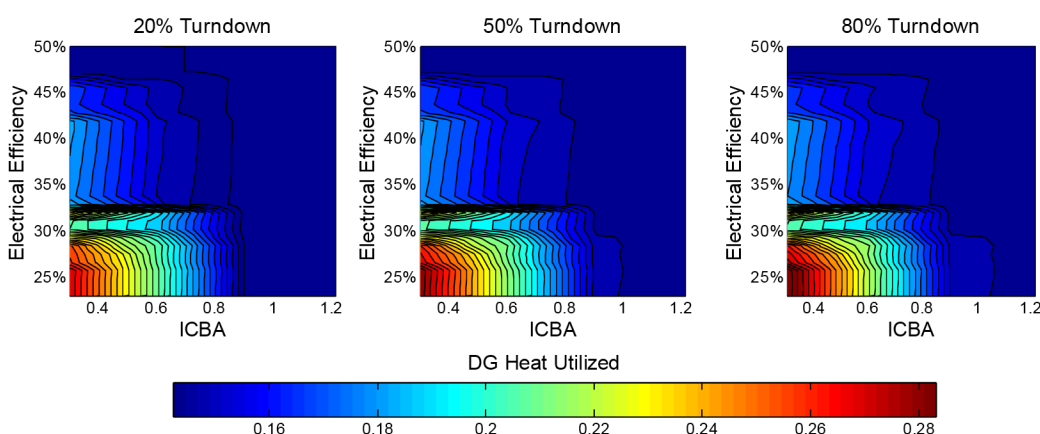
O&M cost is $0.03 per kWh Waste heat utilized is determined for a given electrical efficiency and ICBA.

One of the benefits of distributed generation is increased system efficiency through the utilization of waste heat. Figure 99 shows, for US Navy Palmer Hall and an O&M cost of $0.03 per kWh, total system efficiency. Generators with the highest electrical efficiency have the highest total system efficiency. Along a line of constant efficiency, smaller generators have higher total system efficiency than larger generators due to higher waste heat utilization. Figure 100 shows the percent increase in total system efficiency for US Navy Palmer Hall. Generators that experience the largest increase in total system capacity factor are small and have low electrical efficiency. By utilizing a large portion of the available waste heat, the efficiency for these generators can nearly be doubled through the inclusion of waste heat recovery.

Figure 99: Total System Efficiency for US Navy Palmer Hall, Broken Down by O&M Cost Broken Down by Turndown
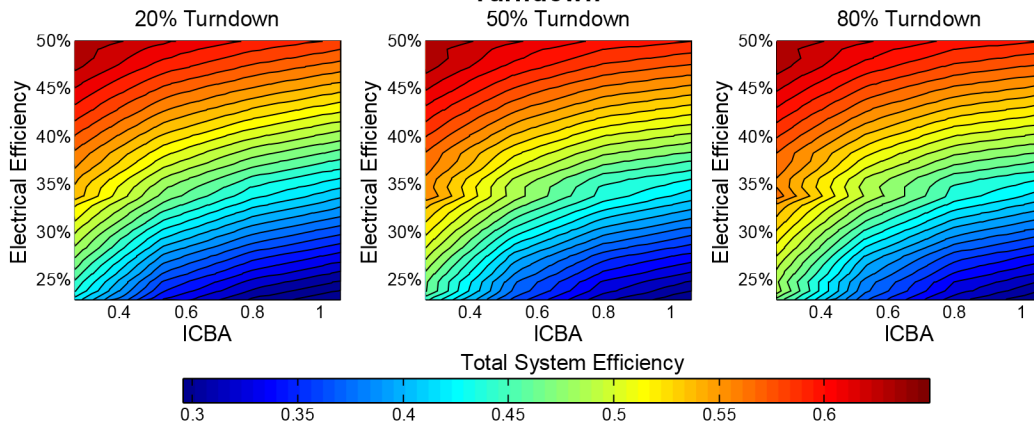
O&M cost is $0.03 per kWh Total system efficiency is determined for a given electrical efficiency and ICBA.

Figure 100: Percent Increase in Total System Efficiency for US Navy Palmer Hall, Broken Down by O&M Cost Broken Down by Turndown

O&M cost is $0.03 per kWh Increase to total system efficiency is determined for a given electrical efficiency and ICBA.

127
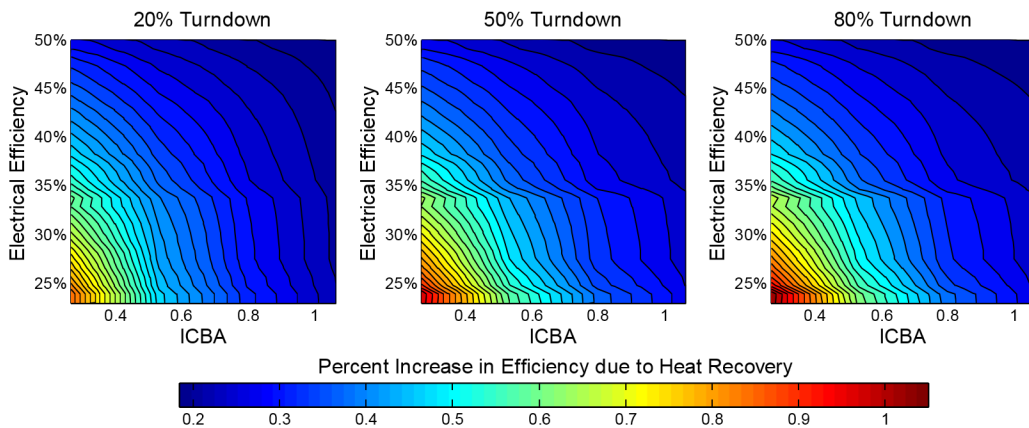
For a building with low levels of coincidence, system efficiency is only slightly improved due to waste heat recovery. Figure 101 shows, for UCI Cal IT2 l and an O&M cost of $0.03 per kWh, total system efficiency. Total efficiency is improved only by a few efficiency points for most installations. Figure 102 shows the percent increase in total system efficiency for UCI Cal IT2. The largest increase is experienced by small generators that have low electrical efficiencies, but only increases total efficiency by a fraction of the electrical efficiency.

Figure 101: Total System Efficiency for UCI Cal IT2, Broken Down by O&M Cost Broken Down by Turndown
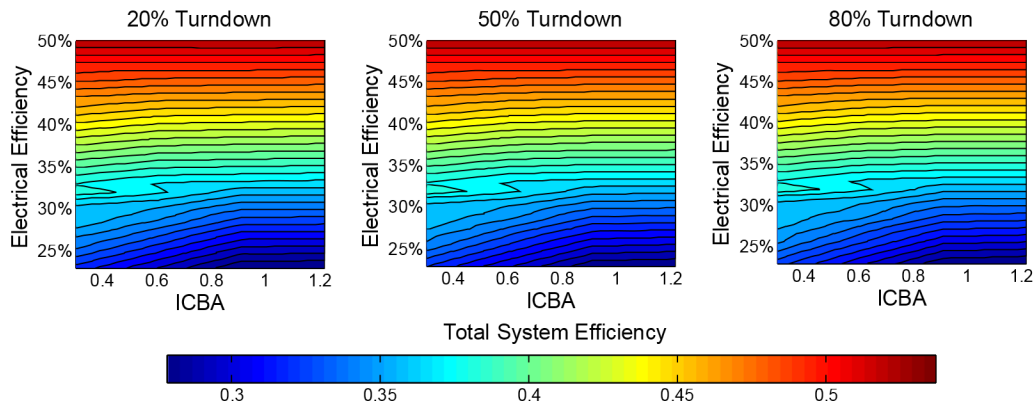
O&M cost is $0.03 per kWh Total system efficiency is determined for a given electrical efficiency and ICBA.

Figure 102: Percent Increase in Total System Efficiency for UCI Cal IT2, Broken Down by O&M Cost Broken Down by Turndown
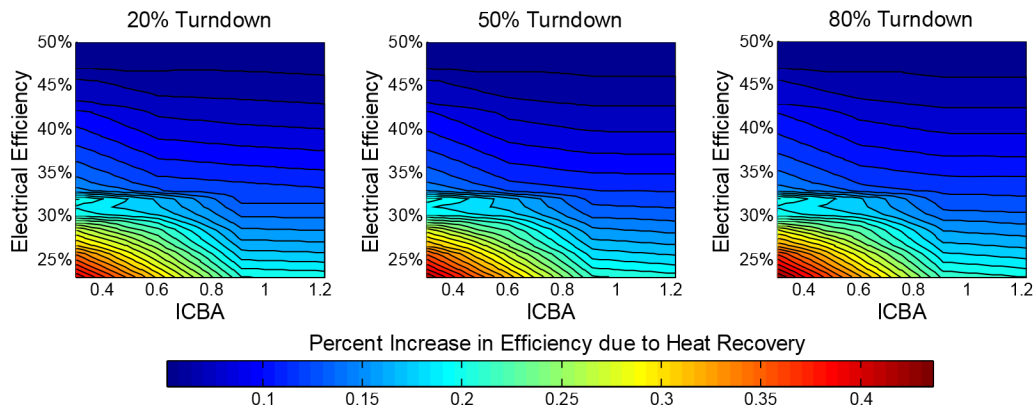
O&M cost is $0.03 per kWh Increase to total system efficiency is determined for a given electrical efficiency and ICBA.

3.4.2 Parent Electric Rates

All results and analysis performed for standby rates apply to building and generator combinations operating under parent electric rates. Any difference in result between parent and standby electric rates is due to the elimination of value due to demand shifting under the parent rates. Without this value, demand charges always apply to on- and mid-peak during the summer and demand charge reduction is accomplished only through maximum utility demand reduction.

TOU-B rates are preferred for all building and generator combinations used in the parametric study. While TOU-A rates may be better suited for providing less expensive electricity to low load factor buildings, none of the buildings with corresponding heat loads had a low enough load factor to warrant the use of TOU-A. As a result, additional costs are incurred when switching a building that prefers TOU-B to TOU-A when implementing DG simply from switching rate structures. These additional costs have a negative effect on payback length that were not experienced while using TOU-B rates.

3.4.2.1 Electric Only

DG that has low electrical efficiency and high O&M cost were previously discussed, which resulted in the conclusion that not enough savings could be produced in order to pay off the cost of capital before the life of the loan expired. This resulted in payback length extending beyond 10 years. The only way to reduce this payback length is to reduce operation cost by increasing electrical efficiency or lowering O&M cost to allow for energy replacement to occur or to lower capital cost associated with purchasing and installing DG.

Lowering capital cost to $2400 per kW does not allow for significant reductions in payback length for low electrical efficiency and high O&M generators, but does allow for comparisons between the generators using standby rates shown in Figure 81 to the same generators operating under the parent rate structure. Figure 103 shows the impact increasing installed capacity has on annual savings and payback length for UCI Cal IT2 when installed generation has low electrical efficiency and high O&M cost. All systems, regardless of turndown ability, do not pay back before 10 years. Any reduction to cost of electricity is shifted to increased natural gas cost, O&M, or finance payment, as seen in Figure 104. This results in zero savings during the life of the loan. While Figure 104 only displays cost information for building and generator combinations with 80 percent turndown, it is representative of costs for all generators with similar electrical efficiency and capital cost, regardless of turndown. Capacity factor behaves under the parent rate structure identically to the capacity factor produced for operation under the standby rate structure shown in Figure 82.

Figure 103: Impact of Encreased Capacity on Annual Savings and Payback Length Versus ICBM and ICBA for UCI Cal IT2 Under the Parent Electrical Rate
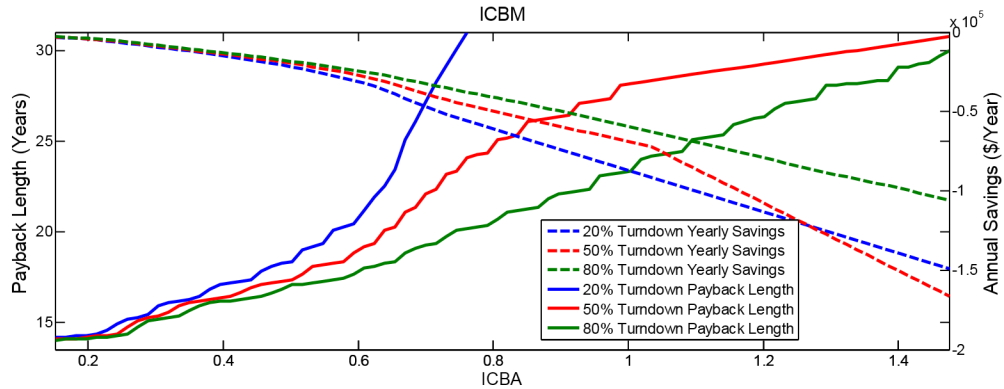
System has an electrical efficiency of 25% and O&M cost is $0.03 per kWh. Capital cost of DG is $2400 per Kw.

Figure 104: Annual cost of energy separated into utility, O&M, and financing cost with corresponding savings versus ICBA for UCI Cal IT2 under the parent electrical rate. System has an electrical efficiency of 25%, O&M cost is $0.03 per kWh, and turndown of 80%. Capital cost of DG is $2400 per kW
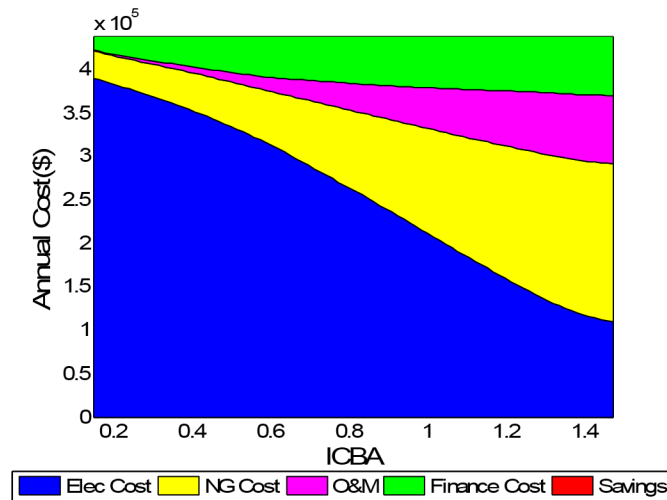
The only building that experiences savings during the life of the loan is the SCAQMD. Having the lowest load factor of the buildings included in the parametric study, generator operation can reduce demand charges while replacing minimal electrical energy, resulting in savings being realized for the building. Figure 105 shows the cost of energy breakdown, including the savings for generators with 80 percent turndown.

Figure 105: Annual cost of energy separated into utility, O&M, and financing cost with corresponding savings versus ICBA for SCAQMD under the parent electrical rate

System has an electrical efficiency of 25%, O&M cost is $0.03 per kWh, and turndown of 80%. Capital cost of DG is $2400 per kW.

Generators with lower turndown experience slightly lower savings, as seen in Figure 106, but savings are not eliminated. These savings are realized even for low turndown generators at large installed capacities because operation is limited to only the maximum electrical demand. While the full demand reduction potential of this generator is not realized, the large demand dynamic variation that leads to a low capacity factor can be eliminated, lowering the total cost of electricity and realizing savings. This occurs for high load factor buildings, but the demand dynamic variation that increase maximum utility demand above the average building demand are much less for high load factors buildings than for low load factors buildings. As a result, the savings produced from eliminating demand dynamic variation for high load factor buildings are erased by losses stemming from producing expensive electricity on-site.

Figure 106: Annual cost of energy separated into utility, O&M, and financing cost with corresponding savings versus ICBA for SCAQMD under the parent electrical rate
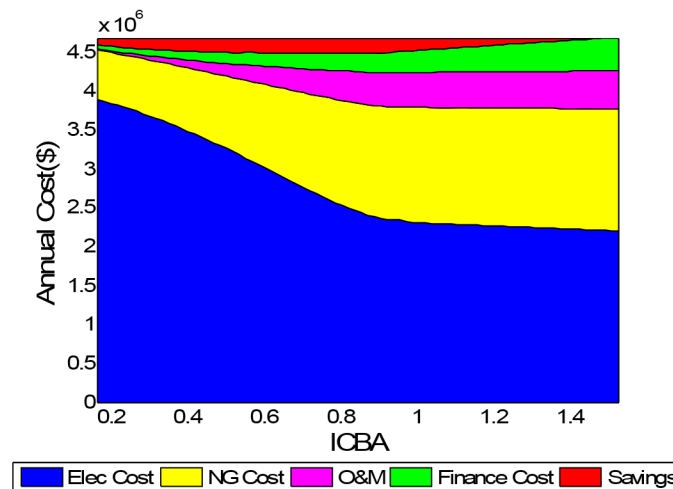
System has an electrical efficiency of 25%, O&M cost is $0.03 per kWh, and turndown of 20%. Capital cost of DG is $2400 per kW.

Despite realizing savings during the life of the loan, payback for SCAQMD does not occur for any generator until after 15 years, as seen in Figure 107. The savings produced from producing electricity on-site do not cover the cost associated with owning and operating DG. Yearly savings are realized for nearly all amounts of installed capacity, but payback length increases as capacity increases. For low efficiency generators with high O&M cost, the economic case is weakened if the parent rate structure is used to determine the cost of electricity over the standby rate structure.

Maximum savings and fastest payback for all buildings except for SCAQMD occur at the lowest tested capacity, regardless of turndown. For SCAQMD, maximum savings occur between 0.8 ICBA and 1 ICBA, depending on turndown. These maximum savings also correspond to payback lengths greater than 20 years. Fastest payback for SCAQMD occurs at the lowest tested capacity.

Figure 107: Impact of increased capacity on annual savings and payback length versus ICBM and ICBA for SCAQMD under the parent electrical rate
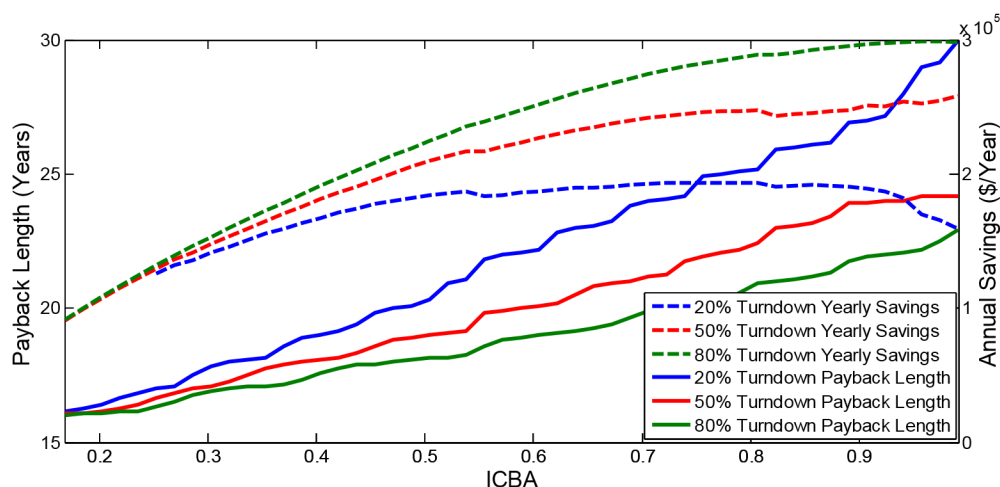
System has an electrical efficiency of 25% and O&M cost is $0.03 per kWh. Capital cost of DG is $2400 per kW

Increasing electrical efficiency and reducing O&M cost so that it is less expensive to produce electricity on-site versus purchasing it from a utility shows improvements to the economics of DG under the parent rate structure. This scenario is presented for UCI Cal IT2 in Figure 108. Comparing Figure 108 to Figure 81 shows that for installations of less than 0.8 ICBA, payback occurs faster under standby rates. However, for parent rate structure, payback length remains relatively flat and does not experience the slight increases to payback length experienced under standby rates. For standby rates, once maximum utility demand has been shifted away from on- and mid-peak during the summer, further increased capacity produces no additional savings from demand shifting. Unable to produce the savings produce by the prior installed capacity, further capacity beyond what is required for demand shifting results in longer payback lengths. This behavior is not experienced under the parent rate structure, where additional capacity has the same cost reducing potential as the already installed capacity, as long as the full capacity can be utilized. Regardless, at low levels of DG capacity, payback occurs quicker under standby rates. Even though a portion of the building load is met for DG capacity less than the average building electrical demand, DG operation affects the electric rates that determine the cost of all utility supplied electricity.

Beyond a 0.8 ICBA, low turndown generator operation is blocked and high turndown generators are forced to run at part load. For 20 percent and 80 percent turndown generators, a longer payback length is observed under the parent rate structure when compared to operation under the standby rate structure. High turndown generators, however, experience a reduced payback length under the parent rate structure.

Figure 108: Impact of increased capacity on annual savings and payback length versus ICBM and ICBA for UCI Cal IT2 under the parent electrical rate
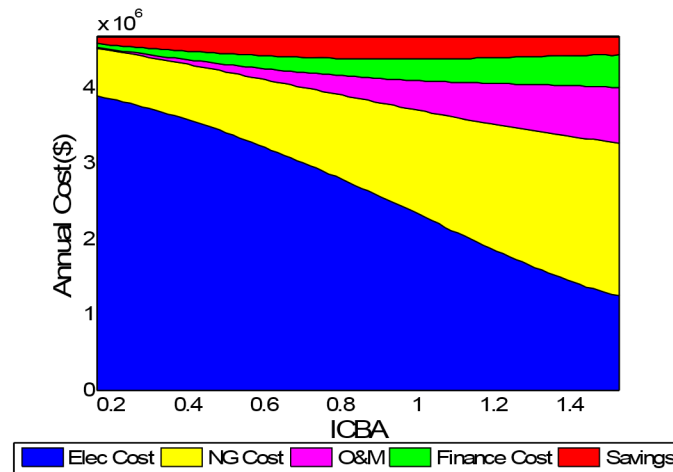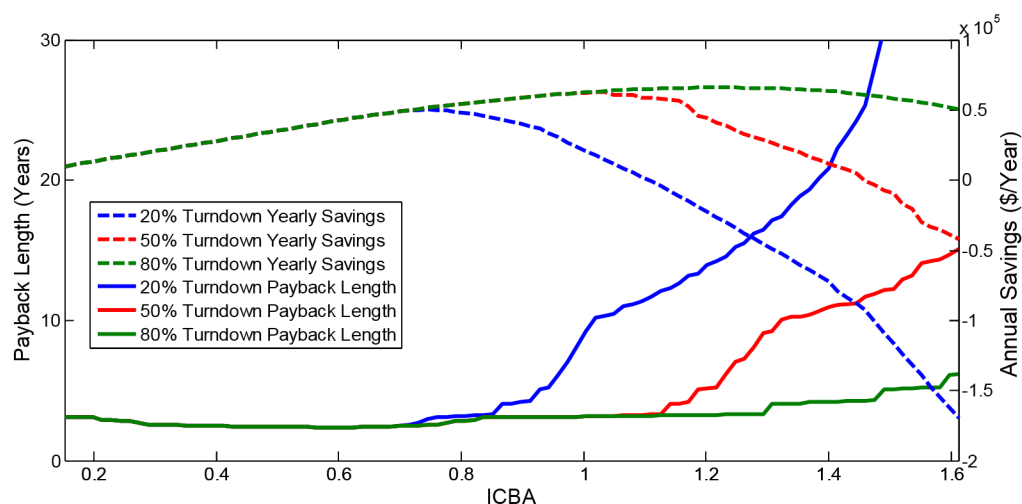

System has an electrical efficiency of 50% and O&M cost is $0.01 per kWh. Capital cost of DG is $2400 per kW.

This is the result of the dispatch strategy and additional fixed costs experienced under the standby rate. Under standby rates, the dispatch strategy allows maximum utility demand to increase during off-peak in order to ensure that on- and mid-peak demand charges are avoided. This behavior allows demand charges to increase even though demand reduction and energy replacement is possible. Since demand shifting has no value under the parent rate structure, the off-peak demand that would be allowed to increase under the standby rate dispatch strategy is eliminated under the parent rate dispatch strategy, reducing demand charges further under the parent rate dispatch strategy. This illustrates that even for specific rate structures, such as the standby rate structure, a single operating strategy does not necessarily minimize cost for all generators.

In addition to the standby rate dispatch strategy error, standby rates include fixed charges, such as the capacity reservation charge, are unavoidable under standby rates. These charges apply regardless of amount of utility electricity consumed by the building.

These two issues allow for operation under the parent rate structure to appear to be more economically attractive than operation under the standby rate structure. If the dispatch strategy is corrected to account for generators that can produce electricity at a lower cost than what is available for purchase from the grid, this difference would disappear between standby and parent rates.

The capacity factor under the parent rate is similar to the capacity factor under the standby rate structure. One distinction between the two is that since demand shifting has no value under the parent rate structure, DG operation is never blocked due to demand shifting. As a result, the capacity factor is 1 for small levels of capacity generation under the parent electric rate structure, as seen in Figure 109 for UCI Cal IT2.

Figure 109: Yearly capacity factor and percentage of building load met versus ICBM and ICBA for UCI Cal IT2 under the parent electrical rate
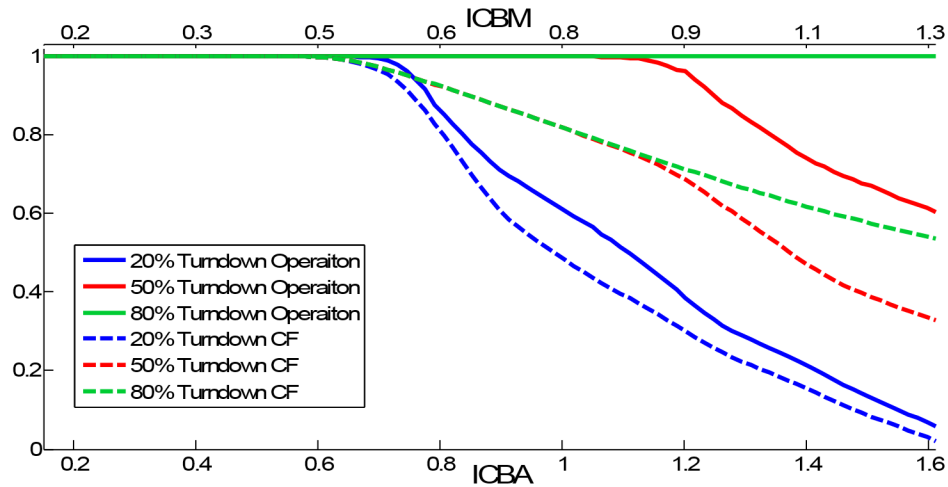
System has an electrical efficiency of 50% and O&M cost is $0.01 per kWh.

Levels of installed capacity where maximum savings and minimum electrical utility costs occur are shown in Table 23 and Table 24 for ICBA and ICBM. A larger difference exists under the parent rate structure between the levels of installed capacity depending on turndown. Difference in DG capacity where maximum savings occur for 20 percent and 80 percent turndown generators depends on the building demand. High load factor buildings experience less of a difference than low load factor buildings between generators with different turndown.

Table 23: ICBA comparison of installed capacity required to reach maximum annual energy savings versus installed capacity required to reach minimum electrical utility cost under the parent electrical rate structure

Building	Maximum Savings (ICBA)			Minimum Electrical Utility Cost (ICBA)		
	20% Turndown	50% Turndown	80% Turndown	20% Turndown	50% Turndown	80% Turndown
Hyatt Irvine	0.709	0.913	1.158	0.913	1.131	1.417
Loma Linda VA	0.788	0.864	1.042	0.915	1.258	1.270
Long Beach VA	0.882	1.095	1.296	0.882	1.336	1.389
Patton Hospital	0.755	1.124	1.540	0.755	1.170	1.540
SCAQMD	0.975	1.260	1.681	0.991	1.361	1.748
St Regis	0.835	1.034	1.352	0.875	1.153	1.365
UCI Bren	0.814	0.942	1.086	0.878	1.165	1.660
UCI Cal IT2	0.745	1.034	1.217	0.776	1.156	1.612
UCI Croul	0.786	1.002	1.203	0.894	1.280	1.665

135

Building	Maximum Savings (ICBA)			Minimum Electrical Utility Cost (ICBA)		
	20% Turndown	50% Turndown	80% Turndown	20% Turndown	50% Turndown	80% Turndown
UCI Nat Sci 1	0.781	1.140	1.219	0.812	1.250	1.640
UCI Nat Sci 2	0.801	1.094	1.109	0.801	1.248	1.649
US Navy Palmer Hall	0.784	1.236	1.236	0.824	1.263	1.356

System has an electrical efficiency of 50% and O&M cost is $0.01 per kWh. Capital cost of DG is $2400 per kW.

Table 24: ICBM comparison of installed capacity required to reach maximum annual energy savings versus installed capacity required to reach minimum electrical utility cost under the parent electrical rate structure

Building	Maximum Savings (ICBM)			Minimum Electrical Utility Cost (ICBM)		
	20% Turndown	50% Turndown	80% Turndown	20% Turndown	50% Turndown	80% Turndown
Hyatt Irvine	0.501	0.646	0.819	0.646	0.800	1.002
Loma Linda VA	0.621	0.681	0.821	0.721	0.991	1.001
Long Beach VA	0.638	0.793	0.937	0.638	0.966	1.005
Patton Hospital	0.491	0.731	1.001	0.491	0.761	1.001
SCAQMD	0.556	0.718	0.958	0.565	0.776	0.996
St Regis	0.617	0.764	0.999	0.646	0.852	1.009
UCI Bren	0.495	0.572	0.659	0.533	0.708	1.009
UCI Cal IT2	0.463	0.643	0.756	0.482	0.718	1.002
UCI Croul	0.475	0.606	0.727	0.541	0.774	1.007
UCI Nat Sci 1	0.477	0.697	0.744	0.496	0.763	1.002
UCI Nat Sci 2	0.490	0.669	0.678	0.490	0.763	1.008
US Navy Palmer Hall	0.584	0.920	0.920	0.613	0.940	1.009

System has an electrical efficiency of 50% and O&M cost is $0.01 per kWh. Capital cost of DG is $2400 per kW.

3.4.2.2 Waste Heat Recovery

Waste heat recovery under the parent rate structures follow the same principles established in Section 3.2.2. Maximum savings and minimum electric utility costs occur at the same level of generation as generators operating in electric only mode except for a few cases. Hyatt Irvine and UCI Croul for 20 percent turndown generators and UCI Nat Sci 1 for 80 percent turndown generators experience slight increases in capacity where maximum savings occur. These small increases in DG capacity are approximately 2 percent for Hyatt Irvine, 4 percent for UCI Croul, and 1 percent for UCI Nat Sci 1.

3.4.3 Maximum Capital Cost

The parametric model examined and captured the economic behavior of numerous types of generators operating for various buildings. While the results presented above establish benchmarks for desired building energy demand and generator performance in order to be attractive economically, the presented results only capture a snapshot of the information produced through the parametric study. In an effort to utilize the parametric study results, a statistical model predicting payback length was developed using analysis of variance. The maximum DG capital cost if a specific payback length for a given building and generators are predicted. The predicted capital cost changes between buildings and between generators with different operational characteristics. For buildings using generators without waste heat recovery, only electric load factor and average monthly heating load are required. Four buildings span these two factors; Loma Linda VA has a high load factor and high average monthly heating, US Navy Palmer has a high load factor and low average monthly heating, SCAQMD has a low load factor and high average monthly heating, and UCI Bren has a low load factor and low average monthly heating.

3.4.3.1 Capital Cost with No Heat Recovery

Assuming standby electrical rates, generator turndown of 50 percent, and no waste heat recovery, the estimated capital cost where payback will take 10 years to occur for various buildings are shown in Figure 110 for ICBM of 0.5 and 0.9. As the cost of producing electricity on-site increases due to either reduced electrical efficiency or increased O&M cost, the estimated capital cost decreases. In addition, DG capital cost also decreases as capacity increases.

US Navy Palmer Hall has a similar load factor to Loma Linda VA, but has a much smaller average monthly heating load. The estimated capital cost for US Navy Palmer Hall experiences similar trends as Loma Linda VA. Capital cost for low operating cost generators is reduced for US Navy Palmer Hall. Due to the higher fuel cost, maximum capital cost is reduced. SCAQMD has a low load factor and high average monthly heating load. For midsized installations, such as DG sized to 0.5 ICBM, capital cost can be as high as $4000 per kW and still experience payback in 10 years. Because of the low electrical load factor, electricity cost is higher for SCAQMD than for other buildings like Loma Linda VA. Replacement of electrical energy at SCAQMD is more valuable, leading to the possibility of higher cost DG paying back. However, as DG capacity increases, capital cost must be reduced if a payback length of 10 years it to be maintained. At this level of DG capacity, SCAQMD can only accept a capital cost that is slightly higher than high electrical load factor buildings. Reducing average monthly heating for a low load factor building reduces the maximum capital cost. The estimated capital cost for UCI Bren is higher than a building with similar average monthly heating but a higher load factor, such as US Navy Palmer Hall. The higher fuel cost experienced by UCI Bren leads to lower allowed capital cost for midsized installations. As capacity increases, the estimated capital cost for UCI Bren approach the same values estimated for SCAQMD estimated for similarly sized DG.

Figure 110: Estimated capital cost for Buildings at which payback takes 10 years for DG operating under standby electric rates with turndown of 50%, and no waste heat recovery
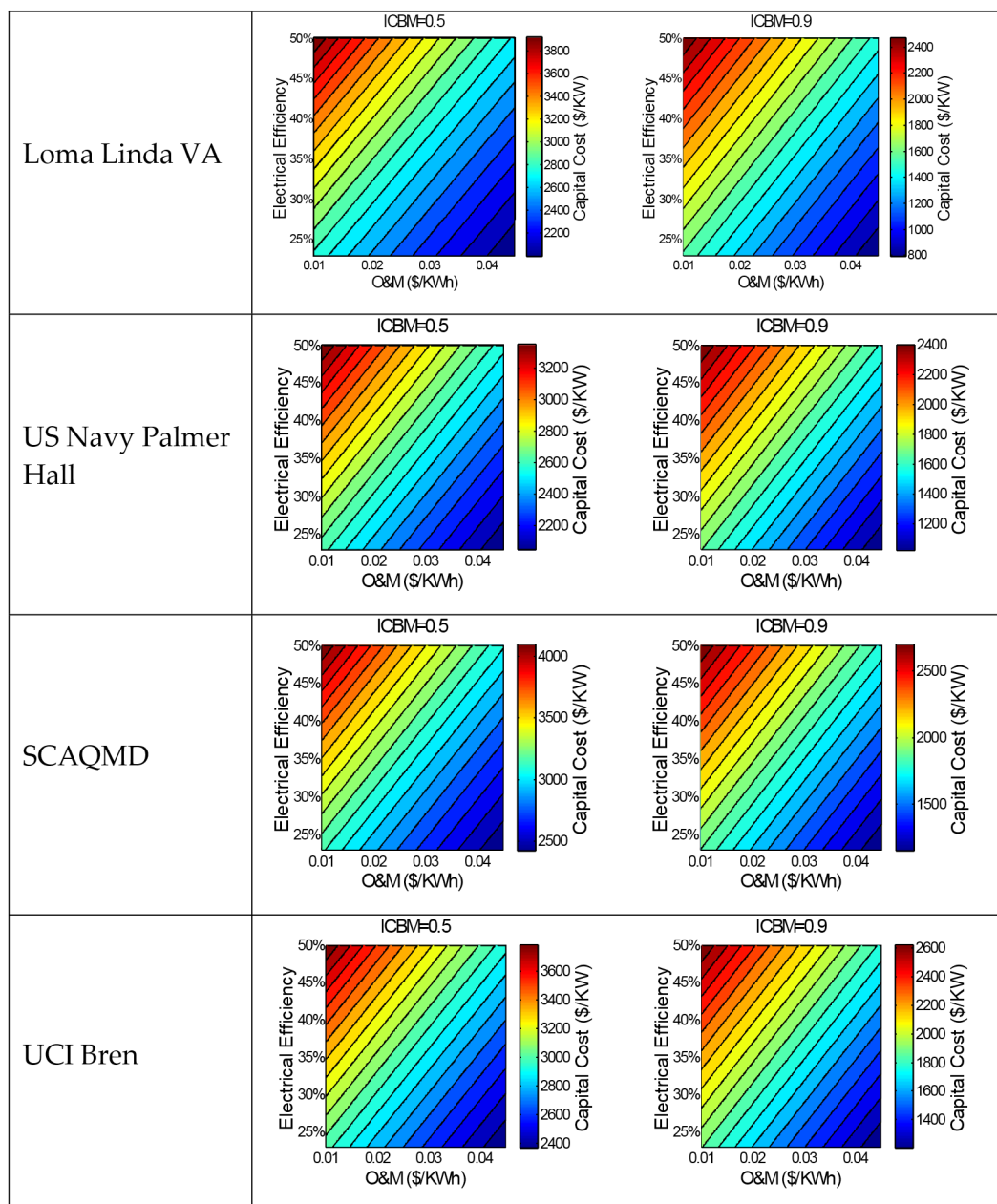
3.4.3.2 Capital Cost with Heat Recovery

Waste heat recovery can produce additional savings that make it possible for DG with higher capital cost to be installed. A building with high coincidence between electrical and thermal loads, such as Loma Linda VA, can install DG with higher capital cost than if they were only pursing electric only DG. This remains true as DG capacity increases for generators with low operating costs. Generators with high operating costs must still have capital costs similar to what is required if the generators were to provide electricity only. Capital cost for buildings

with low coincidence remains approximately equal to the capital cost for DG offering electricity only. This is shown for UCI Bren in Figure 110, which is similar in cost magnitude and trend to Figure 111.

Figure 111: Estimated capital cost for Buildings at which payback takes 10 years for DG operating under standby electric rates with turndown of 50%, and waste heat recovery
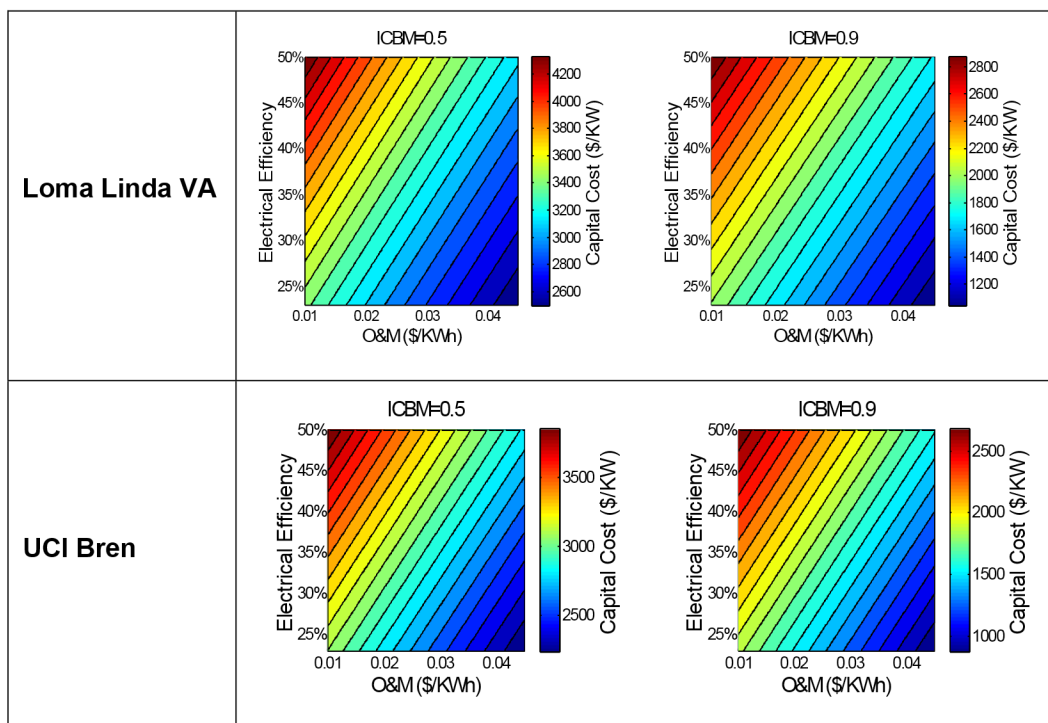
If the parent electric rate is used over the standby electric rate, similar trends emerge as with standby rates. However, the difference in capital cost between DG low and high operating cost under standby rates is much greater under parent rate structures. With demand shifting having no value under the parent rate structure, the value of DG with high operating costs is reduced. Capital cost for DG with high efficiency and low O&M cost is similar to the values found under standby rates. As installations increase, the estimated capital cost under parent rates is much higher than what is allowed under standby rates. This is a result of the standby rate dispatch errors. Better standby rate design can lead to improved economic performance for large DG installations, allowing for generators with higher capital costs than are currently predicted paying back in 10 years under standby rates. Figure 112 shows the estimated capital cost for Loma Linda under parent rate structures. Figure 112 is typical of changes to the estimated capital cost for all buildings presented. When waste heat recovery is included, changes to capital costs similar to what occurs for standby rates occurs under parent rate structures.

Figure 112: Estimated capital cost for Loma Linda VA at which payback takes 10 years for DG operating under parent electric rates with turndown of 50%, and waste heat recovery
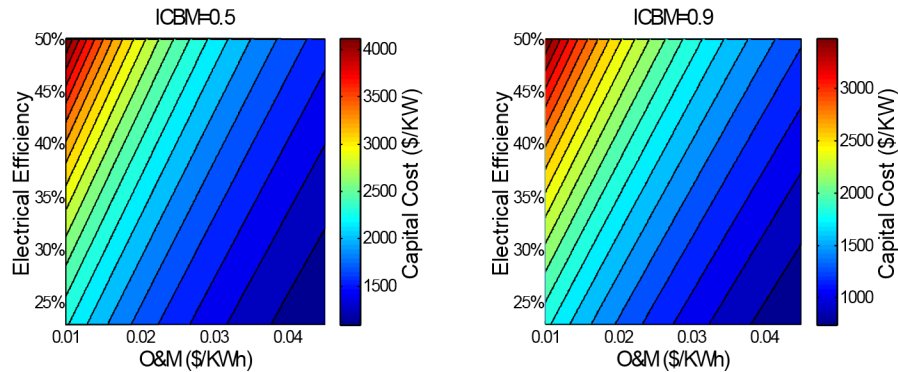
These results highlight the link between the value of the energy produced by DG to the estimated capital cost where a payback of 10 years occur. Generators that are capable of offering more cost reducing activities are capable of supporting a higher capital cost. As the number of cost reducing activities decreases, the capital cost associated with that DG must decrease accordingly. Similarly, the capital cost that can be supported by DG relates to the savings that can be produced under a given rate structure. DG with low electrical efficiency and high O&M cost has value under standby rates that is not present under parent rates, as shown by higher allowed capital cost under standby rates. Concurrently, DG with high electrical efficiency and low O&M cost have similar value under both rate structures.

3.5   Microturbine Emissions

Part load emissions from the C65 MTG can be combined with the corresponding energy produced to give an idea of the emissions produced to meet a given load. This energy production depends on how much energy is utilized from the C65 MTG. Depending on utilization of waste heat, emissions per unit of electricity can vary drastically. Figure 113 shows the amount of heat available from a C65 MTG per unit of electricity generated. Traditionally, waste heat is reported in some form of BTUs. The units of the y-axis of Figure 113 is kWh of waste heat available per kWh electricity generated, allowing for direct comparison between the electrical and thermal products of a C65 MTG. Near full load operation, over twice the amount of energy is available from HR than is produced by the electrical generator. At part load operation, efficiency is reduced, leading to more available waste heat.

Figure 113: Available waste heat from a C65 MTG per kWh electricity generated
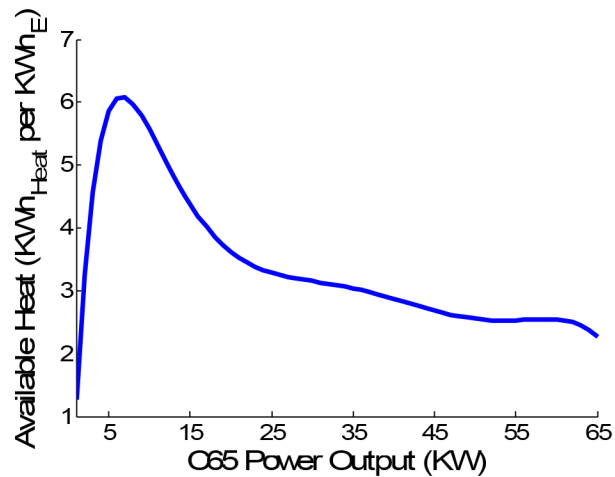
Emission rates per energy production depend on the amount of waste heat recovered. These rates are shown in Figure 114 for CO_2, NO_x, and CO for no waste heat is recovered and all available waste heat is recovered and utilized. The CO_2 emissions curve was determined by assuming that the natural gas fuel is pure methane and that each mole of combusted methane produced one mole of CO_2. Figure 114 shows that waste heat recovery can significantly reduce emission rates, particularly for CO_2. It is clear that the least amount of emissions are produced near or at full load. Figure 115 shows the emissions for operation near or at full load for a C65 MTG.

Figure 114: Part load CO_2, NO_x, and CO emissions for a C65 MTG with 0% waste heat recovery and 100% waste heat recovery

141
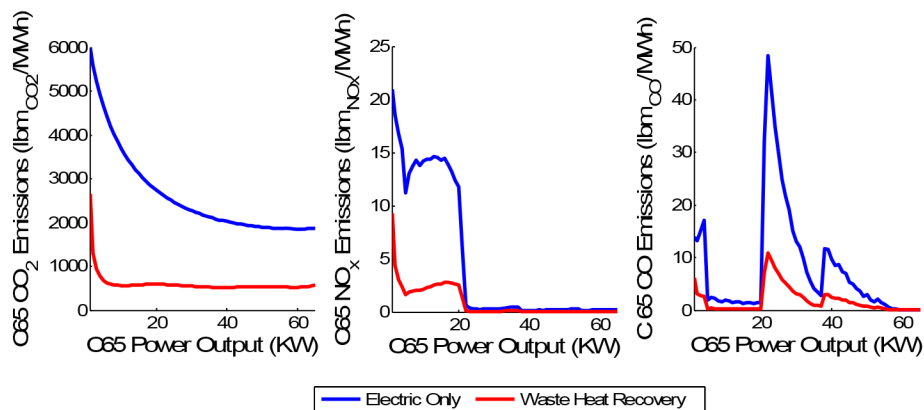
Figure 115: Part load CO₂, NOₓ, and CO emissions for a C65 MTG operating near full load with 0% waste heat recovery and 100% waste heat recovery
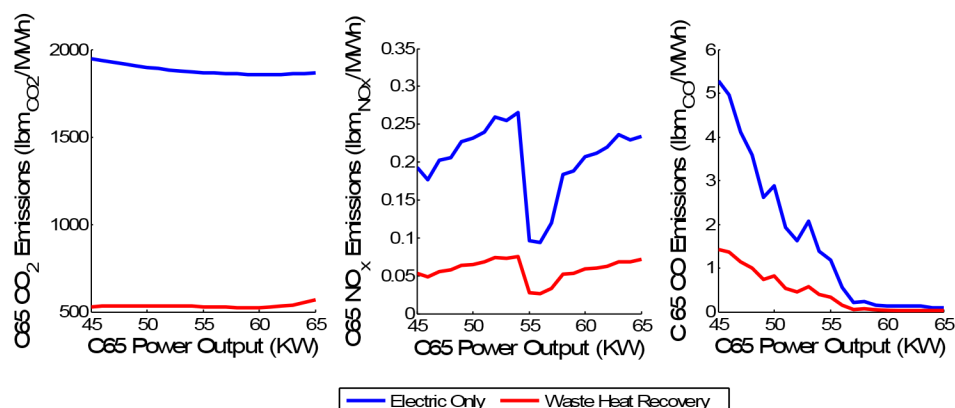
In some areas, such as California, standards and emission limits exist for C65 MTG operation. It is clear that operation of a C65 MTG with no waste heat recovery produces pollutant emissions of NO_x and CO at rates that surpass California Air Resources Board (CARB) limits. CO emissions are below CARB limits at full power operation, but quickly surpass the limits even at near full load operation. If a C65 MTG is to meet these limits, waste heat must be utilized.

It is also clear from these figures that while the pollutant emission limits might be lower than either the CA or US electric grid, a C65 MTG produces carbon emissions at rates that are higher. With a possible benefit of DG being reduced carbon emissions, it is important to determine how much waste heat recovery is necessary for a C65 MTG to reach carbon emissions parity with traditional energy production methods.

The carbon emissions of a C65 MTG are not only compared to the carbon emissions of the electric grid if waste heat is utilized. Since it is assumed that waste heat recovery replaces heat that would have been supplied through the firing of a natural gas boiler, the carbon emissions from the boiler are also avoided. Parity between a C65 MTG with waste heat recovery and traditional energy is achieved when carbon emissions from a C65 MTG is equivalent to the carbon emissions combined emissions of the electric grid and natural gas boiler. Assuming 90 percent of the fuel bound energy is converted into heat in a boiler, natural gas is pure methane, and all methane is converted into CO_2, the emissions factor for a boiler is 483.38 pounds of CO_2 for every MWh of heat produced.

3.5.1 C65 MTG and CARB Standard

If all waste heat available from a C65 MTG is utilized, the generator meets the CARB emission limits only for near or full load operation, as shown in Figure 116. Figure 116 shows the emissions of a C65 MTG normalized to the CARB limits; a C65 MTG is below the emissions limit if the corresponding value in Figure 116 is at or below one on the y-axis. Each individual pollutant drop below the CARB limits during small windows of part load of operation, but the only time when both pollutants are emitted at levels below CARB limits is at and above 57 kW.

Figure 116: NO$_x$, and CO emissions for a C65 MTG operating near full load normalized by the CARB emission limits with 100% waste heat recovery
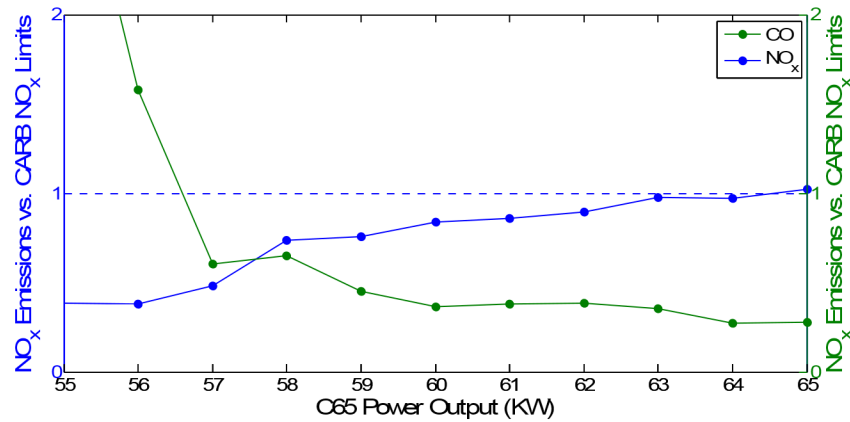
Complete utilization of available waste heat is difficult unless the generator is undersized for the thermal load it is satisfying. In addition, full utilization of heat is not needed for the CARB limits to be met. This is shown in Figure 116 when full waste heat utilization results in the emissions limit to be lower than the CARB limits. Partial utilization of waste heat can lead to satisfaction of CARB limits. Figure 117 shows the percent of waste heat that must be utilized in order for a C65 MTG to meet CARB emission limits.

In order for a C65 MTG to operate at emission rates lower than the CARB limits, the generator needs to be operated at or near full load and a large portion of waste heat must be utilized.

Figure 117: Percent of waste heat to be recovered for C65 MTG to meet CARB limits for NO$_x$ and CO

143
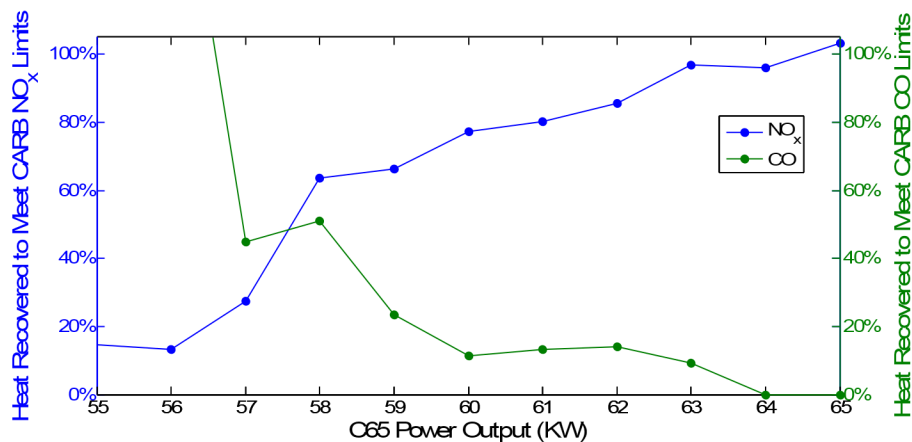
3.5.2 C65 MTG and CA Electric Grid

NO_x emissions produced by the California electric grid are higher than what is produced by a C65 MTG at near or full load. CO emissions are not reported for the California electric grid. If no waste heat is utilized, a C65 MTG produces much more CO_2 than the CA electric grid, as shown in Figure 118. Figure 118 shows the CO_2 emissions from a C65 MTG normalized by the CO_2 emissions from the California electric grid. Waste heat must be utilized if a C65 MTG is to reach CO_2 parity with the California electric grid.

Figure 118: CO$_2$ from a C65 MTG normalized by the California electric grid CO$_2$ emission
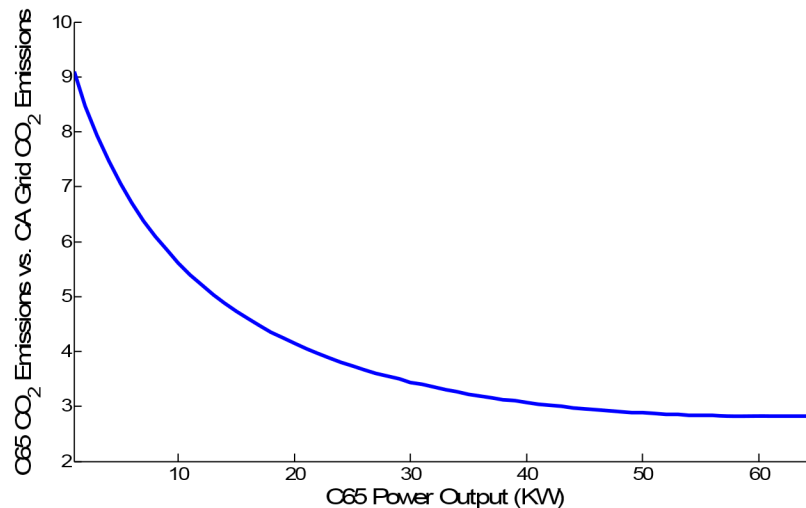
Waste heat recovery can lead to CO_2 parity with the electric grid alone. However, waste heat recovery is replacing thermal loads that would have been met by a natural gas fired boiler, negating the CO_2 emissions associated with natural gas combustion in the boiler. By reducing boiler operation, a C65 MTG can reach CO_2 parity with traditional means used to supply building energy. Figure 119 shows, for part load C65 MTG operation, the amount of heat that must be recovered for parity, the percentage of available waste heat that must be recovered, and the resulting emissions rate at which parity is achieved with the California electric grid and a natural gas fired boiler. At reduced power settings, much more heat must be utilized in order to reach parity with the grid. However, even at very low power settings, parity is achieved at less than 50 percent of the available waste heat being utilized. Ultimately, lower carbon emissions are achieved at close to full load operation. Since only a portion of the waste heat is required to be utilized to reach CO_2 parity, if more waste heat is utilized, a C65 MTG will outperform traditional methods of supplying building energy in therms of carbon emissions. If enough heat is utilized to satisfy the CARB emission limits, a C65 with produce less CO_2 emissions than if the building demand was satisfied through the California electric grid and the firing of a natural gas boiler.

144

The California electric grid CO_2 emissions factor is the average for the entire state of California. This emissions factor is a composite of different generators with varying levels of CO_2 production. C65 MTG operation may lead to the replacement of energy that was produced by less carbon intensive generation, requiring higher levels of heat utilization for CO_2 parity to be achieved. Further breakdown of the state wide CO_2 emissions factor is not readily available and producing area specific emission factors would lead to better understanding of the amount of waste heat recovery required to reach CO_2 parity for a specific area. This work, however, falls outside the scope of this current work.

Figure 119: Amount of heat recovery required, percent of available heat, and C65 MTG CO2 emission rates required for a C65 MTG to reach CO2 parity with the California electric grid
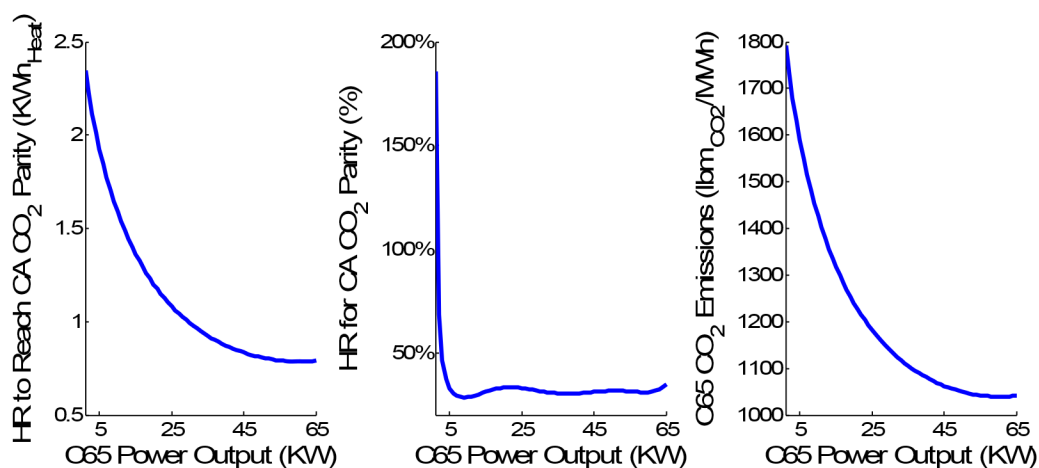
3.5.3 C65 MTG and US Electric Grid

NO_x and CO emissions are produced at a lower rate for a C65 MTG operating at or near full power without heat recovery than by the US electric grid. CO_2 emissions, however, are not. Figure 120 shows the CO_2 emissions from a C65 MTG normalized by the US electric grid CO_2 emissions. The US electric grid produces CO_2 at a higher rate than the California electric grid, resulting in C65 MTG CO_2 emissions without heat recovery being closer to the US electric grid than the California electric grid.

Figure 120: CO_2 from a C65 MTG normalized by the US electric grid CO_2 emission
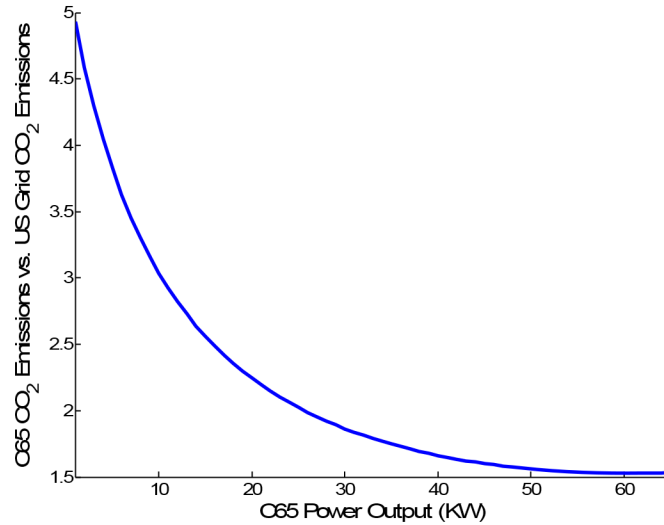
Waste heat utilization brings a C65 MTG closer to parity with the US electric grid and also eliminates CO_2 emissions from a natural gas fired boiler. Figure 121 shows, for part load C65 MTG operation, the amount of heat that must be recovered for parity, the percentage of available waste heat that must be recovered, and the resulting emissions rate at which parity is achieved with the US electric grid and a natural gas fired boiler. Similar trends to the California electric grid are seen for the US electric grid. However, since the US electric grid emits CO_2 at a higher rate than the California electric grid, parity can be reaches with the US electric grid by utilizing less of the available waste heat.

Figure 121: Amount of heat recovery required, percent of available heat, and C65 MTG CO_2 emission rates required for a C65 MTG to reach CO_2 parity with the US electric grid

146
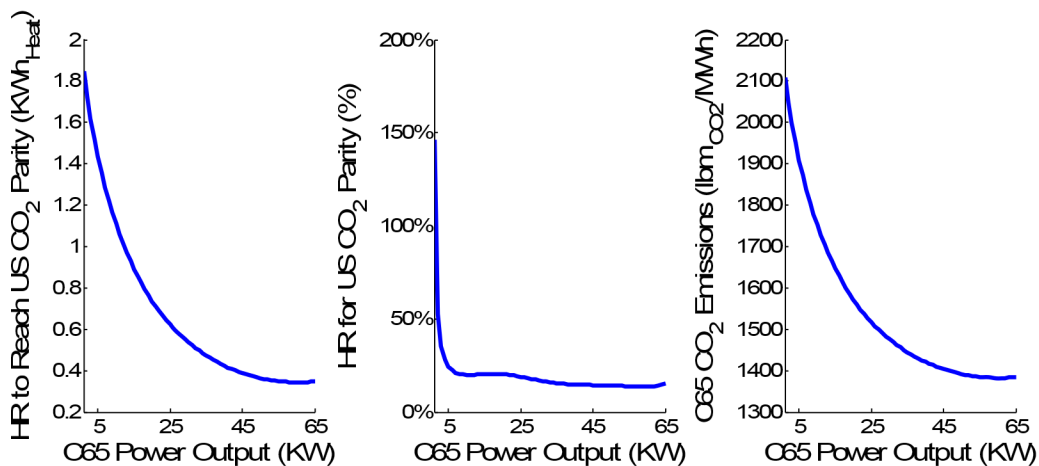
CHAPTER 4:
Economical Dispatch of CCHP Systems Novel Control Algorithms Development, Installation and Verification

4.1 Develop and Test Novel Control Algorithms and Architecture

4.1.1 Plant 'Master Controller' Development

The ELF building has a limited set of fuel cells (5kW) and a PV installation of about 5kW. There are three micro-turbines of 65kW capacity each. Not all of them are in working condition. Due to the limited energy contribution of the fuel cells and PVs and the considerable effort and cost required to include them in the control strategy, we will not implement an active control of these energy resources in the course of this demonstration. In summary, the control implementation will be limited to the control of the micro-turbines and the HVAC system and industrial loads at the ELF building. In simulation and theory these distributed energy resources namely PVs and fuel cells can be considered. The overall architecture of this demonstration is illustrated in Figure 122. As shown in the figure, the smart energy box will be connected simultaneously to two separate networks:

1. The building automation network called FACnet will provide access to the Building Automation Network (via BACnet and SOAP protocols), the Micro-Turbines and Industrial Loads (via Modbus protocol and wireless sensors).

2. The second network is the UC-Irvine public network DMZ or "Demilitarized Zone". It provides access to the internet for weather forecast acquisition.

To implement the novel control algorithm developed in the course of this project we need:

- Weather forecast for energy demand forecasting;

- Historical energy consumption data for the building;

- Historical data on industrial load activity for model calibration and forecasting on industrial loads activities.

- Access to the building automation for control of the HVAC system;

- Access to the Micro-Turbines to controller.

The access to these subsystems we will be done with the use of existing software interfaces and building new ones. The table below list software components created or modified for the demonstration at the ELF building.

Figure 122: Overview of the Master Controller
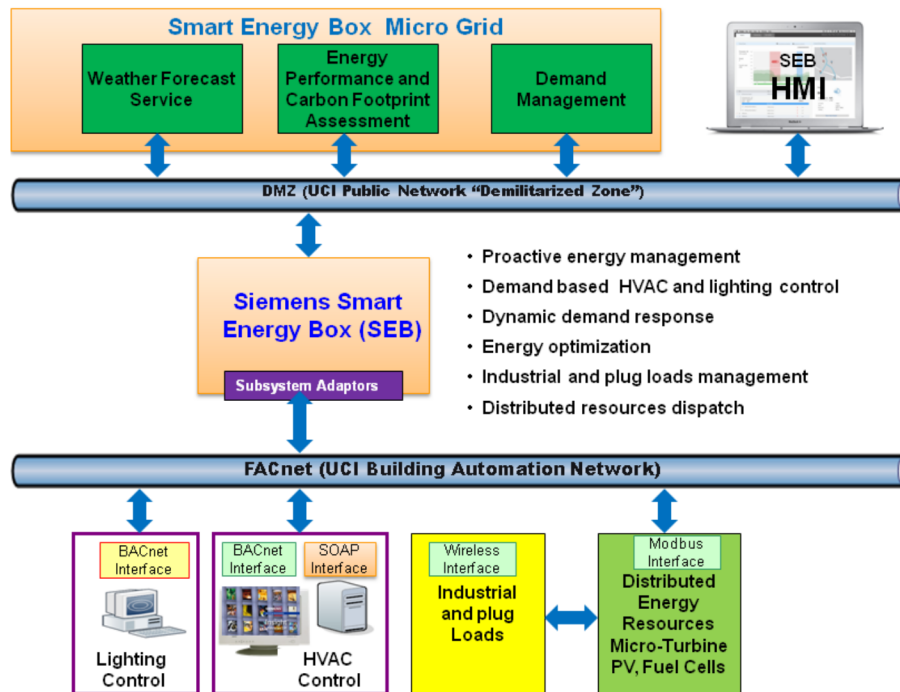
Figure 123: Master Controller Architecture Overview
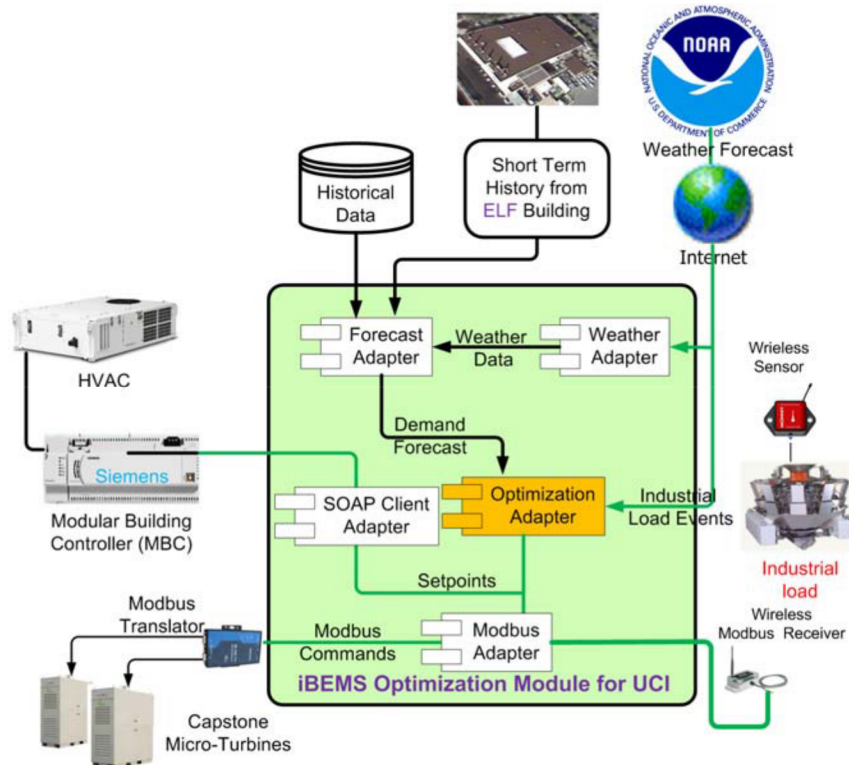
Table 25: Software Components needed for the Demonstration at the ELF Building

Item	Component Name	Description
1	Forecast Adapter	This component predicts the energy usage of the building based on historical knowledge of weather and past energy consumption measurements.
2	Modbus Adapter	This component implements the Modbus TCP protocol to control the Capstone Micro-Turbines at the ELF building, Modbus RTU protocols to monitor industrial load via Modbus Wireless sensors.
3	SOAP Adapter	This component enables the software to connect to the Siemens's Modular Building Controller (MBC) that controls the HVAC system of the ELF building.
4	Weather Adapter	The component provides the interface to read the weather forecast.
5	Optimization Adapter	The Optimization module provides the implementation of the translated Novel Controls developed in the course of this project.

Forecast Adapter: The load forecasting algorithms developed in the course of this project and tested in simulation with Matlab Simulink have been translated to C# and integrated to Siemens iBEMS via the Forecast Adapter component. This component takes as inputs the weather data and historical energy consumption of the building and provides 24 hours look ahead energy consumption predictions. The module also uses the latest available energy consumption data (short term history) to adapt its predictions.

Modbus Adapter: This component is a wrapper of the Modbus TCP protocol necessary to communicate with the Capstone micro-turbines at the ELF building. The Modbus network connection between the SEB and the Capstone micro-turbine system is through a Modbus gateway or Modbus translator. For this project, the model 7112 Plus by Moxa is used. This Modbus translator model is preconfigured to support connectivity with Capstone micro-turbine model C30, C65, and C200. The translator connects to the micro-turbine by serial RS-232 at port P1. Its Serial port RS-485 is reserved for connection with other micro-turbines. The device has two Ethernet ports, LAN1 and LAN2, with factory preset IP addresses. LAN1 designated for configuration while LAN2 is for network connection. The Smart Energy Box will connect to the translator via Ethernet or TCP/IP connection at port LAN2. The general schematic for the network connection is displayed in Figure 124.

Figure 124: Modbus translator UC 7112 Plus Connections
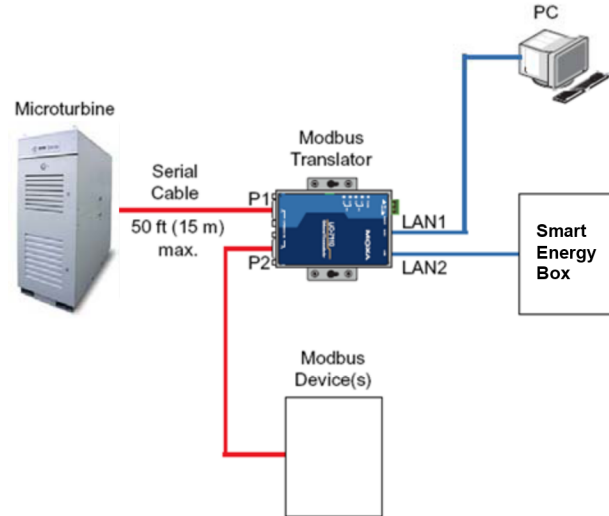
SOAP Adapter: This component will be used to communication with the existing building automation system at the ELF building. The Siemens Modular Building controller (MBC) currently at the ELF Building is a controller with limited feature that does not support BACnet protocols but supports SAOP protocols. Researchers purchased and installed an SAOP server on the Siemens APOGEE Insight server. With that license setpoints of the ELF building for Read/Write can be exposed to SAOP Clients. The SOAP Adapter is a SOAP client Wrapper that allows the optimization module to read and modify setpoints of the building automation controller at the ELF building.

Optimization Adapter: This component is a wrapper of the translated Novel control algorithms. It takes as inputs the energy forecast from the forecast module, the weather data, the industrial load forecast as well as its current status via wireless sensors, the current building controls setpoints and computes new building control setpoints and energy generation setpoints such as the capstone micro-turbines setpoints. The figure below shows the execution sequence of the optimization module.

Figure 125: Optimization Schema of the Smart Energy Box (SEB)
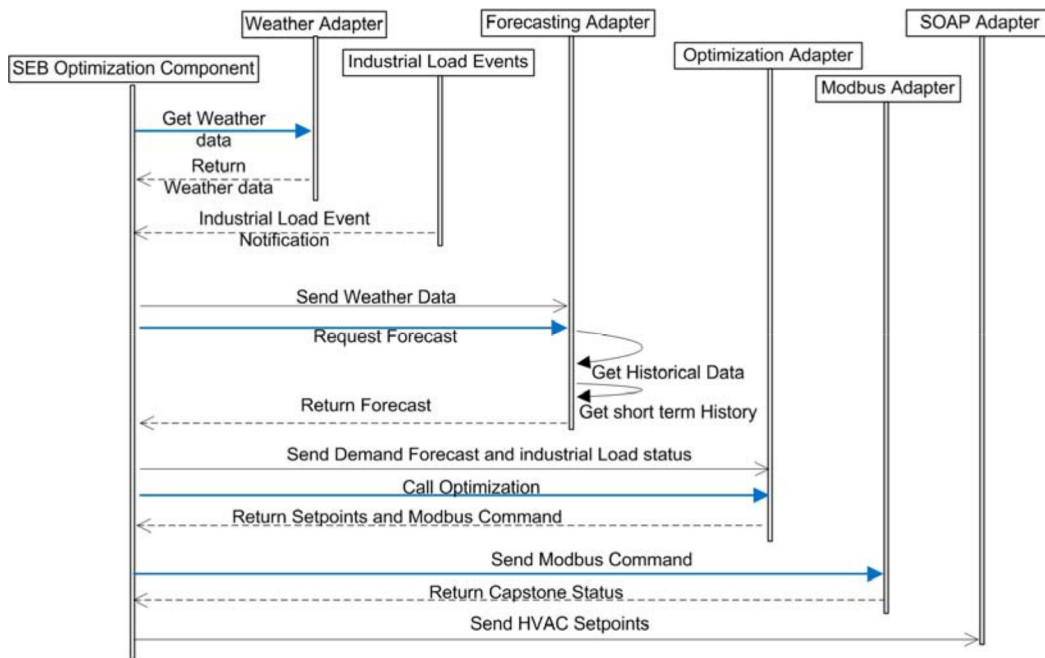
4.1.2 Sub-System Control

The ELF building sub-systems such as micro-turbines, laboratory equipments and supporting equipments required to run those lab's equipment such as air compressors, heaters, etc…. schedule is random. The purpose of the control of these equipments is to mitigate peak loads generated by running these equipments. Since researchers cannot prevent these lab equipments from running when they are needed, the options of control remaining are to offset their load when it happens. There are many ways to determine that these loads are running:

- Monitoring of the central power meter for sudden changes. There is no direct connection to the central power meter at the ELF building therefore this approach cannot be used,

- Sub-metering loads: This option will be used in the future but it is not available for this project.

- Adding sensors on loads: This option has been implemented for some of the loads for example the pressure in the air tank is being monitor with wireless sensor and is being recorded by the SEB.

- Forecasting when the load is likely to come on. Researchers developed and implemented advance techniques of load forecasting based on historical data. These techniques will be discussed in the following sections.

4.1.2.1 Industrial Loads Forecasting

This subsection presents our model developed for forecasting of industrial load dynamic using the ELF building historical data. There are limited sources that accounts for the majority of

151

industrial load in the ELF building (e.g. one 100-kW compressor, two 300-kW compressors and two 500-kW heaters). The separated load data for all equipment were not available, therefore total industrial load was used to predict the probability of having industrial load event in the next time slot. The research was planned into three steps:

- In the first phase, a preliminary statistical analysis was performed to categorize the load dynamic patterns over time and to extract the major features of load data.

- In Step 2, a generalized linear model (GLM) was employed to explain the relationship between time and frequency of industrial load for a given time interval.

- In the next step, the model was fed into a simple algorithm, which determined the industrial load status for the next 15 minutes.

The proposed algorithm returned three values:

- "1" for higher chance;

- "0.5" for moderate chance and;

- "0" for lower chance of having industrial load event in the next 15 minutes.

 In addition, the performance of the proposed approach was investigated using the two years real historical data of the building.

4.1.2.2 Frequency Analysis

In this step, a comprehensive statistical analysis was performed using different quantitative tools to better understand the main patterns of data. The total building load data were recorded every 15 minutes during 24 hours of a day and were available for all months of 2009 and 2010 and a few days of 2011. Figure 126 depicts the descriptive statistics and box plots of the building load data categorized by year. In our analysis, the 2011 load data are not used, since the available data were not sufficient for statistical analysis. The average building energy consumption increased from 2009 and 2010 showing that these two years did not follow the same load pattern. The same results are shown in Table 26, where a Kruskal-Wallis test was applied to investigate the homogeneity of the 2009 and 2010 datasets. The lower value of p-value shows that the two datasets are not homogenous.

Figure 126: Descriptive Statistics and Box Plots of Total Load Data Categorized by Year
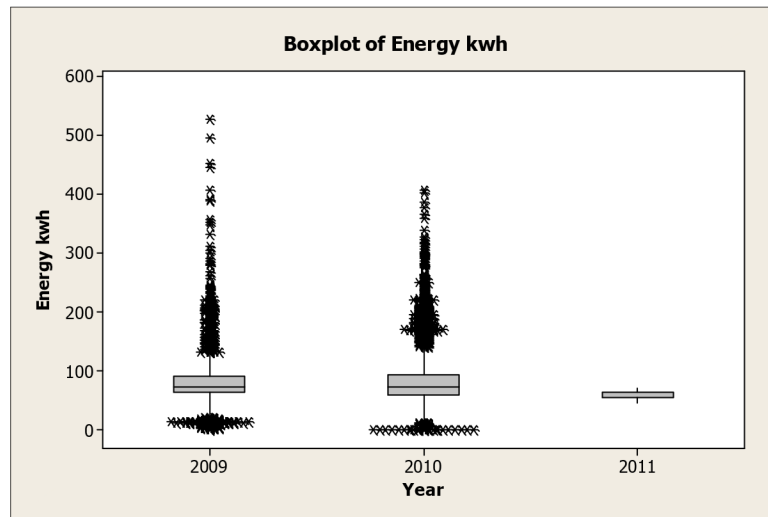
Table 26: Kruskal-Wallis Test for Load data vs. Years

Year	N	Median	Ave Rank	Z
2009	8746	73.80	8819.5	1.73
2010	8760	73.62	8687.6	-1.73
Overall	17506		8753.5	

H = 2.98 DF = 1 P = 0.084

H = 2.98 DF = 1 P = 0.084 (adjusted for ties)

As a result, we built our model based on the 2010 dataset, as it was the last available dataset from the building. Figure 127 present the 2010 frequency of industrial load occurrence categorized by month and weekday. It is shown that the number of industrial load events observed in the last three months is significantly greater than in the other months. In addition, the difference between weekdays and week-ends are significant that should be taken into account in the modeling phase.

Figure 127 (b) and Figure 128 (b) presents the 95 percent confidence interval for the average monthly and daily energy consumptions. The results reveals that month and day are important factors to be considered in the model and can capture a portion of total variability. It implies that the proposed forecast model should include variables that represent the current month and current day.

Figure 127: (a) The frequency of industrial load occurrence categorized by month, (b) 95% Confidence Interval for the average monthly energy consumption (kWh)

(a) Month
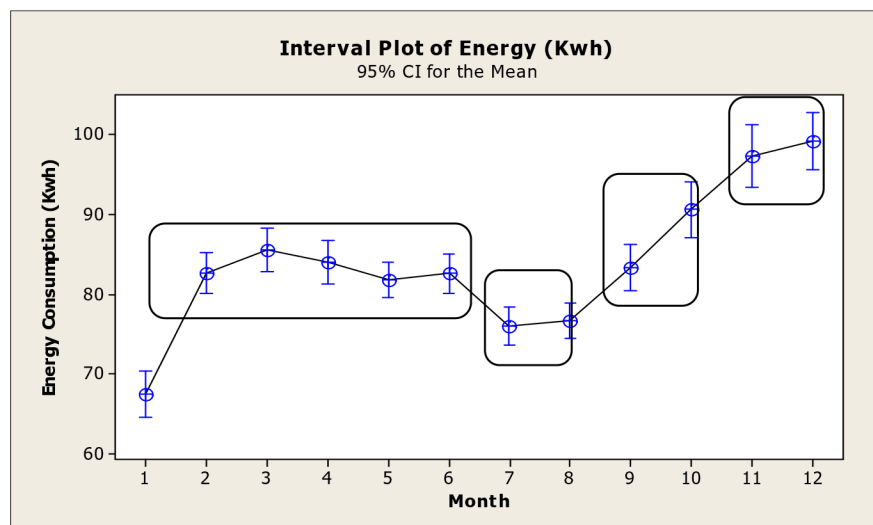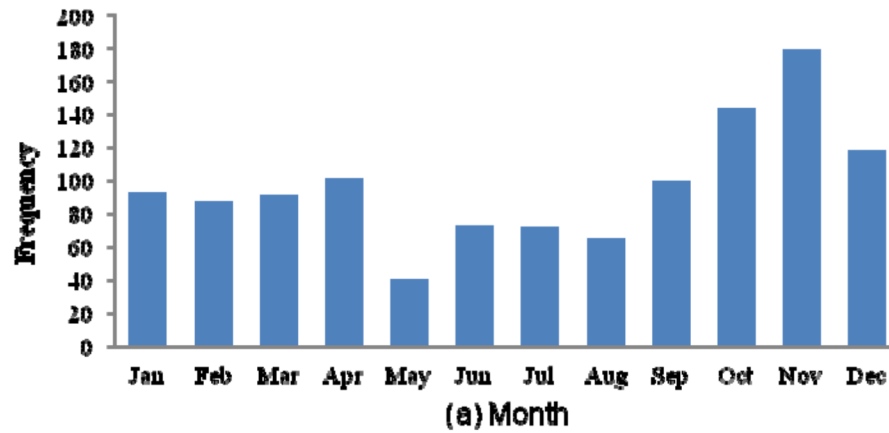
(b)

Figure 128: (a) The frequency of industrial load occurrence categorized by days of the week (b) 95% Confidence Interval for the average daily energy consumption (kWh)

(a) Weekdays
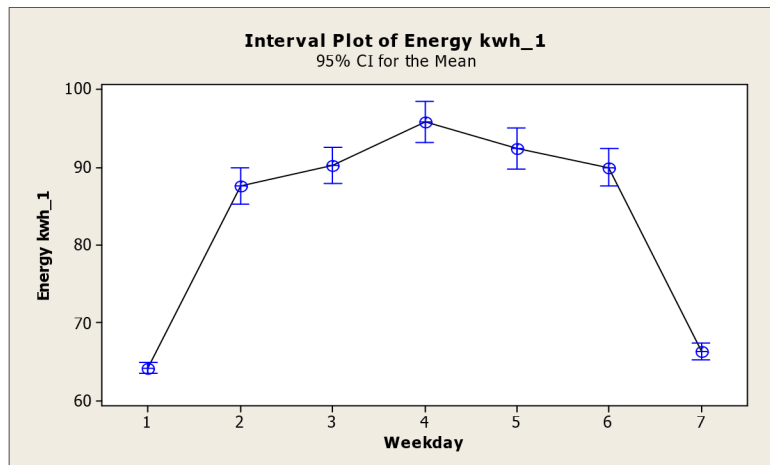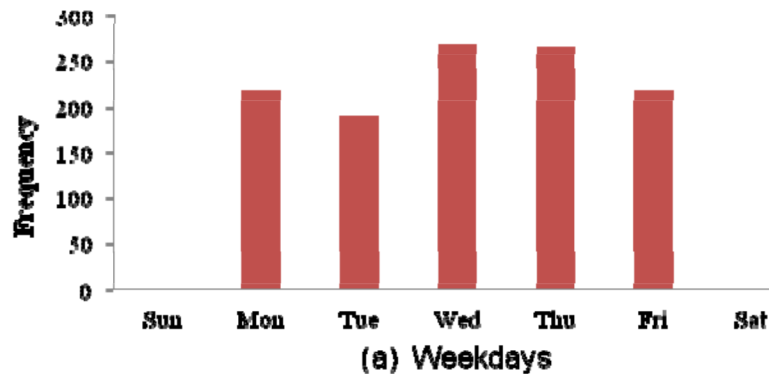
(b)

The frequency of industrial load occurrences categorized by hours is presented in Figure 129. It is observed that the frequency distribution is a unimodal distribution where the probability of having an industrial load event between 15:00 p.m. through 17:00 p.m. is greater than rest of the hours. These simple analyses can help to provide a better insight about the patterns hidden among the building load dataset.

Figure 129: The frequency of industrial load occurrence categorized by hours of the day
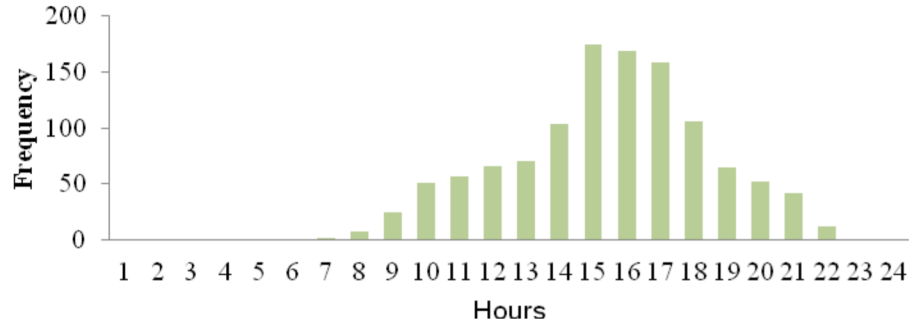
4.1.2.3 The proposed Algorithm

In order to forecast the probability of having an industrial load in the next few hours, a simple algorithm was coupled with the aforementioned Logistic regression model. The proposed algorithm used the results of regression model and the current and past status of the building load to forecast the probability of industrial load. It could return three values (1, 0.5, and 0) as mentioned earlier. The result showed that the proposed approach could effectively predict the future probabilities of industrial load occurrence and at the same time could maintain the false alarm in an acceptable level. By forecasting industrial load for any quarter-hour-ahead, one can take a quick action to manage the energy consumption and lower the total energy cost. The following steps should be done in order to run the proposed algorithm:

Algorithm

{

> **Step 1**: Convert the month, day and hour to the corresponding indicator variables. By adding n-1, separate indicator variables instead of a single variable with n states or values, one can add the categorical values such as months or weekday to the model. For example, if X is the weekday values i.e. Sunday, Monday, …, Saturday, researchers use $\{x'_i = 0 \text{ or } 1 \mid i=1,2,\ldots,6\}$.

> **Step 2**: Input the indicator variables and calculate the initial probability of industrial load, $\hat{\pi}^t_{ijk}(w)$, using Equation 1:

> **Step 3**: If $\hat{\pi}^t_{ijk}(w) > H^u$ then the current state at time t is 1 (Red) implying a higher probability of having industrial load in the next 15 minutes. If $\hat{\pi}^t_{ijk}(w) \leq H^l$, then the current state at time t is zero (Green) implying that there is a lower chance to have an industrial load in the next time slot (next 15 minutes). In this case, go step 1.

> If $H^u \geq \hat{\pi}^t_{ijk}(w) > H^l$ then the current state at time t is 0.5 (Yellow) implying that there is a moderate probability of having industrial load in the system. In this case, go step 4.

156

Step 4: Calculate the probability of industrial load for the p consecutive past data t-1, …, t-p. If there are q ($< p$) time slots with higher probabilities of having industrial loads, then the current state at time t is 1 (Red), otherwise, the current state at time t is 0 (Green)

}

The optimal values of p and q can be found using an optimization method that minimizes Type II error (*Probability of not alerting an industrial load when there is a real industrial load in the building*) while maintaining Type I error (*Probability of false alarm when there is a normal load in the building*). In addition, H^u and H^l are the upper and lower limits for probability values and can be used to adjust the Type I and Type II errors.

Researchers investigated the performance of the proposed method using 2010 real energy data of the ELF building. Table 27 shows the result of the proposed algorithm. Note that for this figure, it is assumed that the industrial load is any load greater than 200 *kW*.

Table 27: The percentages of accurate forecasts, type I and Type II errors (Industrial load > 200 KW)

Value	Count	Percent	Comment
-1	246	0.70%	Type II Error
0	30988	88.44%	Percentage of accurate forecast
1	3806	10.86%	Type I Error
78% of all Industrial Loads were detected correctly Model Accuracy (Signals)			

Value	Count	Percent	Comments
-1	143	0.41%	Actual: Industrial load Detected: Green
-0.5	358	1.02%	Actual: Industrial load Detected: Yellow
0	26463	75.52%	True Signal
0.5	4358	12.44%	Actual: Normal load Detected: Yellow
1	3718	10.61%	Actual: Normal load Detected: Red
56% of Industrial load were flagged Red, 30 % were flagged Yellow, 85% combined			

The proposed model was able to provide correct forecasts for more than 88 percent of time slots during 2010 (For both industrial and normal load cases combined). It identified 78 percent of all industrial loads occurred during year 2010. Note that these results were given by only using Equation 1 and before applying the proposed algorithm. By applying the algorithm, researchers were able to detect 86 percent of all industrial loads during 2010. The algorithm could directly

identify 56 percent of industrial loads (by alarming red signal) and could indirectly identify the other 30 percent (by alarming yellow status).

In addition, the proposed algorithm was investigated when the industrial load considered as any load greater than 160 KW. Table 28 summarizes the results. It shows that by applying the proposed model one could identify 75 percent of all industrial loads. If the proposed model is enhanced by the algorithm, the chance to detect an industrial load increases to 78 percent.

Table 28: The percentages of accurate forecasts, Type I and Type II errors (Industrial load > 160 KW)

Value	Count	Percent	Comments
-1	621	1.77%:	Type II Error
0	31278	89.26%:	Percentage of accurate forecast
1	3141	8.96%:	Type I Error
75% of all Industrial Load is detected correctly			
Model Accuracy (Signals)			

Value	Count	Percent	Comments
-1	527	1.50%	Actual: Industrial load Detected: Green
-0.5	616	1.76%	Actual: Industrial load Detected: Yellow
0	26731	76.29%	True Signal
0.5	4112	11.74%	Actual: Industrial load Detected: Yellow
1	3054	8.72%	Actual: Industrial load Detected: Red
53% of Industrial load were flagged Red			
25% were flagged Yellow			
78% combined			

4.1.3 System Configuration and Optimization

4.1.3.1 ELF Building System Overview

In modeling the ELF building located at University of California, Irvine with EnergyPlus researchers indentified a total of 47 different zones serving different purposes from laboratory (wind tunnel, combustion science, and civil engineering) to office. The building has two floors with a total floor area of 34,000 ft². The cooling and heating demands of the ELF building are supplied by a HVAC system with two Air Handling Units (AHU) and 62 Variable Air Volume (VAV) boxes.

158

The hot water, chilled water, and a major part of its electricity of ELF building are supplied by the UCI central. The chilled (or hot) water supplied from the central plant provides the thermal energy required for the cooling coil of the AHUs (or VAV boxes). The ELF building also has an on-site electricity generation system including two to three 65 kW Capstone micro-turbine (MT) generators, one 5 kW array of Photovoltaic (PV) solar panels (optional), and one 5 kW fuel cell (optional). The electricity and natural gas consumed by the ELF building and its HVAC equipments are purchased from the utility companies (Southern California Edison and Southern California Gas). The systematic diagram of the ELF building energy system is illustrated in Figure 130.

Figure 130: UCI ELF building energy system diagram (Notations: AS – Air Supply, AR – Air Return, CWS – Chilled Water Supply, CWR – Chilled Water Return, HWS – Hot Water Supply, HWR – Hot Water Return, ELS – Electricity Supply, OA – Outside Air, EA – Exhaust Air)
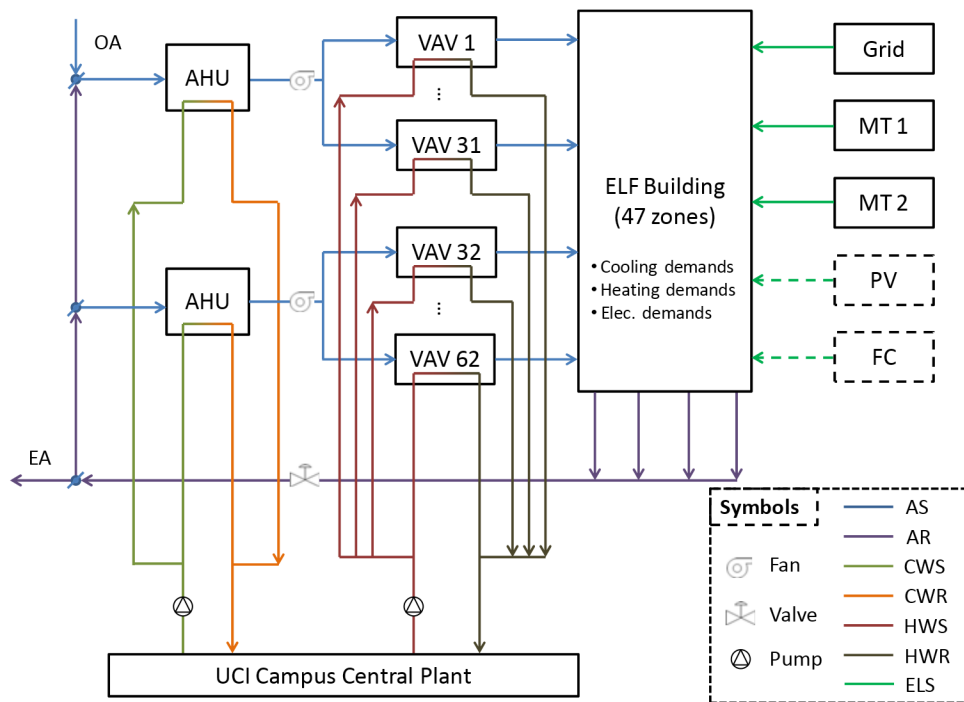
Further analysis of electricity consumption of the ELF building shows that the majority of operational cost comes from demand charge assessed on electricity consumptions peaks. The peaks come from experiment equipments in ELF building: one 100-kW compressor, two 300-kW compressors and two 500-kW heaters. When these equipments are running, their electricity consumption overwhelms all other units such as HVAC, plug-loads and lighting in ELF building and creates huge peaks demand on the electricity consumption profile as shown in Figure 131 .

159

Therefore our control objective is to generate set-points for onsite generation equipments and HVAC system so that the peak electricity consumption is compensated by load shedding and onsite generation, thus reducing possible demand charges.

Figure 131: Comparative Energy consumption for ELF building (simulation vs meter data)
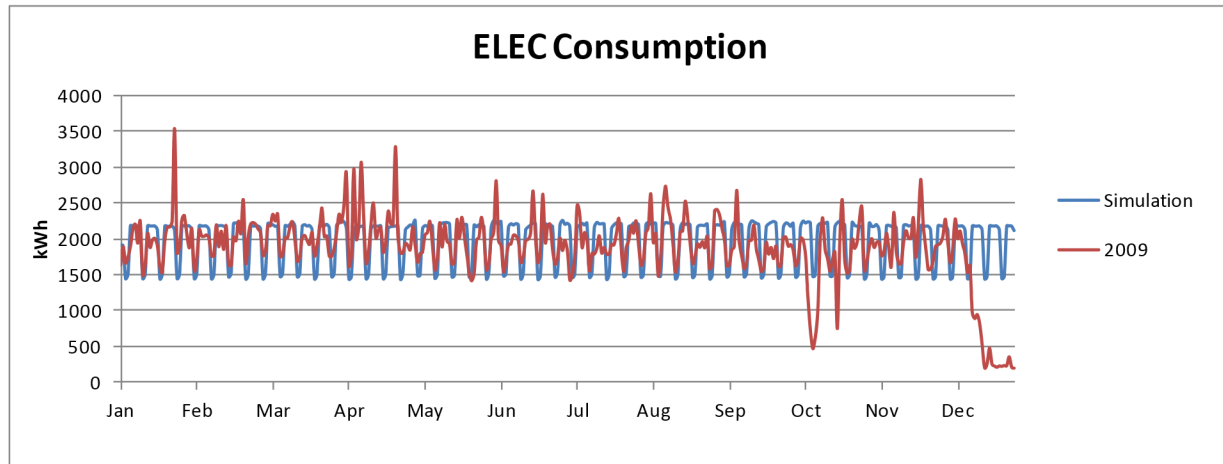
4.1.3.2 HVAC System

The HVAC system is monitored and controlled by APOGEE Insight BMS system. There are two AHUs in the ELF building. The layout and points for them are similar. There are 14 exhaust fans that are DDC with ON/OFF set-points. The points of heating system can be read/write from Smart Energy Box (SEB).

4.1.3.3 Microturbine

The ELF building has three Capstone micro-turbines that can be used for on-site generation. Through Siemens Smart Energy Box, researchers can send ON, OFF and power level set-points to these micro turbines to control their operation.

4.1.3.4 Optimization of ELF Building Operation through Novel Control Algorithm

The novel control system structure is shown in. This control system utilizes two sources of information regarding the operation condition of large equipment s (heaters and compressors in ELF building): the forecast algorithm described in previous section and a set of sensors mounted to heaters and compressors. When a heater or a compressor is about to turn on, sensors will send signal to SEB. Based on this information, control algorithm generates set points for Capstone micro turbines and HVAC system to accommodate the upcoming high energy consumption.

A rule based control logic is used here: when the forecast algorithm predicts high industrial load probability for the next hour, the SEB sample sensor readings more frequently, and tune down the HVAC energy consumption by shutting down some of the fans; when the forecast

algorithm predicts low industrial load probability for next hour, the SEB reduce the sensor reading sampling frequency and stop controlling the energy consumption of HVAC system.

When an equipment turn-on signal is detected by a sensor, SEB will ramp up the gas turbine and set it to proper operation level to meet the upcoming electricity demand as much as possible.

The reason for adopting such control logic is that there is a probability that forecasting algorithm gives false alarm, so directly control micro turbine based on forecasting results is too aggressive. Researchers instead choose to monitor the sensor signal more closely during high risk time periods. When the heater or compressor is turned on and detected by the sensor, the gas-turbine can ramp up very quickly to follow the demand curve.

Figure 132: Control System Structure
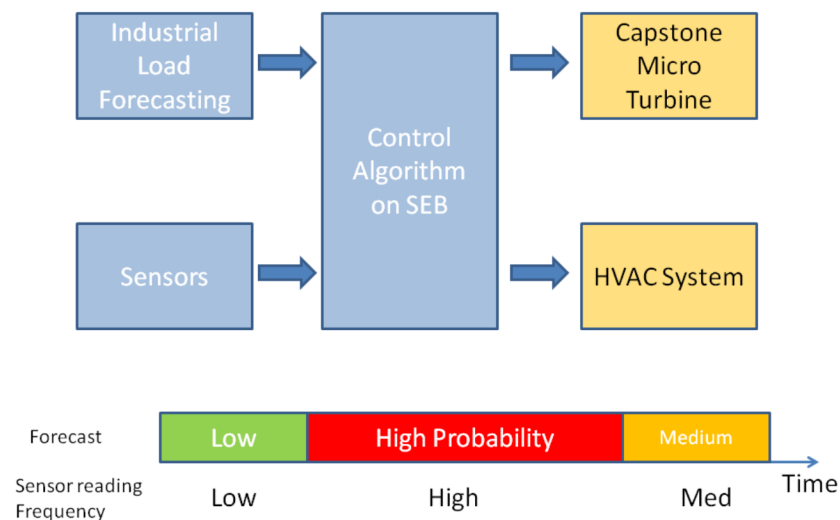
4.2   Translate Novel Control Algorithms to Siemens Controls

The implementation of the control system described in previous sections to Siemens control solution is shown in Figure 133.

The weather forecast is obtained NOAA from weather information service. Although weather data and based load forecast (not industrial load forecast) are not directly used at this time, they are made available for future use when the equipment of ELF are upgraded, for example, to support direct control and add bigger energy storage.

During control system implementation, there is a need to translate the prototypical algorithms of industrial load forecasting and control logic from MATLAB to C/C# and integrate the resulting components to Siemens Smart Energy Box. To make sure the translated version consists with MATLAB prototype provided by Rutgers University, extensive tests were carried out.

The following lists some test results for the electricity load forecasting algorithm. The total forecasting length is chosen as 168 hours (1 week). Researchers trained the parameters using all historical data with the total data length 8760 hours. After executing the code, the trained parameters were first obtained (Figure 134).
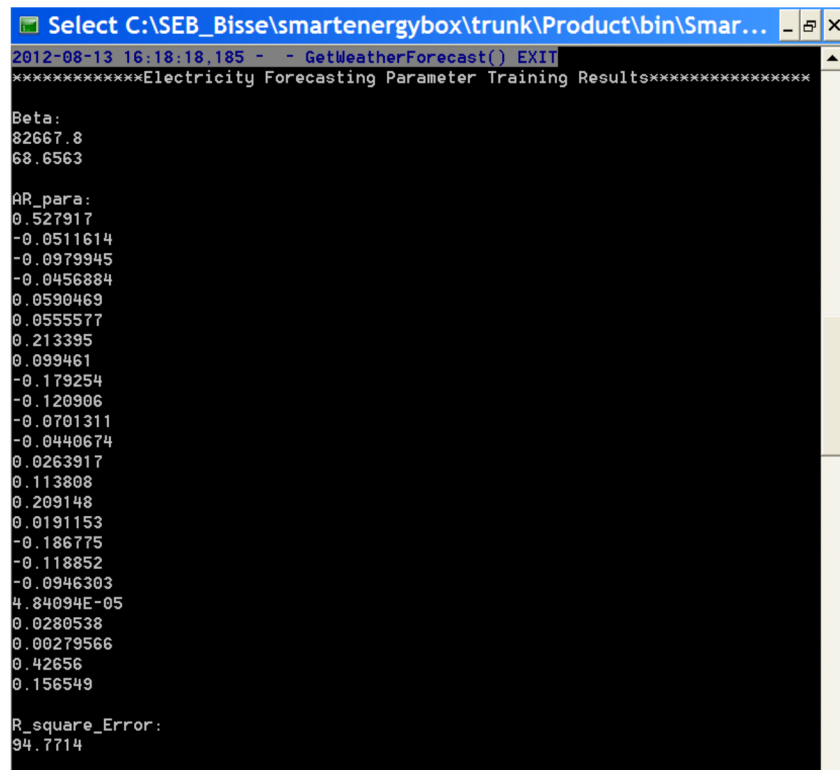
Figure 133: Translating Control Architecture to Siemens Control Solutions
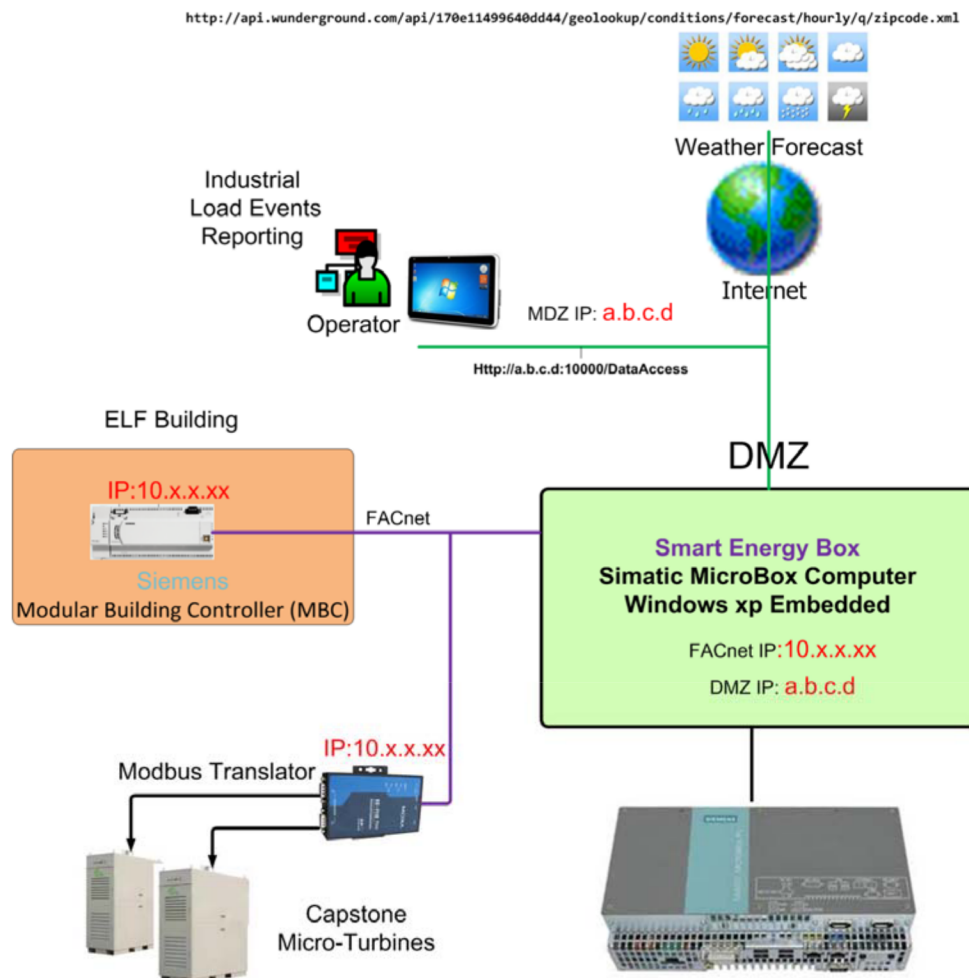
The parameters are then used to predict the electricity loads. The predicting performance is checked by comparing the actual and predicted loads (Figure 135). Researchers changed the

162

total forecasting length to 1176 hours (seven weeks), checked the predicting performance by comparing the actual and predicted loads (Figure 136). Experiment shows that the translated forecasting algorithm has similar performance when compared to the prototype implemented in MATLAB.

Figure 134: Forecast parameters obtained through training using historical data

Figure 135: Comparison of forecast results to actual data for a week

Hour	Actual Electricity Loads	Forecasting Electricity Loads	Forecasting Error
1	5976.024213	0	-5976.024213
2	5976.024213	7386.038243	1410.01403
3	5976.024213	9757.713931	3781.689718
4	5976.024213	13999.5186	8023.494386
5	7653.15859	29268.03979	
6	107287.0052	86851.99573	
7	104186.3286	83398.05027	
8	122536.0262	118249.7009	
9	122268.1031	113639.2326	
10	121820.3928	125809.967	
11	121661.3416	131718.523	
12	124001.32	135232.8806	
13	125271.8471	145738.022	
14	126568.8748	123491.7077	
15	126234.4655	103770.2127	
16	121954.821	109804.362	
17	121728.1019	113254.9108	
18	121888.8834	118932.6372	
19	125248.2836	127082.2714	
20	125422.8701	127740.7116	
21	41792.51946	73506.74374	
22	7653.15859	24551.86948	
23	7653.15859	0	
24	7653.15859	0	-7653.15859

Figure 136: Comparison of forecast results to actual data for 7 weeks

Hour	Actual Electricity Loads	Forecasting Electricity Loads	Forecasting Error
1	5976.024213	0	-5976.024213
2	5976.024213	7386.038243	1410.01403
3	5976.024213	9757.713931	3781.689718
4	5976.024213	13999.5186	8023.494386
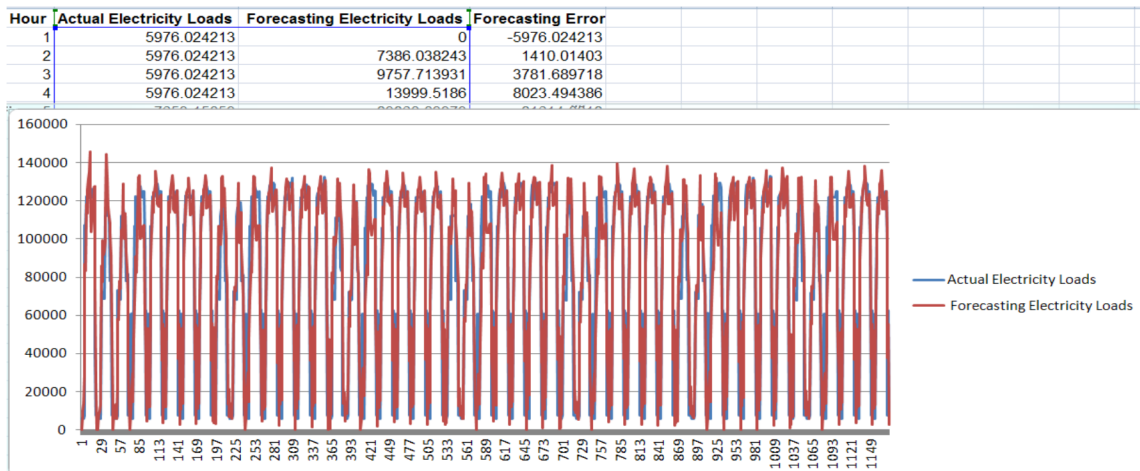
4.3 Installation and Performance of a CCHP System

4.3.1 Microturbine Control

As indicated earlier the iBEMS supports dialog based HMIs such as the one illustrated in Figure 137. In the picture is shown a configuration and display tool for testing of Capstone turbine Control. The window on the right side of the picture below displays command prompt output for the SEB runtime that can be configured to output only relevant data for our demonstration. Figure 138 shows the interface of the Smart Energy Box to control the MTG.

164

Figure 137: SEB command window (left) and Demonstration HMI (right)
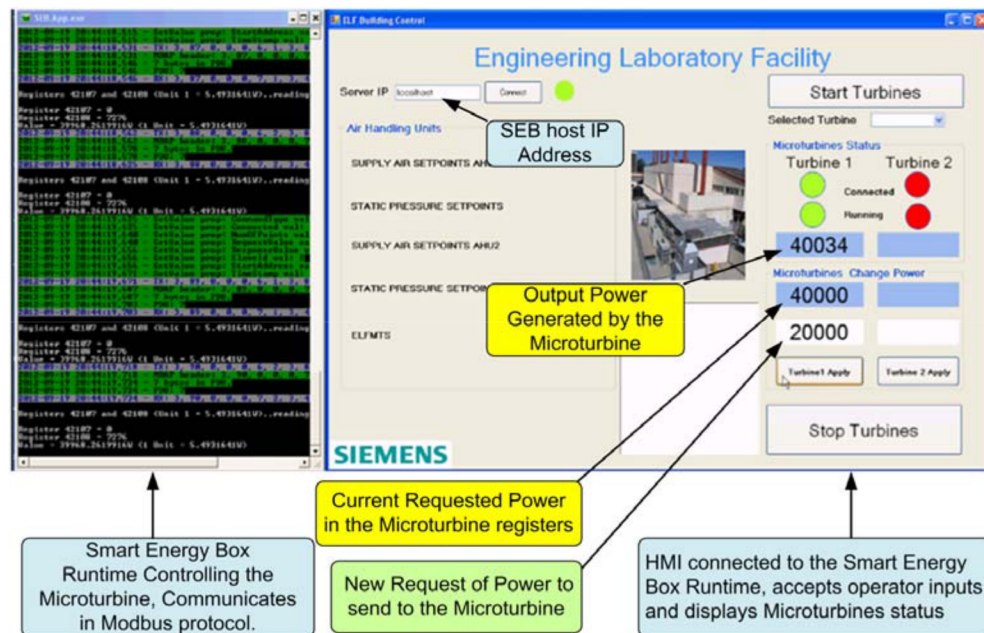
Figure 138: Micro-turbine Controlled by the Smart Energy Box (Left): Capstone Controller Screen, (Right): SEB dialog based interface showing the micro-turbine power level
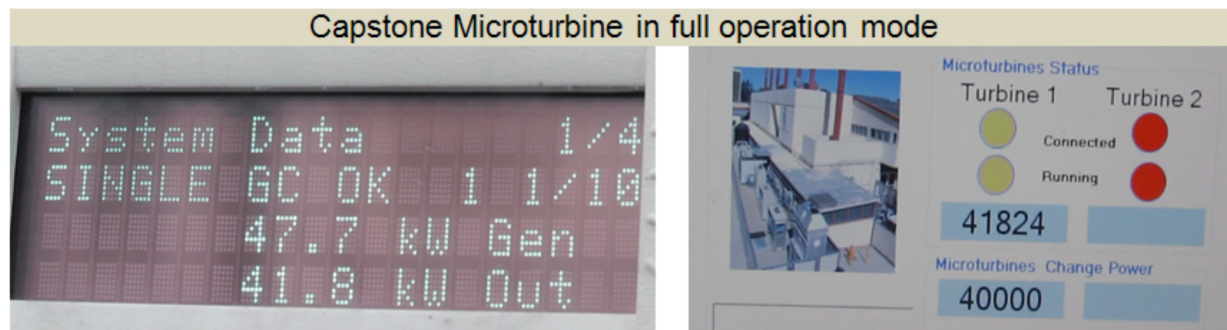
4.3.2 Industrial Load Monitoring with Wireless Sensors

Industrial loads in buildings or commercial facilities are the major cause of peak load demand. By anticipating or detecting when that load occurs provide the opportunity to the SEB to take mitigating actions to reduce the peak load either by reducing demand of other subsystems in the building of firing Microturbine. With forecasting algorithms implemented on the SEB researchers can predict when the industrial load is likely to happen. By monitoring the industrial loads with wireless sensor researchers can detect when the industrial load is active. Figure 139 shows an example of industrial load signal captured by the wireless sensor.

Figure 139: Example of Industrial load signal (compressor pressure) captured by wireless sensor
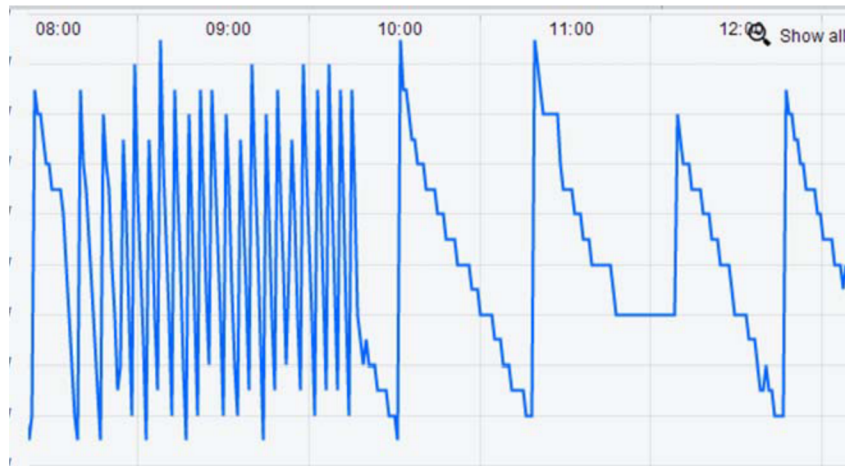
4.3.3 Automated Actions Configuration

As illustrated in Figure 139 above, the SEB can monitor various equipments and devices in a building. The SEB also provides the capability to take action based on the status of the monitored device as illustrated in Figure 140 below.

Figure 140: Illustration of a monitored device signal with location of periods of time when the SEB could take action

The actions are configurable within the SEB configuration xml file. The Metadata type that defines these actions is called **CommandActionRules** and its detailed definition and examples are presented in Appendix A.

166

CHAPTER 5:
Technology Transfer and Production Readiness

5.1 Technology Transfer

The purpose of this project was to develop novel control strategies for dynamic economical dispatch of CHP/CCHP systems with emissions constraints and thermal load following capability. The project was specifically designed to focus efforts on enable the use of CHP/CCHP in under-utilized applications. With the emergence of technologies that can efficiently convert heat into cooling (e.g., absorption chilling technology) the consideration of combined cooling, heating and power (CCHP) offers additional market opportunities that are of interest and can significantly contribute to meeting Industrial Technology Program goals. This Chapter will serve as the starting point for the development of a detailed business plan that can begin to transfer the technology to industry. In this particular case, our industrial partner, Siemens, is the most likely entity to accept the transfer of technology developed in this work.

5.1.1 Product Overview

The project determined the feasibility of dispatching a microturbine generator using different economic control strategies, reducing the cost of energy to the facility. With the outcomes and conclusions of this project, subsequent research and development can focus on the integration and optimization of the CCHP and application of research findings to various buildings and utility rate structures. This would likely be further followed by studies of scale-up, commercial viability and marketability of products that implement this technology to produce useful products for California and U.S. electric market.

5.1.1.1 Product Description

Siemens Corporate Research, the subcontractor for this project, has developed the economical dispatch of CCHP systems novel control algorithms, to achieve dynamic economical dispatch of CHP/CCHP systems with emissions constraints and thermal load following capability. These algorithms are executed by the equipment controllers as component of the control system; therefore they are not complete end-use products, but software enhancements for control application programs.

5.1.1.2 Function and Features

The novel control algorithms and architectures that were developed were also demonstrated to dispatch a microturbine generator in the Engineering Laboratory Facility of the University of California, Irvine. The control algorithms were translated to Siemens controls and were installed to demonstrate the novel control algorithms for economical dispatch of a CCHP system. Implement the control algorithm developed in the course of this project, the product needs include: weather forecast for energy demand forecasting, historical energy consumption data for the building, historical data on industrial load activity for model calibration and forecasting on industrial loads activities, access to the building automation for control of the HVAC system, access to the Micro-Turbines to controller. The access to these subsystems can be done with the use of existing software interfaces and building new ones.

5.1.2 Business Case and Market Analysis

The first market target could be California commercial enterprises and light industrial end-users of electricity and heat. Utilities in the state of California, and Southern California Edison in particular, have been quite progressive with regard to the development and use of CCHP technologies. The technical capabilities of CCHP technologies, especially the primary generators (gas turbines and fuel cells) are not assumed to experience any significant technical performance advances in the period in which the current project will proceed. Although much technological advancement may occur and although technology availability may increase during the course of the project, it is not likely that technology advancement will be focused upon a topic (for example, improving load-following capability) that would have significant impact on the novel control systems developed in this proposal. The regulatory framework is also assumed to be just as it is today with a wide variety of policies that govern CCHP installations throughout the various states of the U.S. It is expected, however, that regulatory policies will change in the near future to support technologies, including CCHP, that will have the benefit of reducing greenhouse gas emissions. Changes in regulatory processes could affect both emissions regulatory bodies as well as utility regulation. All of these possible regulatory changes must be accounted for in the development process with control strategies made flexible enough to accommodate change.

5.1.2.1 Major End-User Market Size

The primary market sector that the research and development products will be applied to is the light industrial market sector. Secondary market sectors are the larger commercial and institutional market sectors. The total industrial market for combined cooling, heating and power is substantial and well recognized. Various estimates of the CCHP market potential in the industrial sector are in the range of 30-90 gigawatts (GW) of electrical capacity in the U.S. [see e.g., Resource Dynamics Corporation, 2003; ONSITE SYCOM, 2000] Most studies also identify gas turbine technologies as leading candidates for near-term CCHP applications in the industrial market, so the focus of the proposed effort is reasonable. The "light" industrial market is defined here as less than 20 MW of electrical capacity.

This light industrial market is currently expected to comprise only a small portion of the overall industrial CCHP market penetration. This is expected even though there is significant market potential in this light industrial size class. For example, Resource Dynamics Corporation estimates that more than 2/3 of the total industrial CCHP market potential is comprised of applications less than 20 MW. [Resource Dynamics Corporation, 2003] This is because of several factors, which include the barriers already identified as: (a) lack of cost-competitive options in this size range, (2) lack of information on the value presented by these smaller systems for potential user, and (3) lack of controls sufficient to deal with the highly dynamic nature and relative non-coincidence of the thermal and electrical loads in many of these light industrial applications. The project directly addresses these barriers and significantly contributes to increased market penetration in the light industrial sector. Researchers estimate that a 20 percent improvement in market penetration in the light industrial sector will be facilitated by the products that evolve from the project alone.

In addition, the team expects that similar increased CCHP market penetration can be enabled in the commercial and institutional sectors with the novel control products that result from the project. These markets have been estimated to be as large as 75 GW of electrical capacity in the U.S. [ONSITE SYCOM, 2000] However, the majority of these markets is less amenable to CCHP applications due to more highly variable loads, lower total energy costs per unit of productivity, less coincidence of thermal and electrical loads, more highly dynamic loads, etc. Thus, researchers estimate a lower contribution to the CCHP market in the commercial and institutional sectors of 12 percent that will be facilitated by the products that evolve from the project.

5.1.2.2 Industrial Market

The total new installed capacity due to the advancements proposed herein is estimated using the following equation:

*New CCHP installed capacity = (fraction attributable to proposed technology) * (total industrial market potential) *(CA market fraction) * (fraction of market targeted)*

With a 20 percent improvement in market penetration in the industrial CCHP market attributed to the technology developed in this proposal, between 1,000 and 4,000 MWe (megawatts of electric capacity) of new CCHP systems will be installed in California [= 0.2* (30 to 90 GW) *(0.25) * 2/3 industrial]. Even if this is limited to those applications between 0.5 – 5MWe the Resource Dynamics study [2003] suggests that this portion of the light industrial market is between 66 percent (current case) and 85 percent (future case). Thus, the range of potential installed CCHP capacity in the 0.5 – 5MWe size classes due to the technology proposed is 670 – 3,400 MWe. If one assumes that the typical installation in the light industrial market is 1 MWe, then the total number of installations in the industrial market sector that are enabled by the novel control technology developed will be between 670 and 3,400 installations.

5.1.2.3 Commercial and Industrial Markets

The commercial and institutional CCHP market is estimated to be as large as 75 GW of total market potential [ONSITE SYCOM, 2000]. The team uses the same means of estimating the total new installed capacity due to the advancements proposed herein, but, assumes only a 12 percent improvement in market penetration due to the product developed in the commercial and institutional sector. Thus, using the following equation:

*New CCHP installed capacity = (fraction attributable to proposed technology) * (total commercial and institutional market potential)* (CA market fraction)*

a 12 percent improvement in market penetration in the commercial and institutional CCHP market sector leads to 2,250 MWe of installed capacity [= 0.12* (75 GW)* (0.25)]. If a typical installation is again assumed to be 1 MWe, then the total number of installations in the commercial and institutional market sectors will be 2,250 installations.

5.1.3 Public Benefits

Public benefits will be realized in at least three areas: (1) energy savings, which will impact the longevity of limited primary energy reserves and the cost of energy supply, (2) criteria pollutant

emissions reductions, which will improve air quality, and (3) greenhouse gas emissions reductions, which will reduce our impact on the global climate.

5.1.3.1 Energy Savings

The combined estimate of increased market applications of CHP/CCHP technology in the light industrial, commercial and institutional markets is between 2,920 and 5,650 MW. If these systems are assumed to have an average electrical efficiency of 36 percent and that 50 percent of the useful heat produced is recovered to replace a boiler, then a total mixed (heat and power) CCHP system efficiency of 68 percent is achieved. When compared to a current average for grid supplied electricity of 33 percent and a 95 percent efficient boiler and assume a 90 percent capacity factor for the CCHP systems savings can be in the range of 9.9 – 29.6 TBtu/year due to the technology proposed. This was estimated by summing the results from the following expressions:

Electrical energy savings/year = (efficiency difference) * (installed capacity, MW) * (capacity factor) * (8766 hours/year) * (3.412E-6 TBtu/MW-hour)

Thermal energy savings/year = (recovered fraction) * (installed capacity, MW) * (capacity factor) * (8766 hours/year) * (3.412E-6 TBtu/MW-hour) / (boiler efficiency)

Interestingly, the energy savings estimate is not very sensitive to the assumed electrical efficiency of the CCHP system. For example with all of the same assumptions except for an increase in average CCHP electrical efficiency up to 40 percent, annual energy savings is estimated to be in the range of 10.4 – 31.2 TBtu/year.

5.1.3.2 Criteria Pollutant Emissions

The proposed effort will lead to significant energy savings in the light industrial, commercial and institutional sectors. The average NOx emissions intensity of electricity provision and natural gas boilers is 0.2 kg NOx/MWh and 0.014 kg NOx/MMBtu, respectively. Thus, the proposed effort is expected to reduce NOx criteria pollutant emissions by roughly between 177 to 531 metric tons of NOx per year.

5.1.3.3 Greenhouse Gas Emissions

In addition, the carbon dioxide (the primary greenhouse gas) emissions intensity of electricity provision and natural gas boilers is 608.2 kg CO_2/MWh and 53.5 kg CO_2/MMBtu, respectively. As a result, the proposed effort is expected to contribute to reductions in carbon dioxide emissions of roughly 0.63 to 1.89 million metric tons annually. Thus, the proposed effort will significantly contribute to reducing the California carbon intensity and contributing to state goals for reduction of greenhouse gas emissions.

5.1.4 Product Development Status and Needs

5.1.4.1 Product Development Status

In this project, physical models of CCHP system components were developed and the economic and environmental analyses strategies were developed. Economic dispatch strategies have been developed and these dispatch strategies can enable Combined Cooling, Heat and Power (CCHP) technologies to reduce overall facility energy costs. The control algorithms and

architectures were developed and translated to Siemens controls and were installed to demonstrate the novel control algorithms for economical dispatch of a CCHP system.

5.1.4.2 Remaining Steps

Before the economical dispatch tools are market ready, robust sets of threshold control parameters, suitable for use with site-specific configurations must be determined. Determining these sets of parameters is out of the scope of the current project. More work is also needed to complete development of the user interface for the economical dispatch tool.

5.1.5 Technology Transfer Actions

5.1.5.1 Manufacture Commitment

There is one participating manufacture (Siemens). The major commercialization partner in this project is Siemens Corporate Research (SCR). SCR works closely with Siemens Building Technologies (SBT). SCR and SBT have significant previous experience and capabilities to translate the novel controls to application software. Significantly, Siemens has applied Model Reference Adaptive Control (MRAC) for Heating Ventilation and Air-conditioning (HVAC), developed a Green Resource Advisor to help end-users design, operate and retrofit their building systems to include "Green Components," and developed distributed optimization and machine learning techniques for building automation and control entitled "Total Plant Optimization."

5.1.5.1 Purchase Incentive

The energy savings and benefits of the results of this project are not dependent upon any code requirements. However, any incentives (e.g., rebates, direct incentives, code recommendations, or points, etc.) will increase the appeal of novel control of CCHP system, both to potential buyers and manufactures.

5.1.5.1 Educating CCHP Engineers and Designers

In current practice, energy managers, architects, commercial building owners, businesses, etc. are not aware of the benefits that CHP/CCHP technology can provide. It is necessary to educate these individuals on the existence, general principals, and benefits of CCHP system and the economical dispatch of a CCHP system. Two articles were submitted to the Journal of Power Sources which will be dedicated to the topics. Case studies of various buildings of this project could be also made available as well.

5.2 Production Readiness

The simulations and demonstration in this project has indicated that the economical dispatch of CCHP system holds the promise of becoming the besting performing control system in the industrial and commercial markets. The technology is on the verge of being commercialized. To determine the steps that will lead to the manufacturing of the technologies developed in this project or to the commercialization of the project's results, a Production Readiness Plan is determined.

5.2.1 Production Process and Current Facilities

The control system for economical dispatch of CCHP system consists of several components: Siemens Smart Energy Box, weather forecast module, demand management module, optimization module. The Siemens Corporate Research has developed the components in the economical dispatch of CCHP systems novel control system, to achieve dynamic economical dispatch of CHP/CCHP systems with emissions constraints and thermal load following capability. These algorithms are executed by the equipment controllers as component of the control system and such software enhancements for control application programs are ready to launch. The Siemens Smart Energy Box is manufacture by Siemens Corp. and is currently available in the market. Combined with the components developed in this project, the production can be completed.

5.2.2 Required Improvements

Before the economical dispatch tools enter the stage of full production, robust sets of threshold control parameters, suitable for use with site-specific configurations must be determined. Building loads and energy consumption patterns and CCHP systems on-site could be largely different. Therefore determining the sets of parameters in the economical dispatch control strategy is required to improve the product. In addition, improvement in the user interface for the economical dispatch tool is also required.

5.2.3 Cost Estimate and Required Investment

The costs associated with full commercialization of the technology developed herein are not known, but, estimated to be well less than $500,000. This estimate is based upon the amount of progress that the current team was able to make with the approximately $400,000 investment of the California Energy Commission. It is believed that a similar investment that targets the development of an energy control product at Siemens Corporation, or other similar entity, that is based upon the findings and developments of the current project is reasonable.

5.2.4 Full Production Ramp-up Plan

While the merits of the economical dispatch of CCHP system product have been proven in the simulations and demonstration, a number of steps must be taken before full production levels can be reached. Further optimization of the algorithm needs to be carried out with more site-specific configurations and control parameters to better accommodate various buildings and facilities as well as various types and integrated systems of distributed energy technologies.

GLOSSARY

CARB	California Air Resources Board
CHP	Combined Heat and Power
CRC	Capacity Reservation Charge
DG	Distributed Generation
EPA	Environmental Protection Agency
EPIC	Electric Program Investment Charge
HR	Heat Recovery
ICBA	Installed Capacity versus Building Average
ICBM	Installed Capacity versus Building Maximum
kW	Kilowatt
kWh	Kilowatt-Hour
MTG	Microturbine Generator
MUD	Maximum Utility Demand
NEI	National Emissions Inventory
NFCRC	National Fuel Cell Research Center
O&M	Operations and Maintenance
SCE	Southern California Edison
SCG	Southern California Gas Company
SEB	Smart Energy Box
SGIP	Self Generation Incentive Program
TOU	Time of Use
UCI	University of California, Irvine

REFERENCES

Flores, Robert. Control of Dispatch Dynamics for Lowering the Cost of Distributed Generation in the Building Environment. University of California, Irvine. Master of Science Thesis, 2013.

Resource Dynamics Corporation, *Cooling, Heating, and Power for Industry: A Market Assessment*, Prepared for the U.S. Department of Energy, 2003.

ONSITE SYCOM Energy Corporation, The Market and Technical Potential for Combined Heat and Power in the Commercial/Institutional Sector, Prepared for U.S. Department of Energy, 2000.

APPENDIX A:
Automated Actions Configuration

The actions are configurable within the SEB configuration xml file. The Metadata type that defines these actions is called **CommandActionRules** and it is defined as follows:

```xml
<MetaObject name="CommandActionRules"  >
    <SimpleProperty name="TiggerVarName"     type="System.String" persistency="persistent" />
    <SimpleProperty name="TiggerVarType"      type="System.String" persistency="persistent" />
    <SimpleProperty name="TiggerStartActionValue"    type="System.String" persistency="persistent" />
    <SimpleProperty name="TiggerStartMinduration"     type="System.String" persistency="persistent" />
    <SimpleProperty name="StartActionStartTime"      type="System.String" persistency="persistent" />
    <EnumProperty name="StartActionCondition"       enumerators="LEQ GEQ EQ LES GRE"
                                                         Persistency="persistent" />
    <SimpleProperty name="StartActionCommand"      type="System.String" persistency="persistent" />
    <SimpleProperty name="TiggerStopActionValue"     type="System.String" persistency="persistent" />
    <SimpleProperty name="TiggerStopMinduration"      type="System.String" persistency="persistent" />
    <EnumProperty name="StopActionCondition"       enumerators="LEQ GEQ EQ LES GRE"
                                                         Persistency="persistent" />
    <SimpleProperty name="StopActionCommand"      type="System.String" persistency="persistent" />
    <SimpleProperty name="StartStopMinduration"      type="System.String" persistency="persistent" />
    <SimpleProperty name="StopActionStartTime"      type="System.DateTime" persistency="persistent" />
    <SimpleProperty name="StopStartMinduration"      type="System.String" persistency="persistent" />
    <SimpleProperty name="Currentcommand"       type="System.String" persistency="persistent" />
    <SimpleProperty name="CurrentcommandStartTime"      type="System.DateTime" persistency="persistent" />
    <SimpleProperty name="Valid"          type="System.Boolean" persistency="persistent" />
</MetaObject>
```

And example of **CommandActionRules** data point definition is illustrated in the figure below.

```
<CommandActionRules name="Start.Microturbine.One"
        TiggerVarName="Compressor.Pressure"    // the name of the trigger variable
        TiggerVarType="ModbusControlPoint"     // define the data type
        TiggerStartActionValue="143"           // threshold to start action
        TiggerStartMinduration="00:00:20"
        StartActionStartTime="00:00:00"
        StartActionCommand="ON"                // start action Command type
        TiggerStopActionValue="153"            // stop action threshold.
        TiggerStopMinduration="00:00:20"
        StopActionCommand="OFF"                // stop action Command type
        StartStopMinduration="00:05:00"
        StopActionStartTime="6/10/2013 12:00:00 AM"
        StopStartMinduration="00:05:00"
        Currentcommand="NONE"                  // current command default NONE
        CurrentcommandStartTime="6/10/2013 12:00:20 AM"
        Valid="false"                          // if false the rule is not executed
        StartActionCondition="LEQ"        // Start action condition <=
        StopActionCondition="GEQ" />      // start action condition >=
```

Figure 141: Illustration of a command Action Rule data point

CommandActionRules properties description

Simple Property Name	Description
TiggerVarName	Name of the variable used to trigger action. In the case of the illustration above, we use compressor pressure variable name **Compressor.Pressure**
TiggerVarType	Defines the variable type of TiggerVarName in this case the variable type is **ModbusControlPoint**
TiggerStartActionValue	Threshold to start action
TiggerStartMinduration	When the threshold is reached it must be maintained for a minimum duration before action could be triggered to avoid starting action on noises.
StartActionStartTime	This variable holds the last time stamp when the start action command was triggered. This variable is used internally. The user is not required to assign a valid value to this
StartActionCondition	Stores the logical condition to test whether action should be executed of not. For example when the TiggerStartActionValue is reached what should be the decision

based on?

If (value <= `TiggerStartActionValue`) then execute Action?

If (value >= `TiggerStartActionValue`) then execute Action?

The condition are defined in the following enumerator

`enumerators="LEQ GEQ EQ LES GRE"`

`LEQ` ➔ Less or Equal

`GEQ` ➔ Greater or Equal

`EQ` ➔ Equal

`LES` ➔ Less

`GRE` ➔ Greater

`StartActionCommand`	This variable holds the command that will be executed. For example in the picture above the command to execute is to start engine "ON" therefore the value held by this variable is **"ON"**. In other circumstances it could be a number to write to a specific register in a controller.
`TiggerStopActionValue`	Threshold to stop action
`TiggerStopMinduration`	When the threshold is reached it must be maintained for a minimum duration before action could be triggered to avoid starting action on noises.
`StopActionCondition`	Stores the logical condition to test whether action should be executed of not. For example when the `TiggerStopActionValue` is reached what should be the decision based on?

 If (value <= `TiggerStopActionValue`) then execute Action?

If (value >= T `TiggerStopActionValue`) then execute Action?

The condition are defined in the following enumerator

`enumerators="LEQ GEQ EQ LES GRE"`

`LEQ` ➔ Less or Equal

_{GEQ} ➔ Greater or Equal

_{EQ} ➔ Equal

_{LES} ➔ Less

_{GRE} ➔ Greater

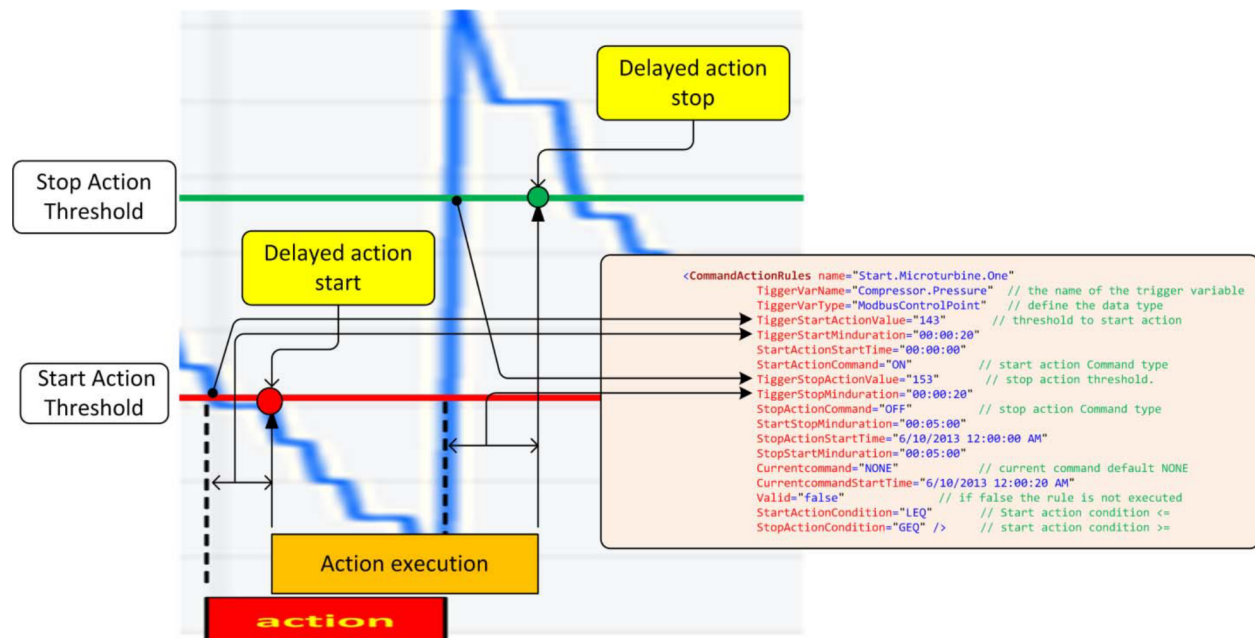|	
`StopActionCommand`	This variable holds the command that will be executed. For example in the picture above the command to execute is to stop engine, **"engine OFF"** therefore the value held by this variable is **"OFF".** In other circumstances it could be a number to write to a specific register in a controller.

Figure 142: Illustration of threshold and minimum start durations

`StopActionStartTime`	This variable holds the last time stamp when the stop action command was triggered. This variable is used internally. The user is not required to assign a valid value to this.
`StartStopMinduration`	Some equipment require a minimum startup time. It is not advised to try to stop them during that time period except for emergency. Therefore, even though a start threshold may be reached, the controller may not issue a start command if the minimum duration of stop-start period has not expired.

StopStartMinduration

Some equipment require a minimum time to shutdown. It is not advised to try to restart them during that time period. Therefore, even though a start threshold may be reached, the controller may not issue a start command if the minimum duration of stop-start period has not expired.
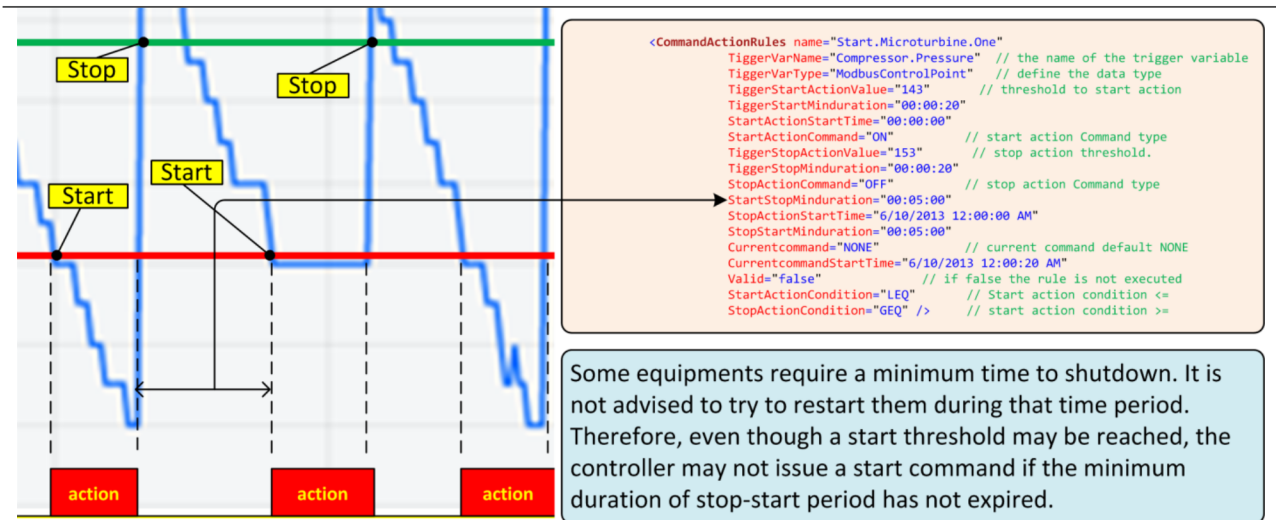

Figure 143: Illustration of stop-start minimum duration

Currentcommand

This variable holds the current command name that is being executed StartActionCommand value or StopActionCommand value or NONE if no command is executed. By default it is NONE. This variable is mostly used internally

CurrentcommandStartTime

This variable holds the last time stamp when the stop action Currentcommand was changed. This variable is used internally. The user is not required to assign a valid value to this.

Valid

This Boolean value enable to configuration to be used when it is TRUE. By default it should be false.